CONFORMAL COOLING AND RAPID THERMAL CYCLING IN INJECTION MOLDING WITH 3D PRINTED TOOLS

by

XIAORONG XU

B.S., University of Science and Technology of China, 1992
M.S., State University of New York at Stony Brook, 1995

Submitted to the Department of Mechanical Engineering in Partial Fulfillment of the Requirements for the Degree of

Doctor of Philosophy
In Mechanical Engineering

at the

MASSACHUSETTS INSTITUTE OF TECHNOLOGY

September 1999

Signature of Author _____
Department of Mechanical Engineering

Certified by _____
Emanuel M. Sachs
Professor of Mechanical Engineering
Thesis Supervisor

Accepted by _____
Ain A. Sonin
Chairman of Graduate Committee

CONFORMAL COOLING AND RAPID THERMAL CYCLING IN INJECTION MOLDING WITH 3D PRINTED TOOLS

by

XIAORONG XU

Submitted to the Department of Mechanical Engineering in Partial
Fulfillment of the Requirements for the Degree of
Doctor of Philosophy In Mechanical Engineering

ABSTRACT

Solid Freeform Fabrication processes such as 3D Printing have demonstrated the potential to produce tools with complex internal geometry. This work explores the application of this capability to improved thermal management for injection molding tooling through: i)cooling lines which are conformal to the mold surface which provide improved uniformity and stability of mold temperature and ii) tools with low thermal inertia which, in combination with conformal fluid channels allow for rapid heating and cooling of tooling, thereby facilitating isothermal filling of the mold cavity.

This work presents a systematic, modular, approach to the design of conformal cooling channels. Recognizing that the cooling is local to the surface of the tool, the tool is divided up into geometric regions and a channel system is designed for each region. Each channel system is itself modeled as composed of cooling elements, typically the region spanned by two channels. Six criteria are applied including; a transient heat transfer condition which dictates a maximum distance from mold surface to cooling channel, considerations of pressure and temperature drop along the flow channel and considerations of strength of the mold. These criteria are treated as constraints and successful designs are sought which define windows bounded by these constraints. The methodology is demonstrated in application to a complex core and cavity for injection molding.

In the area of rapid thermal cycling, this work utilizes the design methods for conformal channels for the heating phases and adds analysis of the packing and cooling phases. A design is created which provides thermal isolation and accommodation of cyclic thermal stresses though an array of bendable support columns which support the molding portion of the tool where the heating/cooling channels are contained. Designed elasticity of the tool is used to aid in packing of the polymer during the cooling phase. Methodology for the design of this structure is presented. A set of tools has been fabricated and subjected to thermal and mechanical tests.

Thesis Supervisor: Emanuel Sachs
Title: Professor of Mechanical Engineering

ACKNOWLEDGEMENTS

I would like to thank Ely Sachs for providing me the opportunity to accomplish something that I will be proud of all my life. Thank you for your consistent support and encouragement. What I learnt from you is the treasure I will take forever.

I would like to thank Professor Samuel Allen and Professor John Lienhard for sitting in my thesis committee and giving me marvelous helps, suggestions and inspirations for the past four years.

I am greatly indebted to our 3DP staffs: Dave Brancazio, Jim Serdy and Julie . They devoted a lot of time and energy in this project and took care of many detailed technical and administrative issues. Without their help this project would have been impossible. I would like to extend my thanks to every student in 3DP lab from whom I learnt a lot. I deeply appreciate their friendship and support.

The work discussed in this thesis is supported by the Technology Re-Investment Project, Cooperative Agreement (DMI - 9420964) funded by DARPA and administered by NSF, and the 3D Printing Industrial Consortium. I would like to thank all the consortium members for their contribution to this project and their tremendous help. Thank Richard Barlik from Hasbro for designing the benchmark part for conformal cooling, Jim Irish, Wayde Schmidt and Ronald White from UTRC, Derek Smith, Dennis Burke from Motorola, for their consistent support and encouragement through the whole the project. I owe millions of thanks to Charles Malstrom, who have proposed the benchmark part for the rapid thermal cycling test and provided a lot of technical guidance.

I want to thank Gerry, Fred and Mark at LMP machine shop and Peter, Steve from MIT central machine shop for their excellent job and tremendous help. My gratitude extends to Ms. Yin-Lin Xie and Mr. John Centorino at Department of Material Science for their help with the furnace work and the mechanical test.

In 1996 I had an opportunity to visit Cornell Injection Molding Program where I got tremendous guidance from Dr. K. K. Wang and Dr. C. A. Hieber in injection mold cooling system design and analysis. I would like to say "thank you" to them and to all CIMPers for their friendship and generous help.

Finally I would like to express my sincere thank to my wife, Xin and my parents. I could not have reached today's point without their encouragement, care and companionship.

Dedicated to
my wife Xin and my parents
for
their consistent love and support

TABLE OF CONTENTS

LIST OF TABLES

LIST OF FIGURES

NOMENCLATURE

ρ_m, ρ_p, ρ_c :	Density of the mold, the plastic part and the coolant respectively
c_m, c_p , c_c :	Specific heat of the mold, the plastic part and the coolant respectively
K_m , K_p , K_c :	Thermal conductivity of the mold, the plastic part and the coolant respectively
α_m, α_p, α_c:	Thermal diffusivity of the mold, the plastic and the coolant respectively
E_m , E_p , E_c:	Energies accumulated in the mold, dissipated from the part and absorbed by the coolant respectively
E_{loss}:	Energy loss through heat transfer oil in rapid heating
E_m:	Young's modulus of the mold
I:	Momentum of inertia
E:	Young's modulus
G_m:	Shear modulus of the mold
μ_c :	Coolant viscosity
μ, η:	Part viscosity
Re_D:	Coolant Reynold number
F_0 :	Froude number
B_i :	Biot number
Q:	Coolant flow rate
v:	Coolant flow velocity
h , h_c :	Heat transfer coefficient between mold and coolant
e:	Cooling channel surface roughness
C_f:	Cooling channel surface friction factor
T_w:	Mold wall temperature
T_{melt}:	Plastic melt processing temperature
T_{eject}:	Plastic ejection temperature
T_{center}:	Part center temperature
$T_{average}$:	Averaged part temperature across the thickness

T_m^s:	Cycle averaged mold temperature at steady operation
$T_m(t)$:	Cycle averaged mold temperature as a function of time
T_m^0, T_{mold}^0:	Initial mold temperature
T_{oil}^0:	Initial oil temperature
T_c:	Coolant temperature
l_m:	Vertical distance from cooling line to mold wall
l_p:	Half the plastic part thickness
H:	Part thickness
D:	Cooling channel diameter
W:	Cooling line pitch distance
L:	Cooling line length
V_m:	Net mold volume
hc_eq:	Equivalent heat transfer coefficient
l_eq:	Equivalent distance from the cooling channel to the mold wall
Δm:	Step length of finite difference nodes for the mold
Δp:	Step length of finite difference nodes for the part, coolant pressure drop
δ:	Horizontal displacement due to thermal expansion/shrinkage
β:	Thermal expansion coefficient for 3DP material
T_j^k:	The temperature of the jth node at the kth time step
T_1:	Temperature at the mold-part interface on part side
T_0:	Temperature at the mold-part interface
T_2:	Temperature at the mold-part interface on mold side
ΔT:	Temperature drop along the cooling line
t_{cycle}:	Injection cycle time
t_{fill}:	Filling time
τ:	mold time constant
Δt:	Step length for the simulation time
$\dot{\gamma}$:	Shear rate
$\dot{\gamma}_{max}$	Maximum shear rate in the part

N:	Required oil channel number
K:	Loss efficient for pipe fitting
P_{cr}:	Critical buckling load
P_{hr}:	Horizontal force applied on the truss columns
M_0:	Moment at the end of truss columns

PAGE(S)
MISSING

CHAPTER 1

INTRODUCTION

CONTENT

1.1 INJECTION MOLDING (IM)

1.1.1 Introduction

Injection molding is a cyclic process used to convert raw material into all types of products. Although the term "injection molding" refers to a general process where the molten material is forced into a mold cavity and solidifies to obtain the final shape, this thesis will only focus on the thermoplastic injection molding. However the concepts discussed in this thesis will also apply to many other molding processes, such as Blow Molding, Casting and Powder Injection Molding.

The injection molding process is the most common process for polymer manufacturing. Major advantages of this process include:

1) High production rate
2) Allowing large volume production
3) Relatively low labor cost per unit
4) Allowing process automation
5) High quality parts with various shapes, colors and finishes
6) Minimal scrap loss because runners and gates are recyclable.
7) Close dimensional tolerances

An injection molding process consists of the successive repetition of four stages: filling, packing, cooling and ejection. In the filling stage, the polymer melt is injected into an empty cavity formed by two halves of the mold. After the cavity has been completely filled, additional melt is packed into the cavity at high pressure in order to compensate for the shrinkage of the part in cooling. The cooling stage continues until the part is solidified to the point where no significant deformation will occur on the part at ejection. Once the mold opens and the part is ejected from the mold, the molding machine starts to prepare for the next injection cycle.

1.1.2 Problems In Injection Molding

Despite its tremendous advantages, the injection molding process also suffers quality problems. These problems can be classified into three categories: appearance, process and properties. Appearance problems include bubbles and voids in the part, discoloration, sink

marks, surface waviness and weld lines. Process problems include excess flash on parting lines, short shots, sprue sticking and erratic ejection. Property problems include brittleness, warpage, uneven shrinkage and cracking. The chief causes of these quality problems are machine parameters (injection speed, injection pressure, holding pressure, etc.), material preconditioning factors (incoming material quality, drying time and temperature, etc.) and mold design factors (gate and runner size, location and shape, cavity layout, cooling line distribution, etc.).

The major reason for various quality problems in injection molding is the coupling feature of the process itself. The coupling feature is addressed from the following two perspectives:

1) Coupling between design and manufacturing

The mold designer has to consider the molding condition and the manufacturing capability in order to determine the design parameters such as the runner size and the gate location. Formerly, mold design was regarded as an art because successful injection molding and high part quality depended heavily on the mold designer's experience and knowledge. Today, with the help of numerical simulation and various CAD packages, the mold design procedure is significantly automated. However, the numerical simulation can only speed up the trial and error iteration, but can not change the coupling feature of the process itself. To begin with, the designer does not know the quality of the resulting part until he runs the flow, cooling and warpage analysis or check the molded art. He has to rely on the performance result to improve his design. Secondly, one of the most important parts of the design, the cooling channel design, unfortunately has to be placed at the end of the design cycle and is thus given the least consideration. Mold designers have other fundamental issues to consider such as the pin ejectors, the gate location and the runner arrangement before they can think about cooling channels. After other elements have been placed, little space and flexibility remain to generate a properly designed cooling channel. Also, the traditional manufacturing processes do not allow the freeform fabrication of complex channel systems inside a small insert. That is why, in many cases, the cooling channel is merely a decoration instead of an effective means for part dimensional control. In extreme cases, the badly designed cooling channels may result in unbalanced cooling and warpage.

2) Coupling between mold filling and part cooling

In a traditional injection molding process, the filling stage is coupled with the cooling stage. On the one hand, when the hot plastic melt makes contact with the cold mold wall, the boundary starts to cool down and creates a skin of frozen layer. This frozen layer hinders the successive flow of the plastic melt

and may lead to defects such as short shot. On the other hand, the non-uniform temperature field in the plastic part during the filling stage introduces residual stresses and molecular orientation. The flow-induced residual stresses and the thermal-induced residual stresses are coupled together and result in a complex residual stress pattern in the part, which is the major reason for many quality problems.

The coupling physics between the filling and the cooling stages significantly effects the process condition setup. The dilemma a mold designer faces in the design of the injection pressure and mold temperature for thin wall molding best addresses this effect. The short shot defect always occurs for thin part molding because the plastic melt freezes before it completely fills the cavity. Three solutions to this problem are increasing the melt temperature, increasing the mold temperature or increasing the injection pressure (therefore shorten the filling time). However, increasing the melt temperature requires a corresponding increase in packing pressure to compensate for the thermal shrinkage. With this modification, one also takes the risk of degrading the polymer melt. The high mold temperature means that a longer cycle time is required before the part can sufficiently solidify. The large injection pressure causes high flow-induced molecular orientation. In the meantime, the high heat and large shear rate caused by viscous shear may degrade the polymer melt. In a word, there is not an effective way for independent control of process parameters. A mold designer must find a compromised solution from different feasible process conditions.

The key to eliminating the problems discussed above is to decouple molding process. In the following chapter we will discuss how the conformal cooling and rapid thermal cycling techniques help to eliminate the coupling that exists in an injection molding process.

1.1.3 Field Review

The ultimate goal in injection molding is to decrease the time and cost of part manufacture, while maintaining or increasing the quality. In order to achieve this goal, the injection molding process has been studied, modified and refined over the last approximately 125 years. Many different methods and techniques have been developed to make the process more productive, controllable and economical. These methods and techniques are classified into two areas: process hardware and molding science.

In the hardware side of the process, different methods such as helical channels, baffled hole system, spiral plug system and heat-pipes have been developed for the uniform and efficient cooling of the part [Pye 1989]. Some mold manufacturers built tools with cooling channels that follow the part shape

by different methods, such as stacking slices of the insert layer by layer with cooling channels milled on each layer [Luling 1997]. Other manufacturers developed the pulse heating and cooling technique for better control of the mold temperature, in order to reduce the energy consumption and enhance uniform cooling conditions [DeGaspari, 1995]. Various novel processes such as injection-compression molding, lost-core molding and co-injection molding have been developed for further improvement of the process quality and variety [Schmidt, 1998]. In 1986, Kim and Suh reported the development of a low thermal inertia mold for isothermal filling [Kim et. al 1986]. The mold was constructed by placing multiple layers of woven graphite, silicon rubber, Teflon and zirconium oxide on the surface of the mold base. The rapid switch of the heating circuit fires the graphite fiber and warms up the mold surface in a very short time so that the isothermal filling occurs. The experiments with low thermal inertia molding showed significant improvement in the part residual stress and molecular orientation. Other advantages of the low thermal inertia molding include lower barrel plastic temperature, lower injection pressure, slower injection rate, the short-shot eliminated part and the uncoupled scheme for mold flow and cooling design and analysis. More recently, Kim and Wadhwa designed a mold which uses thermoelectric devices for rapid heating and cooling [Kim et. al 1987]. Jansen built a fast-response heating elements for the use of isothermal filling by placing a resistance layer between two insulation layers [Jansen et. al 1994].

The scientific modeling of the injection molding process was first introduced in the early 1970's [Kenig and Kamal 1970]. Different methods were proposed to predict the temperature field for mold and part during the cooling stage [Singh 1991, Austin 1985, Chu et. al 1989, Kwon 1982, Turng et. al 1990, Himasekhar et. al 1992, Chen et. al 1991, Hu et al 1995]. The cooling-related quality issues such as residual stress, shrinkage and warpage were also addressed in [Lauze et. al 1989, Rezayat 1989, Thomas et. al 1989, Chen et. al 1991, Titomanlio et. al 1996, Liu et. al 1996, Zoetelief et. al 1996]. Among those simulation algorithms, an iterative hybrid scheme proposed by the Cornell Injection Molding Program (CIMP) became a standard scheme for mold cooling analysis due to its computational efficiency [Kwon 1982, Turng et. al 1990, Himasekhar et. al 1992].

1.2 LAYERED MANUFACTURING (LM)

1.2.1 Field Overview

Layered Manufacturing (LM) is also referred to as "Solid Freeform Fabrication" for its ability to produce complex parts and as "Rapid Prototyping" because often LM can produce a part more quickly than by other means. It represents a promising class of manufacturing processes that convert CAD models

directly into 3D parts. Most of the LM processes are material additive processes, differing from traditional manufacturing approaches of machining, which involve removal of material. 3D objects are constructed by incrementally building up cross-sectional layers of arbitrary complex shapes converted from CAD models. Typical LM processes include stereolithography (SLA), selective laser sintering (SLS), three dimensional printing (3DP), shape deposition manufacturing (SDM), fused deposition manufacturing (FDM), laminated object manufacturing (LOM). [Marcus et. al. 1993].

The capability of LM to produce nearly arbitrary shapes lends itself to rapid, flexible and customized production. Many large industries such as the automotive, electronics and aerospace industries have adopted LM technology as an effective way to reduce the product development cycle in the prototyping stage. As commercial LM technologies improve, complex parts with more materials and better dimensional accuracy will be commercially available. Traditional machine shops with their hazards and noise may be replaced by LM centers, providing quiet environments with less exposure to hazardous materials and less waste. LM will move rapid prototyping to rapid manufacturing.

1.2.2 3D Printing Process

Three Dimensional Printing (3DP) is one of the LM processes that rapidly fabricates three-dimensional parts directly from computer models. A solid object is created by printing a sequence of two-dimensional layers. The creation of each layer involves the spreading of a thin layer of powdered material followed by the selective joining of powder in the layer by ink-jet printing of a binder material. A continuous-jet printhead is raster-scanned over each layer of powder using a computer controlled x-y table. Individual lines are stitched together to form 2D layers, and the layers are stitched together to form a 3D part. Unbound powder temporarily supports unconnected portions of the component, allowing overhangs, undercuts and internal volumes to be created. The unbound powder is removed upon process completion, leaving the finished part [Sachs et. al., 1995]. The 3D Printing process sequence is shown in Figure 1-1.

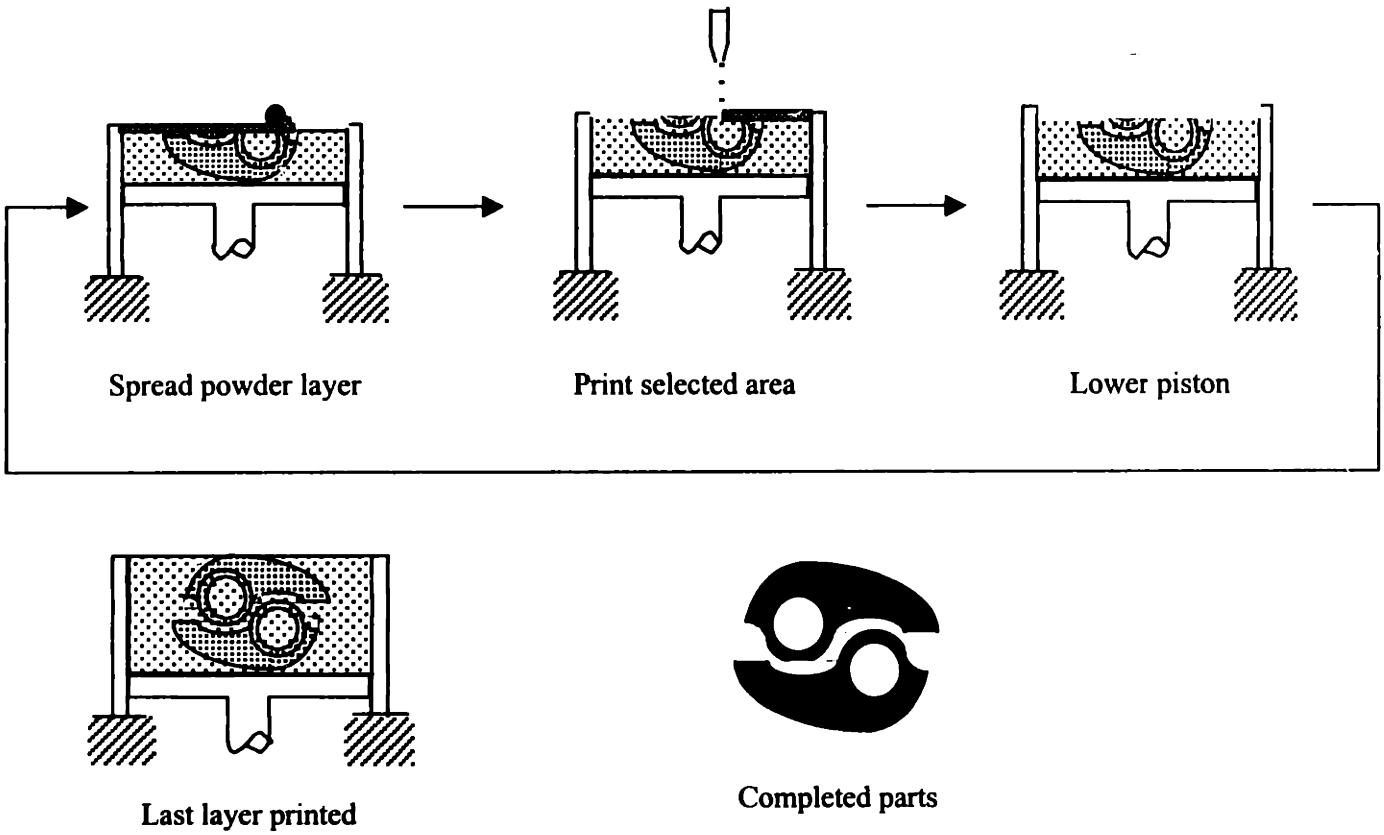

Figure 1-1 Comparison of mold surface temperature histories for straight channel cooling and conformal channel cooling

After the green part is printed, four post-processing steps are taken in order to obtain metal parts with full density: debinding, sintering, infiltration and heat treatment, if needed. The post-process flow is shown in Figure 1-2. The first step is debinding and light sintering. Debinding evaporates the organic binder from the green part. Light sintering gives the skeleton a certain degree of sintering strength. During debinding and light sintering the green part has to be buried in a Zirconia or Aluminia powder bed in order to avoid slumping of the green part due to gravity or high temperature creep. The second step is sintering. Sintering is a solid state diffusion bonding among powder particles. It gives the skeleton enough strength for infiltration. In the third step of infiltration the infiltrant metal, lifted by the capillary force, fills the porosity of the skeleton at a temperature at least 50°C higher than the infiltrant melting point. A full-density part is obtained after solidification. If the tool is hardenable, then additional heat treatment such as annealing, solution treatment, hardening and tempering are required.

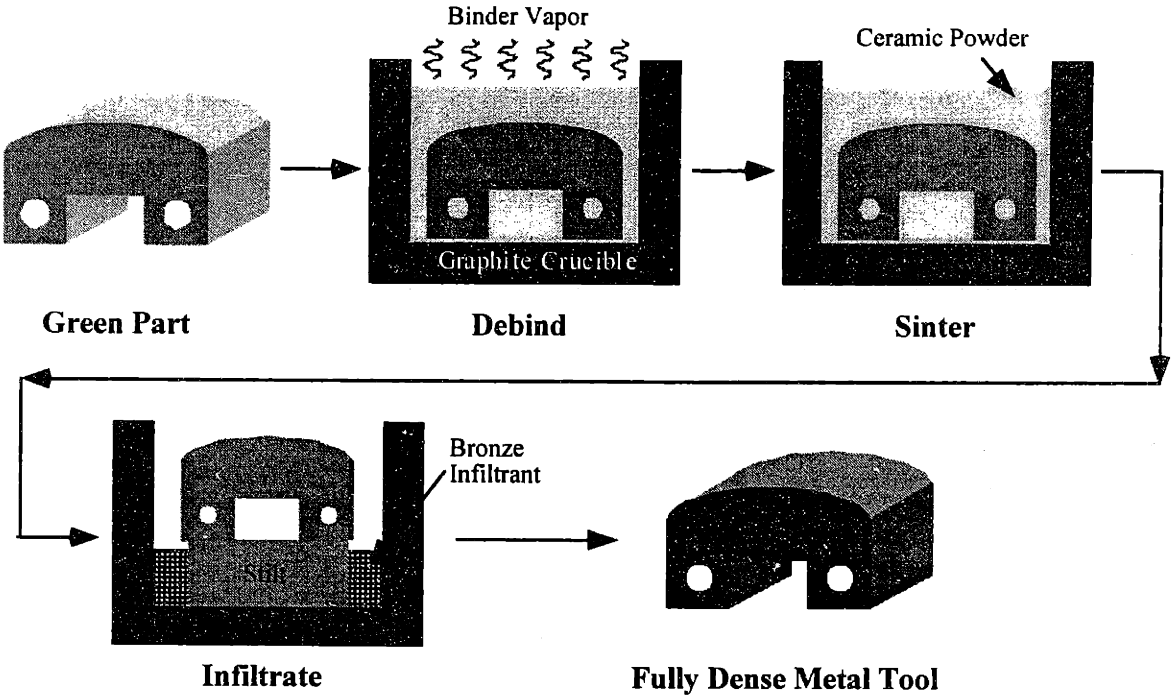

Figure 1-2 Post processing steps for a 3D Printed green part

The 3D Printing process is being exploited for a wide range of applications, including many applications that are being commercialized. Soligen, Incorporated of Northridge, CA provides metal castings made by 3D Printed ceramic molds and cores. Z Corporation of Somerville, MA provides 3D Printing machines for an office modeling application used to produce models to verify geometry. Therics, Incorporated of Princeton, NJ is developing various medical applications based on 3D Printing technology. Specific Surfaces of Franklin, MA is using 3D Printing to create ceramic filters for hot gas filtration. ExtrudeHone Corporation of Irwin, PA provides machines and services for the fabrication of metal tooling and metal parts by 3D Printing. Several other application areas are under development, including fine resolution metal parts and ceramic parts for electronic and structural applications. Military applications under development include ceramic cores for lost-wax casting, dies for injection of ceramic cores, tools for resin transfer molding, die casting tools with conformal cooling and structural ceramic parts for high performance engines.

Among various applications for the 3D Printing technique, a special area of interest is injection molding. The 3D Printing process appeals to the injection molding industry for at least the following reasons: 1) It builds visual models to assist in the design of a prototype for molding. 2) It permits fast tooling with complex geometric features. 3) It allows the freeform fabrication of complex internal

channels inside the mold, providing a more uniform molding temperature, and therefore higher part quality. 4) Special structures can be designed on mold inserts for low thermal inertia and better performance of injection molding. 5) The 3D Printing process helps to set up a clean interface between mold design, mold fabrication and injection process control

1.3 MOTIVATION

The emergence of Layered Manufacturing processes such as 3D Printing has demonstrated significant advantages over traditional manufacturing processes. The lessons and technologies learned from Layered Manufacturing have the potential to redefine the traditional processes, such as injection molding, for higher part quality and short production cycle. My motivation in this project is to explore this potential by using injection molding as an example.

1.3.1 Defining a clear interface between design and manufacturing

A manufacturing process is basically a process that converts the draft of a design into three dimensional parts by applying energy in the forms of temperature, pressure, etc. The injection molding process is a typical manufacturing process that shares several common features with other processes. The designer's draft input is converted into the final part output by applying energy in the forms of molding temperatures and pressures, by defining geometric constraints through the cavity shape and by the constitutive law of polymer rheology. The successful output of the final part depends not only on the process conditions such as temperatures and pressures, but also on the geometric constraints that are directly defined in the design draft.

Figure 1-3 shows elements involved in the injection molding process, which are categorized into three domains: design domain, manufacturing domain and constitutive law. It is obvious from this figure that the elements involved in an injection molding process are coupled with each other. For example, the part geometry determines the pressure and temperature distribution as well as the filling pattern. In the mean time, the pressure and the temperature distributions are coupled with each other through the Spencer-Gilmore equation and through the polymer viscosity feature. This coupling consequentially influences the accuracy of the geometry and leads to defects such as short shot. The coupling between design and manufacturing domains results in many trails and errors in the product development cycle for injection molding. My objective is to minimize the coupling effect in injection molding and to define a clear interface between mold design, mold fabrication and injection process control.

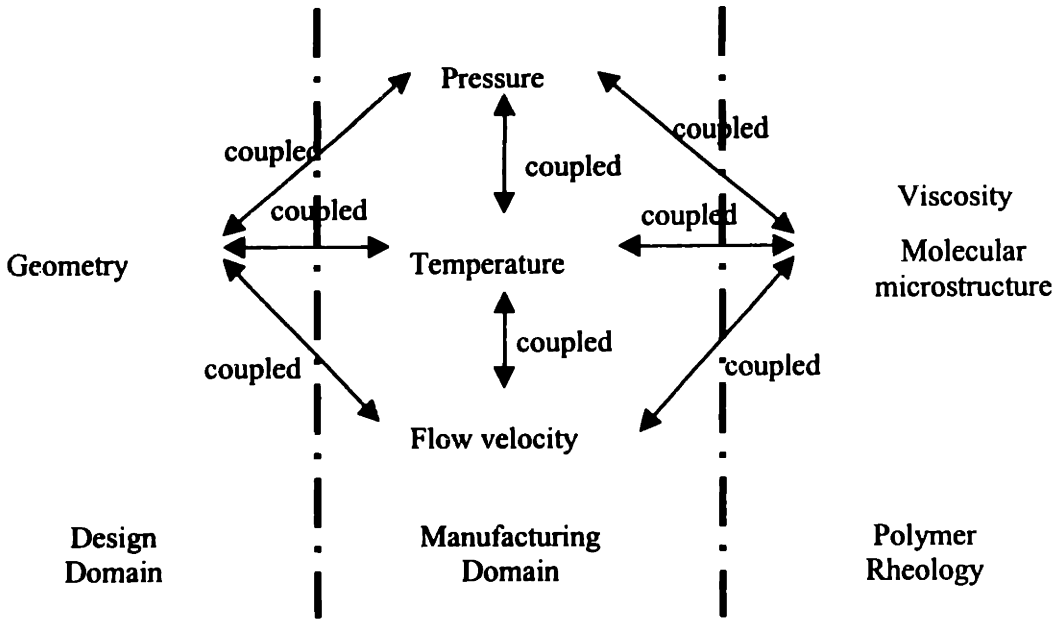

Figure 1-3 Components in an injection molding process and their coupling features

1.3.2 More effective control of the mold temperature in injection molding

Mold temperature is very important, influencing both the part quality and the production rate in an injection molding process. However, in the past, mold temperature control has not received enough attention. Even though cooling channels are the principal means of mold temperature control, they are always designed at the end of the entire mold cycle. The consequence is that the cooling channels designed are not always effective in temperature control. The lack of the efficiency of the cooling channels on mold temperature control is not only because of the limited space left for the cooling line but also because of the lack of a proper manufacturing process that can fabricate channels that follow the part shape.

Another problem for the traditional molding process is that a coolant with constant flow rate and temperature is used for the entire molding cycle, regardless the different mold temperature requirements for the filling stage and the cooling stage. As we know, an injection cycle consists of four successive stages of mold filling, packing, cooling and ejection. At the filling stage the hot plastic melt fills the mold cavity under a certain injection pressure. The high mold temperature will help eliminate the short shot defect and reduce the flow-induced residual stress and orientation. At the cooling stage, a low mold temperature will reduce the required cooling time and therefore shorten the cycle time. However, because the coolant can not promptly control the mold temperature, a constant flow is always used for successive cycles. In this case molding engineers expect that the mold will reach a certain steady state operation after

a long time of warming up, where the mold temperature is at a certain compromised value to satisfy the requirements both for no-short shot filling and for rapid cooling. This solution increases the warming-up time, introduces residual stresses and makes it difficult to independently control different process parameters such as the injection pressure, injection speed and melt temperature.

The 3D Printing process provides us with an easy and effective way for mold temperature control. On the one hand, by constructing cooling channels conformal to the part shape, uniform and efficient cooling can be achieved. On the other hand, the mold temperature can be dynamically controlled by running hot and cold oils alternately through conformal channels, in order to satisfy different temperature requirements for the filling and the cooling stage. In the filling stage, the mold is rapidly heated up so that the mold is at a high temperature for better performance during filling. In the cooling stage, the mold is rapidly cooled down in order to shorten the cycle time. Figure 1-4 shows this ideal thermal cycle. It can not be successfully achieved unless a low thermal inertia tool is constructed. The 3D Printing process has the potential to build a low thermal inertia tool that satisfies the requirement for dynamic mold temperature control.

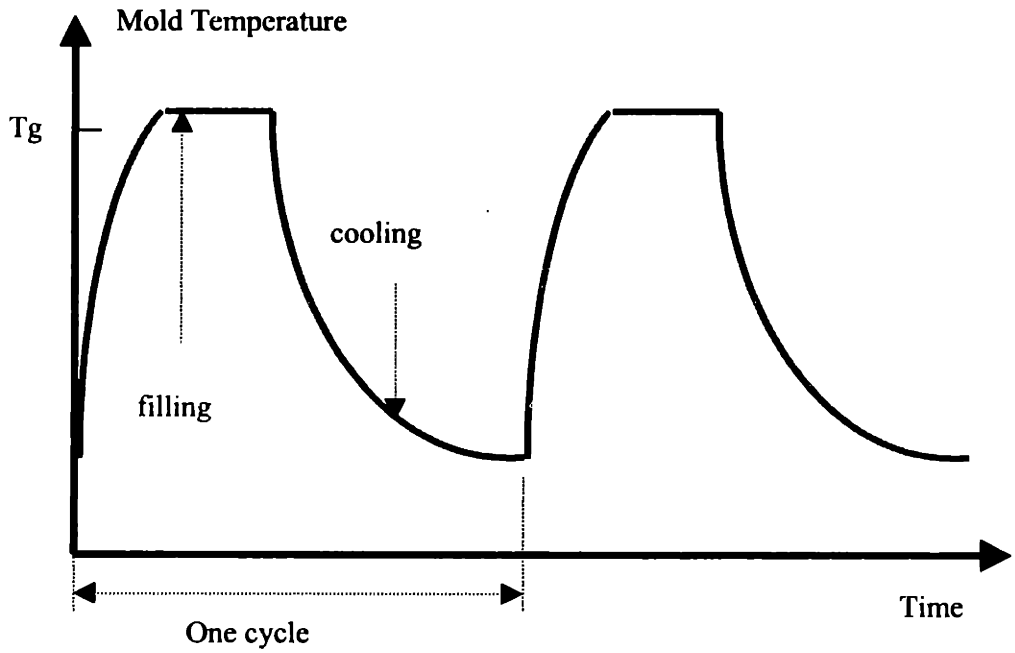

Figure 1-4 An ideal thermal cycle

1.3.3 Simplified production flow in injection molding

The coupling features in injection molding that are described in section 1.3.2 significantly reduce the efficiency of the production cycle in injection molding. The traditional mold making procedure is

iterative, complex and full of trial and error. Figure 1-5 shows the production flow for a traditional injection molding process. Once a prototype part is proposed, a tool is designed based on this part and the numerical simulation is performed to evaluate the moldability as well as the process parameter setup. The designed tool is then sent to the machine shop for fabrication. The tool fabrication process may find design problems in the prototype part or in the tool that need modification. The fabricated tool is then subject to the molding test. The molding test yields an appropriate setup for the process parameters such as the injection pressure profile and speed. For parts with quality problems, the trouble shooting is performed and the design of the part and the tool needs to be modified again with the help of numerical analysis.

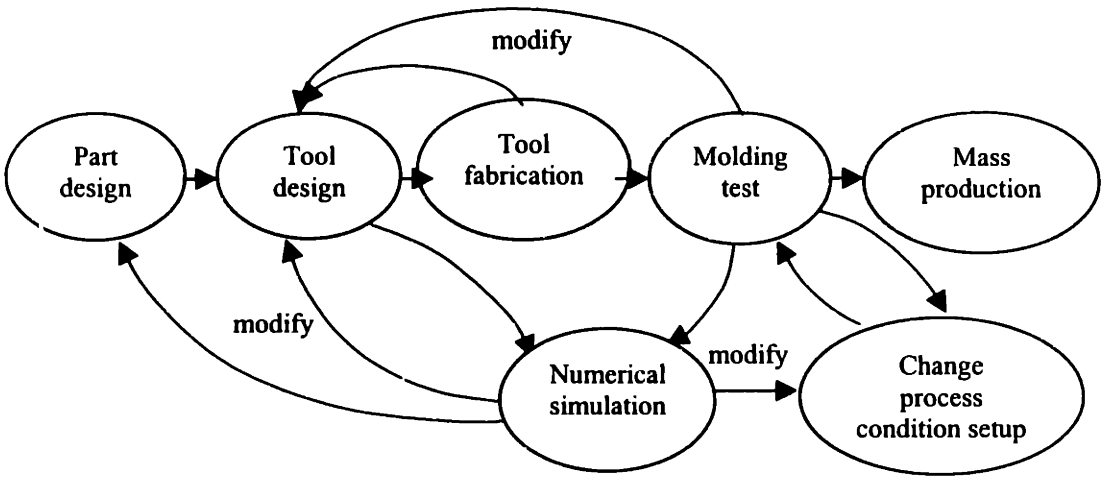

Figure 1-5 Production flow for traditional injection molding

As one can see from the above figure, the production flow is time consuming and full of design loops. The modern mold CAD software speeds up these design loops but is not able to change the coupling feature of the production flow itself. The reason is that the existing CAD packages are actually analysis tools instead of synthesis tools. Before these tools can be used, an initial design of the part, the runner system and the process condition should be provided. The CAD system then simulates the flow and cooling of the polymer melt. The simulation results are interpreted and used to modify the original design. This kind of the design loop continues until a satisfactory design is achieved.

As the geometric features of the mold and cooling channels get more and more complex, the analysis tool becomes insufficient for the design purpose. Even on a workstation, it easily takes over 24 hours to obtain an optimal design of the gates and runners for a part with intermediate complexity, let alone complex cooling channel design. What we really need is a simple synthesis tool that can directly

convert part geometry and design requirements into proper cooling channels and process parameters. With such a systematic design methodology, we are able to achieve the straight forward production flow as sketched in Figure 1-6.

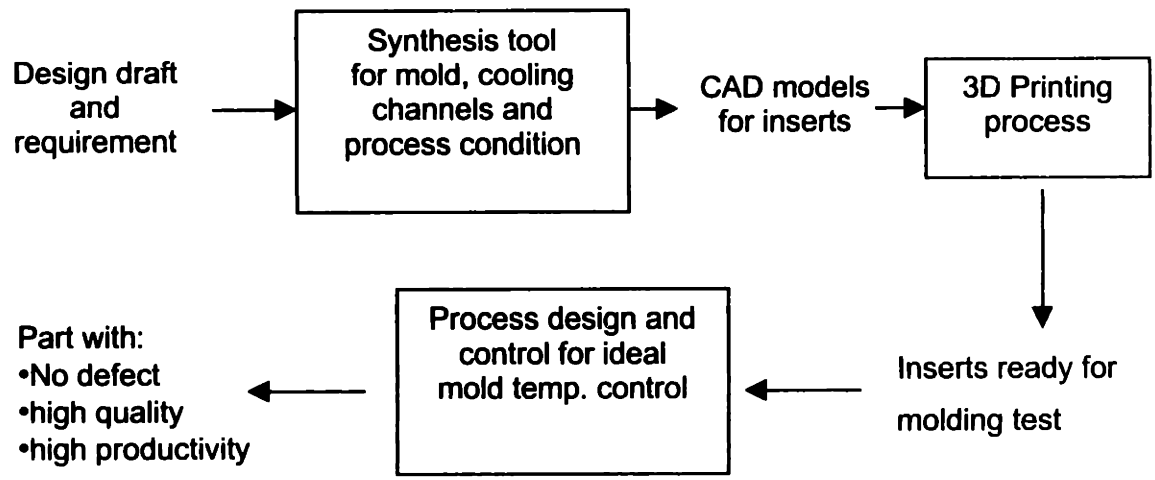

Figure 1-6 A simplified production flow for injection molding

In the above production flow the synthesis tool is the systematic design methodology we have proposed for conformal cooling and rapid thermal cycling. The ideal mold temperature profile is the rapid thermal cycle. We will discuss them in detail in the following chapters.

1.4 CONTENTS AND THESIS ORGANIZATIONS

This thesis consists of 6 chapters and focuses on two topics: conformal cooling and rapid thermal cycling. For each topic we will discuss concepts, design rules and fabrication issues. Conformal cooling refers to the concept of placing cooling channels that follow the part shape. Rapid thermal cycling refers to the concept of dynamically controling the mold temperature by alternate use of hot and cold oil. Chapter 1 is the introduction. It gives a review of injection molding related research and background, as well as the motivations of this project. Chapter 2 presents the theoretical framework for the conformal cooling technique. It explores the physical foundation of conformal cooling, makes an operational definition of conformal cooling and discusses a systematic design methodology for creating conformal cooling channels. It also analyze the heat transfer in conformal cooling by 1D and 2D models, based on single bit called "cooling cell". Chapter 3 describes the practical implementation of the design methodologies discussed in chapter 2. In this chapter, six design rules are proposed for conformal cooling

channel and process parameter design. A software package has also been developed to help the conformal cooling channel design. The use of design rules and the software tool are illustrated with a complex cooling channel design case. Chapter 4 introduces the topic of rapid thermal cycling. In chapter 4, a concept of rapid thermal cycling is proposed and explored. Each stage involved in a rapid thermal cycle is modeled. The theoretical base for the idea of using the mold deflection to compensate for the part shrinkage is explored. Chapter 5 shows the practical application of the theory and the concepts discussed in chapter 4 through the development of a design case. The chapter is divided into two major parts: design issues and fabrication issues. The design issues for the tool in rapid thermal cycling include benchmark part selection, cooling channel design, process parameter design, mold structural design, oil delivery system design and mold base assembly design. In this part, a tool with truss support and conformal channels is proposed for mechanical strength, buckling resistance, low thermal stress, relief of the thermal expansion/shrinkage, and for providing elastic deformation for part shrinkage compensation. In the second part, manufacturing issues are explored in detail. The manufacturing problems are studied using sample truss structures. The process control and quality problems in each step of the 3DP process and in the post processing are discussed in detail. Chapter 6 discusses testing and proposed future work. The testing includes a mechanical and a thermal test. The mechanical test evaluates the load deflection curve, strength and buckling resistance of the truss structure designed. The thermal test evaluates the thermal response and temperature uniformity of the benchmark tool. The test results provide a good reference for the future molding operation. At the end of this chapter, the project is concluded and the future research work is proposed.

1.5 REFERENCES

1. Chen S., S. Yu, A. Davidoff, "Hybrid Mehods for Injection Mold Cooling Process Simulation and Mold Cooling System Analysis", *ANTEC'91*, p499 - 503
2. Chen S., N. Cheng, K. Jeng, "Post-Filling Simulation and Analyses of Shrinkage and Warpage of the Injection Molded Parts", *ANTEC'91*, p493 - 498
3. DeGaspari J., " Mold Cooling", *Plastics Technology*, October 1995, p49
4. Fay J., *Introduction to Fluid Mechanics*, MIT Press, 1995
5. Himasekhar K., J. Lottey, K. Wang, "CAE of Mold Cooling in Injection Molding Using a Three Dimensional Numerical Simulation", *Journal of Engineering for Industry*, vol. 114, May-92, p213 - 221

6. Hu S., N. Cheng, S. Chen, "Effect of Cooling System Design and Process Parameters on Cyclic Variation of Mold Temperatures - Simulation by DRBEM", *Plastics, Rubber and Composites Processing and Applications*, Vol. 23, No. 4, 1995, p221 - 231
7. Kwon T., "Mold Cooling System Design Using Boundary Element Method", *ASME Journal of Eng. for Industry*, Vol. 110, p384 - 394
8. Lauze Y., J. Hetu, "Temperature Prediction of Part and Mold Using Finite Element Simulations", *ANTEC'94*, p809 - 812
9. Liu S., "Modeling and Simulation of Thermally Induced Stress and Warpage in Injection Molded Thermoplastics", *Polymer Engineering and Science*, Vol. 36, No. 6, Mar-96, p807 - 818
10. Marcus H., D. L. Bourell, "Solid Freeform Fabrication Finds New Applications", Advanced Materials & Processes, Sept – 1993, p28 - 35
11. Marcus H., D. L. Bourell, "Solid Freeform Fabrication Finds New Applications", Advanced Materials & Processes, Sept – 1993, p28 - 35
12. Mills A., *Heat and Mass Transfer*, Irwin Press, Chicago, 1995
13. Pye R., "Injection mould design", Longman, 1989
14. Rezayat M., T. Burton, "Combined Boundary-Element and Finite - Difference Simulation of Cooling and Solidification in Injection Molding",
15. Rezayat M., "Numerical Computation of Cooling-Induced Residual Stress and Deformed Shape for Injection-Molded Thermoplastics", *ANTEC'89*, p341 - 343
16. Rosato D., "Injection Mold Design Handbook", Van Hostrand Reinhold Comp., NY, 1985, Chapter 7, p160 - 234
17. Sachs E., M. Cima, P. Willams, D. Brancazio, J, Cornie, "Three dimensional printing: rapid tooling and prototypes directly from a CAD model", *Transactions of the ASME: Journal of Engineering for Industry*, vol 114, no.4, Nov -1992, p481 - 488
18. Sachs E., E. Wylonis, M. Cima, S. Allen,S. Micheals, E. Sun, H. Tang, H. Guo, "Injection Molding Tooling by Three Dimensional Printing: a Desktop Manufacturing Process", *ANTEC'95*
19. Sachs E., S. Allen, H. Guo, J. Banos, M. Cima, J. Serdy, D. Brancazio, "Progress on Tooling by 3D Printing: Conformal Cooling, Dimensional Control, Surface Finish and Hardness", Solid Freeform Fabrication Proceedings, Sept-1997, p115-123
20. Schmidt L., "Opportunities or the Next Decade in Injection Molding", *Plastic Engineering*, October 1998, p27-31
21. Singh K., "Design of Mold Cooling System", *Injection and Compression Molding Fundamentals*, A. Isayev Ed., Marcel Dekker, 1991, p567 – 605p
22. Tadmore Z., C. Gogos, "Principles of Polymer Processing", Wiley, 1979, p584 - 610

23. Thomas R., N. McCaffery, "The Prediction of Real Product Shrinkage Calculated from a Simulation fo the Injection Molding Process", *ANTEC'89*, p371 - 375
24. Titomanlio G., K. Jansen, "In-Mold Shrinkage and Stress Prediction in Injection Molding", *Polymer Engineering and Science*, Vol. 36, No. 15, Aug-96, p2041 - 2049
25. Turng L., "Application of the Boundary Element Method to the Cooling-Line Design for Injection Molds", *CIMP Technical Report*, No. 56, Jan-87
26. Turng L., K. Wang, "A computer - aided cooling line design system for injection molds", *Journal of Eng. for Industry*, vol 112, May-90, p161
27. Zoetelief W., L. Douven, A. Housz, "Residual Thermal Stresses in Injection Molded Products", *Polymer Engineering and Science*, Vol. 36, No. 14, Jul-96, p1886 - 1896

CHAPTER 2

CONFORMAL COOLING

CONTENT

FIGURES

2.1 INTRODUCTION

2.1.1 Motivation

The cooling of injection molding tooling is crucial to the performance of the tooling, influencing both the rate of the process and the resulting quality of the parts produced. However, cooling line design and fabrication has been confined to relatively simple configurations primarily due to the limits of the fabrication methods used to make tools, but also due to the lack of a design methodology appropriate for cooling lines.

For many years mold designers have been struggling for the improvement of the cooling system performance, despite the fact that the cooling system complexity is physically limited by the fabrication capability of the conventional tooling methods. Different methods such as helical channels, baffled hole system, spiral plug system and heat-pipes have been developed for the uniform and efficient cooling of the part [Pye 1989]. Some mold manufacturers built tools with cooling channels follow the part shape by different methods such as stacking slices of the insert layer by layer with cooling channels milled on each layer [Luling 1997]. Other manufacturers[1] developed the pulse heating and cooling technique for better control of the mold temperature in order to reduce the energy consumption and enhance uniform cooling condition.

The emergence of Solid Freeform Fabrication (SFF) processes offers injection mold manufacturers new degrees of freedom in mold tooling. The SFF processes are additive processes that construct 3D objects by incrementally building up cross sectional layers of arbitrary complex shapes converted from CAD models. Typical SFF processes include stereolithography, selective laser sintering, three dimensional printing, solid ground curing, laminated object manufacturing, etc. [Marcus &Bourell 1993]. The ability to fabricate 3D features with almost arbitrary complexity makes these processes extremely useful for fabricating parts and tools that cannot be practically made by other techniques. One example of the applications is to fabricate complex cooling channels inside injection molds in order to improve the uniformity of cooling. The 3D Printing Lab at MIT has been participating in the injection molding tooling project for several years [Sachs et. al 1992, Sachs et. al 1995, Sachs et. al 1997]. The

[1] One company is called REPS. They have a web page at: http://www.reps.co.uk/. The other company is: CITO Products Inc., 1002 South 12th St, Watertown, Wisconsin 53094,Phone: 414-261-2606

industrial application of 3D Printed tools with serpentine conformal cooling channels built inside have achieved the simultaneous improvement of the cycle time by 15% and the part distortion by 9% [Sachs et. al 1997]. With the manufacturing flexibility offered by SFF processes such as 3D Printing, more complex cooling channel systems such as that shown in Figure 1b can be fabricated for the further improvement of the cooling performance.

The emergence of new processes that can be used to create tools with conformal cooling channels placed with almost arbitrary complexity not only offers the designer new degrees of freedom in the design of injection molding tools but also simplifies the methodology used to design cooling channels. The work discussed in this thesis seeks to develop a methodology for the design of cooling channels that both simplifies the design and results in substantially improved performance. The methodology described in this thesis will greatly simplify the design of complex channels such as those of Figure 2-1.

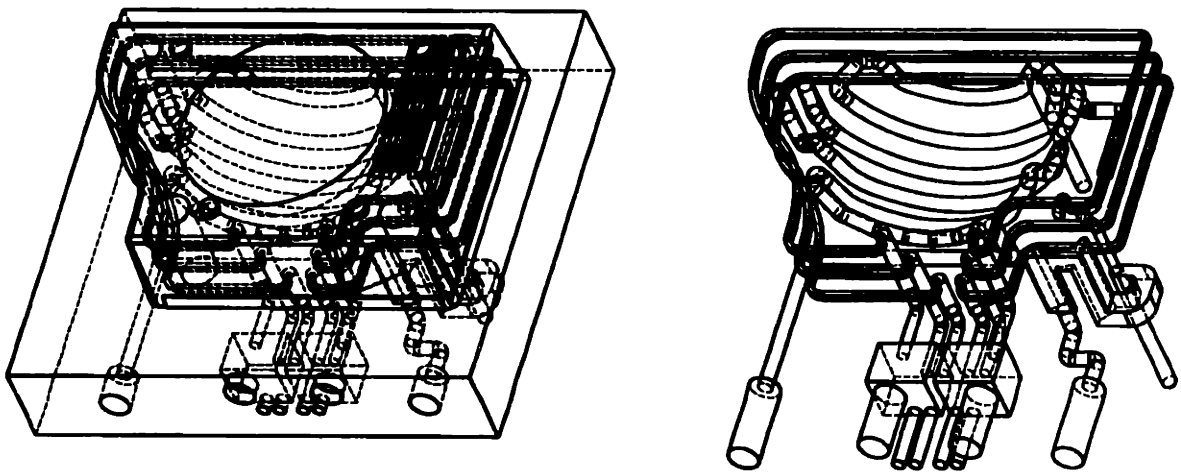

Figure 2-1 Left: solid model for the core insert with internal conformal cooling channels. Right: Solid model for the conformal cooling channels set

2.1.2 Related work

Before scientific analysis was introduced into injection molding, the design of the mold cooling system was dominated by designers' experience and simple formula [Tadmore et. al 1979, Pye 1989, Rao 1991, Rosato 1985]. It is not until early 80's that the mold cooling simulation was paid more and more attention. Different methods were proposed to predict the temperature field for the mold and the part during the cooling stage [Singh 1991, Austin 1985, Chu et. al 1989, Kwon 1982, Turng et. al 1990,

Himasekhar et. al 1992, Chen et. al 1991, Hu et al 1995]. The cooling related quality issues such as residual stress, shrinkage and warpage were also addressed in [Lauze et. al 1989, Rezayat 1989, Thomas et. al 1989, Chen et. al 1991, Titomanlio et. al 1996, Liu et. al 1996, Zoetelief et. al 1996]. Among those simulation algorithms, an iterative hybrid scheme proposed by Cornell Injection Molding Program (CIMP) became a standard scheme for mold cooling analysis due to its computational efficiency [Kwon 1982, Turng et. al 1990, Himasekhar et. al 1992]. Today most of the mold design packages such as C-MOLD are equipped with this analysis scheme. This scheme treats the plastic part as one-dimensional transient heat transfer and the mold as three-dimensional heat transfer. The periodic transient mold temperature field within an injection cycle is separated into a quasi-steady component and a time–varying component. The quasi-steady component reflecting the cycle–averaged temperature field is obtained by solving the Laplace equation for the entire mold using the boundary element method. The solution is then used as the boundary for 1D part temperature field. The iterative reference between the boundary element solution of the cycle-averaged mold temperature field and the finite difference solution of the part temperature field continues until a steady temperature boundary is achieved at the mold-part interface. Compared with the finite element simulation that needs to calculate the internal nodes, the hybrid scheme discussed above significantly reduces the computational time because only the boundary nodes are considered for obtaining the cycle-averaged mold temperature field.

The emerging techniques for freeform fabrication of the injection molding tools place a new challenge to the mold design and analysis strategy due to the increased complexity in cooling channel geometry. This situation motivates us to develop a systematic tool for conformal cooling line design. Compared with the existing cooling analysis software, the methodology discussed in this paper builds a synthesis tool instead of an analysis tool for the design of the complex conformal cooling channels which take the full advantage of SFF processes.

2.2 HEAT TRANSFER MODEL FOR CONFORMAL COOLING

As the name implies, conformal cooling is used to signify cooling channels that conform to the surface of the mold cavity. However, in this paper, the term "conformal cooling" has a further significance that is related to the transient heat transfer within the mold. When a mold is started up it takes some time before the mold reaches a steady state operating temperature. Figure 2-2 shows the mold surface temperature histories recorded by the thermocouples for both the mold with conformal cooling channels and that with straight cooling channels [Sachs et. al 1995]. As one can see from the figure, the mold surface temperature of the core with straight cooling channels tracked over 25 successive injections

starting from the coolant temperature of 12° C and reaching a cycle average steady state temperature of approximately 55° C. However, if the cooling lines are placed very close and conformal to the mold surface the steady state condition is reached very quickly. As illustrated in Figure 2-2 the cycle average temperature of a conformally cooled core reaches its steady state value after one injection cycle. Our operational definition of conformal cooling then is that the cycle average temperature shown in Figure 2-4 reaches its steady state value within one injection cycle. As shown by experiments, the difference of the mold surface temperature profiles we just discussed above significantly effects the part quality and productivity.

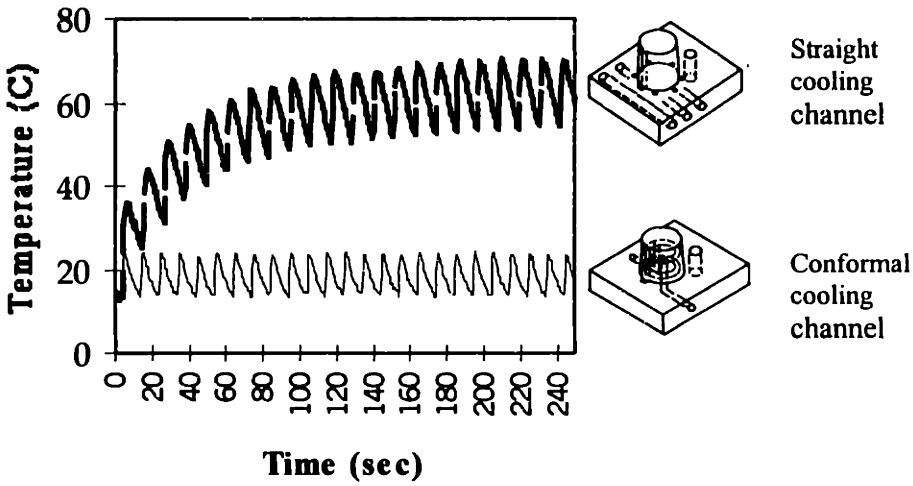

Figure 2-2 Comparison of mold surface temperature histories for straight channel cooling and conformal channel cooling

The difference between two cases shown in Figure 2-2 has to do with the rate of the energy transfer into the mold over successive injections and the thermal inertia of the mold. As the hot plastic comes in during each successive injection, heat transfer takes place across the plastic mold interface and a heat pulse is conducted through the mold material itself. This heat pulse warms up the mold material as it propagates toward the cooling channels and is eventually removed in the cooling water. If the cooling channels are far from the mold's surface, successive heat pulses keep raising the temperature of the mold until the heat pulse propagating in is balanced by heat extraction by the coolant. If the cooling channels are close to the mold surface, the effective thermal mass of the tool is confined to that region between the surface and the cooling channels and is much reduced. In addition, the conduction path from the surface of the

tools to the cooling lines is reduced. As a result, the steady state condition is reached much more rapidly and can in fact be attained within one injection cycle.

Heat transfer for conformal cooling is analyzed based on the energy balance for the active portion of the mold defined as a "cooling cell". A cooling cell is the portion between the mold surface and the cooling lines including a slice of part with half the thickness, a segment of mold and a cooling channel, as shown in Figure 2-3. The outside boundary of the cooling cell is assumed adiabatic.

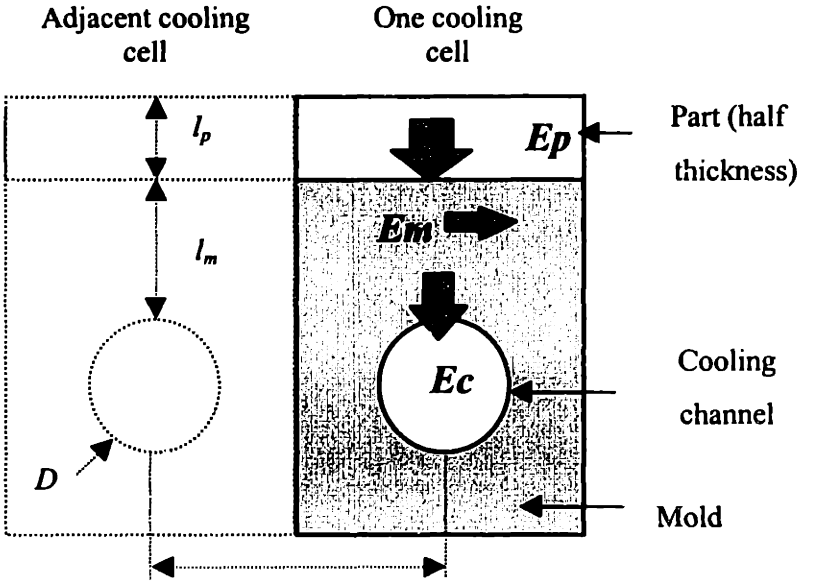

Figure 2-3 Sketch of the energy flow in an individual cooling cell

An energy balance may be written for the active portion of the mold, that is the portion between the surface and the cooling lines:

$$E_P = E_M + E_C \qquad (2\text{-}1)$$

where E_p is the energy loss from the plastic part to the mold, E_m is the energy accumulation in the mold and E_c is the energy loss through the coolant.

For the mold surface temperature profile sketched in Figure 2-2 if we average the transient temperature over each injection cycle we obtain the cycle averaged mold temperature profile as shown in Figure 2-4 in solid line.

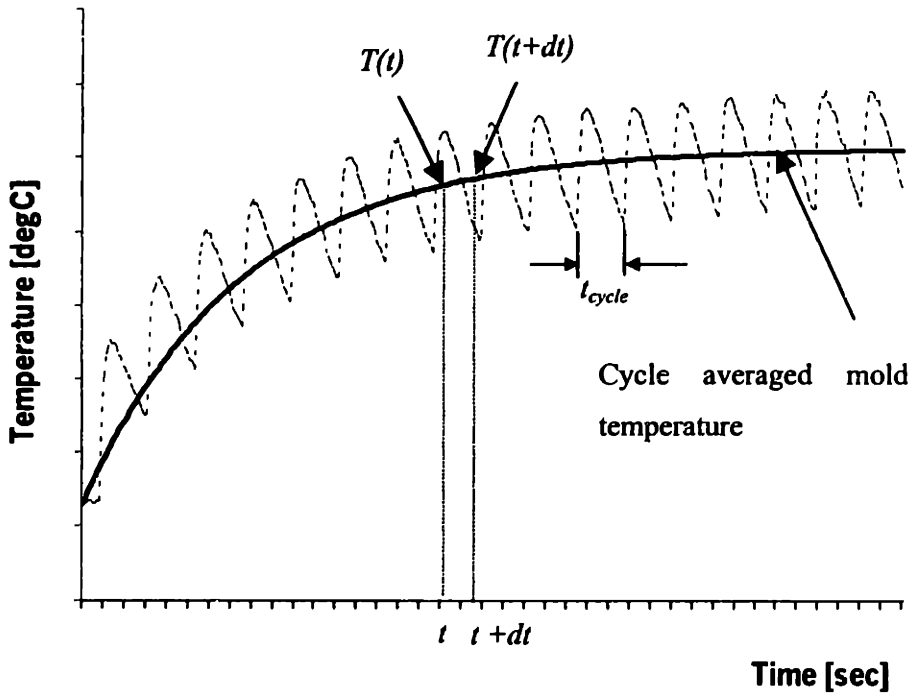

Figure 2-4 Cycle averaged mold surface temperature curve

Let us consider a small time step of dt after t seconds of molding in the cycle averaged mold temperature curve. The averaged energy loss per unit depth of the plastic part during period dt is:

$$E_p = \rho_p c_p l_p W(T_{melt} - T_{eject})dt / t_{cycle} \qquad (2\text{-}2)$$

where ρ_p is the density of the part, c_p is the specific heat of the part, T_{melt} is the plastic melt temperature, T_{eject} is the part ejection temperature, t_{cycle} is the injection cycle time, l_p is half the part thickness, W is the cooling line pitch distance.

The energy accumulation in the mold during time period dt is:

$$E_m = \rho_m c_m l_m W(T_m(t+dt) - T_m(t)) \qquad (2\text{-}3)$$

where ρ_m is the density of the mold, c_m is the specific heat of the mold, $T_m(t+dt)$ and $T_m(t)$ are cycle averaged mold surface temperatures at time t and $t+dt$ respectively, l_m is the vertical distance from the top of the cooling channel to the mold wall.

The energy transfer from the plastic part to the coolant is by heat conduction through the mold and then by convection to the coolant. Figure 2-5 is the thermal circuit model showing two thermal resistance in series. The cycle averaged temperature at the mold-coolant interface is defined as T_a. The

heat flux from the mold to the mold-coolant interface is equal to that from the mold-coolant interface to the coolant. The total energy dissipation to the coolant per unit depth of the mold is expressed as:

$$E_c = K_m W(T_m - T_a)dt / l_m = \tfrac{1}{2} h\pi D(T_a - T_c)dt \qquad (2\text{-}4)$$

where h is the heat transfer coefficient at mold - coolant interface, D is the hydraulic diameter of the cooling channel. Only half of the cooling channel surface is counted for the heat flow calculation.

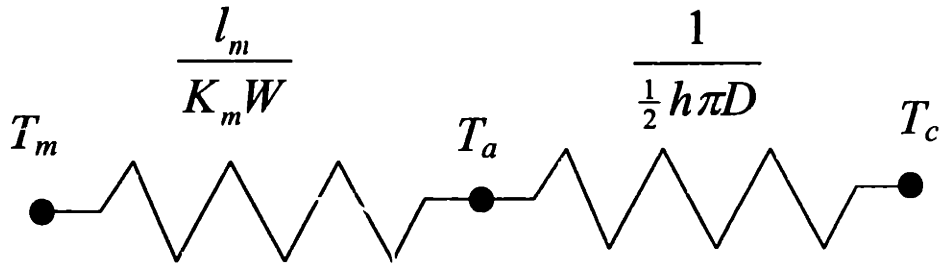

Figure 2-5 The thermal circuit model for the mold and the coolant heat transfer

By solving equation (2-4) the explicit form of the averaged mold - coolant interface temperature T_a is expressed as:

$$T_a = \frac{K_m W T_m + \frac{1}{2} h\pi D l_m T_c}{K_m W + \frac{1}{2} h\pi D l_m} \qquad (2\text{-}5)$$

The energy loss per depth of the part through the coolant during time period dt is therefore:

$$E_c = \frac{h\pi D(T_m - T_c)K_m W dt}{2K_m W + h\pi D l_m} \qquad (2\text{-}6)$$

Substituting the expressions of E_m, E_c and E_p in equation (2-1) with expressions (2-2), (2-3) and (2-6) yields:

$$\rho_m C_m l_m \frac{T_m(t+dt) - T_m(t)}{dt} + \frac{h\pi D K_m}{2K_m W + h\pi D l_m}(Tm - Tc) - \frac{\rho_p C_p l_p (T_{melt} - T_{eject})}{t_{cycle}} = 0 \qquad (2\text{-}7)$$

As $dt \to 0$, the above equation is transformed to a first order differential equation with respect to the mold surface temperature T_m:

$$\rho_m C_m l_m \frac{dT_m}{dt} + \frac{h\pi DK_m}{2K_m W + h\pi D l_m}(T_m - T_c) = \frac{\rho_p C_p l_p (T_{melt} - T_{eject})}{t_{cycle}} \quad (2\text{-}8)$$

The first term in equation (2-8) captures the thermal mass of the tool and the build-up of heat as the temperature of the tool increases. The second term in equation (2-8) captures the transfer of heat by conduction through the mold and then convection into the cooling fluid. The right hand side of equation (2-8) captures the source of the heat, which is the cooling down of the plastic.

This first order differential ordinary differential equation has the solution of the form shown in equation (2-9), where T_{ms} is the cycle averaged mold temperature at steady state and τ is the time constant of the system. Equations (2-10) and (2-11) give the expressions for cycle averaged mold temperature and the mold time constant respectively. Our definition of conformal cooling can now be stated formally by requiring that τ be less than or equal to one injection cycle time. Figure 2-6 shows a prediction of equation (2-9) superimposed on the experimental results previously shown in Figure 2-2. As can be seen, there is reasonably good prediction with the cycle average temperature.

$$T_m(t) = T_{m0} + (T_{ms} - T_{m0})e^{-t/\tau} \quad (2\text{-}9)$$

$$T_{ms} = T_c + \frac{\rho_p c_p l_p (2K_m W + h\pi D l_m)(T_{melt} - T_{eject})}{h\pi D K_m t_{cycle}} \quad (2\text{-}10)$$

$$\tau = \frac{\rho_m c_m l_m^{\,2}}{K_m}\left(1 + \frac{2WK_m}{h\pi D l_m}\right) \quad (2\text{-}11)$$

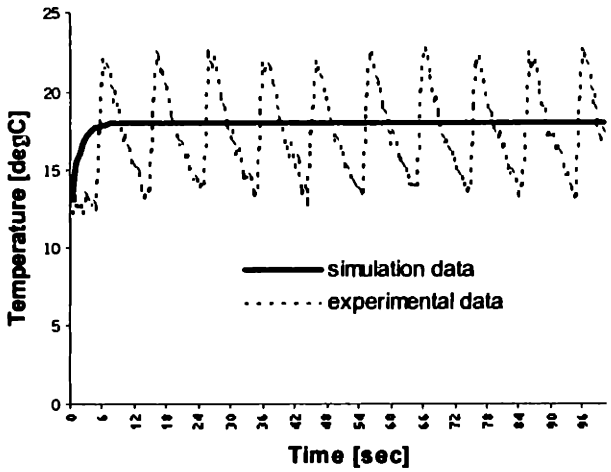

Figure 2-6 Comparison of the experimental data and the simulation result for the mold surface temperature

In equation (2-11) the second term inside the parenthesis on the right side of the equation is negligible as long as we have:

$$\frac{2WK_m}{h\pi Dl_m} << 1 \qquad (2\text{-}12)$$

In a limiting the heat transfer coefficient h goes to infinity, the expression for the time constant reduces to the form shown in equation (2-13). In this simplified expression we see that the important material property for the mold is the thermal diffusivity which is $K_m / \rho_m c_m$. We also see that the time constant is proportional to the square of the distance between the surface of the mold and the cooling channels. This simplified expression makes clear the importance of considering this as a transient heat transfer calculation. If this were a steady state heat transfer problem then doubling the thermal conductivity of the mold would allow the channels to be placed twice as far away. However, as we can see from equation (2-13) if we double the thermal conductivity and place the channels twice as far away the time constant in fact increases by a factor of 2. Thus, while the material properties are important, the geometry (as seen by the square of the distance in equation (2-13)) is even more important.

$$\tau = \frac{\rho_m c_m l_m^2}{K_m} \qquad (2\text{-}13)$$

For a typical design, the cooling channel pitch distance W is about 10mm, the channel size D is about 5mm, the distance from the channel to the mold wall l_m is about 3 mm, the heat transfer coefficient h is about 30,000. The resulting $\frac{2WK_m}{h\pi Dl_m}$ in equation (2-12) is about 0.39, which is smaller than 1. This indicates that for a rough estimation purpose we can eliminate the second term inside the parenthesis in expression (2-11) and use (2-13) to estimate the time constant of the mold.

2.3 1D HEAT TRANSFER ANALYSIS FOR CONFORMAL COOLING

The proposal of the conformal cooling concept significantly simplifies the heat transfer analysis. Before this concept is proposed the mold cooling analysis is based on a standard scheme first proposed by Cornell Injection Molding Program (CIMP). This scheme treats the plastic part as one-dimensional transient heat transfer and the mold as three-dimensional heat transfer. The periodic transient mold temperature field within an injection cycle is separated into a quasi-steady component and a time–varying component. The quasi-steady component reflecting the cycle–averaged temperature field is obtained by solving the Laplace equation for the entire mold using the boundary element method. The solution is then used as the boundary for 1D part temperature field. The iterative reference between the boundary element solution of the cycle-averaged mold temperature field and the finite difference solution of the part temperature field continues until a steady temperature boundary is achieved at the mold-part interface.

The analysis scheme for conformal cooling is in many ways similar to that proposed by CIMP. The only exception is that the cycle averaged mold temperature in conformal cooling is directly obtained from the energy model discussed in the previous section. A complete algorithm for conformal cooling simulation is illustrated by a flow chart shown in Figure 2-7.

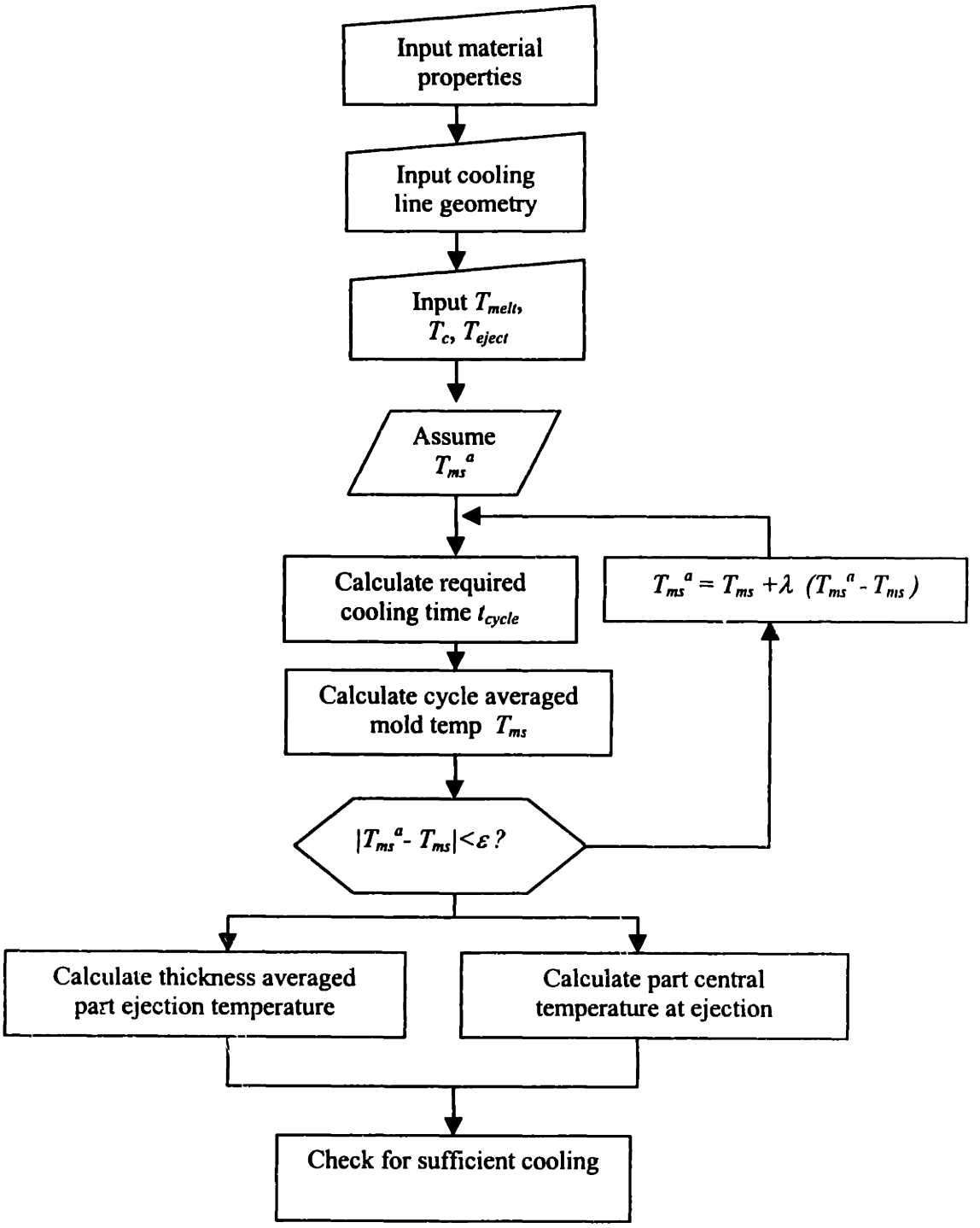

Figure 2-7 Flow chart for 1D cooling simulation

As shown in Figure 2-7, the first step of the simulation is to input the thermal properties of the mold, the plastic and the coolant, the cooling channel size, the cooling line location and the process temperatures. Then we assume a cycle averaged mold temperature value T_{ms}^a and use it as the boundary condition to calculate the part ejection temperature and the cooling time. After that the cycle averaged

mold temperature (denoted as T_{ms}) is recalculated based on the 1D heat transfer model we derived in equation (2-10). The recalculated T_{ms} will then substitute the presumed T_{ms}^{a} with a certain relaxation factor λ. This operation iterates until the difference between the presumed T_{ms}^{a} and the recalculated T_{ms} is less than a certain infinitesimal value ε. This algorithm is proved convergent and has successfully estimated the cycle average mold temperature profile with reasonably high accuracy, as shown in figure 2-6.

The part heat transfer during cooling stage is modeled as one-dimensional heat conduction. The temperature field is obtained by Fourier series. The temperature at the center of the part and the thickness averaged part temperature at the end of cooling stage are expressed by equation (2-14) and (2-15) respectively [Turng 1987].

$$T_p^{center} = T_{ms} + \sum_{n=0}^{\infty} \frac{2}{n\pi}[1-(-1)^n](T_{melt} - T_{ms})\sin(\frac{n\pi}{2})e^{-\frac{a_p n^2 \pi^2 t_{cycle}}{4l_p^2}} \qquad (2\text{-}14)$$

$$T_p^{average} = T_{ms} + \sum_{n=0}^{\infty} \frac{2}{(2n+1)^2\pi^2}(T_{melt} - T_{ms})e^{-\frac{a_p (2n+1)^2 \pi^2 t_{cycle}}{4l_p^2}} \qquad (2\text{-}15)$$

where T_{ms} represents the cycle averaged mold temperature, T_{melt} is the polymer melt temperature, and t_{cycle} is the injection cycle time.

In the above iterative algorithm, after we have presumed the cycle averaged mold temperature T_{ms}^{a} , we can use equation (2-15) to calculate the cycle time if we let T_{ms} in equation (2-15) equal to T_{ms}^{a}, and $T_p^{average}$ equal to the required ejection temperature T_{eject}. Since the higher order terms in the Fourier series are much smaller than the first term and are therefore negligible, equation (2-15) can be expressed in a simplified form:

$$T_{eject} = T_{ms} + \frac{2}{\pi^2}(T_{melt} - T_{ms})e^{-\frac{a_p \pi^2 t_{cycle}}{4l_p^2}} \qquad (2\text{-}16)$$

The required cycle time t_{cycle} can be obtained by the following expression:

$$t_{cycle} = -\frac{4l_p^2}{\alpha_p \pi^2}\ln\frac{\pi^2(T_{eject} - T_{ms})}{8(T_{melt} - T_{ms})} \qquad (2\text{-}17)$$

The by-product of the algorithm discussed above is the part ejection temperature. To ensure sufficient cooling, it is required that at the time of ejection the part center temperature T_p^{center} be less than the glass temperature for thermoplastic material, and the thickness averaged part temperature $T_p^{average}$ is less than the required ejection temperature. These criteria are used for the rough evaluation of sufficient cooling condition.

2.4 2D NUMERICAL ANALYSIS FOR CONFORMAL COOLING

The numerical simulation discussed here is based on the finite difference analysis of the heat transfer in the individual cooling cell. At the beginning of the cooling stage, the mold temperature and the part temperature are assumed uniformly distributed. As shown in Figure 2-8, one-dimensional meshes are constructed for the part while two-dimensional meshes are for the mold.

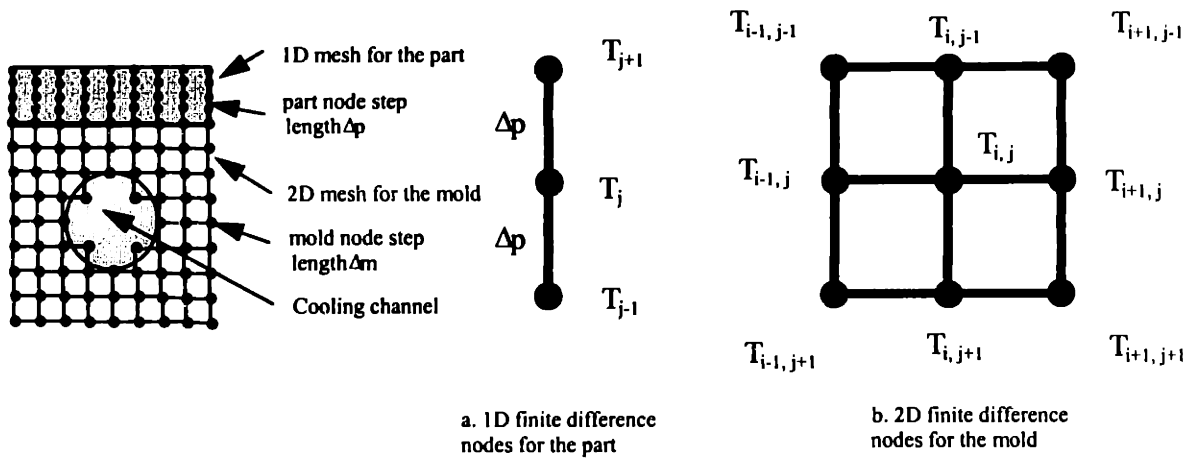

a. 1D finite difference nodes for the part

b. 2D finite difference nodes for the mold

Figure 2-8 Sketch of the finite difference nodes for the part and the mold Left: unit cooling cell. Middle: part. Right: mold

2.4.1 Part heat transfer

As shown in Figure 2-8, all the nodes for the part are belong to three basic types: those inside the part, those at the centerline of the part and those on the mold –part interface. The length step for the simulation is Δp, the time step is Δt. The explicit form of the 1D unsteady heat conduction at nodes inside the part is given by equation (2-18) [Mills 1995]. In equation (2-18), T_j^{k+1} is the temperature on the *jth* node at time $(k+1)\Delta t$, T_{j-1}^{k} is the temperature on the *(j-1)th* node at time $k\Delta t$, T_{j+1}^{k} is the temperature on

the *(j+1)th* node at time $k\Delta t$, T_j^k is the temperature on the *jth* node at time $k\Delta t$, F_0 is the Froude number for the part obtained by equation (2-19), α_p is the thermal diffusivity for the part.

$$T_j^{k+1} = F_0(T_{j-1}^k + T_{j+1}^k) + (1-2F_0)T_j^k \tag{2-18}$$

$$F_0 = \frac{\alpha_p \Delta t}{\Delta p^2} \tag{2-19}$$

For nodes on the part centerline, the adiabatic boundary condition is assumed. The node temperature is expressed by the following equation:

$$T_j^{k+1} = 2F_0 T_{j-1}^k + (1-2F_0)T_j^k \tag{2-20}$$

For nodes at the mold - part interface an instant contacting temperature T_0 is observed once the hot plastic melt of T_2 contacts the cold mold wall of T_1, as shown in Figure 2-9. The interface temperature is derived based on the fact that the heat flux from the part is equal to the heat flux toward the mold and is expressed by equation (2-21).

$$\frac{T_1 - T_0}{T_0 - T_2} = \frac{\sqrt{K_p c_p \rho_p}}{\sqrt{K_m c_m \rho_m}} \tag{2-21}$$

where K_p,, c_p,, ρ_p, are thermal conductivity, specific heat and density for the plastic part respectively, K_m,, c_m,, ρ_m, are thermal conductivity, specific heat and density for the plastic part respectively.

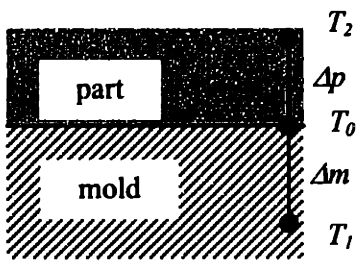

Figure 2-9 Sketch of nodes close to the part-mold interface

Δm and Δp in Figure 2-9 are length steps for the mold and the part respectively. Their relationship is defined by equation (2-22). This equation ensures that the heat flux from the part side to the interface is equal to that from the interface to the mold side during the whole cooling time.

$$K_p \frac{(T_2 - T_0)}{\Delta p} = K_m \frac{(T_0 - T_1)}{\Delta m} \tag{2-22}$$

If the contact thermal resistance between the mold and the part is considered, equation (2-22) is then replaced by the following equation:

$$K_p \frac{(T_2 - T_0)}{\Delta p} = h_p (T_0 - T_1) \tag{2-23}$$

Notice that in equations (2-18) and (2-20), the temperature value at node j at time $(k+1)t$ is obtained by the temprature values of its neidhorhood as well as its temperature at time kt. In order to maintain the simulation stability, the second term on the right side of equations (2-18) and (2-20) should be positive. This lead to the stability criterion expressed by the equation below:

$$F_0 \leq \frac{1}{2} \tag{2-24}$$

2.4.2 Mold heat transfer

The explicit forms of the node temperatures at different positions of the mold are listed in equation (2-25) through (2-29) [Mills 1995]. The outer boundaries of the cooling cell are assumed adiabatic. At the mold - coolant interface, a constant heat transfer coefficient is assigned based on the cooling channel roughness and the coolant flow rate. The node temperatures at different positions in the mold are listed below:

a) For nodes inside the mold:

$$T_{i,j}^{\,k+1} = F_0 (T_{i-1,j}^{\,k} + T_{i+1,j}^{\,k} + T_{i,j-1}^{\,k} + T_{i,j+1}^{\,k}) + (1 - 4F_0) T_{i,j}^{\,k} \tag{2-25}$$

b) For nodes on the outer boundary of the mold:

$$T_{i,j}^{k+1} = 2F_0[T_{i-1,j}^{k} + \frac{1}{2}(T_{i,j+1}^{k} + T_{i,j-1}^{k})] + (1-4F_0)T_{i,j}^{k} \quad (2\text{-}26)$$

c) For nodes at the exterior corners of the mold: $T_{i,j}^{k+1} = 2F_0(T_{i-1,j}^{k} + T_{i,j-1}^{k}) + (1-4F_0)T_{i,j}^{k}$ (2-27)

d) For nodes at the mold - coolant interface:

$$T_{i,j}^{k+1} = 2F_0[T_{i,j+1}^{k} + \frac{1}{2}(T_{i-1,j}^{k} + T_{i+1,j}^{k}) + B_i T_c^{k}] + (1-4F_0-2F_0B_i)T_{i,j}^{k} \quad (2\text{-}28)$$

e) For nodes at interior corners of the mold - coolant interface:

$$T_{i,j}^{k+1} = \frac{4}{3}F_0[\frac{1}{2}(T_{i-1,j+1}^{k} + T_{i,j-1}^{k}) + T_{i,j+1}^{k} + T_{i+1,j}^{k} + B_i T_c^{k}] + (1-4F_0-\frac{4}{3}F_0B_i)T_{i,j}^{k} \quad (2\text{-}29)$$

In above equations, F_0 is the Froude number of the mold, and Bi is the Biot number of the mold. F_0 and Bi are obtained from equation (2-30) and (2-31) respectively:

$$F_0 = \frac{\alpha_m \Delta t}{\Delta m^2} \quad (2\text{-}30)$$

$$B_i = \frac{h_c \Delta m}{K_m} \quad (2\text{-}31)$$

The heat transfer coefficient h_c in equation (2-31) is assumed constant over the mold - coolant interface. For laminar flow, the Nusselt number N_u is obtained by equation (2-32) and the heat transfer coefficient h_c is then expressed by equation (2-33):

$$N_u = 3.66 + \frac{0.065(\frac{D}{L})R_{eD}P_r}{1+0.004[(\frac{D}{L})R_{eD}P_r]^{2/3}} \quad \text{(laminar flow)} \quad (2\text{-}32)$$

$$h_c = \frac{N_u K^c}{D} \quad \text{(laminar flow)} \quad (2\text{-}33)$$

For the turbulent flow heat transfer coefficient is obtained from the Dittus and Boelter equation (2-34):

$$h_c = 0.023 R_{eD}^{0.8} P_r^{0.4} \frac{K^c}{D} \qquad \text{(turbulent flow)} \qquad (2\text{-}34)$$

In order to make the simulation convergent the last terms on right sides of equations (2-25) to (2-28) should be positive. This gives the stability criteria as below:

$$F_o \leq \frac{1}{4(1+B_i)} \qquad (2\text{-}35)$$

2.5 CONFORMAL COOLING DESIGN METHODOLOGY

The introduction of conformal cooling significantly simplifies the injection molding cooling system design methodology. In the conformal cooling situation, the mold heat transfer is localized in a small region between two adjacent cooling channels. The local mold heat transfer enables us to divide the part, mold and coolant system into simple bits and do the analysis and design on each bit. From the design point of view the localized heat transfer suggests that we first design a cooling "cell" composed of the small region between the adjacent cooling lines and then map the solution to the entire mold. The flexibility of SFF processes makes this modular approach possible by minimizing the manufacturing constraint that must be applied. This strategy simplifies the cooling line design by providing a sequential approach to obtain a global solution by adding many local solutions. As the design procedure is much simplified, the resulting cooling lines can be quite complex and take full advantage of the flexibility of SFF processes. Figure 2-10 shows how SFF processes simplify the cooling channel design methodology using an example of designing cooling channels for a hemispherical part. As one can see from the figure, straight cooling channels fabricated by conventional manufacturing processes result in 3 dimensional dessign and analysis over the entire mold which is very time consuming. As a contrast, SFF processes allows the freeform fabrication of conformal channels which digitizes the cooling system into individual bits. One dimensional or two dimensional simple analysis is then performed on each bit in order to obtain the global solution of the entire cooling system.

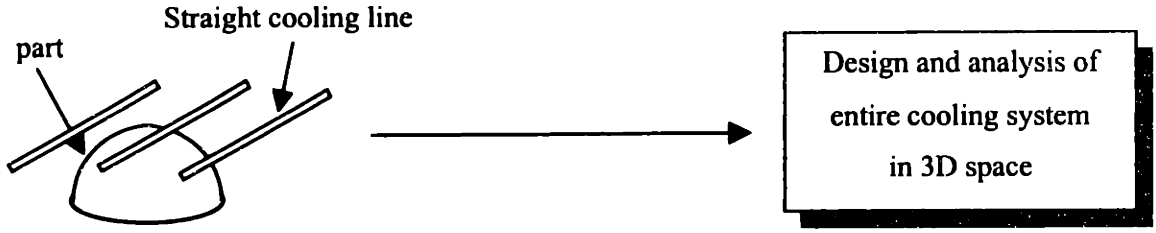

(a) Traditional manufacturing processes build straight cooling channels that lead to 3D design and analysis of entire cooling system.

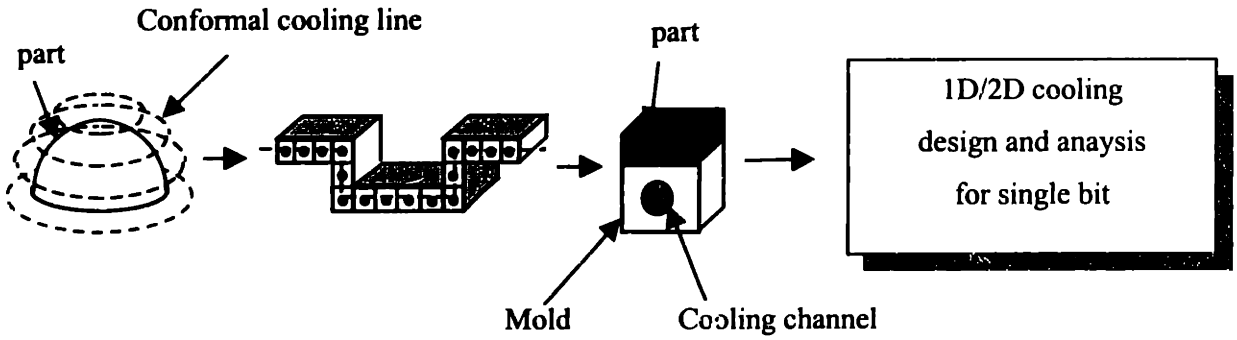

(b) SFF processes build conformal cooling channels that lead to 1D/2D design and analysis for single bit.

Figure 2-10 Simplification of the cooling channel design methodology for conformal cooling channels made by SFF processes

Figure 2-11 illustrates the steps of this design methodology by a generic part with a hemispherical dome and a flat bottom. As shown in the figure, the part is first divided into two cooling zones (a hemisphere and a flat surface) based on its geometry. Then in each cooling zone the conformal cooling surface is constructed and the cooling channel topological structure is defined. After that the system of cooling channels is further decomposed into small elements called cooling cells. The heat transfer analysis and the cooling system design is based on these cooling cells and is then mapped to the entire mold. This modularized design strategy is not sensitive to the part geometry, therefore it keeps the same design simplicity no matter how complex the part geometry is.

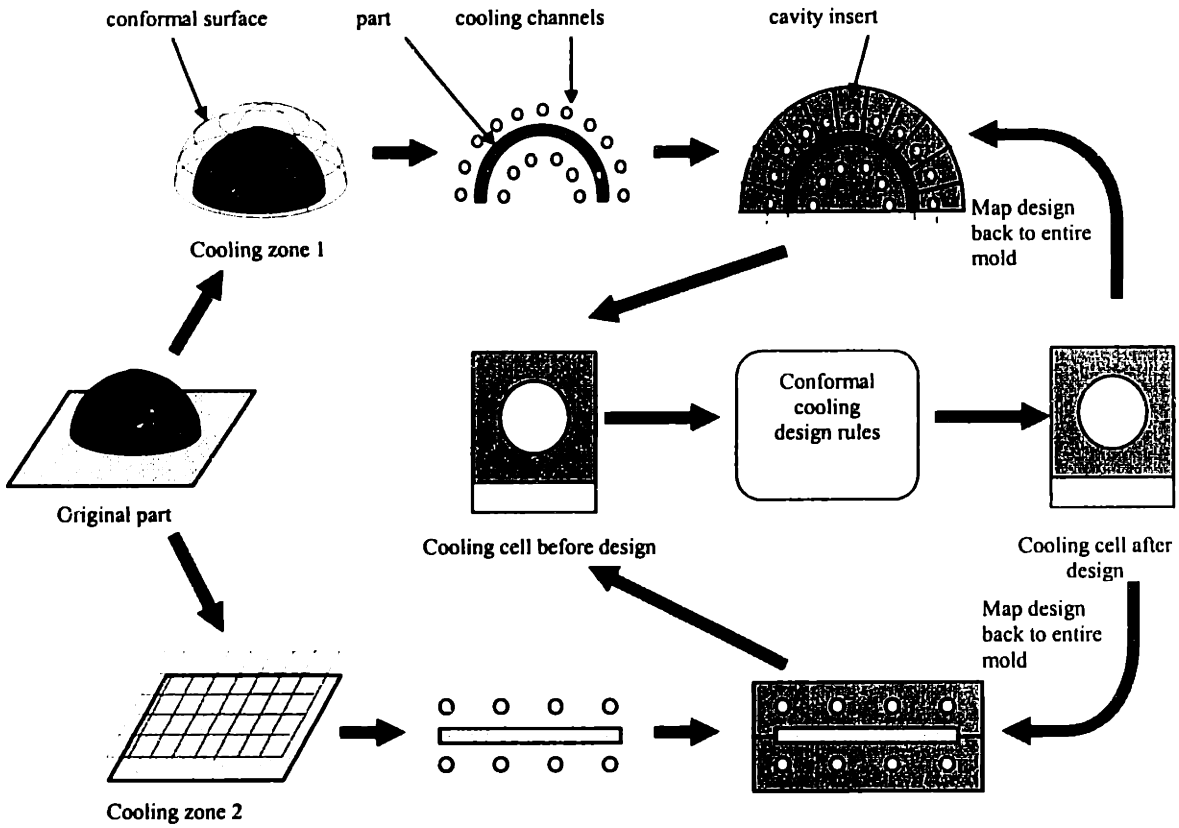

Figure 2-11 Conformal cooling design flow for a generic part

2.6 CONCLUSION

Solid Freeform Fabrication processes such as 3D Printing has demonstrated the potential to fabricate tools for injection molding with complex conformal channels built inside to improve the cooling uniformity and efficiency for high part quality and productivity. The complexity of the resulting cooling channels places a challenge to the existing injection molding CAD software. The work discussed in this chapter builds the theoretical foundation and the design methodology for complex conformal cooling channel design. First the thermodynamic model for conformal cooling is developed to predict the cycle averaged mold temperature profile as well as the part ejection temperature. The conformal cooling criterion is proposed base on this model. Then the finite difference methods are used to simulate the part and the mold heat transfer in a small area around the individual cooling channel. Finally a systematic methodology for conformal cooling channel design is illustrated by the design of a generic part.

2.7 REFERENCES

1. Austin C., "Mold cooling", *ANTEC '85*, p764 - 768
2. Chen S., S. Yu, A. Davidoff, "Hybrid Mehods for Injection Mold Cooling Process Simulation and Mold Cooling System Analysis", *ANTEC'91*, p499 - 503
3. Chen S., N. Cheng, K. Jeng, "Post-Filling Simulation and Analyses of Shrinkage and Warpage of the Injection Molded Parts", *ANTEC'91*, p493 - 498
4. Chu E., M. Kamal, S. Goyal, "A Computer Simulation of the Injection Molding Process Including Filling, Packing and Solidification", *ANTEC'89*, p344 - 347
5. Himasekhar K., J. Lottey, K. Wang, "CAE of Mold Cooling in Injection Molding Using a Three Dimensional Numerical Simulation", *Journal of Engineering for Industry*, vol. 114, May-92, p213 - 221
6. Hu S., N. Cheng, S. Chen, "Effect of Cooling System Design and Process Parameters on Cyclic Variation of Mold Temperatures - Simulation by DRBEM", *Plastics, Rubber and Composites Processing and Applications*, Vol. 23, No. 4, 1995, p221 - 231
7. Kwon T., "Application of the Boundary Integral Method to the Nonisothermal Flow of a Polymeric Fluid Advancing in a Thin Cavity of Arbitary Shape", *CIMP Technical Report*, No. 38 Jan-82
8. Kwon T., "Mold Cooling System Design Using Boundary Element Method", *ASME Journal of Eng. for Industry*, Vol. 110, p384 - 394
9. Lauze Y., J. Hetu, "Temperature Prediction of Part and Mold Using Finite Element Simulations", *ANTEC'94*, p809 - 812
10. Liu S., "Modeling and Simulation of Thermally Induced Stress and Warpage in Injection Molded Thermoplastics", *Polymer Engineering and Science*, Vol. 36, No. 6, Mar-96, p807 - 818
11. Luling M., "Cooling Channels that Follow Part Shape", *Injection Molding*, Feb. 1997, p70-72
12. Marcus H., D. L. Bourell, "Solid Freeform Fabrication Finds New Applications", Advanced Materials & Processes, Sept – 1993, p28 - 35
13. Mills A., *Heat and Mass Transfer*, Irwin Press, Chicago, 1995
14. Pye R., "Injection mould design", Longman, 1989
15. Rao N., "Design formulas for plastics engineers", Hanser, 1991, chapter 6
16. Rezayat M., T. Burton, "Combined Boundary-Element and Finite - Difference Simulation of Cooling and Solidification in Injection Molding",

17. Rezayat M., "Numerical Computation of Cooling-Induced Residual Stress and Deformed Shape for Injection-Molded Thermoplastics", *ANTEC'89*, p341 - 343
18. Rosato D., "Injection Mold Design Handbook", Van Hostrand Reinhold Comp., NY, 1985, Chapter 7, p160 - 234
19. Sachs E., M. Cima, P. Willams, D. Brancazio, J, Cornie, "Three dimensional printing: rapid tooling and prototypes directly from a CAD model", *Transactions of the ASME: Journal of Engineering for Industry*, vol 114, no.4, Nov -1992, p481 - 488
20. Sachs E., E. Wylonis, M. Cima, S. Allen,S. Micheals, E. Sun, H. Tang, H. Guo, "Injection Molding Tooling by Three Dimensional Printing: a Desktop Manufacturing Process", *ANTEC'95*
21. Sachs E., S. Allen, H. Guo, J. Banos, M. Cima, J. Serdy, D. Brancazio, "Progress on Tooling by 3D Printing: Conformal Cooling, Dimensional Control, Surface Finish and Hardness", *Solid Freeform Fabrication Proceedings*, Sept-1997, p115-123
22. Singh K., "Design of Mold Cooling System", *Injection and Compression Molding Fundamentals*, A. Isayev Ed., Marcel Dekker, 1991, p567 - 605
23. Tadmore Z., C. Gogos, "Principles of Polymer Processing", Wiley, 1979, p584 - 610
24. Thomas R., N. McCaffery, "The Prediction of Real Product Shrinkage Calculated from a Simulation fo the Injection Molding Process", *ANTEC'89*, p371 - 375
25. Titomanlio G., K. Jansen, "In-Mold Shrinkage and Stress Prediction in Injection Molding", *Polymer Engineering and Science*, Vol. 36, No. 15, Aug-96, p2041 - 2049
26. Turng L., "Application of the Boundary Element Method to the Cooling-Line Design for Injection Molds", *CIMP Technical Report*, No. 56, Jan-87
27. Turng L., K. Wang, "A computer - aided cooling line design system for injection molds", *Journal of engineering for industry*, vol 112, May-90, p161
28. Xu X., E. Sachs, S. Allen, M. Cima, "Designing Conformal Cooling Channels for Tooling", *Proceedings of 9th Solid Freeform Fabrication Symposium*, Austin, TX, 1998.
29. Zoetelief W., L. Douven, A. Housz, "Residual Thermal Stresses in Injection Molded Products", *Polymer Engineering and Science*, Vol. 36, No. 14, Jul-96, p1886 - 1896

CHAPTER 3

DESIGN AND FABRICATION OF TOOLS FOR CONFORMAL COOLING

CONTENT

FIGURES

3.1 BENCHMARK PART PROPOSED FOR CONFORMAL COOLING TEST

Although conformal cooling is proposed as a new concept in recent years the idea is not new because in a lot of design cases mold designers always try to place the cooling channel with as uniform distance to the mold surface as possible to improve the cooling uniformity. This work is effective for 2D flat, simple parts such as a disc or a plate. However mold designers will feel frustrated if they have to face the cooling channel design for a complex 3D parts with small geometric features because there was no proper design methodology nor fabrication methods to make cooling channels conformal to the mold surface. 3D Printing process has demonstrated its potential to build complex conformal channels in the tool. The conformal cooling design methodology introduced in the last chapter provides a convenient way to handle the design issues associated with conformal cooling. Now the question is which part can best demonstrate the advantages of conformal cooling, from both fabrication and design point of views.

The following are some basic requirements for the benchmark part design:

1) It should have 3 dimensional features that allows the freeform build-up of conformal channels in 3D space.
2) It should have delicate geometric features in which it would be difficult for traditional mold designers and fabricators to place cooling channels.
3) The resulting complexity of the conformal cooling channel should challenge the existing mold design and analysis software
4) The geometric features of the benchmark part should favor the current manufacturing capability of the Solid Freeform Fabrication processes. For this purpose the part should not be designed too big (>10") or too small (< ¼").
5) The design should not violate common sense in injection molding. For example if the part thickness in a local area is extremely large (say larger than3/8") the sink mark will be inevitable no matter how uniform the cooling is.

The members of 3D Printing Industrial Consortium have put a lot of effort on designing the benchmark part for conformal cooling test. The result is a design sketched in Figure 3-1. In this design we are going to mold a box with the top open. On the bottom plate of the box stand several features of interest. These features include:

1. A hemisphere dome which is always very difficult to cool uniformly by traditional cooling methods.
2. Three posts very close to the wall which makes the cooling channel placement very difficult.

3. Delicate texture features on the bottom for testing the improvement of the surface quality by conformal cooling
4. A rectangular post with a slot in middle which is also a very common industrial feature

Besides, the surrounding wall of the part is designed with different thickness to test the wrapage improvement by conformal cooling.

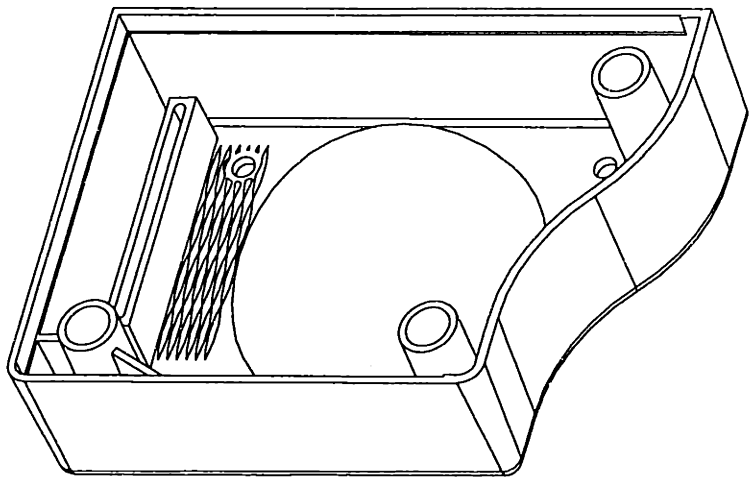

Figure 3-1 Benchmark part proposed for conformal cooling test

3.2 DESIGN RULES

After the benchmark part is proposed the next step is to design the corresponding conformal cooling channel set. As we have discussed in chapter 2 the localized heat transfer by conformal cooling allows us to develop a simple design methodology to deal with complex cooling channel design. In order to implement this design methodology a set of design rules are required. In this chapter, six design rules are proposed and design windows are constructed for the cooling line design based on individual cooling cells. These rules include design for conformal cooling condition, design for coolant pressure drop, design for coolant temperature uniformity, design for sufficient cooling, design for uniform cooling and design for mold strength and deflection.

3.2.1 Design for conformal cooling condition

In chapter 2 we have proposed the criterion for conformal cooling condition. This criterion should be observed throughout the whole design procedure in order to validate other design rules discussed below and to allow good control of the mold surface temperature. In order to reach the conformal cooling

criterion, a mold designer can use different methods such as increasing the heat transfer coefficient, increasing the channel diameter, decreasing the distance between the cooling lines and the mold wall and choosing mold material with a high thermal diffusivity. However it is observed from equation (2-13) that a closer distance from the cooling channel to the mold surface is more effective than a material with high thermal diffusivity in improving the conformal cooling condition.

3.2.2 Design for coolant pressure drop

The allowable pressure drop of the coolant along the conformal cooling channel is constrained by the available pumping pressure of the chiller. The objective of the cooling line design for pressure drop is to find a proper combination of the coolant flow rate, the cooling channel diameter and the cooling line length so that the resulting total pressure drop is smaller than a given pressure budget. The fluid mechanics of the incompressible flow can be used to predict the coolant pressure drop that is the function of the cooling line length, the cooling line diameter and the coolant flow rate [Fay 1995].

$$P = \frac{L}{2D}\rho v^2 C_f \qquad (3\text{-}1)$$

where C_f in equation (3-1) is the cooling channel surface friction factor which differs for different flow regions:

$$C_f = \frac{16}{R_{eD}} \qquad \text{(for laminar flow)} \qquad (3\text{-}2)$$

$$C_f = \frac{0.25}{1.8^2}\left(\log_{10}\left[\left(\frac{e}{3.7D}\right)^{1.11} + \frac{6.9}{R_{eD}}\right]\right)^{-2} \qquad \text{(for turbulent flow)} \qquad (3\text{-}3)$$

In the above equations, R_{eD} is the Reynolds number of the coolant flow e is the surface roughness of cooling channels.

3.2.3 Design for the coolant temperature uniformity

The objective of the design for the coolant temperature uniformity is to check and make sure that the coolant temperature variation along the length of the cooling line is maintained within a certain range. Under the conformal cooling condition no thermal energy is accumulated in the mold. Therefore the energy dissipated from the part in each injection cycle as its temperature drops from the melt temperature

down to the ejection temperature is completely dissipated by the coolant. The heat exchanger analysis in [Mills 1995] yields a simple expression of the coolant temperature increase ΔT in the cooling stage:

$$\Delta T = \frac{\rho_p c_p l_p wL}{\rho_c c_c Q} \cdot \frac{(T_{melt} - T_{eject})}{t_{cycle}} \qquad (3\text{-}4)$$

where l_p is half the plastic part thickness, w is the cooling line pitch distance, L is the cooling line length, Q is the coolant flow rate and t_{cycle} is the injection cycle time. ρ_c, c_c, ρ_p, c_p are the densities and specific heats for coolant and part materials respectively. Equation (3-4) indicates that during the steady injection cycles the heat pulse due to the cooling down of the plastic part is totally converted to the temperature rise of the coolant flow. In order to reduce the coolant temperature drop, the designer can use the coolant with large specific heat, increase the coolant flow rate, decrease the pitch distance between two adjacent cooling channels or reduce the length of the cooling line.

3.2.4 Design for sufficient cooling

The objective for the sufficient cooling criterion is to ensure that the part is totally solidified at ejection. Typically the part ejection temperature depends on the polymer material and is given in advance. The mold designer has to decide how much cooling time is required to cool down the part for a special cooling channel configuration. Recognizing that the conformal cooling condition significantly simplifies the cooling analysis the algorithm proposed in this section tries to provide mold designer a quick tool to estimate the required cooling time.

As we have discussed in section 3.1, the cooling analysis scheme adopted by most of mold design software is computationally expensive and not efficient for the design and analysis of complex cooling channels. With the concept of conformal cooling, this scheme is much simplified. As the matter of fact, the steady cycle averaged mold temperature can be directly derived from equation (2-10). However, if you check equation (2-10) you will notice that the cycle averaged mold temperature T_{ms} is a function of the cycle time t_{cycle} and the part ejection temperature T_{eject}.. Although the part ejection temperature is usually given in advance, the resulting cycle time is unknown. We developed the following iterative algorithm to find the cycle time t_{cycle} and the steady cyclic mold temperature T_{ms}:

Step 1. Assume the cycle averaged mold temperature T_{ms}.

Step 2. Calculate the cycle time t_{cycle} for the required part ejection temperature according to 1D part heat transfer.

Step 3. Calculate the part ejection temperature at the end of t_{cycle}.

Step 4. Calculate the cycle averaged mold temperature T_{ms} based on equation (2-10).

Step 5. Replace T_{ms} in step 1 by the cycle averaged mold temperature value obtained in step 4.

Step 6. Follow the iterations from step 1 to 5 until the cycle averaged mold temperature T_{ms} reaches a steady value.

For more detailed descriptions on the algorithm, please refer to chapter 2.

3.2.5 Design for uniform cooling

The term "cooling uniformity" in this paper has both global and local meanings. The global uniformity is the cooling rate variation over the entire mold. It is guaranteed by keeping the coolant temperature uniform. The local cooling uniformity refers to the variation of the mold surface temperature within the individual cooling cell sketched in Figure 3-2. The local cooling uniformity is defined by the difference of the cycle averaged temperatures on the mold surface right above the cooling channel and at the middle of two adjacent channels, i.e. points A and B in Figure 3-2.

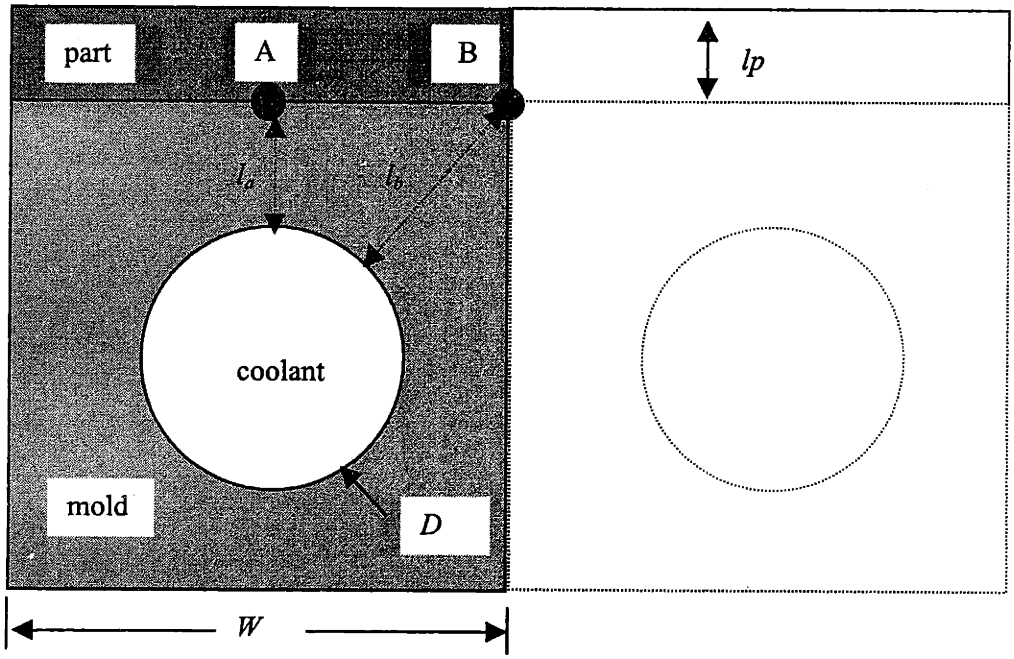

Figure 3-2 Sketch of a cooling cell and its adjacent cell for cooling uniformity analysis

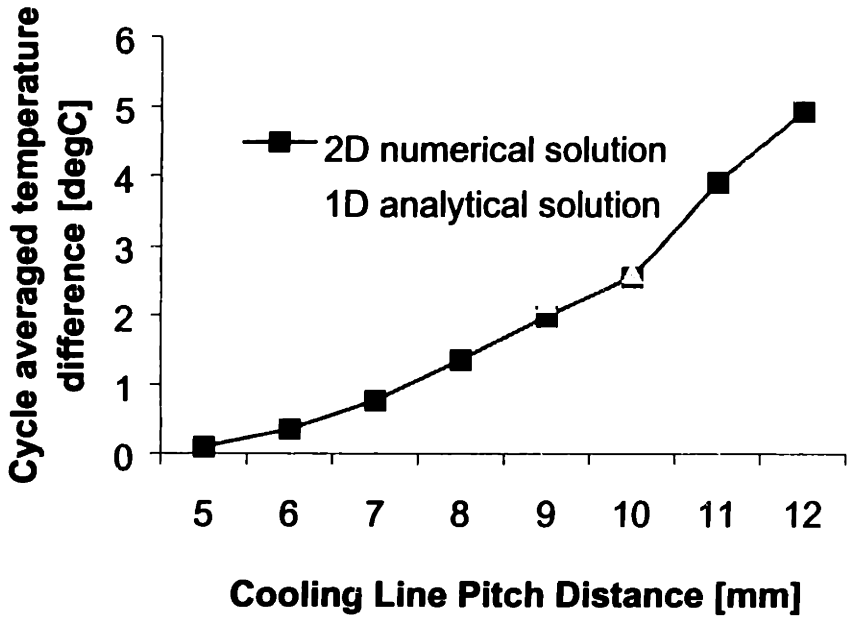

Figure 3-3 Comparison of the analytical and numerical solutions for cycle averaged mold surface temperature

The cycle averaged mold surface temperatures at point A and point B in Figure 3-2 are derived from equation (2-10) and are expressed below:

$$T_{ma} = T_c + \frac{\rho_p c_p l_p (2K_m W + h\pi D l_a)(T_{melt} - T^a_{eject})}{h\pi D K_m t_{cycle}} \tag{3-5}$$

$$T_{mb} = T_c + \frac{\rho_p c_p l_p (2K_m W + h\pi D l_b)(T_{melt} - T^b_{eject})}{h\pi D K_m t_{cycle}} \tag{3-6}$$

where l_a and l_b are the depth of the heat diffusion into the mold at point A and point B respectively. T^a_{eject} and T^b_{eject} are part ejection temperatures at A and B respectively. The cycle averaged temperatures T_{ma} and T_{mb} are obtained following the same routine as discussed in section 3.4. The local cooling uniformity of the mold is thereby defined as the absolute value of the cycle averaged temperature difference between point A and point B:

$$\Delta T_{ab} = \mid T_{ma} - T_{mb} \mid \tag{3-7}$$

Figure 3-4 plots the local cooling uniformity and compares it with the numerical result for different cooling line pitch distance. The numerical result was obtained by 2D finite element analysis using PDease® software package. The material properties used for analysis are those of polystyrene (part), 316 stainless steel (mold) and 30 °C water (coolant). The calculation is based on 2mm part thickness, 4mm cooling channel diameter and 3mm vertical distance from cooling line to mold wall. The heat conduction distances l_a and l_b in equation (3-5) and (3-6) are chosen to be distances from point A and B to the wall of the cooling channel respectively. As one can see from the figure, the analytical and numerical solutions match very well in a certain pitch distance range. More accurate prediction can be achieved by adding adjustment factors to l_a and l_b.

3.2.6 Design for mold strength and deflection

Rao suggested using the rectangular channel shown in Figure 3-4 to model the mold stress and delection around cooling channels [Rao 1991]. According to this model, the maximum tensile stress in the mold under a certain injection pressure P_m is:

$$\sigma_{max} = \frac{0.5 P_m D^2}{l_m^2} \tag{3-8}$$

The maximum shear stress in the mold is:

$$\tau_{max} = \frac{0.75 P_m D}{l_m} \tag{3-9}$$

The maximum mold surface deflection under pressure P_m is:

$$f_{max} = \frac{P_m D^2}{l_m}\left(\frac{D^2}{32 E_m l_m^2} + \frac{0.15}{G}\right) \tag{3-10}$$

The above expressions represent the worst loading condition because the commonly used cooling channels are circular shaped and have smaller stress and deflection. The numerical simulation shows that the stress concentration is reduced by over 50% if we choose channels with round corners.

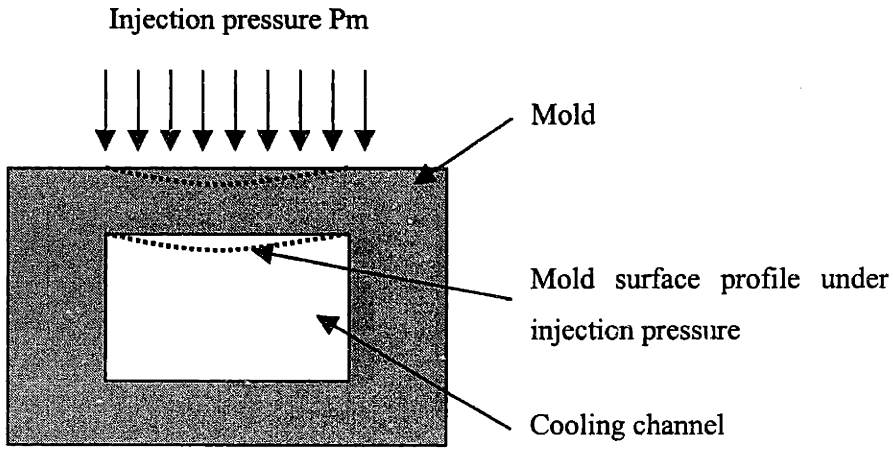

Figure 3-4 Sketch of a cooling cell under the injection pressure

3.2.7 Design windows for conformal cooling

The design rules discussed above defined the relationships between individual design parameters such as the cooling channel diameter, length, coolant flow rate, etc. With these rules and other physical constraints, it is possible to construct design windows that guide the selection of mold parameters and cooling conditions. Figure 3-5 shows an example of such design windows represented by the cooling line length versus the cooling channel diameter. The cooling line pitch distance in this window is set to be 10mm. The coolant (water) flow rate is 3GPM and the distance from mold wall to cooling channel is 3mm. The pressure budget is 50psi and the maximum temperature drop is 2 degC. As can be seen from the figure, the feasible choice of the cooling line length and the cooling channel diameter is the shaded area surrounded by the pressure drop criterion, the temperature drop criterion, the manufacturing capability criterion and the part geometry criterion. The manufacturibility criterion defines the ease of manufacturing for a specified cooling channel. The major challenge for small channel manufacturing is powder removal. The smaller the cooling channel, the more difficult to clean the powder from, and the shorter the cooling channel length could reach. On the other hand a small increase of the cooling channel diameter will result in a significantly large increase of the feasible cooling channel length. This is why in Figure 3-5 the manufacturibility curve shows a nonlinear increase with respect to the cooling channel diameter.

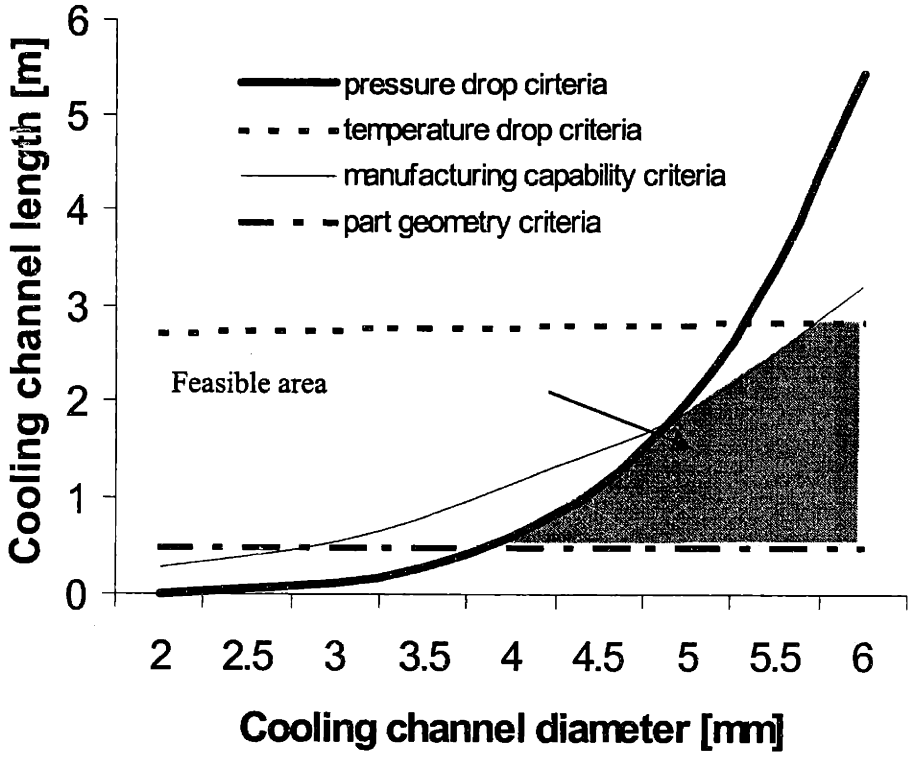

Figure 3-5 A conformal cooling design window defined by the cooling channel diameter and length

Figure 3-6 is another example of the design window defined by the cooling channel distance to the mold wall l_m and the cooling channel diameter D for a consistent cooling line pitch distance W (for the graphic reference, please see Figure 2-5). As one can see from Figure 3-6, the mold wall thickness limits the allowable distance from the cooling channel to the mold wall, the channel pitch distance limits the maximum cooling channel size. The cooling uniformity curve defines the feasible combination of l_m and D. As the channel size decreases it has to be placed further away from the mold surface in order to maintain the mold surface temperature uniformity for a given pitch distance W. The conformal cooling criterion defines the feasible area of l_m and D that satisfies the conformal cooling condition. This criterion can be directly derived from equation (2-11). As the cooling channel diameter increases the channel has to be placed closer to the mold wall. However the conformal cooling condition is not very sensitive to the cooling channel size change because the dominate term that determines the mold time constant is the distance from the channel to the mold wall l_m, instead of the channel size D. The strength criterion ensures that the local strength of the mold is enough to survive the process pressures. The larger the channel size the further the channel should be placed away from the mold surface.

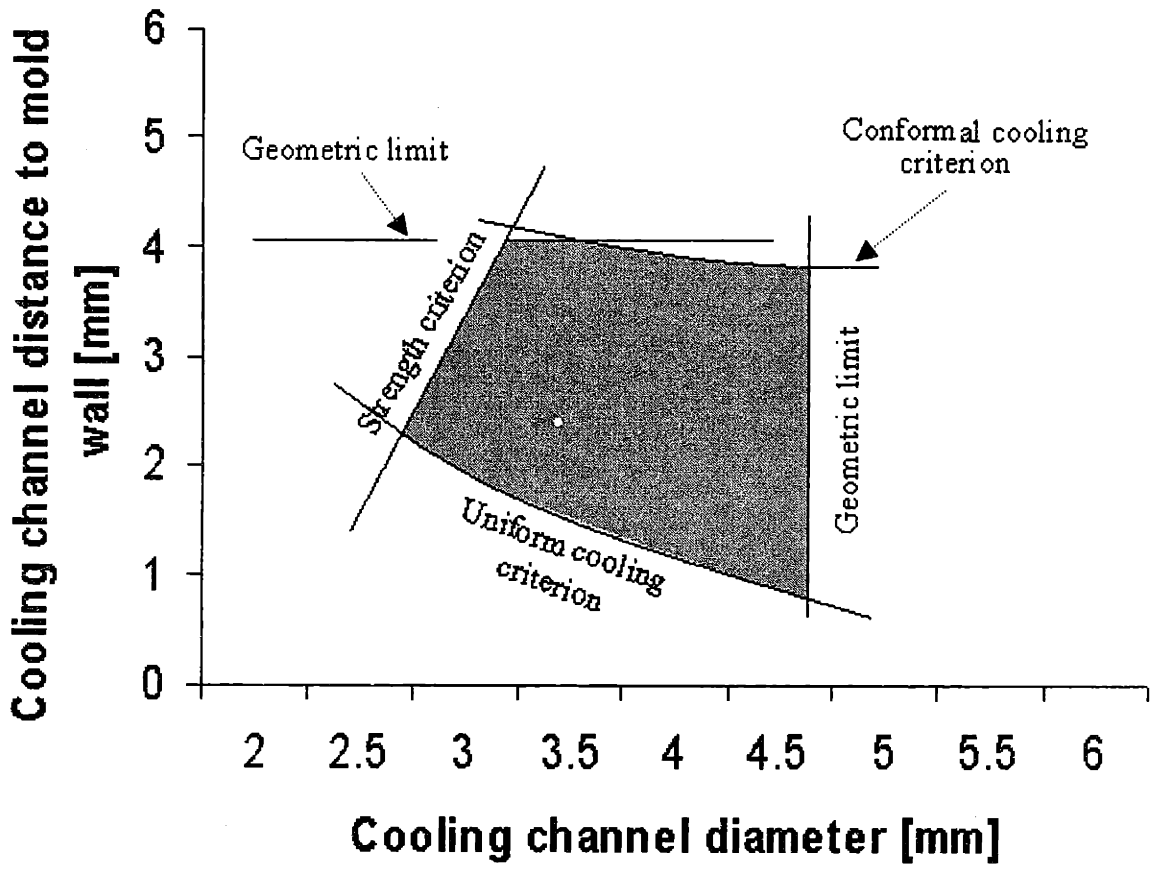

Figure 3-6 Another example of the design window defined by cooling channel diameter and cooling channel distance to mold wall

3.3 A SOFTWARE PACKAGE FOR CONFORMAL COOLING

3.3.1 Introduction

A computer program called "Conformal Cooling" has been developed at 3D Printing Lab of MIT as a test bed for the conformal cooling design methodology. The software package is written in Visual Basic 5.0 and is run in Window 95/NT environment. The software helps the mold designers to determine the proper set of design parameters such as the cooling channel size and location as well as process condition parameters such as the cooling time and the coolant flow rate. It automatically checks the validity of each design criterion and prompts suggested solutions for design problems such as the high coolant pressure and insufficient cooling. Compared with the existing injection molding CAD software,

this package is simple, easy to use and takes very short computational time. The cooling system design for an entire mold using this package takes only 20 minutes.

3.3.2 Flow chart and structure of the "Conformal Cooling" package

Figure 3-7 illustrates the flow chart for cooling channel design using "Conformal Cooling" software package. The design flow consists of 3 stages: information input, design rule verification and design result reporting. As the first step of the design the user enters the budgets for the coolant pressure drop, the coolant flow rate and the chiller power capacity. Then in the material property window, the user loads, edits or inputs the material property data for the mold, the part and the coolant respectively. After the material properties have been selected, the designer defines the design problem by assigning process parameters such as the part thickness, the injection pressure, the desired cooling time and the cooling area. As the final stage for information input, a graphic interface is provided for setting up the cooling channel size and location. After all the design information has been entered, the design engine starts to check the validity of the design according to the following five design rules: design for pressure drop, design for coolant temperature variance, design for mold strength and deflection, design for part ejection temperature and design for conformal cooling condition. Any violation to these design rules will be notified. The corresponding suggestions are itemized. Once the design satisfies all the design rules, the user is able to run the numerical simulation to see the temperature distribution pattern during the cooling stage. After all the design and analysis work is done a design report is created listing all the major design parameters and critical results.

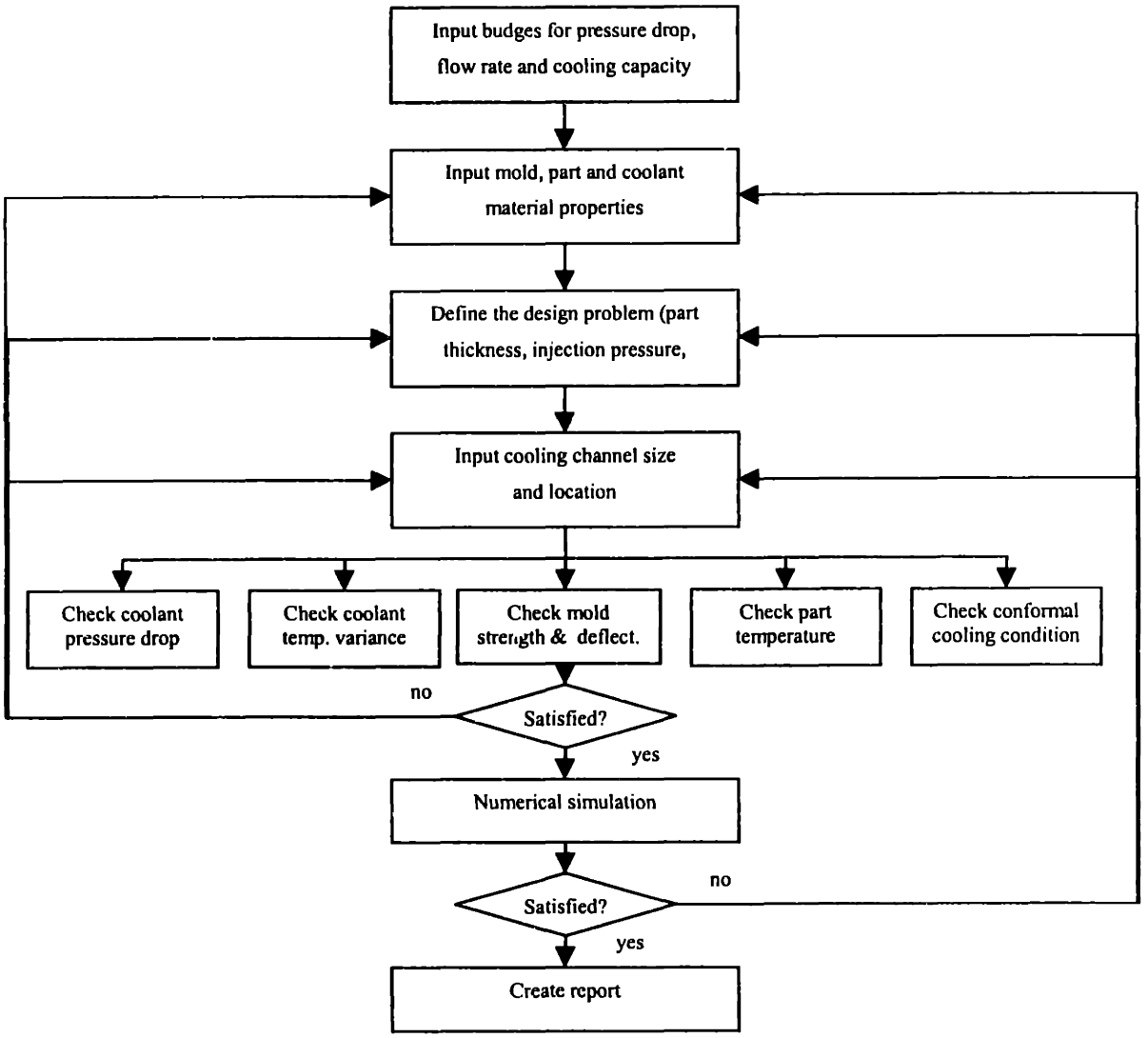

Figure 3-7 Flow chart for the Conformal Cooling software

Figure 3-8 illustrates the hierarchy structure of the software. On the top level is the project manager window which consists of four sub modules: design information input, rough design, simulation and accessory. The design input module is further divided into sub modules of material property definition, cooling line geometry definition, chiller system specification and design problem configuration. The rough design module consists of functions for evaluating the coolant pressure drop, the coolant temperature variance, the mold strength, the part ejection temperature and the conformal cooling condition. The simulation module includes sub modules for simulation parameter setup, image manipulation (shift and zoom), temperature distribution displaying and the temperature profile plotting. The accessory module includes an alarm clock, a calculator and a unit converter between the English unit and the SI unit.

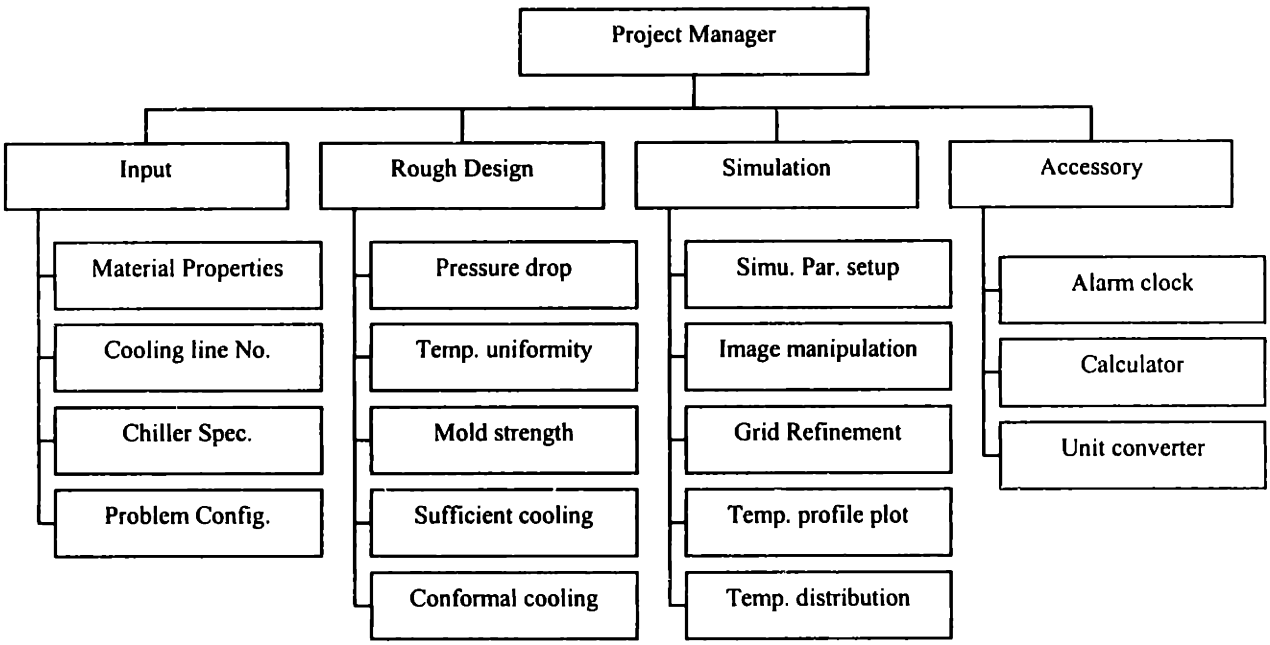

Figure 3-8 Hierarchy structure for the Conformal Cooling software

3.3.2.1 Major user interface

Figure 3-9 shows the main user interface for the "Conformal Cooling" package. On the top of the window are two rows of buttons for design information input and design result evaluation respectively. Four buttons on the left side of the upper row read the process budget input window, the material property input window, the design problem configuration window and the cooling line geometry input window respectively. Three buttons on the right side of the upper row are the calculator, the unit converter and the alarm clock. The buttons in the lower row are for users to verify the design validity. Eight buttons in this row are used to check the mold strength, the mold surface deflection, the coolant pressure drop, the coolant temperature variance, the part temperature at center, the part averaged temperature, the conformal cooling condition and the numerical heat transfer simulation respectively. Directly below these buttons is an information booth where the design result corresponding with eight buttons is displayed. On the right side of the information booth is a spread sheet listing all the input data, the intermediate data and the result related with the design procedure. With this spread sheet the designer can easily check the current design status such as the Reynolds number, the heat transfer coefficient, etc. Below the information booth and the spread sheet is the design suggestion window where all the possible solutions for the design problems are listed in case that a design violates a certain design rule. By clicking any suggestion items, the user is led to the corresponding design input window where the related design parameter can be modified. On the bottom of the design information booth sit side by side five status indicators showing the current design status based on five design rules. Each status indicator is painted with either green or

red colors. The green color indicates that the design passes the corresponding design rule, while the red color shows that the design violates the corresponding rule. In the latter case, a warning message will blink below the suggestion window urging the designer to make modifications. The design is said accomplished when all the status indicators turn green. Let us take the design shown in Figure 3-9 as an example. The information booth is showing the part temperature data because the temperature evaluation button was just clicked. It seems that the central temperature of the part at the end of cooling is 116 degC which is higher than the plastic glass temperature (about 100degC for PS). it means that the plastic melt is not totally solidified at ejection. The suggested solutions to this problem are listed below. They include increasing the coolant flow rate, setting longer cooling time, using the mold material with higher thermal conductivity, etc. Since this design violates the sufficient cooling criterion, the corresponding design status indicator keeps red (indicated in Figure 3-9 as a dotted text box).

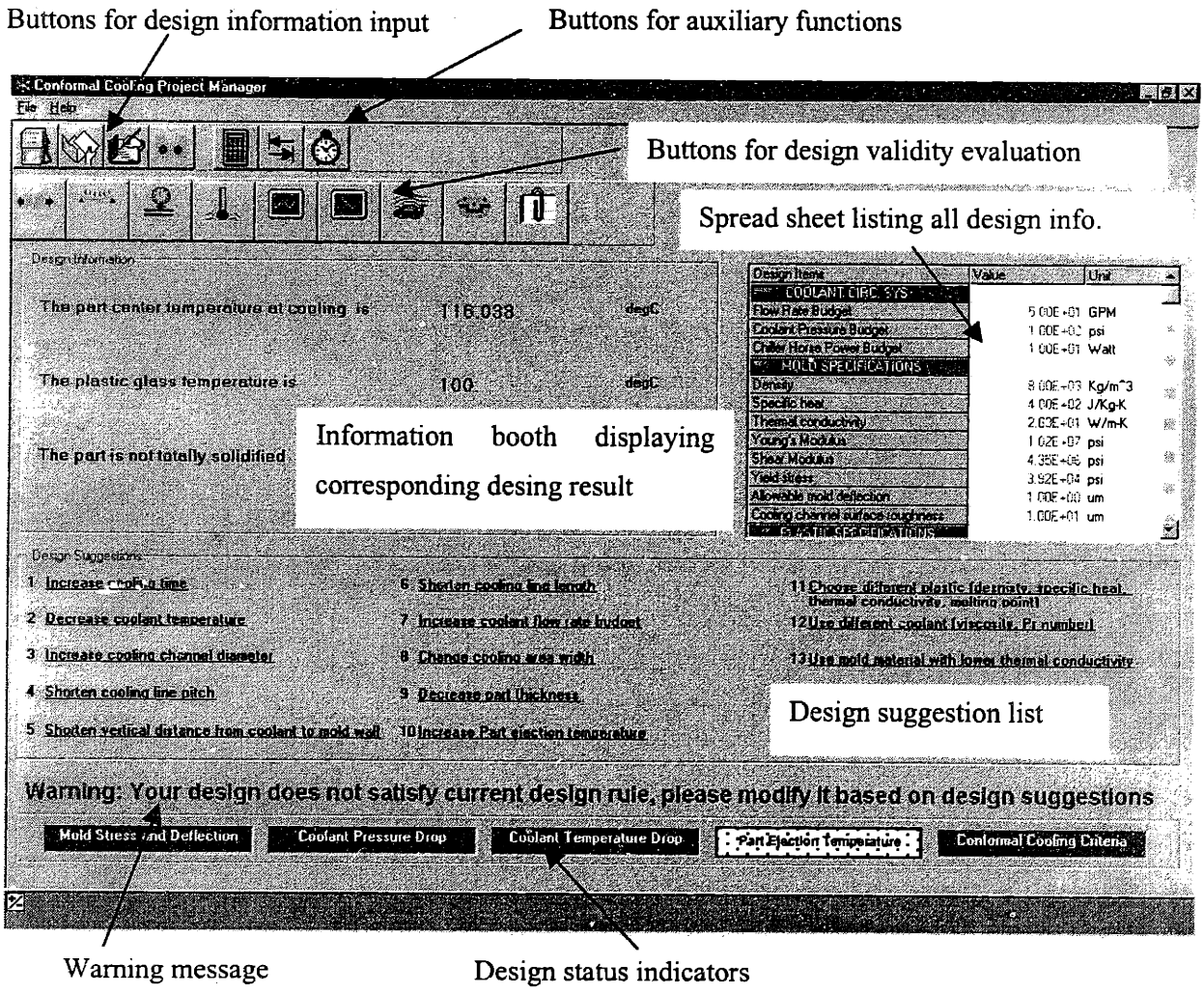

Figure 3-9 Main user interface for conformal cooling

3.3.2.2 Mold, part and coolant material properties input

Figure 3-10 shows the window for entering, editing and loading material properties for the mold, the part and the coolant. In this window, default material property values are assigned first. The user can enter, modify and load the material property data. Once the material property data have been entered they can be saved into a database for the future use.

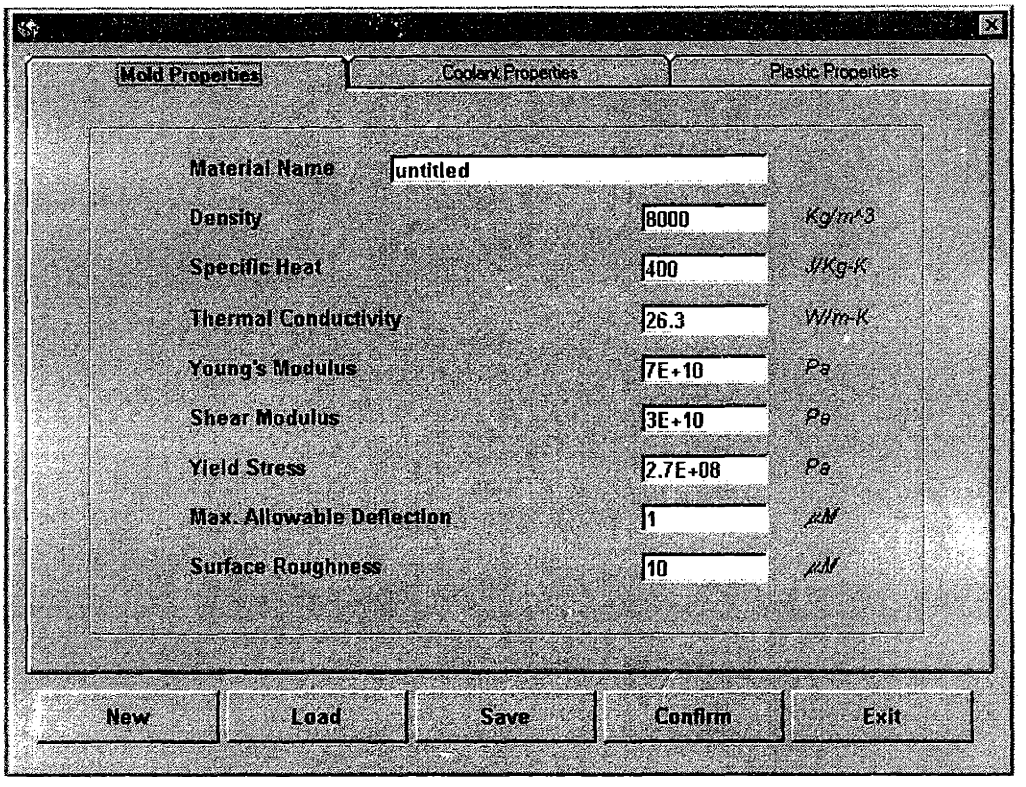

Figure 3-10 Interface for material property input

3.3.2.3 Design problem configuration

The window shown in Figure 3-11 is used to configure the design problem. The configuration setup in this window includes the cooling area, the part thickness, the cooling line length, the width of the cooling area, the coolant temperature, the desired cooling time, the injection pressure, the allowable temperature drop along the cooling line and the part ejection temperature. The default setup is used at the beginning of the design. After the confirm button is clicked the new configuration will used to update the default one.

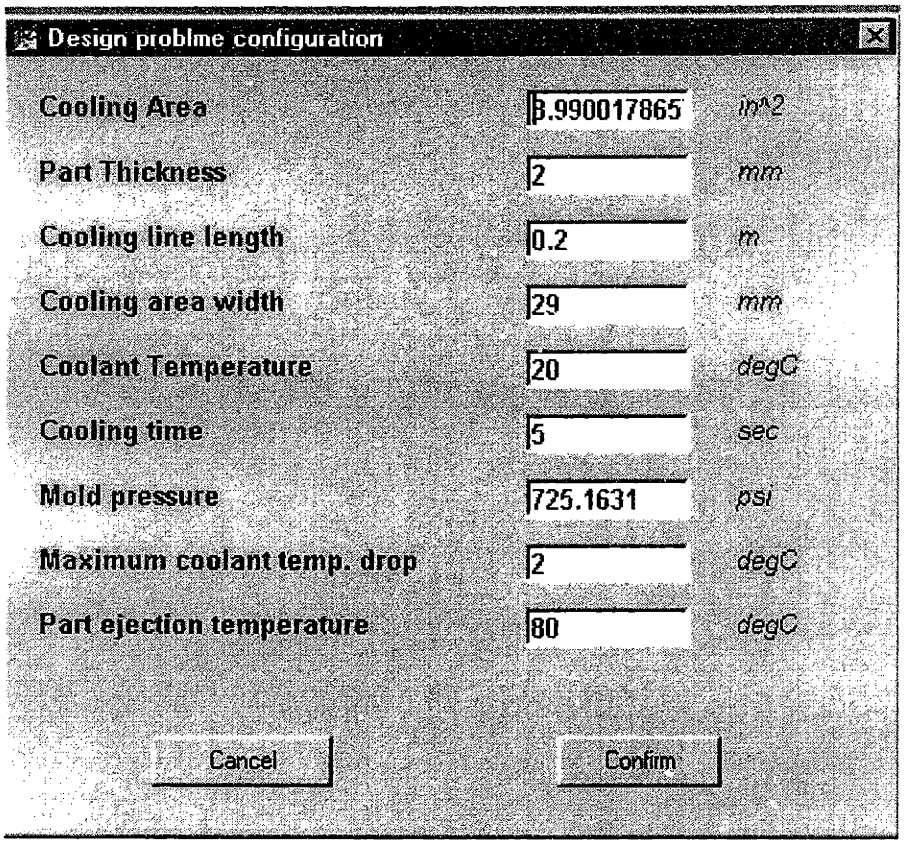

Figure 3-11 Interface for design problem configuration

3.3.2.4 Cooling channel size and location design

The cooling channel design window shown in Figure 3-12 defines the size and the location of the cooling channel. on the left side is the sketch of a single cooling unit (a segment of the part, a segment of the mold and a cooling channel). To the right and the bottom of this figure are bars used to change the mold thickness, the vertical distance from the cooling channel to the mold wall, the cooling channel pitch distance and the cooling channel diameter. The change of these design parameters simultaneously updates the shape of the cooling unit sketched above. Four buttons on the lower right side is used to zoom in/out and repaint the sketch. Below these buttons are radio boxes defining if the cooling channel is centered or non-centered.

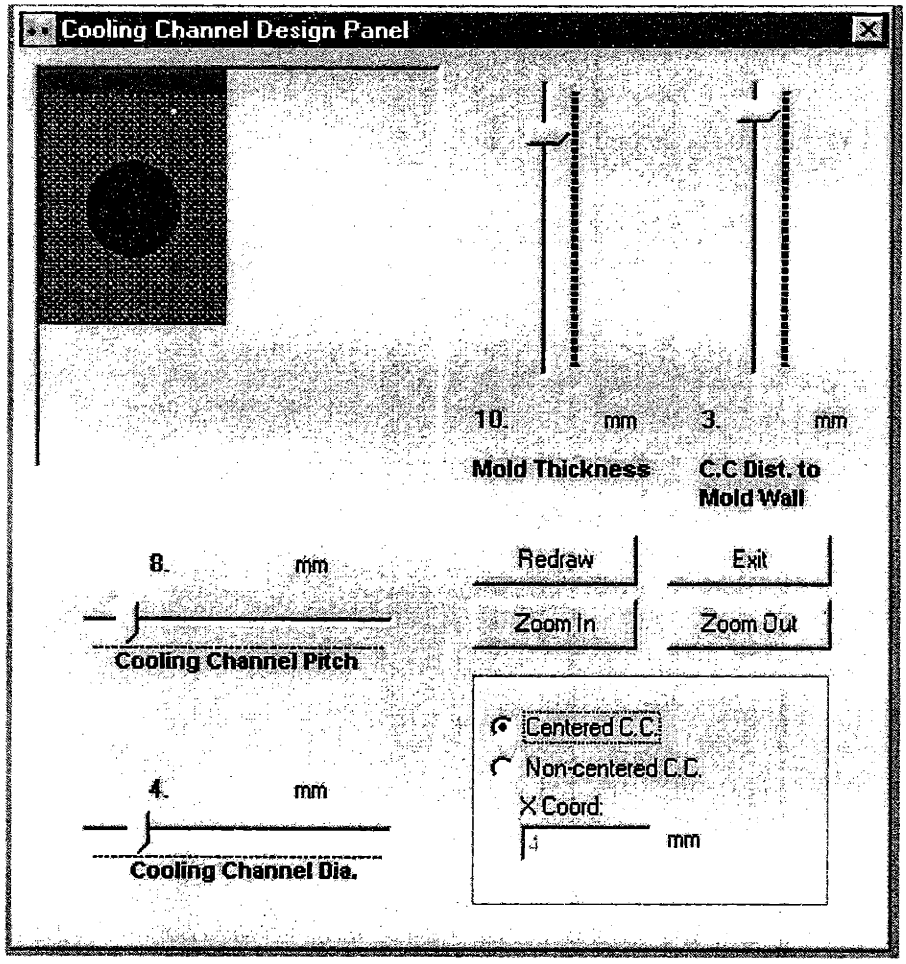

Figure 3-12 Interface defining the cooling channel geometry

3.3.2.5 Numerical simulation

The numerical simulation window performs the 2D simulation of the cooling cell. On the top of the window are buttons to control the simulation and display. Right below these buttons is a canvas sketched with a unit cooling cell with the part, the mold and a cooling channel. The temperature distribution is marked by different palette colors. On the right side of this canvas is the temperature distribution across the thickness of the part at the end of the cooling stage. Below the canvas is the plot of the temperature profile along the horizontal cross section of mold. At the lower right corner of the window are some radio boxes and buttons used to change the scales of the temperature profile plots. It also indicates the x y coordinates and temperature values at any point where the user's mouse clicks on the unit cooling cell.

The simulation is based on the finite different analysis. The resolution of the simulation can be improved by refining the simulation setup. The left most button on the third row with an icon of rulers is used for simulation parameter set up. One it is clicked, a simulation setup window is invoked, as shown in Figure 3-13. In the simulation setup window, the grid numbers for both the part and the mold are defined. The total simulation time and the time interval for image updating is also defined. The resulting time step and the length step for simulation are then calculated according to stability conditions. The larger the grid number the longer time it takes to simulate and the higher accuracy the simulation can reach.

One more thing to mention is that the original distribution of the Conformal Cooling package has a bug in the simulation module (conf.bas). After fixing this bug, the temperature distribution simulated by this package shows high agreement with that simulated by other commercial finite element packages.

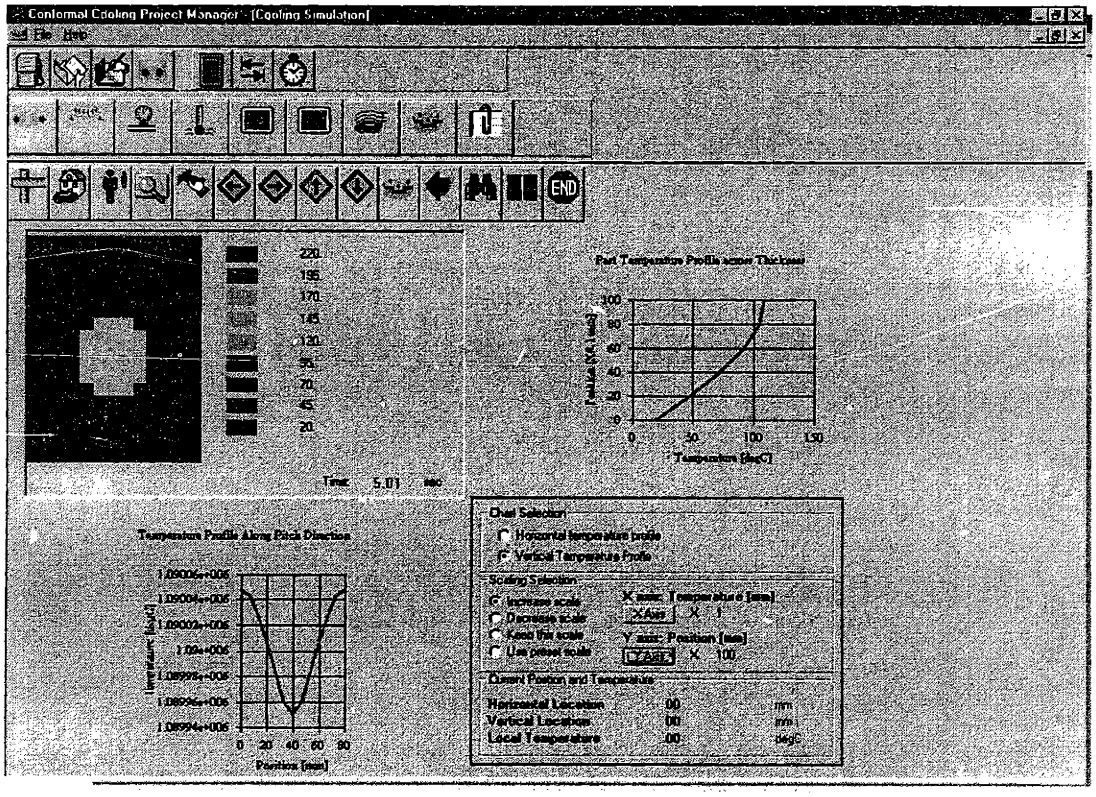

Figure 3-13 Interface for numerical simulation

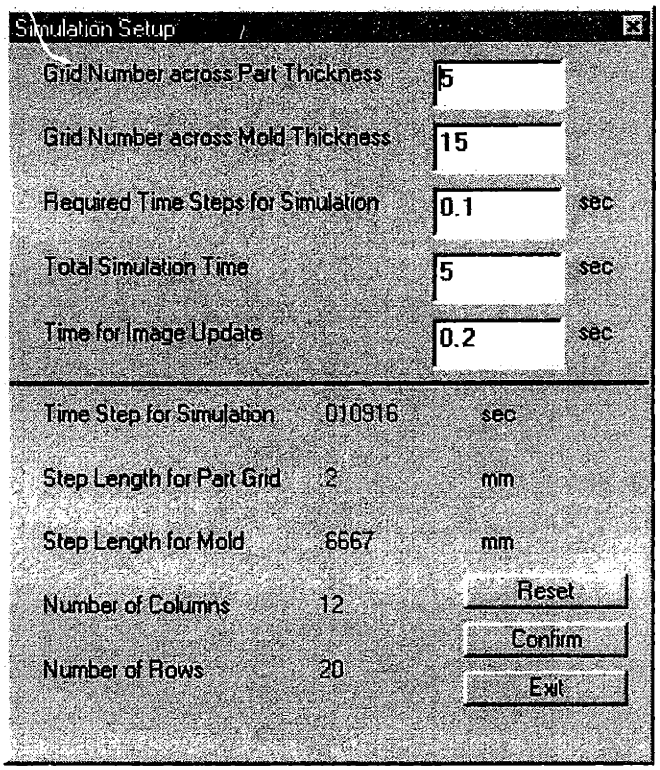

Figure 3-14 Interface simulation parameter setup

3.3.2.6 Design report

The design report window summarizes the design result using the conformal cooling software. Figure 3-15 shows a typical report interface. The results are listed by 3 categories. In the category of geometry design, the part thickness, surface area, mold thickness, cooling line length, pitch distance, distance from cooling line to mold wall and cooling channel size are listed. In the second category, the desired cooling time, the total number of cooling lines required, the coolant flow rate, the required horse power, and the pressure supply are listed. In the third category, the cycle averaged mold temperature, the plastic ejection temperature and the coolant temperature variance are listed. All these results provide mold designers enough information to construct the conformal cooling lines in a 3 D space providing that the 3D model of the part is given.

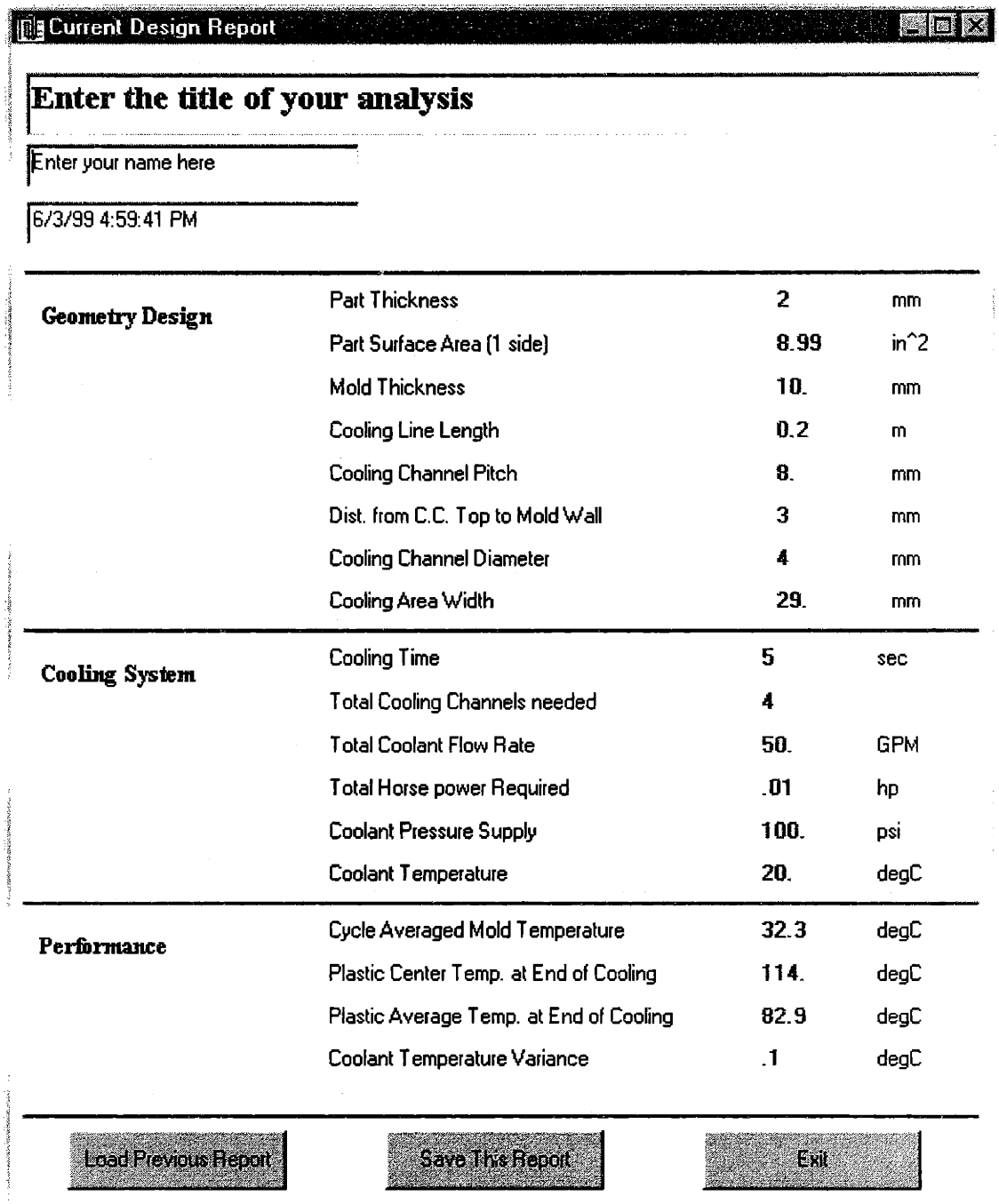

Figure 3-15 Design report window

3.3.3 Cooling channel design for proposed part

The cooling channel design for the part proposed in section 3.1 exactly follows the systematic design methodology discussed in the previous chapter. Figure 3-16 shows the design flow. The part is firstly divided into two cooling zones. For each cooling zone, the topologic structure is defined and the

cooling line is separated into different sections with different cross section shapes based on the part geometry. These sections are further decomposed into individual cooling cells and the design rules are applied to these cells to obtain the local solution of the cooling channel parameters. The 2D numerical simulation is also used for the evaluation of the transient performance of each cooling cell. The cooling line design results for the core insert of the benchmark tool are listed in table 3-1. On the top row of the table the cooling system is divided into two cooling zones: zone 1 that the surrounds the wall of the part and zone 2 that surrounds the bottom. The oil channel topology is designed in the second row. For the cooling zone 1 there is a single inlet (section 1) divided into 3 parallel branches (section 2) and then combined into a single outlet (section 3). The cooling channel cross section type for sections 1 and 3 are circular, while those for section 2 are rectangular with corner rounded. The part geometry requires that the cooling line length for section 2 is 0.43m. If we set the hydraulic diameter for cooling channels in section 2 be 2.3mm, the resulting pressure drop is 29.6 psi. The conformal cooling condition yields a cooling line pitch distance of 10mm and the vertical distance from cooling lines to the mold wall of 2.5mm This design leads to the maximum stress of 8704psi for an injection pressure of 5000psi. After the desired cooling time of 10 seconds, the averaged part temperature reaches 62.95degC. For the cooling zone2, it is a single line divided into 3 sections. Section 1 and 3 are the inlet and the outlet with circular cross section shapes. Section 2 is the serpentine circular cooling channel that follows the hemispherical dome of the part. For section 2, the cooling channel diameter is 4mm. The cooling line length is 1.15m. The flow rate is 3 GPM. This leads to a pressure drop of 37.5psi and a Reynolds number of 62,100. The conformal cooling condition requires that the vertical distance from the cooling channel to the mold wall is 5mm and the pitch distance for the cooling line is 10 mm. Under an injection pressure of 5000psi the maximum stress built around the cooling channel is 7909psi. The part ejection temperature is 64.9 degC for a desired cooling time of 10 seconds.

The concept of conformal cooling and the methodology for conformal cooling channel design have been used by members of the 3D Printing Industrial Consortium to guide their design [Latham et al. 1999].

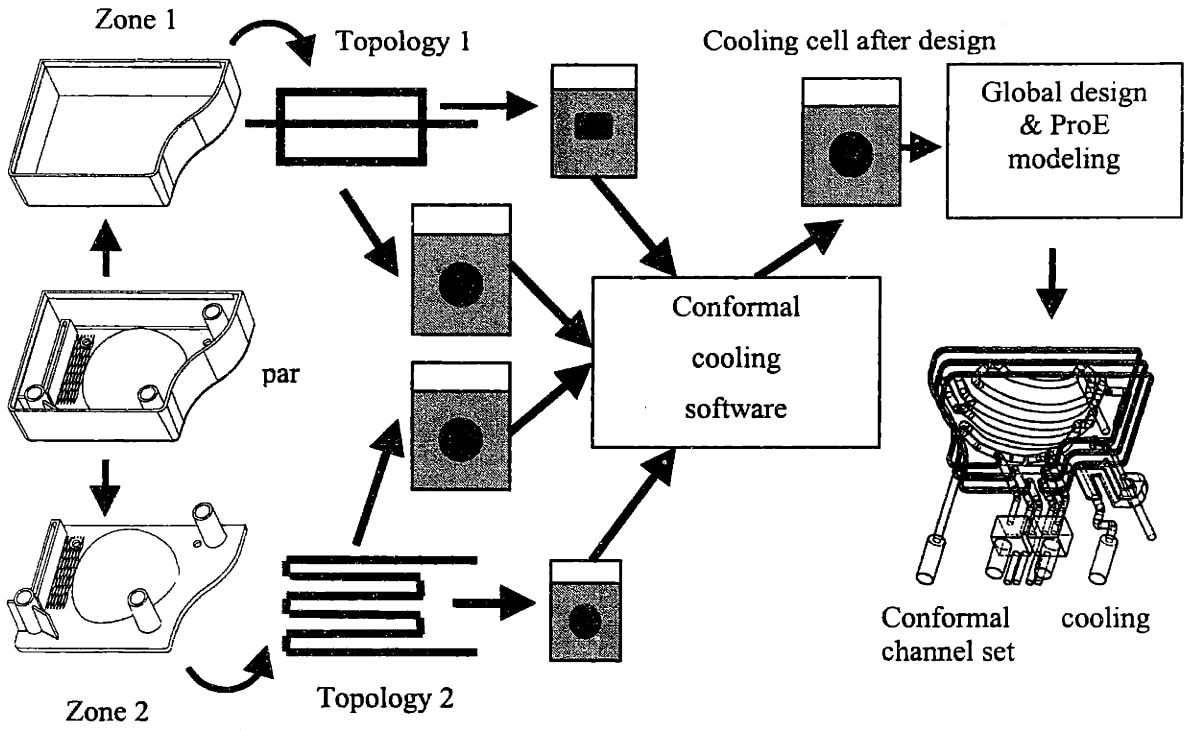

Figure 3-16 Conformal cooling channel design procedure for benchmark part

	Cooling zone 1		Cooling zone 2	
Cooling zone Topological Structure	1 2 3 section 1: inlet section 2: 3 parallel lines section 3: outlet		1 2 3 section 1: inlet section 2: serpentine cooling line section 3: outlet	
Section No.	1, 3	2	1, 3	2
Cross Section Shape	●	⬬	●	●
Hydraulic Diameter	6.35 mm	2.3 mm	8 mm	4 mm
Cooling Line Length	.03 m	.43 m	.03 m	1.15 m
Pitch Distance	10 mm	10 mm	10 mm	10 mm
Coolant Flow Rate	3	1	3	3
Reynolds	2800	36,000	2220	62,100
Coolant Pressure Drop	<<1psi	29.6 psi	<<1psi	37.5 psi
Total Pressure Drop	~ 30 psi		~38 psi	
Vert. Dist. To Mold Wall		2.5 mm		5 mm
Cooling Time		10 sec		10 sec
Max. Stress		< 13,000 psi		< 8094 psi
Part Ave. Temp.		62.95		64.9

Table 3-1 Conformal cooling design results for the benchmark tool

3.4 SOLID MODELING BY PROENGINEERING

After the design parameters and process conditions for all the cooling cells have been determined, the solutions are mapped back to the whole mold to construct the entire conformal cooling system. The cooling system model is then subtracted from the insert model to get the mold insert with internal cooling channels. After all the .STL file is created for solid freeform fabrication. An important issue that a designer should pay attention to is that an additional tolerance has to be added to the original CAD model in order to compensate the process shrinkage and leave room for post-process machining. For simple geometry, the tolerance is added by offsetting the entire surface of the insert. However this method faces difficulties when we try to offset the outer surface of the core insert. The small texture feature on the top of the core insert makes it impossible to offset the surface in normal direction. Our solution is to pick up this area for translating offsetting, while keep the rest of the surfaces normal offset. The entire routine for the tooling design of the benchmark part discussed in this chapter is listed below:

1) Create the solid model for the benchmark part
2) Create the core and the cavity inserts by mapping the geometric feature to two blocks.
3) For core insert, copy the texture feature into a small block
4) Use this small block with texture feature to make a negative block
5) Hide the texture feature from the original core insert and offset the entire insert
6) Use the negative block obtained from step 4 as a die to carve the texture feature on the top of the core insert. The carved feature will offset from the original position by translation along the vertical direction
7) Obtain the insert with tolerance offset and the texture feature
8) Create the conformal cooling channel set from the part
9) Subtract the conformal cooling channel set from the insert obtained from step 7 in order to get the final solid model of the insert with texture feature, tolerance offset and internal channels.

The above steps are sketched in Figure 3-17.

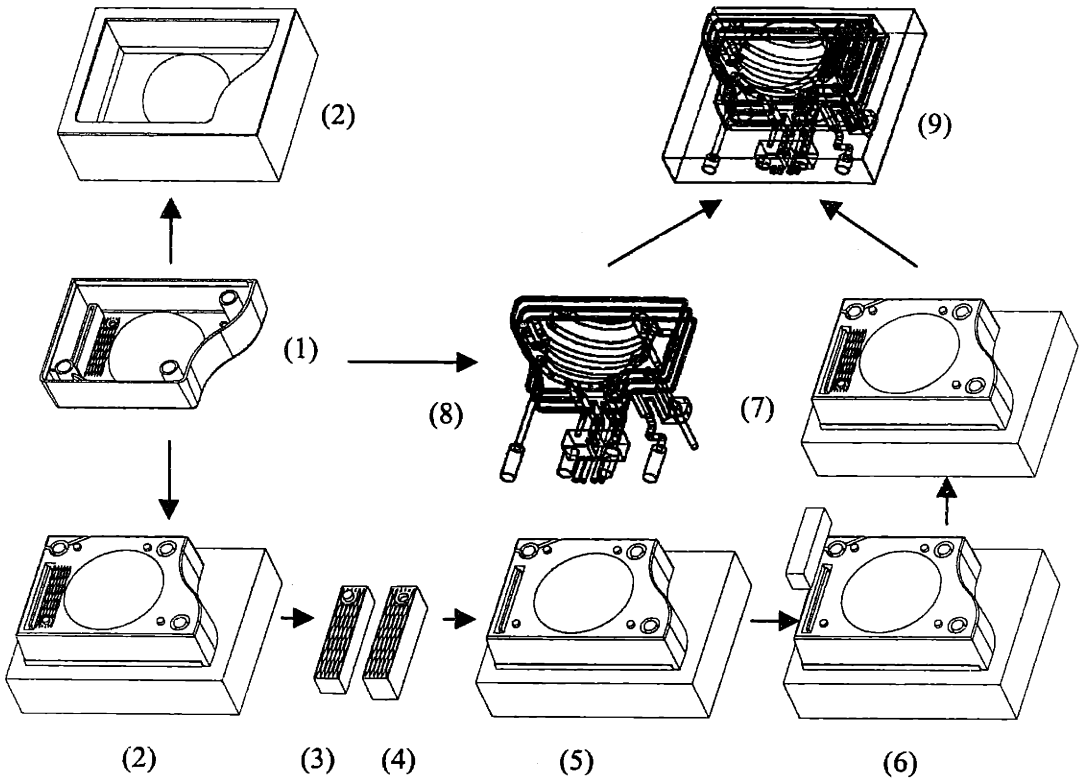

Figure 3-17 Steps to make offset to the benchmark tool for the manufacturing tolerance

This design has been fabricated by 3D Printing process. Figure 3-18 shows the green part of the core insert. As one can see from the cut-away view of the green part, small cooling channels have been placed conformal to the mold wall.

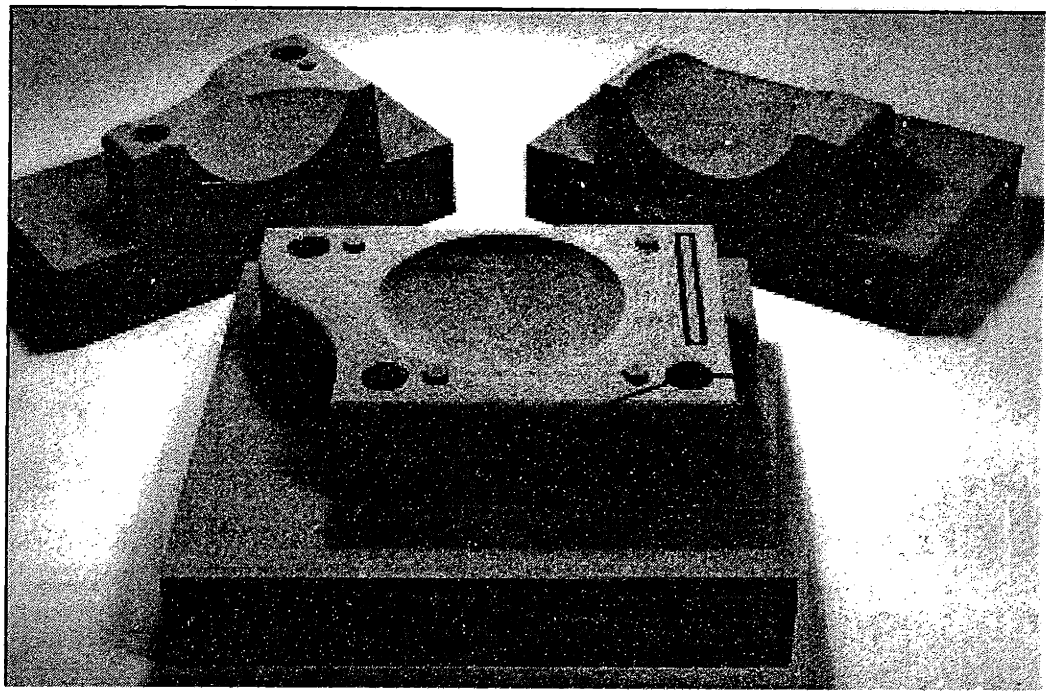

Figure 3-18 Green part of the benchmark tool for conformal cooling fabricated by 3DP process

3.5 CONCLUSION

Solid Freeform Fabrication processes such as 3D Printing can create injection molding tooling with complex cooling channels offering the potential for substantial improvement in production rate and part quality. This capability raises the challenge of designing the complex cooling channels required to realize these improvements.

This work presents a systematic method for the design of cooling channels for tooling. First the mold surface is decomposed into manageable sections called cooling zones. Then a system of cooling channels is designed for each cooling zone. This system of cooling channels is further decomposed into smaller elements called cooling cells that are easy to analyze. The cooling cell is a sandwich structure covering the part, the mold and the cooling channel region between two adjacent cooling lines. Six design rules are applied in order to create design windows for the individual cooling cell. These design rules include design for conformal cooling condition, design for coolant temperature drop, design for part ejection temperature, design for sufficient cooling, design for mold strength and deflection and design for cooling uniformity. After the design for individual cooling cell is finished, the solution is mapped back to the mold in order to build the entire conformal cooling system.

3.6 REFERENCES

1. Fay J., *Introduction to Fluid Mechanics*, MIT Press, 1995
2. Latheam T., J. Irish, "Low Cost, High Performance Tooling by 3D Printing", Technology Re-Investment Program Final Report, 1999, pVI.4AII-1
3. Mills A., *Heat and Mass Transfer*, Irwin Press, Chicago, 1995
4. Rao N., "Design formulas for plastics engineers", Hanser, 1991, chapter 6
5. Sachs E., S. Allen, M. Cima, X. Xu, J. Banos, J. Serdy, D. Brancazio, H. Guo, "Fabricating Metal Tooling and Metal Parts by 3D Printing", *Naval Research Reviews*, three/1998, p9-18
6. Xu X., E. Sachs, S. Allen, M. Cima, "Designing Conformal Cooling Channels for Tooling", *Proceedings of 9th Solid Freeform Fabrication Symposium*, Austin, TX, 1998.
7. Xu X., E. Sachs, S. Allen, M. Cima, "Design Tools for Rapid Thermal Cycling", ANTEC'99, New York City, NY, 1999.

CHAPTER 4

RAPID THERMAL CYCLING

CONTENT

FIGURES

4.1 INTRODUCTION

4.1.1 Field review

In a traditional injection molding process the polymer melt is fed through a runner system and gates into the mold cavity. It is then packed under high pressure and cooled until solidification. Although this process has become one of the most popular processes for polymer manufacturing it still has some inherent shortcomings [Kim 1983]. The most significant shortcoming is that the filling stage is coupled with the cooling stage. As the polymer melt contacts the cold mold wall a layer of frozen skin is formed near the mold surface. This kind of "solidification while filling" results in at least two problems. First it reduces the flow passage so that a higher injection pressure and larger injection speed is required for a successful injection. In extreme cases the flow passage is totally blocked before the cavity is filled and the short shot defect occurs. Second the coupling between the filling stage and the cooling stage introduces very complex patterns of residual stresses that are difficult to analysis and control. These stresses are categorized into flow-induced stresses and thermal-induced stresses. The flow-induced stresses are due to shear and normal stresses that develop during the non-isothermal flow of the polymer in the filling and the packing stages. The thermal-induced stresses are due to the non-uniform and unbalanced cooling as well as the shrinkage during the packing and cooling stages. The residual stresses directly effect the dimensional accuracy and mechanical property of the injection molded part. For this purpose a lot of research work have been done to predict the molded-in residual stresses[Isayev 1987, Akay et al. 1996, Titomamlio et al. 1996, Liu 1996, Zoetelief et al 1996] and to optimize the process conditions [Jansen et al. 1996, Leo et. al 1996, Lee et. al 1995, Kang et. al 1995] for high part quality. However the successive improvement of the process conditions is hindered by the inherent shortcoming of the process itself, that is the coupling effect between the filling and the cooling stages.

The coupling between the filling stage and the cooling stages has to do with the placement of the cooling channel. Ideally speaking the mold temperature control during the filling stage and the cooling stage should be separated because a higher temperature will benefit the filling stage but a lower mold temperature will speed up cooling. However in the traditional molding process the mold temperature is controlled by the coolant and/or the heater of a constant target temperature during the entire injection cycle, regardless different requirements for the filling stage and the cooling stage. A typical case in injection molding is that the coolant with low temperature is pumped through the mold to speed up the cooling. However the coolant also keeps the mold temperature low during the filling stage, which results

in molding defects such as the short shot and the surface quality problems. These defects are traditionally adjusted by applying large injection pressure, high injection speed and high melt temperature. However the change of these process parameters will lead to other side effects which eventually make the process control and the trouble shooting very difficult.

A fundamental solution is to make the temperature control independent for the filling stage and the cooling stage. A passive way is change the coolant flow for different stages of the process. An example is the pulse cooling technique. An active way is to dynamically cycle the mold temperature by periodical heating and cooling. An example is called rapid thermal cycling, which will be discussed in detail in this chapter.

The pulse cooling technique was first introduced by CITO Products, Inc [CITO 1997]. Instead of the traditional continuous circulation unit, the pulse cooling unit uses the timed injection of coolant to control the mold surface temperature. This method improves the part quality, shortens the injection cycle time and reduces the energy consumption. For details on pulse cooling test result please refer to [Mincy 1992] and [Wooldridge et. al 1988].

Rapid thermal cycling used to be investigated under the name of "low thermal inertia molding". In 1986 Kim and Suh reported the development of a low thermal inertia mold for isothermal filling [Kim et. al 1986]. The mold was constructed by placing multiple layers of woven graphite, silicon rubber, Teflon and zirconium oxide on the surface of the mold base. The rapid switch of the heating circuit fires the graphite fiber and warm up the mold surface in a very short time so that the isothermal filling occurs. The experiments with low thermal inertia molding showed the significant improvement in the part residual stress and the molecular orientation. Other advantages of the low thermal inertia molding include the lower barrel plastic temperature, the lower injection pressure, the slower injection rate, the short-shot eliminated part and the uncoupled scheme for mold flow and cooling design and analysis. More recently Kim and Wadhwa designed a mold which uses thermoelectric devices for rapid heating and cooling [Kim et. al 1987]. Jansen built a fast-response heating elements for the use of isothermal filling by placing a resistance layer between two insulation layers [Jansen et. al 1994].

4.1.2 Overview of the MIT Project in Rapid Thermal Cycling

In reviewing the literatures in mold temperature control, it is noticed that the existing tooling methods are not efficient enough for rapid thermal cycling. The low thermal inertia mold with heating

elements on the surface suffers potential problems such as the short tool life, the non-efficient cooling and the difficulty to build heating element for the complex geometry. The emergence of the Solid Freeform Fabrication processes provides a straightforward way for the mold temperature control. In previous chapters we have discussed the conformal cooling technique. The industrial application of 3D Printed tools with conformal cooling channels have achieved the simultaneous improvement of the cycle time by 15% and the part distortion by 9% [Sachs et. al 1997]. Now we are moving one step further beyond conformal cooling. We proposed that the mold temperature be rapidly cycled by running hot and cold oil alternately through conformal channels [Xu et. al 1999]. A tool with low thermal inertia is the key for the successful implementation of this proposal. In this section we give a conceptual design of the low thermal inertia mold sketched in Figure 4-1 that satisfies the process requirements.

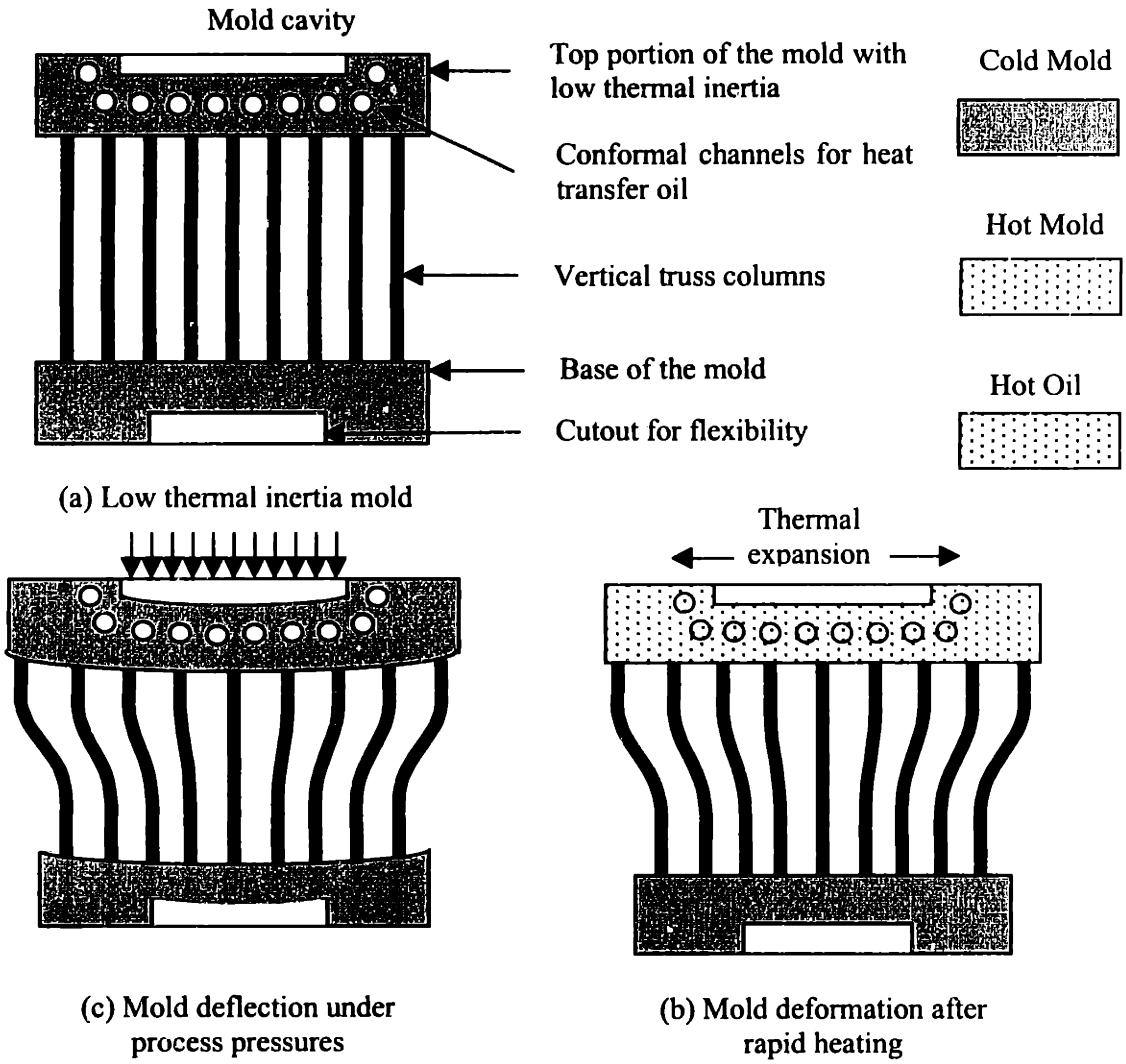

Figure 4-1 Concept of the low thermal inertia mold

Figure 4-1(a) shows the cavity insert of the low thermal inertia mold. It consists of a top plate, vertical truss columns and a bottom base. The top portion of the mold is a shell with low thermal mass. The conformal channels are embedded in the shell to provide the uniform and efficient temperature control to the cavity surface. The top shell is supported by vertical truss columns. The small cross section areas of truss columns minimize the heat conduction and insulate the top shell from the rest of the mold. With this design the top portion of the mold always keeps such a low thermal inertia that its temperature can be rapidly changed by hot and cold oil flowing through the embedded conformal channels. The functions of the truss structure are further illustrated in Figure 4-1(b) and 4-1(c). Figure 4-1(b) sketches the situation when the compressive process pressure (injection or packing pressure) is applied on the cavity surface. The flexibility of the truss structure and the cutout from the bottom of the mold allows a predictable deflection of the mold which has the potential to hold extra polymer melt for the compensation of the part shrinkage during the cooling stage. This idea will be further explored below. The truss structure also allows the free expansion /shrinkage of the top portion of the mold due to the temperature change, as shown in Figure 4-1(c). The displacement of the truss columns relieves thermal stresses in the shell and helps to extend the tool life.

The low thermal inertia mold discussed above is going to be used in a rapid thermal cycling process sketched in Figure 4-2. In the process the hot and the cold oil alternately flow through conformal channels embedded in the top portion of the mold to dynamically control the mold temperature. Before the injection cycle starts the hot oil flows through the conformal channel so that the shells of the core and the cavity inserts are heated up. Then two halves of the mold are clamped together to start the cycle. In the filling stage the shell portion of the mold keeps hot so that the plastic melt fills the cavity isothermally. At the end of the filling stage additional melt is packed into the cavity by the mold surface deflection under a certain packing pressure. Then the packing pressure is maintained and the heat transfer oil is switched to the cold to rapidly cool down the shell and the part. After the part is totally solidified it is ejected from the mold. In the mean time the heat transfer oil is switched back to the hot to heat up the top portion of the mold preparing for the next injection cycle.

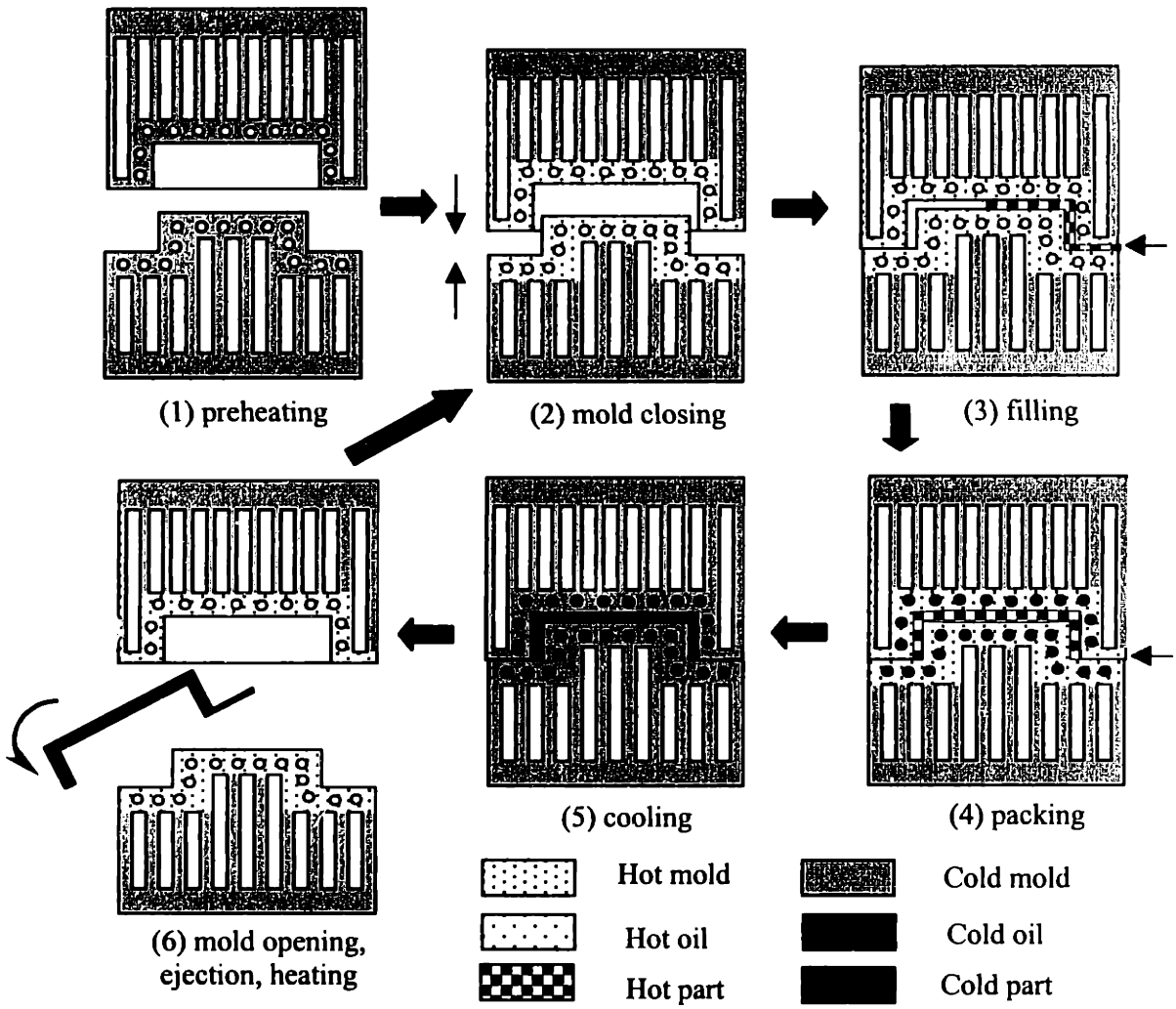

Figure 4-2 Procedure for rapid thermal cycling

The successful implementation of the process described above heavily depends on the ability to freely fabricate the insert shown in Figure 4-1. The Solid Freeform Fabrication (SFF) processes such as 3D Printing provides this freedom. The 3D Printing process has demonstrated its potential to build truss structures for rapid thermal cycling [Sachs et. al 1995]. The early stage experiment has shown advantages of rapid thermal cycling in improving the birefringence patterns of the molded part [Sun 1995]. The experimental success encouraged the further investigation of the physical background and the design methodology for rapid thermal cycling. In this chapter we will discuss models simulating four stages of a rapid thermal cycle (i.e. rapid heating, isothermal filling, packing and rapid cooling). In the next chapter we will discuss the detailed design and fabrication issues for rapid thermal cycling.

4.2 RAPID HEATING

At the beginning of a rapid thermal cycle, the mold cavity is rapidly heated up by the heat transfer oil flowing through conformal channels embedded in the shell portion of a low thermal inertia mold. This section models the rapid heating stage and guides the tool design and the heater selection. The models and analysis in this section are based on a simple mold plate shown in Figure 4-3, where 5 parallel channels are placed with uniform spacing in a thin shell. At $t = 0$ the insert mold temperature $T_{mold}{}^{0}$= 30 degC, the oil temperature $T_{oil}{}^{0}$= 220 degC. The rapid heating lasts for 2 seconds. Major dimensions of the tool are shown in the figure. As one will see in chapter 5, the model sketched here is actually half of the benchmark tool we have designed for the rapid thermal cycling test.

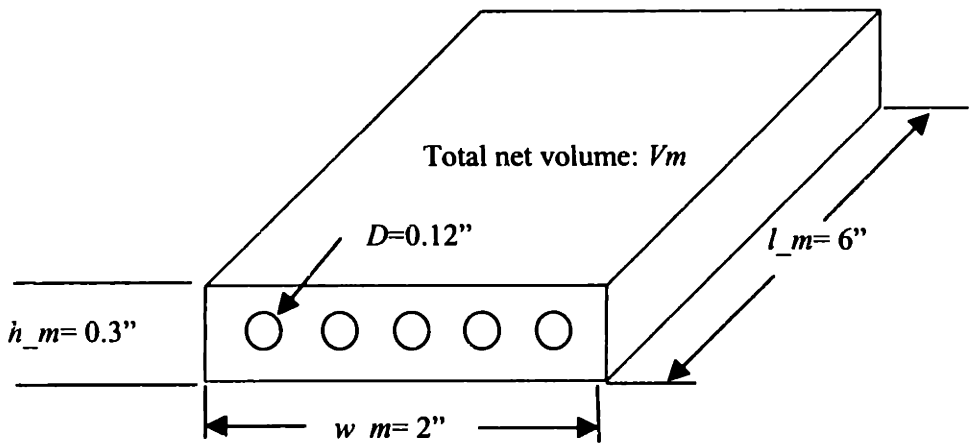

Figure 4-3 Sketch of the mold with conformal channels for rapid heating analysis

4.2.1 Analytical model for rapid heating

In chapter 2, we have discussed the mold heat transfer under the conformal cooling condition and have derived an expression for the mold time constant (equation 2-11) which is an indicator of the thermal response rate of the mold to the external energy change. This definition captures the characteristic thermal response of the mold regardless the process difference. Therefore the definition is also valid for the rapid heating case. In this chapter equation (2-11) is rewritten as below:

$$\tau = \frac{\rho_m c_m l_m^{\,2}}{K_m} + \frac{2\rho_m c_m l_m W}{h\pi D} \qquad (4\text{-}1)$$

In the above equation the first term captures the conductive heat transfer through the mold thickness, the second term captures the convective heat transfer through the heat transfer oil. As we have discussed in chapter 2, these two terms have similar order of the magnitude level while the second term is slightly smaller than the first.

Two extreme cases for equation (4-1) are infinite heat transfer coefficient and infinite thermal conductivity. The former corresponds with a constant cooling channel wall temperature. In this case the second term of equation (4-1) can be eliminated and the mold time constant τ_k is defined as:

$$\tau_k = \frac{\rho_m c_m l_m^{\,2}}{K_m} \tag{4-2}$$

This equation defines the mold time constant as a function of the mold material properties and the oil channel location with respect to the mold wall. It is used in the design stage to roughly estimate the mold surface temperature response without considering the detail issues of the cooling line design.

The other extreme case is when the mold material has the infinite thermal conductivity. In this case the first term of equation (4-1) can be eliminated and the mold time constant τ_h is expressed as:

$$\tau_h = \frac{\rho_m c_m l_m W}{\frac{1}{2}\pi D h} \tag{4-3}$$

This is actually the lumped model for rapid heating assuming that there is no temperature gradient in the mold. If we multiply the numerator and denominator by the cooling line length L, we obtain the mold time constant as a function of the mass of the mold material that needs to be heated and the total surface area of the conformal channels:

$$\tau_h = \frac{c_m M}{hA} \tag{4-4}$$

where M is the total mass of the mold, A is the total surface area of the conformal channels, h is the heat transfer coefficient.

In a practical design case, equation (4-1) is used for rough estimation of the mold time constant without the considering the oil channel design details, equation (4-4) helps to find the required oil channel

size and flow rate in order to hit the target mold response time in rapid heating. In the design of the benchmark tool discussed in the next chapter, the ratio between the conductive and the convective terms in equation (4-1) is about 1:0.88.

Since we have defined the mold time constant, the response of the mold temperature to the given oil temperature can thus be expressed as:

$$T_m(t) = T_{oil}{}^0 + (T_m{}^0 - T_{oil}{}^0)e^{-t/\tau} \qquad (4\text{-}5)$$

where $T_{oil}{}^0$ is the oil temperature, $T_m{}^0$ is the initial mold temperature, τ is the mold time constant defined by equation (4-1).

For a mold with the size discussed in previous section and with the initial temperature of 30 degC, if we heat up the mold using the hot oil of 220 degC with a flow rate of 5GPM, the mold surface temperature will end up with 173 degC after 2 seconds.

4.2.2 2D numerical model for rapid heating

A 2D numerical model is proposed to simulate the heat transfer of the mold and the oil along the oil line. Figure 4-4 shows how 3D mold and oil channels are converted to the 2D equivalence. As shown in the figure, two parallel plates of infinite length in the z direction are used to model the mold. The hot oil flow is simulated as a one-dimensional flow in y direction between two parallel plates. In order to make this conversion valid, the following two rules should be observed: 1) the product of the heat transfer coefficient and the cooling area at the mold and hot oil interface should be the same for the 3D model as that for the 2D model. 2) the 2D model should have the same thermal mass as the 3D model. The application of above two rules yields the equivalent heat transfer coefficient *hc_eq* and the equivalent distance from the oil channel to the mold wall *l_eq* as below:

$$hc\_eq = \frac{h \cdot \pi D}{2w} \qquad (4\text{-}6)$$

$$l\_eq = ((2l_m + D) \cdot w - \frac{1}{4}\pi D^2)/2w \qquad (4\text{-}7)$$

where h is the heat transfer coefficient of the hot oil, D is the oil channel diameter, w is the oil channel pitch distance, and l_m is the distance from the oil channel to mold wall.

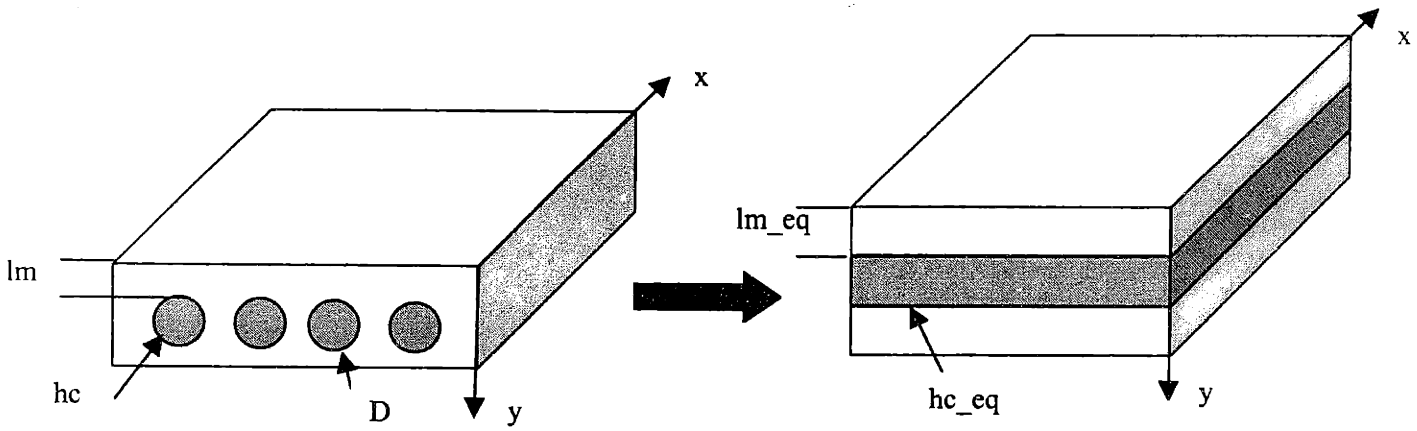

(a) Actual mold and oil channels (b) 2D equivalence of the mold and oil channels

Figure 4-4 Conversion from the 3D circular hot channel model to its 2D equivalence

The *xy* plane projection of the 2D equivalent model in Figure 4-4(b) is sketched in Figure 4-5. The flow direction and the equivalent distance from the oil channel to the mold wall *l_eq* can be clearly seen from this figure.

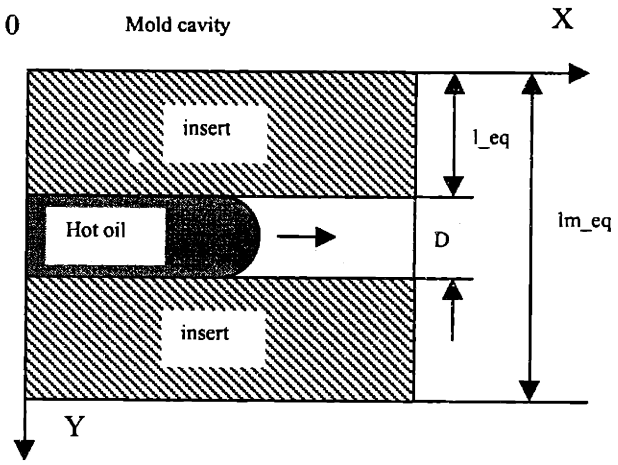

Figure 4-5 2D sketch of the mold and the hot oil on xy plane

A Microsoft Excel spreadsheet was designed for 2D heat transfer analysis during rapid heating. A Visual Basic macro function was written and embedded into the spreadsheet to simulate the transient heat transfer when hot oil flows through the insert. The mold and the oil temperature distribution after 0.1, 0.5, 1.0, 1.5 and 2 seconds of rapid heating are shown in Figure 4-7. In these figures the x axis is the distance along the oil channel and the y axis is the vertical distance to the mold surface. The labels "upper" and "lower" correspond with the upper and lower boundary of the wall of cooling channels. Between "upper" and "lower" is the hot oil temperature. The mold material for this simulation is 316 stainless steel with thermal conductivity of 26.3 W/m-K.

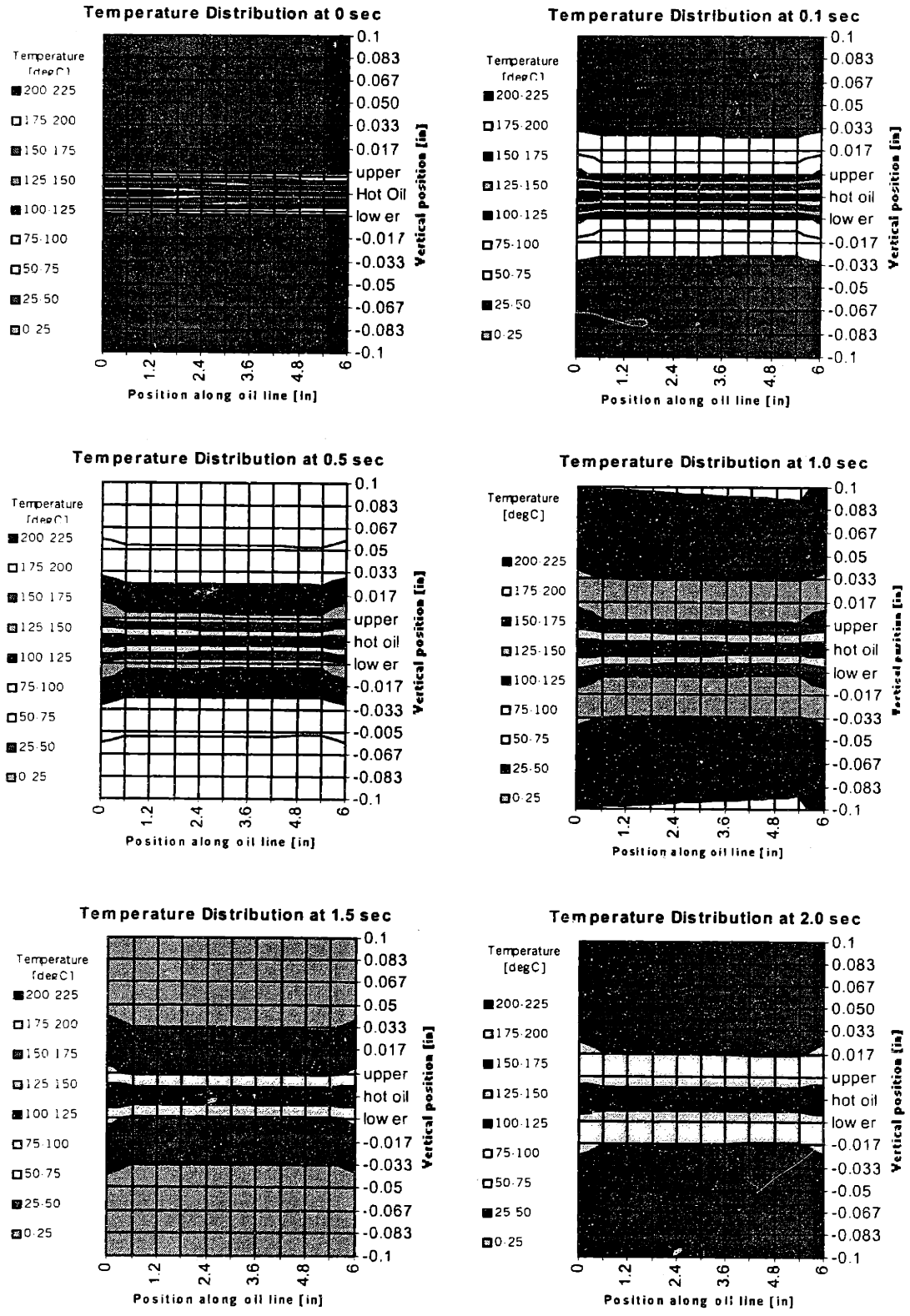

Figure 4-6 Mold surface temperature distribution after 0, 0.1,0.5,1.0,1.5 and 2 seconds of rapid heating

y coord \x coord [in]	0.59	1.18	1.77	2.35	2.94	3.53	4.12	4.71	5.30	5.89	6.50
0.1	156.6	154.1	154.0	153.9	153.8	153.6	153.5	153.4	153.3	153.2	155.5
0.083	157.5	155.0	154.9	154.8	154.6	154.5	154.4	154.3	154.2	154.1	156.4
0.067	160.3	157.6	157.5	157.4	157.3	157.2	157.1	156.9	156.8	156.7	159.2
0.05	164.8	162.0	161.8	161.7	161.6	161.5	161.4	161.3	161.1	161.0	163.7
0.033	171.1	167.8	167.7	167.6	167.5	167.4	167.3	167.2	167.0	166.9	170.1
0.017	179.3	175.1	175.0	174.9	174.8	174.7	174.6	174.5	174.3	174.2	178.3
upper	190.4	183.6	183.5	183.4	183.3	183.2	183.1	183.0	182.9	182.8	189.4
hot oil	220.0	219.9	219.8	219.7	219.6	219.5	219.4	219.3	219.3	219.2	219.2
lower	190.4	183.6	183.5	183.4	183.3	183.2	183.1	183.0	182.9	182.8	189.4
-0.017	179.3	175.1	175.0	174.9	174.8	174.7	174.6	174.5	174.3	174.2	178.3
-0.033	171.1	167.8	167.7	167.6	167.5	167.4	167.3	167.2	167.0	166.9	170.1
-0.05	164.8	162.0	161.8	161.7	161.6	161.5	161.4	161.3	161.1	161.0	163.7
-0.067	160.3	157.6	157.5	157.4	157.3	157.2	157.1	156.9	156.8	156.7	159.2
-0.083	157.5	155.0	154.9	154.8	154.6	154.5	154.4	154.3	154.2	154.1	156.4
-0.1	156.6	154.1	154.0	153.9	153.8	153.6	153.5	153.4	153.3	153.2	155.5

Table 4-1 Mold temperature profile after 2 seconds of rapid heating

Table 4-1 lists the mold temperature distribution after 2 seconds of rapid heating. The first row is the x position along the oil channel. The first column is the y position across the mold thickness. Label "hot oil" corresponds with the hot oil line. Label "upper" is the upper boundary of the oil channel. Label "lower" is the lower boundary of the channel. Label "0.1" corresponds with the mold surface, which is 0.1 inch away from the oil channel. As one can see from the table the mold temperature rises up to 154 degC with a variation less than 2 degC after 2 seconds of rapid heating. The oil temperature along the channel rises by less than 1 degC after 2 seconds of rapid heating.

4.2.3 Comparison of the analytical and the numerical models

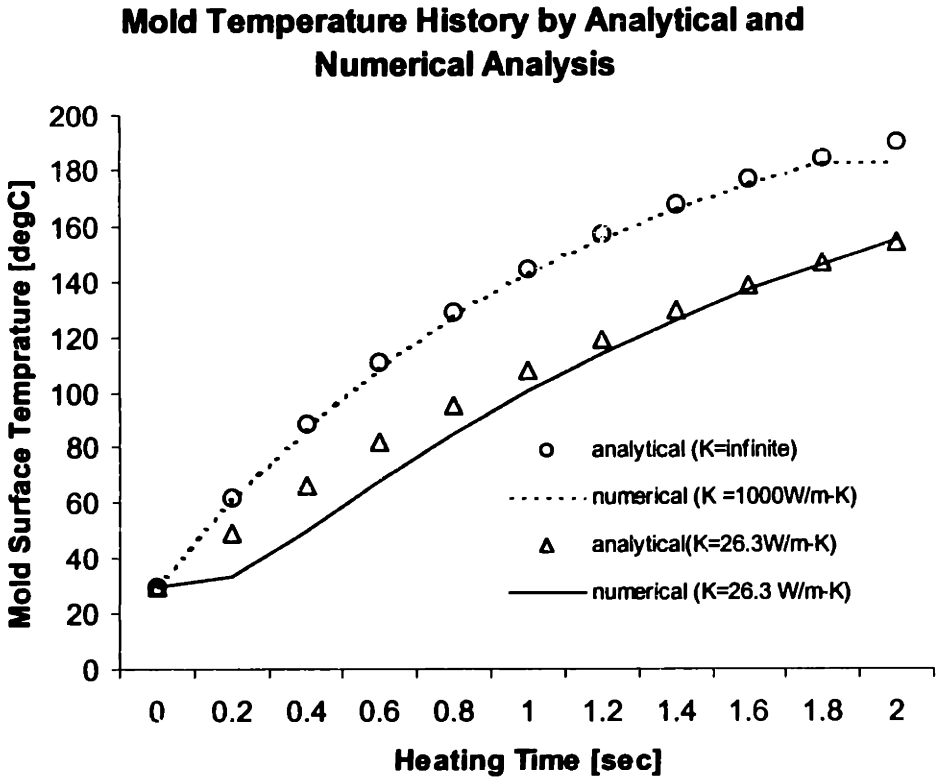

Figure 4-7 Analytical and numerical results for the mold surface temperature history in rapid heating

In the last two sections we have discussed the analytical and the numerical models for rapid heating. Figure 4-7 plots the averaged mold surface temperature histories predicted by these two models for both the low thermal conductivity (26.3 W/m-K) and the extremely high thermal conductivity (1000 W/m-K). The former is a typical value for 3D printed stainless steel / bronze. The latter is an approximation of the lumped object because the mold temperature tends to be uniformly distributed as the thermal conductivity increases. For the analytical model we first calculated the equivalent distance from the oil channel to the mold surface and the equivalent heat transfer coefficient based on equations (4-6) and (4-7). Then we put these equivalent parameters into equation (4-1) to get the mold time constant. This time constant is an averaged time constant of the entire mold. As to the numerical simulation the mold temperature value is obtained by averaging the mold surface temperature values at different locations. As one can see from the figure, the numerical and the analytical results show a high agreement.

4.2.4 Heat transfer analysis along the oil line

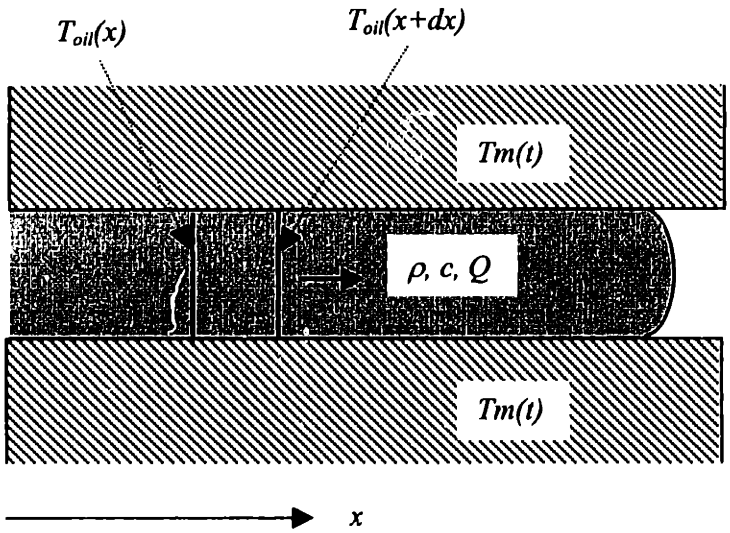

Figure 4-8 Sketch for the heat transfer analysis along the oil line

Figure 4-8 shows the mold and the oil heat transfer along the oil line. The heat exchanger analysis in [Mills 1995] yields the following expression for the hot oil temperature $T_{oil}(x,t)$:

$$\rho c Q \frac{dT_{oil}}{dx} = -h\pi D(T_{oil} - T_m) \qquad (4\text{-}8)$$

This equation yields the hot oil temperature as a function of the heating length and the mold wall temperature:

$$T_{oil} = T_m + (T_{oil}^0 - T_m)e^{-\frac{h\pi D}{\rho c Q}x} \qquad (4\text{-}9)$$

In the above expression, h is the heat transfer coefficient, L is the oil channel diameter, ρ is the density of the heat transfer oil, c is the specific heat of the oil, Q is the flow rate of the oil, T_m is the mold wall temperature history. Equation (4-9) is used to design the oil channel size and the flow rate for the maximum oil temperature drop along the channel. The application of the above equation to the mold sketched in Figure 4-3 with hot oil flow rate of 5GM yields a oil temperature drop along the oil line from 10degC (beginning of rapid heating) to 3degC(after 2 seconds of rapid heating). The numerical simulation shows a temperature drop from 5degC to 1degC. The relatively larger temperature value predicted by the analytical model is caused by using the lumped mold temperature to represent the actual oil channel wall temperature.

4.2.5 Energy consumption for rapid heating

From the design point of view it is very important to figure out the total energy consumed during rapid thermal cycling. According to the lumped model discussed in section 4.2.1, the total energy consumed by heating the mold for t seconds is:

$$E_m(t) = \rho_m c_m V_m (T_m(t) - T_m^0) \tag{4-10}$$

where T_m^0 is the initial mold temperature, V_m is the total volume of the mold.

For the tool proposed in Figure 4-1, the energy consumed by the truss support should also be included in consideration of the heater's power calculation. The heat diffusion distance to the truss columns in a given heating time t_{heat} (typically 2 seconds) is:

$$l_t = \sqrt{\alpha_m t_{heat}} \tag{4-11}$$

The total volume of the mold V_m in equation (4-10) is therefore the summation of the top plate of the mold and part of the truss columns with length l_t:

$$V_m = n[w(2l_m + D) - \frac{1}{4}\pi D^2] + A_t l_t \tag{4-12}$$

where n is the total number of conformal channels, w is the cooling line pitch distance, l_m is the distance from the oil channel to the mold wall, D is the oil channel diameter, A_t is the cross section area of the entire truss columns, l_t is the heat diffusion distance into truss columns.

The application of above equations on the tool sketched in Figure 4-3 with a thermal conductivity of 26.3 W/m-K yields a total energy consumption of 25,030 J. If the cycle time is designed 10 seconds, a heater of at least 2.5kw should be selected.

For the 2D model in section 4.2.2 a numerical expression of the total energy loss is obtained by integrating the difference of the oil temperature and the mold temperature along the oil channel within a given heating time:

$$E_{loss} = \iint h_c \cdot 2w \cdot (T_o(t,x) - T_m(t,x)) \cdot dmdt \tag{4-13}$$

where $T_0(t,x)$ is the oil temperature history, $T_m(t,x)$ is the mold temperature history .

The numerical expression in (4-13) yields a total energy consumption of 23393 J for the same tool sketched in Figure 4-3. This result is very close to that predicted by the lumped model. Similar

calculation for the final benchmark tool discussed in chapter 5 indicates that a 20KW heater is required for rapid heating of two mold inserts.

4.3 ISOTHERMAL FILLING

In an isothermal filling stage, the mold is heated up to a high temperature above the polymer glass temperature so that no vitrifrication happens in filling. The practical advantages of isothermal filling include a smaller process pressure, the elimination of the short shot defect, the lower injection pressure, the lower melt temperature, the isotropic mechanical behavior of the molded part and the birefringence pattern improvement for the molded part. The theoretical significance of isothermal filling is that it uncouples the filling stage and the cooling stage. In the following sections we will discuss governing equations for isothermal filling.

4.3.1 Polymer property and rheology

The molecular structure of polymers used in injection molding directly influences the physical and rheological properties of the material. Two basic types of materials are thermosets and thermoplastics [Bown 1978, Belofsky 1995]. Thermosetting materials are formed by a cross-linking process. In such a process molecules of separate entities are chemically bonded together to form a rigid three dimensional lattice structure. Typical thermosetting materials include Phenol-formaldehyde (PF), Urea-formaldehyde(UF) and Laminating resins (UP). Thermosetting materials will not re-melt on heating. The second group of plastic materials is thermoplastics. Thermoplastics are formed without chemical joining. Therefore these materials can be made fluid by heating and solidifying by cooling for a number of times. Thermoplastic materials are further classified into amorphous and semi-crystalline types according to their ability to form a regular lattice shape as the melt cools. Typical amorphous thermoplastics are PS, PC, PEEK, PMMA, ABS, etc. Typical semi-crystalline materials are PP, LDPE, HDPE, PTFE, PET, etc. The crystalline nature of a bulk polymer has a major effect on its properties. Amorphous polymers are typically transparent, with high toughness, high ductility, low density and lower residual stresses. Semi-crystalline polymer is typically opaque, with high strength, high stiffness and high fatigue resistance. To some extent the morphology can be controlled by varying processing parameters such as the cooling time. In the rapid thermal cycling project we will first focus on thermoplastic materials instead of thermosetting ones because of the following reasons: 1) injection molding of the thermosetting plastic molding requires major modification of the injection molding machine because of the chemical reaction involved. 2) thermosetting plastic materials are typically opaque and make the evaluation of the molecular orientation and the residual stress difficult. 3) thermoplastic materials are more commonly used in the

plastic industry because they are recyclable and help to protect the environment. 4) injection molding of the thermoplastic materials involves more design and fabrication problems that can be solved by introducing SFF processes and new design methodology. It is reasonable to start the project with thermoplastic materials. As the rapid thermal cycling process matures, this technique can also be used for a wide range of the molding processes such as reaction injection molding, compression molding and die casting.

In this project amorphous thermoplastics such as PS and PC are used because their transparent features make the observation of residual stresses relatively easier. The models and design rules in this thesis are therefore based on these types of materials. However this does not mean that the rapid thermal cycling process discussed here only limited to amorphous materials. On the contrary the process is especially beneficial to semi-crystalline and thermoset materials in the sense that the dynamic control of the process temperature will significantly influence the polymer microstructure.

The flow behavior of the polymer melt is studied by polymer rheology[Kennedy 1995]. For a Newtonian flow the shear stress and shear rate is proportional, and the viscosity μ is the constant of proportionality:

$$\tau = \mu \dot{\gamma} \tag{4-14}$$

Viscosity μ is further expressed as a function of fluid temperature and pressure defined in the following equation [Kennedy 1995]:

$$\mu(T,P) = \mu_0 e^{E/R[1/T-1/T_0]} e^{\beta(P-P_0)} \tag{4-15}$$

where E is the empirical activation energy for the material, R is the universal gas constant, μ_0, T_0, P_0, are reference values; and β is an empirical pressure coefficient.

Newtonian flow is a simple assumption of the polymer flow. Most thermoplastic melts show Newtonian behavior at very low shear rates or very high shear rates. For the in-between values of shear rates, the polymer flow is non-Newtonian. Various models have been developed to predict the non-Newtonian viscosity as a function of the shear strain/shear stress. These models include the power law model, the second order model, the Ellis model, the Carreau model and the Cross model.

1) The power law model:

$$\mu = m\dot{\gamma}^{n-1} \tag{4-16}$$

where n is the flow index, m is the consistency which is further defined by the expression below in order to account for the effect of temperature and pressure [Kennedy 1995]:

$$m = m_0 e^{E/R[1/T-1/T_0]} e^{\beta(P-P_0)} \tag{4-17}$$

2) The second order model [Kennedy 1995]:

$$\ln\mu = A_0 + A_1 \ln\dot{\gamma} + A_2 T + A_3 (\ln\dot{\gamma})^2 + A_4 T \ln\dot{\gamma} + A_5 T^2 \tag{4-18}$$

where the A_i are constants depending on the polymer materials.

3) The Ellis model [Kennedy 1995]:

$$\mu = 1 + \left(\frac{\tau}{\tau_{1/2}}\right)^{\alpha-1} \tag{4-19}$$

where $\tau_{1/2}$ is the value of shear stress for which $\mu = \mu_0/2$ and α-1 is the slope of the graph $\ln[\mu_0/\mu)$-2] versus $\ln(\tau/\tau_{1/2})$.

4) Carreau model [Kennedy 1995]:

$$\frac{\mu - \mu_\infty}{\mu_0 - \mu_\infty} = [1 + (\lambda\dot{\gamma})^2]^{(n-1)/2} \tag{4-20}$$

where μ_∞ is the viscosity at infinite shear rate, μ_0 is the viscosity at zero shear rate, n is melt index ranging from 0 to 1, and λ is a time constant.

5) Cross model [Kennedy 1995]:

$$\mu = \frac{\mu_0}{1 + (\mu_0\dot{\gamma}/\tau^*)^{1-n}} \tag{4-21}$$

where t^* is the shear stress at the transition between Newtonian and power law behavior.

In a rapid thermal cycling process, the isothermal filling ensures that no solidification occurs during the filling stage. This makes the traditional process conditions such as a high injection speed, a high melt temperature or a high injection pressure not necessary. As we will discuss in the following chapters, the shear rate in an isothermal filling stage is very low so that the Newtonian model can be used to roughly estimate the isothermal flow.

4.3.2 Governing equations for injection molding

The general equations that govern the behavior of a fluid motion are the equation of continuity, the equations of motion and the equation of energy, as shown below [Tadmor & Gogos 1988]:

Equation of Continuity:

$$\frac{\partial \rho}{\partial t}+\frac{\partial}{\partial x}(\rho v_x)+\frac{\partial}{\partial y}(\rho v_y)+\frac{\partial}{\partial z}(\rho v_{zx})=0 \tag{4-22}$$

Equations of Motion:

x component:

$$\rho\left(\frac{\partial v_x}{\partial t}+v_x\frac{\partial v_x}{\partial x}+v_y\frac{\partial v_x}{\partial y}+v_z\frac{\partial v_x}{\partial z}\right)=-\frac{\partial P}{\partial x}+ \\ \frac{\partial}{\partial x}\left(2\mu\frac{\partial v_x}{\partial x}\right)+\frac{\partial}{\partial y}\left(\mu\left(\frac{\partial v_y}{\partial x}+\frac{\partial v_x}{\partial y}\right)\right)+\frac{\partial}{\partial z}\left(\mu\left(\frac{\partial v_x}{\partial z}+\frac{\partial v_z}{\partial x}\right)\right)+\rho g_x \tag{4-23}$$

y component:

$$\rho\left(\frac{\partial v_y}{\partial t}+v_x\frac{\partial v_y}{\partial x}+v_y\frac{\partial v_y}{\partial y}+v_z\frac{\partial v_y}{\partial z}\right)=-\frac{\partial P}{\partial y}+ \\ \frac{\partial}{\partial y}\left(2\mu\frac{\partial v_y}{\partial y}\right)+\frac{\partial}{\partial x}\left(\mu\left(\frac{\partial v_y}{\partial x}+\frac{\partial v_x}{\partial y}\right)\right)+\frac{\partial}{\partial z}\left(\mu\left(\frac{\partial v_x}{\partial z}+\frac{\partial v_z}{\partial x}\right)\right)+\rho g_y \tag{4-24}$$

z component:

$$\rho\left(\frac{\partial v_x}{\partial t}+v_x\frac{\partial v_z}{\partial x}+v_y\frac{\partial v_z}{\partial y}+v_z\frac{\partial v_z}{\partial z}\right)=-\frac{\partial P}{\partial z} \\ +\frac{\partial}{\partial z}\left(2\mu\frac{\partial v_z}{\partial z}\right)+\frac{\partial}{\partial y}\left(\mu\left(\frac{\partial v_y}{\partial x}+\frac{\partial v_x}{\partial y}\right)\right)+\frac{\partial}{\partial z}\left(\mu\left(\frac{\partial v_x}{\partial z}+\frac{\partial v_z}{\partial x}\right)\right)+\rho g_z \tag{4-25}$$

Equation of Energy:

$$\rho c_v\left(\frac{\partial T}{\partial t}+v_x\frac{\partial T}{\partial x}+v_y\frac{\partial T}{\partial y}+v_z\frac{\partial T}{\partial z}\right)=k\left[\frac{\partial^2 T}{\partial x^2}+\frac{\partial^2 T}{\partial y^2}+\frac{\partial^2 T}{\partial z^2}\right]+$$

$$2\mu\left\{\left(\frac{\partial v_x}{\partial x}\right)^2+\left(\frac{\partial v_y}{\partial y}\right)^2+\left(\frac{\partial v_z}{\partial z}\right)^2\right\}+ \qquad (4\text{-}26)$$

$$\mu\left\{\left(\frac{\partial v_x}{\partial y}+\frac{\partial v_y}{\partial x}\right)^2+\left(\frac{\partial v_x}{\partial z}+\frac{\partial v_z}{\partial x}\right)^2+\left(\frac{\partial v_y}{\partial z}+\frac{\partial v_z}{\partial y}\right)^2\right\}$$

In above equations, μ is the viscosity which depends on the invariant of the rate of deformation tensor and temperature. v_x, v_x, v_x are x, y and z components of the velocity vector, P is the pressure, T is the temperature. The coordinate system for the above equations is defined in Figure 4-9. The polymer flow is in xy plane. z is the part thickness direction.

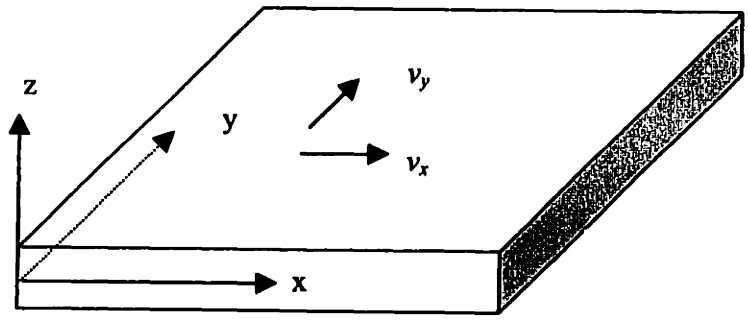

Figure 4-9 Coordinate system for the flow analysis in injection molding

In order to derive the governing equations for the polymer flow in the filling stage of a typical injection molding process, the following assumptions are made:

1) The polymer melt is incompressible
2) The thermal conductivity of the material is constant
3) The cavity thickness is very small so that the velocity component in the thickness direction (z direction) is negligible compared with those in other directions (x and y directions)
4) Gravitational forces are negligible
5) Inertial forces are negligible
6) Energy change due to volumetric change of the polymer melt in x and y directions is negligible
7) Energy change due to conduction in x and y directions is negligible
8) Convective heat transfer in z-direction is negligible

It is also beneficial to list characteristic values for typical injection molding processes:

- Cavity thickness: H = 1e-3 m
- Cavity length: $L >> H$
- Melt velocity: V = 1e-1m/s
- Cavity pressure: p_0 = 1e7 Pa
- Melt viscosity: μ =1e4 Ns/m^2
- Thermal expansion coefficient: β = 1e-3 1/K
- Melt density: ρ = 1e3Kg/m^3
- Temperature difference between mold and melt: ΔT = 1e2 K

- Melt thermal conductivity: K = 1e-1 W/m-K
- Specific heat of melt: c_p = 1e3 J/kg-K

The above assumptions and characteristic values enable us to drop out several terms in order to simplify the governing equations for injection molding. The simplification follows the procedure below:

In the equation of continuity (4-22):

1) For incompressible flow the density is not a function of time, therefore the first term is dropped out.
2) Under the assumption that the polymer flow keeps the uniform density in the filling stage, the density term can be removed from (4-22)

Therefore we have a simplified form of the continuity equation as:

$$\frac{\partial v_x}{\partial x}+\frac{\partial v_y}{\partial y}+\frac{\partial v_z}{\partial z}=0 \qquad (4\text{-}27)$$

In equations of motion (4-23) –(4-25), starting from the left side, the first terms are changes of momentum, the second to the fourth terms are inertial forces. On the right side, the first terms are pressure gradient, the second to the fourth terms are viscous forces and the last terms are forces due to gravity. The order of magnitude analysis can be performed for each term in the momentum equations in order to determine if it is negligible. For convenience let us first define the ratio of the cavity thickness versus the cavity length as:

$$\delta = H/L << 1 \qquad (4\text{-}28)$$

Let us do the order of magnitude analysis for x component of the momentum equations.

$$O\left[\rho\frac{\partial v_x}{\partial t}\right]=O\left[\rho\frac{V}{t}\right]=O\left[\rho\frac{V^2}{H}\right]=O\left[10^4\delta\right] \qquad (4\text{-}29)$$

$$O\left[\rho v_x\frac{\partial v_x}{\partial x}\right]=O\left[\rho V\frac{V}{L}\right]=O\left[10^4\delta\right] \qquad (4\text{-}30)$$

$$O\left[\rho v_y\frac{\partial v_x}{\partial y}\right]=O\left[\rho V\frac{V}{L}\right]=O\left[10^4\delta\right] \qquad (4\text{-}31)$$

$$O\left[\rho v_z \frac{\partial v_x}{\partial z}\right] = O\left[\rho \delta V \frac{V}{H}\right] = O[10^4 \delta] \tag{4-32}$$

$$O\left[\frac{\partial P}{\partial x}\right] = O\left[\frac{P}{L}\right] = O[10^{10} \delta] \tag{4-33}$$

$$O\left[\frac{\partial}{\partial x}\left(2\mu \frac{\partial v_x}{\partial x}\right)\right] = O\left[2\frac{V}{L^2}\right] = O[10^9 \delta] \tag{4-34}$$

$$O\left[\frac{\partial}{\partial y}\left(\mu \frac{\partial v_y}{\partial x}\right)\right] = O\left[\mu \frac{V}{L^2}\right] = O[10^9 \delta] \tag{4-35}$$

$$O\left[\frac{\partial}{\partial x}\left(\mu \frac{\partial v_x}{\partial y}\right)\right] = O\left[\mu \frac{V}{L^2}\right] = O[10^9 \delta] \tag{4-36}$$

$$O\left[\frac{\partial}{\partial z}\left(\mu \frac{\partial v_x}{\partial z}\right)\right] = O\left[\mu \frac{V}{H^2}\right] = O[10^9] \tag{4-37}$$

$$O[\rho g_x] = O[10^4] \tag{4-38}$$

The above analysis leads to a simplified form of the x component of the momentum equations as:

$$\frac{\partial p}{\partial x} = \frac{\partial}{\partial z}(\mu \frac{\partial v_x}{\partial z}) \tag{4-39}$$

The similar analysis for y and z comments yields:

$$\frac{\partial p}{\partial y} = \frac{\partial}{\partial z}(\mu \frac{\partial v_y}{\partial z}) \tag{4-40}$$

$$\frac{\partial p}{\partial z} = 0 \tag{4-41}$$

Following the same procedure discussed above we can also obtain the simplified form for the energy equation as below:

$$\rho c_p (\frac{\partial T}{\partial t} + v_x \frac{\partial T}{\partial x} + v_y \frac{\partial T}{\partial y}) = K \frac{\partial^2 T}{\partial z^2} + \mu[(\frac{\partial v_x}{\partial z})^2 + (\frac{\partial v_y}{\partial z})^2] \tag{4-42}$$

Equations (4-20), (4-32), (4-33), (4-34) and (4-35) form the governing equations for the polymer flow in an injection molding process.

Now let us take a look at the isothermal filling process where the following characteristic values are observed different from the normal injection molding:

- Cavity thickness, H = 1e-3m (It is theoretically true that we can make the part thickness as small as possible with isothermal filling. However other issues limits the smallest thickness we can reach. The target part thickness in this project is larger than 0.02")
- Melt velocity: V = 1e-2m/s (lower injection speed is allowed)
- Cavity pressure: p_0 = 5e3 psi (lower injection pressure is allowed)
- Melt viscosity: μ =1e3 Ns/m^2 (high mold temperature leads to low viscosity)
- Temperature difference between mold and melt: ΔT = 1K

The order of magnitude analysis yields the same expressions for the continuity equation and the momentum equations as the typical injection molding process. However for the energy equation there is a little bit different. In the expression of the energy equation, we have:

$$O\left[\rho c_p \frac{\partial T}{\partial t}\right] = \left[\rho c_p \frac{\Delta T V}{L}\right] = \left[10^7 \delta\right] \tag{4-43}$$

$$O\left[\rho c_p v_x \frac{\partial T}{\partial x}\right] = \left[\rho c_p \frac{\Delta T V}{L}\right] = \left[10^7 \delta\right] \tag{4-44}$$

$$O\left[\rho c_p v_y \frac{\partial T}{\partial y}\right] = \left[\rho c_p \frac{\Delta T V}{L}\right] = \left[10^7 \delta\right] \tag{4-45}$$

$$O\left[K \frac{\partial^2 T}{\partial z^2}\right] = \left[K \frac{\Delta T}{H^2}\right] = \left[10^5\right] \tag{4-46}$$

$$O\left[\mu \left(\frac{\partial v_x}{\partial z}\right)^2\right] = \left[\mu \frac{V^2}{H^2}\right] = \left[10^6\right] \tag{4-47}$$

Obviously the above analysis yields similar levels magnitude for each terms. However the heat conduction term (first term on the right side of equation 4-26) is one magnitude lower than the viscous shear terms (second and third term on the right side). This means that in the isothermal filling the majority of the energy that lead to the temperature increase of the melt is due to the viscous shear. Although we can not neglect the heat conduction term in a serious analysis it is reasonable to consider only the viscous shear in estimating the polymer melt temperature rise. We will discuss this issue in the next section.

Typical molten polymers are non-Newtonian and exhibit viscoelastic effects. However the current research and the MoldFlow software does not account for viscoelasticity [Kennedy 1995]. Therefore we will also neglect the viscoelastic effect. W can define a class of fluids termed *generalized Newtonian fluids* which has the constitutive equation as below [Kennedy 1995, Tamdor & Gogos 1974]:

$$\underline{\tau} = \mu(\dot{\gamma})\underline{\dot{\gamma}} \tag{4-48}$$

where $\underline{\tau}$ is the stress tensor, $\mu(\dot{\gamma})$ is the viscosity function and $\underline{\dot{\gamma}}$ is the shear rate tensor.

In engineering design practice a constant viscosity of the polymer melt is always used to roughly estimate the pressure drop and the flow rate in the filling stage [Rao 1991, Malloy 1994, Middleman 1977]. For isothermal flow this estimation is reasonable because the isothermal flow eliminates the temperature variation in the melt which is one of major causes of the viscosity variation.

Another issue in isothermal filling is that the so called isothermal filling is not strictly isothermal. According to the energy equation (4-26), the viscous shear generates the heat that propagates through the melt and results in a minor temperature variation in the melt and the mold, even if the initial mold and melt temperatures are kept uniform. This part of heat should be taken into account in the design of a rapid thermal cycling process because the resulting melt temperature increase may degrade the polymer. This consideration sets an upper limit to the maximum injection speed that can be achieved.

4.3.3 One dimensional analysis for isothermal flow

In this chapter one-dimensional models are discussed for the simulation of the isothermal flow. The objective of these models is to provide mold designers with simple tools to estimate the filling process before using any sophisticated flow analysis packages. Two commonly used shapes are discussed: a thin part modeled by a slab and a runner modeled by a cylinder.

4.3.3.1 Thin part

Figure 4-10 shows the cross section of the polymer melt flowing between two parallel mold plates. The coordinate system is selected the same as that shown in Figure 4-8.

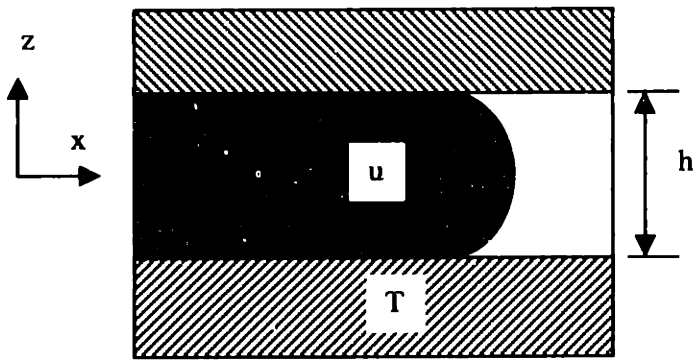

Figure 4-10 One dimensional isothermal melt flow through the mold cavity

The flow shown in Figure 4-10 is actually Poiseuille flow. The momentum equation for this flow is [Middelman 1977, :Malloy 1994]:

$$\frac{\partial p}{\partial x} = \mu \frac{\partial^2 u}{\partial z^2} \tag{4-49}$$

This equation yields [Malloy 1994]:

$$\Delta p = \frac{12 \mu L Q}{H^3 W} \tag{4-50}$$

where Δp is the pressure drop along the flow direction, Q is total flow rate, W is the width of the slab, L is the length of the slab, h is the thickness of the cavity and μ is the viscosity.

The maximum shear strain occurs at the mold wall boundary and is expressed as [Malloy 1994]:

$$\dot{\gamma}_{max} = \frac{H}{2 \mu L} \Delta p \tag{4-51}$$

The viscous shear heat is obtained by the energy equation in one dimensional case:

$$\rho c_p \left(\frac{\partial T}{\partial t} + u \frac{\partial T}{\partial x} \right) = K \frac{\partial^2 T}{\partial z^2} + \mu \left(\frac{\partial u}{\partial z} \right)^2 \tag{4-52}$$

For the steady polymer flow the first term on the left side of equation (4-52) is eliminated. This leads to a second order partial differential equation with respect to x and z. As we have discussed before,

the thermal conduction term is smaller than the viscous shear term. If we eliminate the first term on right side of equation (4-52), the resulting energy equation turns to be:

$$\rho c_p u \frac{\partial T}{\partial x} = \mu (\frac{\partial u}{\partial z})^2 \qquad (4\text{-}53)$$

If we consider the average velocity U and the nominal shear rate $\dot{\gamma}_B$, the above equation is expressed as:

$$\rho c_p U \frac{\partial T}{\partial x} = \mu \dot{\gamma}_B^{\,2} \qquad (4\text{-}54)$$

where U and $\dot{\gamma}_B$ are defined as:

$$U = \frac{Q}{HW} \qquad (4\text{-}55)$$

$$\dot{\gamma}_B = \frac{6U}{H} \qquad (4\text{-}56)$$

The resulting temperature rise as a function of the filling time is expressed below:

$$\Delta T = \frac{36 \mu L^2}{\rho c_p H^2 t_{fill}} \qquad (4\text{-}57)$$

An alternate expression by the nominal shear rate is:

$$\Delta T = \frac{6 \mu L}{\rho c_p H} \dot{\gamma}_B \qquad (4\text{-}58)$$

In above equations L is the length of the part, h is the thickness of the part, t_{fill} is the filling time. For the PC part with the length of 5" and the thickness of 0.1", if we set the melt temperature as 572 degC and the filling time as 2 seconds, the resulting temperature rise due to viscous heat is roughly 7.1 degC.

It is interesting to notice that Middleman [Middleman 1977] estimated the viscous heat based on the first law of thermodynamics. The resulting temperature rise is at the same order of magnitude as this analysis.

In the filling stage the polymer melt contacts the mold wall and cools down. The averaged temperature of the melt can be roughly estimated by equation (2-14). The rough estimation of the melt temperature drop due to conductive heat transfer can b obtained by neglecting the higher order terms in equation (2-14). The resulting temperature drop is thus:

$$\Delta T = \frac{2}{\pi^2}(T_{melt} - T_{mold})(1 - e^{-\frac{a_p \pi^2 t_{fill}}{H^2}}) \qquad (4\text{-}59)$$

The above expression yields a 10.3 degC melt temperature drop in 2 seconds for a mold temperature of 212degF in a conventional molding cycle. However for a rapid thermal cycle, if we set the mold temperature as 450degF, the resulting temperature drop due to thermal conduction is estimated 3.5degC for the same part discussed above. This estimation indicates that the temperature rise due to viscous heating is larger than the temperature drop due to heat conduction in the rapid thermal cycling process. This can explain why in isothermal filling the melt temperature at several spots is even higher than its original value, according to the flow analysis by MoldFlow in chapter 5.

4.3.3.2 Runner

The momentum equation for the Newtonian flow in a circular channel is [Middleman 1977]:

$$\frac{\partial p}{\partial x} = \frac{\mu}{r}\frac{\partial}{\partial r}(r\frac{\partial u}{\partial r}) \qquad (4\text{-}60)$$

The solution of the above equation yields [Middleman 1977, Malloy 1994]:

$$\Delta p = \frac{8\mu L Q}{\pi R^4} \qquad (4\text{-}61)$$

where Δp is the pressure drop along the flow direction, Q is total flow rate, R is the radius of the channel, L is the length of the channel and μ is the viscosity.

The maximum shear strain occurs at the mold wall boundary and is expressed as:

$$\dot{\gamma}_{max} = \frac{R}{2\mu L}\Delta p \qquad (4\text{-}62)$$

The viscous shear heat is obtained by the following energy equation:

$$\rho c_p(\frac{\partial T}{\partial t}+u\frac{\partial T}{\partial r})=\frac{K}{r}\frac{\partial}{\partial r}(r\frac{\partial T}{\partial r})+\mu\dot{\gamma} \qquad (4\text{-}63)$$

The viscous introduced temperature rise and thermal conduction introduced temperature drop in the runner system can be analyzed in the same way as shown in section 4.3.3.1 and will not be redundantly discussed here.

4.4 PACKING STAGE

4.4.1 Introduction

In a rapid thermal cycling process, an isothermal filling stage is followed by a packing stage where a relatively high packing pressure is applied at the gate, the coolant rapidly replaces the hot oil and the part starts to cool down. Packing pressure keeps until the gate is sealed. The major purpose for packing is to hold the polymer melt and supply the cavity with additional melt in order to compensate the shrinkage due to cooling. However the packing stage in a rapid thermal cycle faces three challenges. First of all, without frozen-while-filling as in a conventional molding process, the averaged melt temperature at the end of filling reaches a high point which leads to a large volumetric shrinkage in cooling. Second, while the hot oil is used for rapid heating purpose, it takes time to switch back to cold due to thermal inertia and the time delay of the circulation system. Third, the structure of the low thermal inertia mold does not allow a high packing pressure, therefore less amount of volumetric shrinkage can be compensated by pressure. Due to its importance in part dimensional control it is very necessary to investigate the packing process and define a proper process condition. Three different methods are proposed for better dimensional control: compensating shrinkage by mold deformation, setting a longer packing time and lowering the melt temperature.

4.4.2 State equations for polymer material

The polymer melt in the packing stage is considered compressible. The density of the melt changes with the process pressure and temperature. The pressure-volume-temperature relation for polymer materials during the packing stage is governed by a state equation first proposed by Spencer and Gilmore[Spencer et. al.]:

$$(P+P_0)(\frac{1}{\rho}-\frac{1}{\rho_0})=R_0T \qquad (4\text{-}64)$$

where P_0, ρ_0 and R_0 are material specified constants. For Polystyrene P_0 = 186Mpa, ρ_0 = 1220 Kg/M^3, and R_0 = 80 J/Kg-K.

A more complex expression of the PVT relation is given by Tait equation [Chen et. al]:

$$\rho = V_0(T)^{-1}[1 - C\ln(1 + \frac{P}{B(T)}]^{-1} \quad (4\text{-}65)$$

where V_0 and B are further expressed by functions of the temperature:

$$V_0(T) = b_1 + b_2(T - b_3) \quad (4\text{-}66)$$

$$B(T) = b_3 e^{-b_4 T} \quad (4\text{-}67)$$

In above equations, b_1, b_2, b_3, b_4, and b_5 are material specified constants. For polystyrene, b_1 = 9.6E-04 m^3/Kg, b2 = 2.2E-07 m^3/Kg-degC, b_3 = 2.44E+8N/m^2, b_4 = 4.14E-3/degC and b_5 = 100 degC.

The PVT relationship suggests that it is possible to use a high packing pressure to compensate most of the volumetric change during cooling. However a high packing pressure is not favorable for a rapid thermal cycling process because the tool strength has been somewhat sacrificed a little bit in order to achieve a low thermal inertia. In the next chapter we will discuss alternative methods for dimensional control given a relatively low packing pressure.

4.4.3 Part shrinkage control

Dimensional control is a key issue for most of manufacturing processes including injection molding. Packing and cooling stages in injection molding experience violent changes of process pressure and temperature which consequently introduce uncertainty in part dimensional accuracy. The state equation discussed above is one aspect of how the process pressure and temperature influence the final part dimension. There are other effects such as the warpage caused by process introduced residual stresses. A conventional method for part dimensional control is to use a large packing pressure. The theoretical base is the PVT relationship discussed above. As we know the volume of the polymer material becomes smaller when the molten polymer solidifies. A large packing pressure helps to compensate part of material shrinkage during cooling. We say "part of shrinkage" because the packing pressure for zero shrinkage is as high as 50,000psi, while a typical packing pressure for conventional injection molding ranges from 10,000psi to 20,000psi. The rest of the part shrinkage is compensated by packing additional melt through the gate into the mold cavity while the polymer is gradually solidified. The disadvantage of this method is the residual stress caused by the second flow and the non-uniform density distribution of the part.

The rapid thermal cycling project proposes two novel strategies for dimensional control. One is to lower the melt temperature, the other is to control the mold deformation.

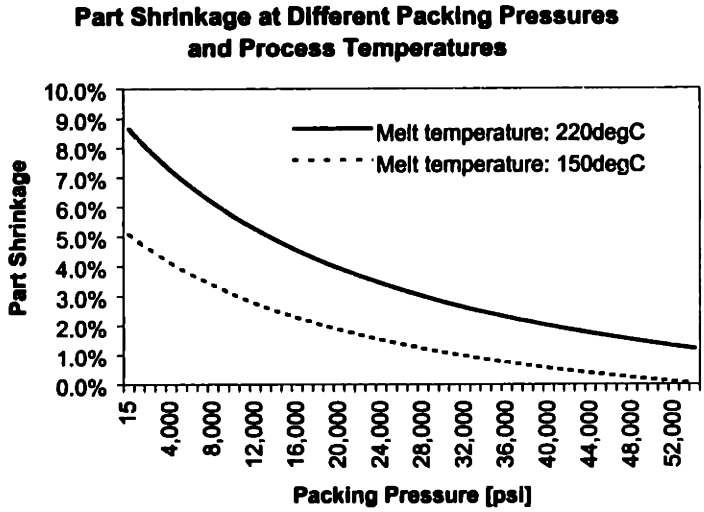

Figure 4-11 Part shrinkage versus packing pressure for different melt temperature for PS

The isothermal filling allows a relatively lower melt temperature that is beneficial for shrinkage compensation. The benefit is demonstrated in Figure 4-11 in which Polysterene material of different initial temperatures (220degC and 150degC) is packed under different packing pressures. The shrinkage values are calculated based on an ejection temperature of 50 degC. This figure suggests: a) with a maximum packing pressure of 5000 psi used in rapid thermal cycling, it is hard to compensate most of the thermal shrinkage. b) a lower processing temperature can be used as a substitute of high packing pressure for the part shrinkage control.

The second method for dimensional control is to design the stiffness of the insert so that the cavity deforms an amount under a given packing pressure in order to hold extra polymer melts that exactly compensates the part shrinkage. A mold insert with the truss support proposed in Figure 4-1 can be modeled as an elastic beam fixed with both ends and supported with the spring suspension, as sketched in Figure 4-12. This model yields equations for mold surface deflections at different locations shown in equation (4-62). In these equations the first term on the left side represents the mold surface deflection under the process pressure p_0, the second term corresponds to the deflection by the bending moment M, the n by n matrix is the stiffness matrix. The last term $(f_1, f_2, \ldots, f_n)$ represents the reactions of individual

springs and is further represented by (ky_1, ky_2, ..., ky_n), where k is the stiffness influence coefficient of the truss supports. The iterative calculation of these equations yields the deformed mold surface profile as plotted in Figure 4-13. This plot is based on a stainless steel mold supported by 9 springs with the equivalent spring constant of 1.75e+8 N/m. The mold thickness is 10mm. The mold projection area is 0.01m^2. The distributed injection pressure on the mold is 10,000 psi.

$$\begin{bmatrix} y1 \\ y2 \\ \cdots \\ yn \end{bmatrix} = \begin{bmatrix} \delta p1 \\ \delta p2 \\ \cdots \\ \delta pn \end{bmatrix} + \begin{bmatrix} \delta M1 \\ \delta M2 \\ \cdots \\ \delta Mn \end{bmatrix} + \begin{bmatrix} s_{11} & s_{12} & \cdots & s_{1n} \\ s_{21} & & & \\ \cdots & & & \cdots \\ s_{n1} & & \cdots & s_{nn} \end{bmatrix} \cdot \begin{bmatrix} f1 \\ f2 \\ \cdots \\ fn \end{bmatrix} \qquad (4\text{-}68)$$

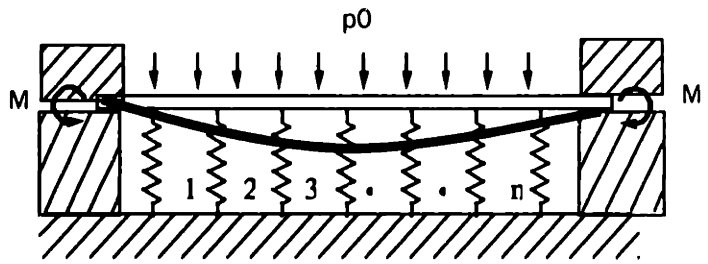

Figure 4-12 The beam-spring model for mold surface deflection prediction

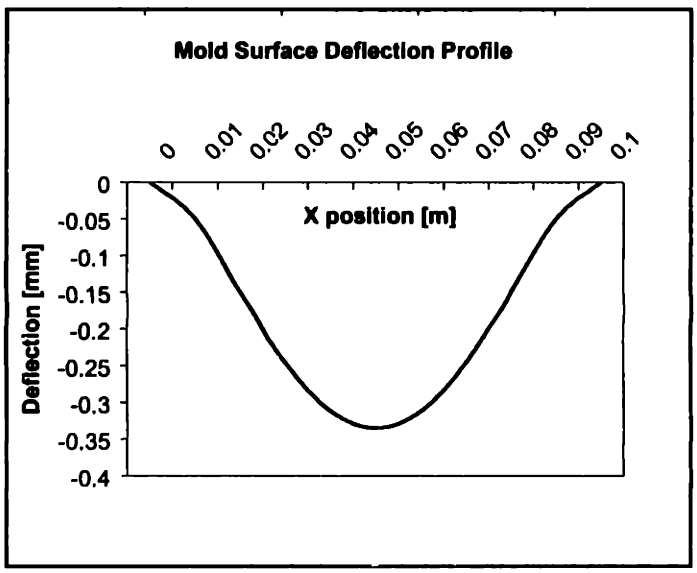

Figure 4-13 The mold deflection predicted by the beam-spring model

With the part shrinkage predicted by the P-V-T curve and the mold deflection predicted by the beam-spring model, it is possible to find an optimal operational point where the mold deflection compensates the part shrinkage, as shown in Figure 4-14. In this case, no packing of the additional melt through the gate is required at a proper operational point A. The part density and other mechanical properties are expected to be more uniform than the traditional molding method.

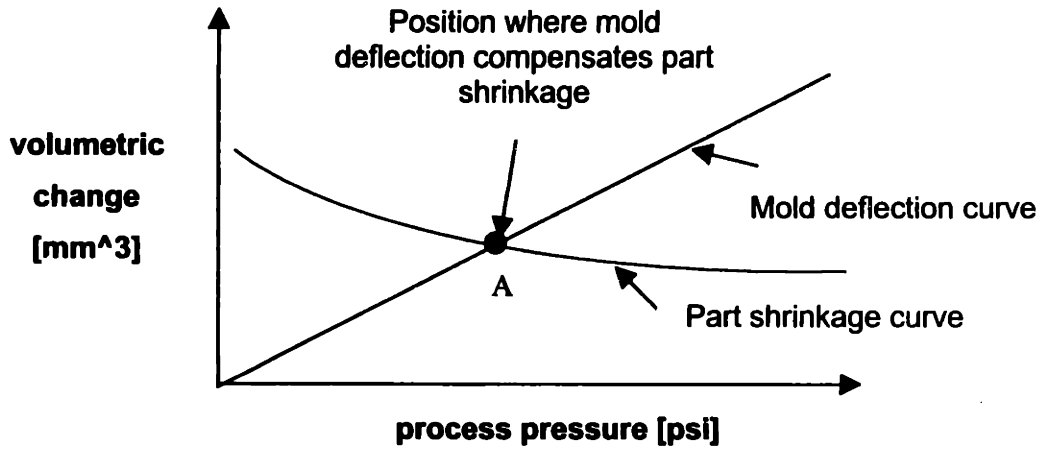

Figure 4-14 Sketch of the volumetric change versus process pressure curve for part cooling and mold deflection

4.5 COOLING STAGE

The cooling of the part starts right after the filling stage when the mold is cooled by the cold oil. With the 3D Printing technique complex internal cooling channels can be built inside the mold to achieve the conformal cooling effect. In the last chapter we have discussed the design methodology for conformal cooling based on the cycle averaged analysis. In this chapter we will build one-dimensional models for the transient heat transfer during the cooling stage. We will first discuss cooling of the part and the runner with consistent mold temperature boundary, then we will build a thermal circuit to simulate the mold and the part cooling.

4.5.1 Estimation of the cooling time with constant mold temperature

4.5.1.1 Part

An infinite plate with boundaries of constant temperature boundary simulates the plastic part in cooling stage. The temperature at the center of the part after a cooling time of t is expressed as a Fourier series [Mills 1995]:

$$T_{center} = T_w + \sum_{n=0}^{\infty} \frac{2}{n\pi}[1-(-1)^n](T_{melt} - T_w)\sin(\frac{n\pi}{2})e^{\frac{a_p n^2 \pi^2 t}{H^2}} \qquad (4\text{-}69)$$

where T_{center} is the temperature at the center of the part, T_w is the mold wall temperature, T_{melt} is the plastic melt temperature, α_p is the thermal diffusivity of the polymer material, H is the thickness of the part, t is the cooling time.

The averaged part temperature at ejection is therefore:

$$T_{average} = T_w + \sum_{n=0}^{\infty} \frac{2}{(2n+1)^2 \pi^2}(T_{melt} - T_w)e^{\frac{a_p (2n+1)^2 \pi^2 t}{H^2}} \qquad (4\text{-}70)$$

Since only the first term of the Fourier series is significant, we keep the first term and neglect the higher orders. This lead to a simple expression of the required cooling time as a function of the melt temperature, the ejection temperature and the mold temperature [Rao 1991]:

$$t = \frac{1}{\alpha}(\frac{H}{\pi})^2 \ln\left[\left(\frac{8}{\pi^2}\right)\left(\frac{T_w - T_{melt}}{T_w - T_{eject}}\right)\right] \qquad (4\text{-}71)$$

where α is the thermal diffusivity of the polymer, T_{eject} is the part ejection temperature averaged across the part thickness.

4.5.1.2 Runner

The runner system of the mold is simulated as an infinitely long cylinder with a radius R. The time for the center of the runner to reach the ejection temperature is [Malloy 1994]:

$$t = \frac{R^2}{5.78\alpha} \ln\left[1.6023\left(\frac{T_w - T_{melt}}{T_w - T_{eject}}\right)\right] \qquad (4\text{-}72)$$

The time for the averaged runner temperature reaches the ejection point is:

$$t = \frac{R^2}{5.78\alpha} \ln\left[0.692\left(\frac{T_w - T_{melt}}{T_w - T_{eject}}\right)\right] \tag{4-73}$$

With the equations above in mind a mold designer can design the size of the runner for the same cooling time as that of the part.

4.5.2 Thermal circuit model for transient heat transfer in cooling stage

We have discussed the analytical estimation for the cooling of the part with the constant mold temperature boundary. In this section we will discuss thermal circuit models for cooling stage heat transfer. The significance of thermal circuit models is that we can use the system dynamic method to study the mold and part heat transfer problems and to predict the transient heat transfer of the mold and the part.

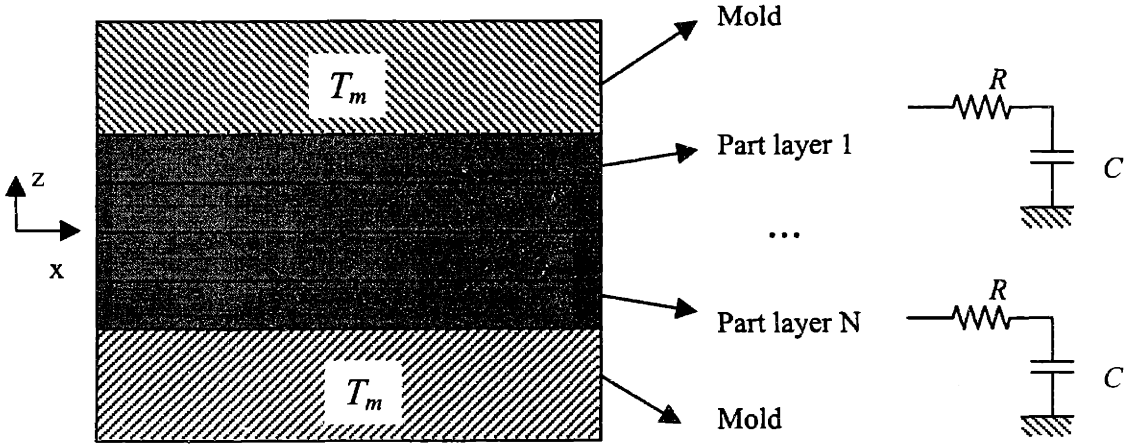

Figure 4-15. Plastic slab cooled in an infinite mold with constant boundary temperature

Figure 4-15 shows a simple model where a part with uniform thickness cooled between two infinite mold plates with constant temperature T_m. In this scenario the part is cut into parallel layers of thickness dp and each layer is represented by a thermal resistance R and a thermal capacitance C. The resistance R and the capacitance C are based on unit area on yz plane and are defined by the following equations respectively:

$$R = \frac{dp}{K_p} \tag{4-74}$$

$$C = \rho_p c_p dp \tag{4-75}$$

where K_p is the thermal conductivity of the part, ρ_p is the density of the part and c_p is the specific heat of the plastic material.

Since the circuit analogy of the constant mold temperature is the DC voltage source, the thermal circuit of the entire part and mold system is thus represented by the circuit model below:

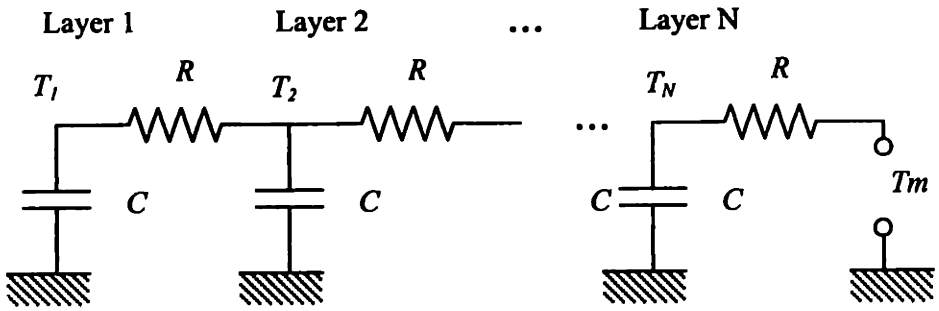

Figure 4- 16. Thermal circuit for the plastic slab cooling under constant mold boundary temperature

In Figure 4-16, T_1, T_2, ..., T_N represent the plastic bulk temperature for N layers respectively, T_{N+1} is the mold – part interface temperature and T_m is the mold temperature. The governing differential equations of the above thermal circuit are:

$$\frac{dT_1}{dt} = -\frac{1}{RC}(T_1 - T_2) \tag{4-76}$$

$$\frac{dT_2}{dt} = \frac{1}{RC}(T_1 - 2T_2 + T_3) \tag{4-77}$$

$$\frac{dT_3}{dt} = \frac{1}{RC}(T_2 - 2T_3 + T_4) \tag{4-78}$$

•••

$$\frac{dT_N}{dt} = \frac{1}{RC}(T_N - 2T_{N+1} + T_m) \tag{4-79}$$

The system dynamic expression of the about state equations is:

$$\frac{d\overline{X}}{dt} = \overline{\overline{A}} \cdot \overline{X} + \overline{B} \tag{4-80}$$

where the state variable vector $\overline{X}$, the matrix $\overline{\overline{A}}$ and the constant vector $\overline{B}$ are represented by the following equations respectively:

$$\overline{X} = \begin{bmatrix} T_1 \\ T_2 \\ \dots \\ T_{N+1} \end{bmatrix} \tag{4-81}$$

$$\overline{\overline{A}} = \frac{1}{RC}\begin{bmatrix} -1 & 1 & 0 & 0 & \dots & 0 \\ 1 & -2 & 1 & 0 & \dots & 0 \\ 0 & 1 & -2 & 1 & \dots & 0 \\ \dots & \dots & \dots & \dots & \dots & \dots \\ 0 & 0 & \dots & 1 & -2 & 1 \\ 0 & 0 & \dots & 0 & 1 & -3 \end{bmatrix} \tag{4-82}$$

$$\overline{B} = \frac{1}{RC}\begin{bmatrix} 0 \\ 0 \\ \dots \\ 2T_m \end{bmatrix} \tag{4-83}$$

The initial condition for the above equations is:

$$\overline{X}(0) = T_{melt}\begin{bmatrix} 1 \\ 1 \\ \dots \\ 1 \end{bmatrix} \tag{4-84}$$

where T_{melt} is the plastic melt temperature.

The thermal circuit model described above demonstrated a very good approximation to the standard Fourier series solution. Figures 4-17 and 4-18 compares the part central temperature history and the part thickness averaged temperature history predicted by the Fourier Series, 3rd order thermal circuit (3 plastic layers) and the 8th order thermal circuit (8 plastic layers) respectively. The simulation is based

on the plastic material with the density of 1000 Kg/m^3, thermal conductivity of 0.15 W/m-K, specific heat of 1747 J/Kg-K. The mold material is 316 stainless steel with the density of 8000 Kg/m^3, the thermal conductivity of 26.3 W/m-K and the specific heat of 400 W/m-K. The part thickness is 2mm. The initial part temperature is 220 degC. The mold temperature is 30 degC. Obviously the thermal circuit analogy gives a very close temperature profile to the Fourier Series solution. As the order of the thermal circuit increases the simulation accuracy is also improved.

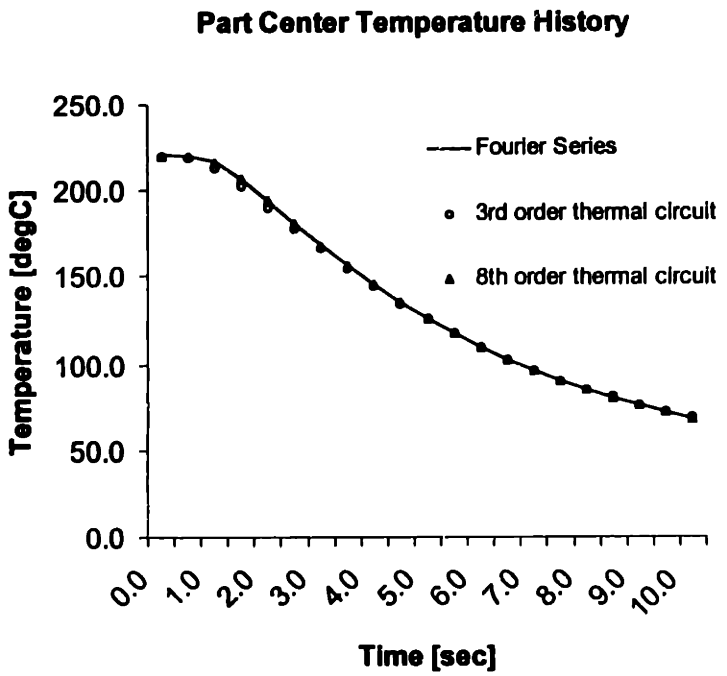

Figure 4-17. Simulation results for part central temperature history by different models

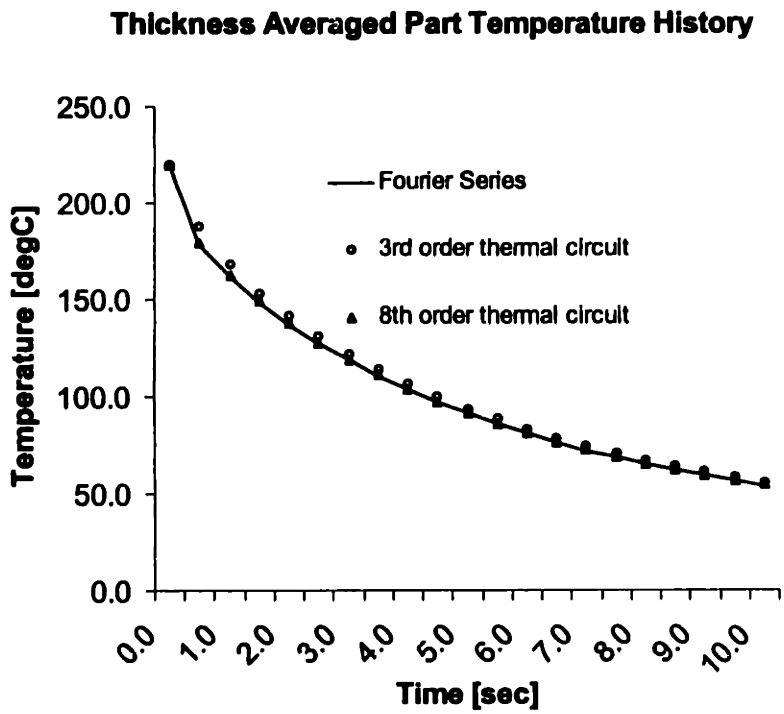

Figure 4-18. Simulation results for thickness averaged part temperature history by different models

4.6 CONCLUSION

In this chapter we have discussed the physical background behind the rapid thermal cycling process. Four stages of a rapid thermal cycle are analyzed: rapid heating, isothermal filling, packing and rapid cooling. For the rapid heating stage, a one dimensional lumped model and a 2 dimensional numerical model have been proposed to simulate the mold and the hot oil heat transfer. The mold time constant defined in chapter 2 has been used to describe the mold temperature response in rapid heating. The analytical model has been compared with the numerical simulation with high agreement. The heat transfer analysis along the oil line has also been modeled and the oil temperature drop was estimated. Issues such as the heating time and the energy consumption have been discussed. For the isothermal filling stage, we started from the governing equations for general fluid motion. In order to obtain governing equations for thin wall injection molding, we have made several assumptions such as the incompressible melt flow, the constant melt thermal conductivity, the negligible velocity component in thickness direction, etc.. After the order of magnitude analysis the simpler forms of equations of motion and energy equation were obtained. Once we have obtained the governing equations for traditional injection molding, we derived simple analytical expressions to estimate the isothermal flow. The injection pressure, the maximum shear rate and the viscous heating were also discussed based on the simple analytical models. For the packing stage, we discussed the Spencer-Gilmore equation that governs the pressure, the volumetric shrinkage and the temperature of the polymer melt. Starting from this equation we explored the idea of using the mold deflection to compensate the part shrinkage. For the cooling stage, we have developed the thermal circuit model to simulate the transient heat transfer of the part. The model has the potential to optimize the mold temperature for minimum residual stress in the part. As a summary the work discussed in this chapter aims at building up the theoretical foundations to guide the design work in the next chapter.

4.7 REFERENCES

1. Akay M., S. Ozden, "Prediction of Process-Induced Warpage in Injection Molded Thermoplastics", *Polymer Engineering and Science*, Vol 36, No 13, 1996, p1839-1846
2. Belofsky H., "Plastics: Product Design and Process Engineering", Hanser, 1995
3. Bown J., "Injection Moulding of Plastic Components", McGraw-Hill, 1978
4. Chen S., N. Cheng, K. Jeng, "Post-Filling Simulation and Analysis of Shrinkage and Warpage of the Injection Molded Parts", *ANTEC'91*, p493-498

5. CITO Product, Inc. "*Mold Surface Temperature Conrol for Highest Quality Production and Shortest Molding Cycle*", Product Catalogue, 1997
6. Isayev A., "Orientation, Residual Stress and Volumetric Effects in Injection Molding", *Injection and Compression Molding Fundamentals*, Marcel Dekker, 1987
7. Jansen K., G. Titomanlio, "Effect of Pressure History on Shrinkage and Residual Stresses-Injection Molding with Constrained Shrinkage", *Polymer Engineering and Science*, Vol 36, No 15, 1996, p2029-2040
8. Jansen K., A. Flaman, "Construction of Fast-Response Heating Elements for Injection Molding Applications", *Polymer Engineering and Science*, Vol 34, No 11, 1994, p894-897
9. Kang S., C. Hieber, K. Wang, "Optimum Design of Process Consitions to Minim Stresses in Injection Molded Parts", *ANTEC'95*, 1995, p991 - 996
10. Kennedy P., "Flow Analysis of Injection Molds" , Hanser, 1995
1. Kim B., "Low Thermal Inertia Injection Molding", Ph.D. Thesis, MIT, 1983
11. Kim B., R. Wadhwa, "A New Approach to Low Thermal Inertia Molding", *Polym.-Plast. Technol. Eng.*, 26(1), 1987, p1-22
12. Kim B. and N. Suh, "Low Thermal Inertia Molding", Polym.-Plast. Technol. Eng., 25(1), 1986, p73-93
13. Lee B., B. Kim, "Optimization of Part Wall Thickness to Reduce Warpage of Injection-Molded Parts Based on the Modified Complex Method", *Polym. – Plast. Technol. Eng.*, 34(5), 1995, p793-811
14. Leo V., C. Cuvelliez, "The Effect of the Packing Parameters, Gate Geometry, and Mold Elasticity on the Final Dimensions of a Molded Part", *Polymer Engineering and Science*, Vol 36, No 15, p1961-1971
15. Liu S., "Modeling and Simulation of Thermally Induced Stress and Warpage in Injection Molded Thermoplastics", *Polymer Engineering and Science*, Vol. 36, No. 6, Mar-96, p807 - 818
16. Malloy R., "Plastic Part Design for Injection Molding", Hanser, 1994
17. Middleman S., "Fundamentals of Polymer Processing"
18. Mincy M., "Comparison Between Cooling Thermal Plastic Molds Using Pulse Modulated and Closed Loop, Warm Water, Circulating Flow Method", 1992
19. Rubin I., "Injection Molding Theory and Practice", John Wiley & Sons, Inc, 1972
20. Sachs E., E. Wylonis, M. Cima, S. Allen,S. Micheals, E. Sun, H. Tang, H. Guo, "Injection Molding Tooling by Three Dimensional Printing: a Desktop Manufacturing Process", *ANTEC'95*
21. Sachs E., S. Allen, H. Guo, J. Banos, M. Cima, J. Serdy, D. Brancazio, "Progress on Tooling by 3D Printing: Conformal Cooling, Dimensional Control, Surface Finish and Hardness", *Solid Freeform Fabrication Proceedings*, Sept-1997, p115-123

22. Spencer R. and G. Gilmore, "Residual Strains in Injection Molded Polystyrene", Modern Plastics, December 1950

23. Sun E., "Implementation of Low Thermal Inertia Injection Molds Using Conformal Passages", M.S. Thesis, MIT, 1995

24. Tadmor Z., C. Gogos, "Principles of Polymer Processing", John Wiley & Sons, 1979

25. Titomamlio G., K. Jansen, "In-Mold Shrinkage and Stress Prediction in Injection Molding", *Polymer Engineering and Science*, Vol 36, No 15, p2041-2049

26. Wooldridge C., E. Schwartz, "Mold Temperature Control: Comparison of Moldmonitor Pulse Cooling System to Continuos Circulation System", GE report PAC-88-098, 1988

27. Xu X., E. Sachs, S. Allen, M. Cima, "Design Conformal Channels for Tooling", *Proceeding of 9th Solid Freeform Fabrication Symposium*, in press

28. Zoetelief W., L. Douven, A. Housz, "Residual Thermal Stresses in Injection Molded Products", *Polymer Engineering and Science*, Vol. 36, No. 14, Jul-96, p1886 - 1896

CHAPTER 5

TOOLING DESIGN AND FABRICATION FOR RAPID THERMAL CYCLING

CONTENT

FIGURES

5.1 INTRODUCTION

In the last chapter we have discussed the theoretical foundation of the rapid thermal cycling process. Two critical components are required for the successful implementation of this process: a heat exchanging system with high efficiency and short response time and a tool with low thermal inertia. This chapter addresses these issues from two aspects: design and manufacturing. In the fist several sections we discuss the design of the benchmark part, the conformal channel, the process parameter, the tool structure, the oil delivery system and the mold base assembly. After that we will explore fabrication issues such as green part printing, debinding/ sintering, infiltration and post-machining/ assembling.

The focus of this chapter is the tool design and fabrication. The destination is to develop the systematic methodology for the design and fabrication of the low thermal inertia tool that is subject to an unfavorable working condition during the rapid thermal cycling. The target mold temperature change is about 100degC in 1 to 2 seconds. The maximum process pressures is about 5000psi. The target mold time constant is about 1 to 2 seconds. The tool should have the flexibility to compensate the shrinkage of the part during cooling (This idea has been explored in Chapter 4). A conceptual design of such a low thermal inertia tool is proposed in Figure 5-1. The tool consists of a top plate and a bottom plate connected by thousands of vertical truss columns. On the top of the parting face are runners, gates and the cavity. Underneath the cavity are conformal channels embedded inside the insert for rapid and uniform control of the mold surface temperature. The top plate is supported by truss structures of different sizes. We will discuss how to design and fabricate inserts with such complex features in following sections.

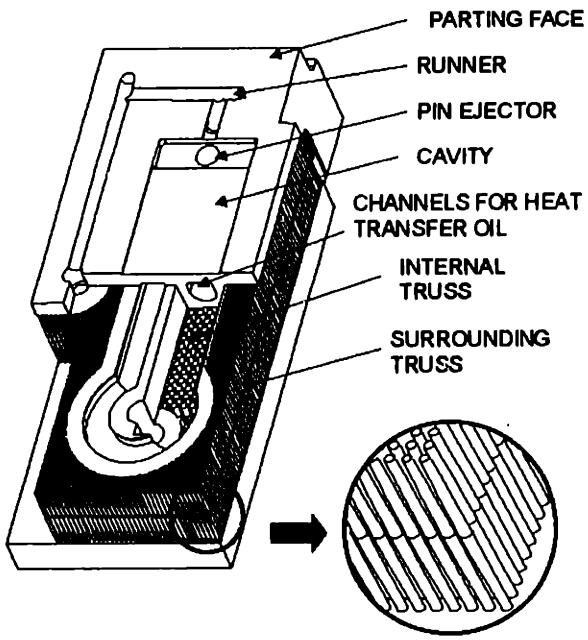

Figure 5-1. Conceptual design of the tool for rapid thermal cycling

5.2 DESIGN ISSUES IN RAPID THERMAL CYCLING

5.2.1 Part design

5.2.1.1 Functional Requirements

The goal of the prototype part design for rapid thermal cycling test is to fully demonstrate the advantage of the 3D printed low thermal inertia tool over the traditional tools. The following design requirements are considered in selecting the benchmark part:

1) The part should have sections with thickness that covers a broad range of industrial interests. Both thick part molding and thin part molding should be considered.
2) The molding material should be commonly used in industry and should be transparent so that birefringence patterns can be easily visualized.
3) The part geometry should allow the formation of the welding line so as to compare the welding line strength with that formed by traditional process.
4) The part geometry should ease the strength test and other mechanical property test on an Instron machine.
5) The post-machining and surface finishing of the tool should be of no difficulty.
6) The cavity depth should be adjustable.

5.2.1.2 Proposed benchmark part

A benchmark part shown in Figure 5-2 was proposed by members of 3D Printing Industrial Consortium. This design consists of two thicker areas (0.1") separated by a thin web. The starting thickness for the middle web area is 0.05. The molding of the thicker parts is first proceed and then extends to the thinner parts by facing the top surface of the insert. The part is fed from both sides of the cavity. At the center of each thicker area, a tapered hole is placed for the welding line visualization and for the strength test. The size of the part is 1.5" X 5". The molding material is either Polystrene (PS) or Polycarbonate (PC) because they are transparent and easy to visualize birefringence patterns and also because that the process temperature for these two resins are within or close to the range for the existing oil circulation system. The physical properties of these two materials are listed in table 5-1. The target molding material for the design discussed below is PC but the tool designed is also suitable for PS molding. For reasons I have discussed in chapter 4, thermosetting materials can also be molded by rapid thermal cycling, but are not the main focus of the current project.

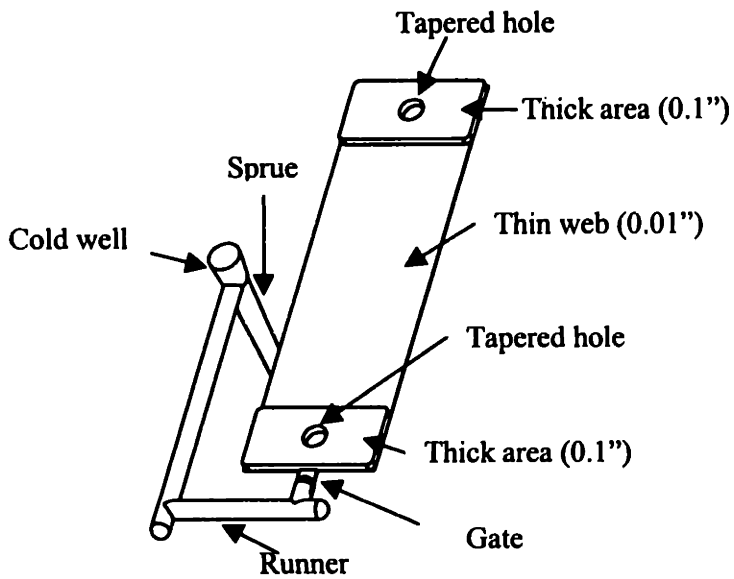

Figure 5-2 The benchmark part designed for rapid thermal cycling test

	Polycarbonate (PC)	Polysterene (PS)
Supplier	GENERIC (LEXAN 141,GE EUROPE)	GENERIC (SUMIBRIGHT, SUMITOMO)
Grade	PC001	PS001
Solid Density	1193.1 Kg/m^3	1050 Kg/m^3
Melt Density	1058.2 Kg/m^3	902.5 Kg/m^3
Thermal Conductivity	0.23 W/m-K	0.22 W/m-K
Specific heat	1881 J/Kg-K	2144 J/Kg-K
Viscosity	234.3 Pa.s at 275°C, 1000s^{-1} 351.2 Pa.s at 295°C, 100s^{-1} 165.3 Pa.s at 295°C, 1000s^{-1} 61.1 Pa.s at295°C, 10000s^{-1} 247.9 Pa.s at 315°C, 100s^{-1} 122.7 Pa.s at 315°C, 1000s^{-1}	68.9 Pa.s at 235°C, 1000s^{-1} 288.1 Pa.s at 255°C, 100s^{-1} 55.8 Pa.s at 255°C, 1000s^{-1} 9.7 Pa.s at255°C, 10000s^{-1} 244.2 Pa.s at 275°C, 100s^{-1} 49 Pa.s at 275°C, 1000s^{-1}
Ejection Temperature	145°C (293°F)	101°C (213.8°F)
No Flow Temperature	175°C (347°F)	131.2°C (268.2°F)
Min. Melt Temperature	280°C (536°F)	180°C (356°F)
Max. Melt Temperature	320°C (608°F)	260°C (500°F)

Table 5-1 Generic material properties from MoldFlow database

5.2.1.3 Gate, Runner and Sprue Design

The runner design should consider the following issues [Pye 1989, Rubin 1972]:

1) The size of the runner must be big enough to permit the melt to pass through and fill the cavity before the runner freezes. Runners below 3/32" in diameter are seldom used in traditional injection molding practice.
2) The pressure loss through the runner increases as the runner length increases. Therefore the runner diameter and length should be adjusted in order to maintain a small pressure loss.
3) Runner size should not be so big that it dominates the injection cycle. It is undesirable to make the runner larger than 3/8" for most materials except the rigid PVCs and the acrylics.
4) The runner size should be in a range consistent with the conventional cutting tool size.

An empirical formula for the runner diameter is expressed below [Pye 1989]:

$$D = \frac{\sqrt{W} \times \sqrt[4]{L}}{8} \tag{5-1}$$

where D is the desired runner diameter in inch, W is the weight of molding in oz, L is the runner length in inch.

No literature is found explaining how to derive equation (5-1), however a simple analysis below will show that the objective of this equation is to maintain a certain injection speed v_{inj} and the injection pressure p_{inj}.

The weight of molding W is expressed by the following equation:

$$W = \rho V = \rho Q t = \rho t v_{inj} A = \rho t v_{inj} \frac{1}{4} \pi D^2 \tag{5-2}$$

where V is the total volume of the part, Q is the flow rate of the melt through the runner system, t is the filling time and v_{inj} is the injection speed. If we maintain a constant filling time and a constant injection speed, the runner diameter will be proportional to the square root of the part weight:

$$D \propto \sqrt{W} \tag{5-3}$$

On the other hand, according to equation (4-50) the pressure drop in the runner system is proportional to the runner length and inversly proportional to the fourth power of the runner diameter. For a constant pressure drop and melt flow rate, we have:

$$D \propto \sqrt[4]{L} \tag{5-4}$$

where l is the length of the runner.

Applying above design rules and formula to the benchmark part shown in Figure 5-2 yields the runner size of 3/32". However the mold flow simulation shows the loss of the injection pressure by up to 30% when using runners of this type. Therefore we finally design the runner with a diameter of 1/8", which leads to a 10% pressure loss in the runner system.

In the practical design, we place the runner and the gate system on the cavity insert only. The runner cross-sectional shape and dimension is sketched in Figure 5-3.

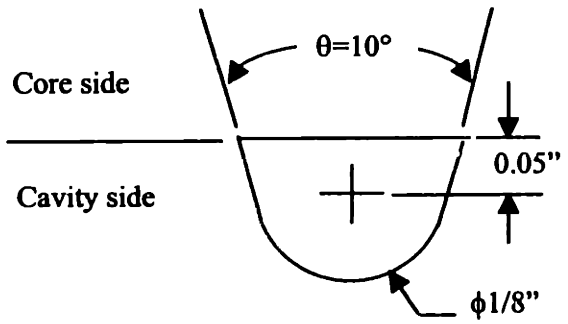

Figure 5-3 Cross section shape of the runner

The gate design follows the rules below:

1) The gate should be able to freeze after the cavity is filled.
2) The gate should allow simple degating with little mark after the part is ejected.
3) The gate should allow extra melt packed into the cavity to compensate the part shrinkage.

The typical design for the length of the gate is between 0.02" to 0.03". The width of the gate is obtained by the following equation [Pye 1989]:

$$W = \frac{n\sqrt{A}}{30} \qquad (5\text{-}5)$$

where A is the surface area of the cavity, n is a material constant. For polycarbonate $n = 0.7$.

Similarly there is no literature indicating how equation (5-5) is derived. However a simple analysis below will show that this equation ensures that the gate solidifies right after the filling stage completes.

From equation (4-71) we know that the cooling time of a slab is proportional to the square of the thickness and inversely proportional to the thermal diffusivity of the material. After applying this equation to the gate, we have the total cooling time required for the gate as below:

$$t_{cool} \approx cW^2 \qquad (5\text{-}6)$$

where c is a constant depending on different polymer materials (i.e. different thermal diffusivity, mold temperature, melt temperature and ejection temperature).

On the other hand the total filling time depends on the volume of the cavity and the flow rate of the polymer melt. That is:

$$t_{fill} \approx \frac{Ah}{Q} \tag{5-7}$$

where A is the surface area of the cavity, h is the part thickness, Q is the polymer flow rate.

For a constant melt flow rate if we require that the gate solidifying time t_{cool} be equal to the melt filling time, we can obtain the following relationship between the gate width and the cavity surface area:

$$W \propto n\sqrt{A} \tag{5-8}$$

The depth of the gate h is determined according to the thickness of the molded part t:

$$h = nt \tag{5-9}$$

The application of above design rules and formula results in our design of a rectangular edge gate with the width of 1/16", depth of 0.07" and length of 0.03".

The runner cross-sectional shape and dimensions are sketched in Figure 5-3. The size of the runner is designed to reduce the pressure loss while maintain the melt temperature. The MoldFlow 9.0 package does not support the irregular runner cross section shape, therefore a circular cross section with equivalent hydraulic diameter is used for analysis purpose. MoldFlow simulation shows that a runner of 0.1" diameter results in a 30% loss in injection pressure. By increasing the runner diameter to 1/8", the pressure loss is dropped down to 10%.

The sprue is designed as a tapered cylinder. The simulation result by MoldFlow shows that the cycle time is dominated by the cooling of the sprue. Therefore the sprue size is a very important design parameter. The sprue with averaged diameter of ¼" results in a cooling time of more than 30 seconds providing that the mold temperature is kept at 212 degF. By reducing the sprue size to 0.2" the cooling time is dropped down to 20 seconds. In the design of the benchmark tool, we use the sprue with the end diameter 5/32" and the tapered angle 2°. This design is compatible with the smallest D-M-E standard sprue bushing (A0451).

5.2.1.4 Mold filling time and injection pressure

The filling stage in a rapid thermal cycling process is modeled as isothermal, where the plastic melt keeps a high temperature while filling the cavity. Under the isothermal condition only the mass conservation and the momentum conservation are used to solve the flow equations. Because of reasons discussed in section 4.3.1 we use the Newtonian flow to roughly estimate the mold filling. For the

benchmark part the total pressure drop in the cavity is obtained by the following equations [Belofsky 1995]:

$$\Delta p = \frac{12\mu L_1 Q}{h_1^3 W} + \frac{12\mu L_3 Q}{h_2^3 W} \qquad (5\text{-}10)$$

where Q is the flow rate of the polymer melt, L_1, h_1, L_2 , h_2 are lengths and thickness of different sections of the part respectively, W is the width of the part. The application of this equation to the benchmark part yields a pressure drop of 20,000psi for a part with $h_1 = 0.1$", $h_2 = 0.01$" and filling time of 2 seconds. This result is consistent with the Moldflow simulation result. In the above analysis we use Polycarbonate, the material properties for PC are shown in table 5-1.

The above estimation indicates that a large injection pressure of up to 20,000psi is required to fill a thin cavity of 0.01" in a couple of seconds, even the filling is nearly isothermal. In order to reduce the injection pressure, three methods are proposed: 1) increasing the web thickness h_2. 2) usin g multiple gates. 3) extending the filling time. The Design of Experiment (DOE) method is used in order to obtain a proper operational window for rapid thermal cycling.

5.2.1.5 Maximum shear rate

The filling estimation discussed above assumes that the polymer melt keeps a constant and uniform temperature during filling. However this is not strictly true because the viscous shear may introduce the extra heat that raises the mold temperature and lead to overheating or degrading of the polymer material. Besides large shear rate also have other negative effect on the polymer material properties and should be avoided. In chapter 4 we have derived that the maximum shear rate as a function of the injection pressure and the cavity geometry (equation 4-51). This equation is rewritten below::

$$\dot{\gamma}_{max} = \frac{h}{2\mu L}\Delta p \qquad (5\text{-}11)$$

The application of this equation on the benchmark part yields a maximum shear rate of 1700 s^{-1} for a part of 2mm thick, with the melt temperature of 572 degF, the filling time of 2 seconds and the injection pressure of 20,000 psi. This shear rate results in about 9degC temperature rise of the polymer melt due to the viscous heating.

5.2.2 Cooling channel design

In this section we will discuss the design of the conformal cooling channels for the part sketched in Figure 5-2. The design methodology has been discussed in Chapter 2 and 3. However the practical use

of this design methodology in rapid thermal cycling needs to take some extra considerations. The major issues in cooling channel design for rapid thermal cycling are highlighted below:

5.2.2.1 Design for mold surface temperature response

In chapter 4 we have used the mold time constant derived from the conformal cooling analysis (equation 4-1) to estimate the temperature response rate of the mold to the hot oil in the rapid heating stage. For the benchmark part shown in Figure 5-2, if we place oil channels with hydraulic diameter of 0.12" conformal to the mold wall with an offset distance of 0.1", the resulting mold time constant is about 1.07seconds for an overall oil flow rate of 10GPM. This calculation used the equivalent distance of the oil channel to the mold wall and the equivalent heat transfer coefficient. The result indicates that the mold reaches about 60% of its steady temperature value after about 1 second of heating. A shorter distance from the oil channel to the mold wall will lead to more rapid response of the mold surface temperature to the oil temperature change. However the lower limit of the distance from the oil channel to the mold wall is also constrained by other design issues such as the temperature uniformity and the mold strength.

5.2.2.2 Design for sufficient heating

The design work for sufficient heating can be divided into 2 subtasks: 1) the heater design and 2) the oil channel design. For the heater design, we first obtain the averaged mold temperature as a function of heating time by equation (4-5). After 2 seconds of rapid heating, the mold temperature reaches 154 degC for the oil temperature of 220 degC and the distance from the oil channel to the mold wall of 0.1". The total energy consumption during rapid heating is 58184 J. If we assume an injection cycle time of 10 seconds, the heater's power requirement for each side of the insert should be no less than 6KW.

The other important subtask is the oil channel design. The oil channel should provide enough surface area for effective transfer of the thermal energy from the oil circulation system to the tool. By applying equation (4-4), we can easily obtain the required surface area for oil channels:

$$A = \frac{c_m(M_m + M_t)}{h\tau} \tag{5-12}$$

where c_m is the specific heat of the mold material, M_m is the mass of the mold, M_t is the effective mass of the truss support considering the thermal diffusive distance l_t , h is the heat transfer coefficient, τ is the characteristic heating time.

The required oil channel number is:

$$N = \frac{A}{DL} \tag{5-13}$$

where L is the averaged length of these channels, D is the channel size and A is the total oil channel area calculated by equation (5-12).

Equations (5-12) and (5-13) is for rough estimation of the required oil channel surface area and circuit number. It assumes that the characteristic heating time τ is approximately the mold time constant. In the case that the mold time constant is longer than the desired heating time, we may have to consider increasing the oil temperature so that the mold can still reach the target temperature after rapid heating.

5.2.2.3 Design for heating/cooling uniformity

The uniform heating/ cooling is achieved by: a) reducing the temperature variation on the mold surface between two adjacent oil channels; b) reducing the temperature variation along the oil channel. The issues on temperature uniformity on the mold surface between two adjacent oil channels have been discussed in detail in chapter 3 and will not be redundantly repeated here. The temperature variation along the oil line can be obtained by the analytical analysis in section 4.2.4 or by the numerical simulation discussed in section 4.2.2. The analysis is based on the benchmark part shown in Figure 5-2. The overall flow rate of the coolant is 10GPM. The inlet oil temperature is 220degC. The initial mold temperature is 30degC. The analytical analysis for the benchmark tool yields the oil temperature drop from 9.4degC (at the beginning of rapid heating) to 1.5 degC (at the end of rapid heating). These values are higher than those by numerical simulation because of the reason explained in section 4.2.4.

5.2.2.4 Design for pumping pressure

The pressure drop for a turbulent pipe flow is expressed by the following equation:

$$P = \frac{L}{2D}\rho v^2 C_f \qquad (5\text{-}14)$$

where L is the length of the channel, D is the size of the channel, v is the flow velocity and C_f is the friction factor, a function of the flow rate, the channel size and the channel surface roughness. For the benchmark tool we have designed, there are 10 channels with hydraulic diameter of 0.1" forming 5 sets of cooling circuits. The total length for each cooling circuit is 14" long. If we use the 20GPM Mokon unit to supply the cold oil for both the core and the cavity insert, each cooling circuit will share a flow rate of 2GPM. This flow rate results in a pressure drop of less than 10 psi. The rest of the pressure supply from the Mokon unit will be dissipated in pipe connections, fittings and corners.

The pressure losses through fittings, corners and valves are called local losses..They are calculated by a loss coefficient K, a function of component geometry and Reynolds number. The pressure drop through the component with a loss coefficient K is:

$$\Delta P = K \cdot \frac{1}{2} \rho v^2 \qquad (5\text{-}15)$$

If we regard the pressure loss through these components as the increase of an equivalent length of the oil pipe, the equivalent length is:

$$L_{eq} = \frac{K}{C_f} D \qquad (5\text{-}16)$$

K values for typical pipe components are listed in Figure 5-4 to 5-7 below. For more detailed descrition on these issues please refer to chapter seven of "Fundamentals of Fluid Mechanics" [Gerhart and Gross 1985]

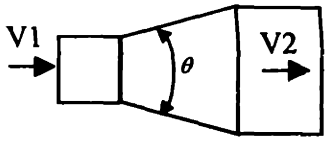

Conical gradual expansion

Expansion Cone Angle	K
15	0.35
30	0.9
45	1.1
60	1.2

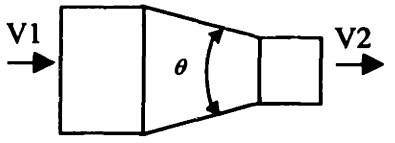

Conical gradual contraction

Contraction Cone Angle	K
30	0.02
45	0.04
60	0.07

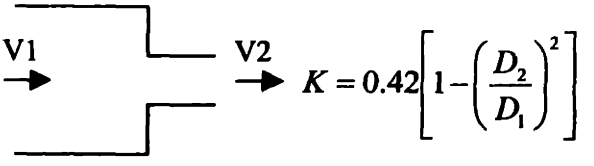

Sudden contraction

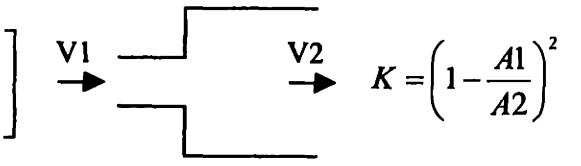

Sudden expansion

Figure 5-4 Typical values of loss coefficient for a gradual/sudden expansion/contraction connections

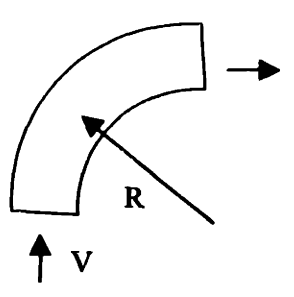

Circular pipe bend

$$K_{total} = K_{Figure} + f\frac{\left(\frac{\pi R}{2}\right)}{D}$$

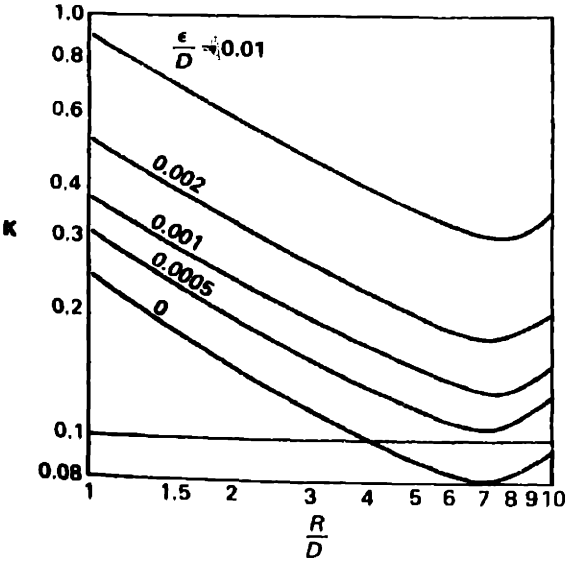

Figure 5-5 Flow in a bend of a circular pipe

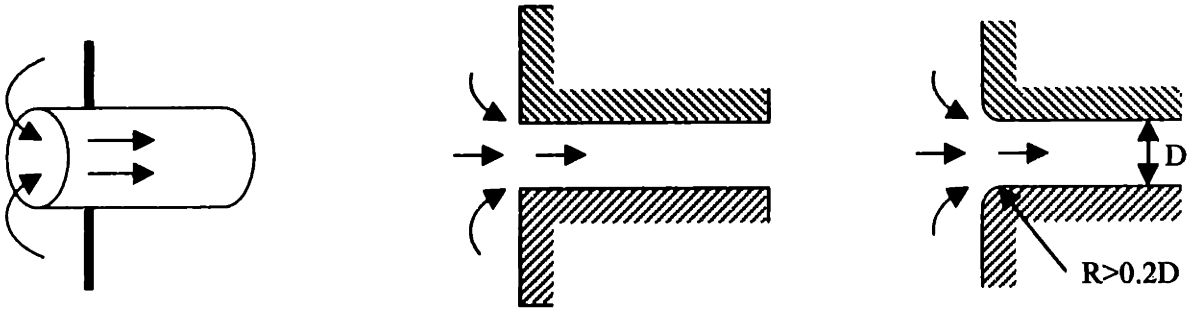

Reentrant

$K \approx 0.8-1.0$

Square edge

$K \approx 0.4-0.5$

Well-rounded

$K \approx 0.05$

Figure 5-6 Loss coefficients for pipe entrances

Loss coefficients for commercial pipe fittings (screwed or soldered)

Nominal Dia. (in)	1/2	1	2	4
Valves(fully open)				
Globe	14	8.2	6.9	5.7
Gate	0.30	0.24	0.16	0.11
Swing check	5.1	2.9	2.1	2.0
Angle	9.0	4.7	2.0	1.0
Elbows				
45° standard	0.39	0.32	0.30	0.29
90° standard	2.0	1.5	0.95	0.64
180° standard	2.0	1.5	0.95	0.64
Tees				
Line flow	0.90	0.90	0.90	0.90
Branch flow	2.4	1.8	1.4	1.1

Figure 5-7 Loss coefficients for commercial pipe fittings

5.2.2.5 Cooling channel design result

Following the same strategy as discussed in chapter 2, we have successfully determined the major parameters necessary to construct conformal channels for the benchmark tool for rapid thermal cycling

test. In terms of the detail design we have also considered other issues such as balancing oil flows in different channels, minimizing the pressure loss by rounding every sharp corners, etc. Our effort results in a set of conformal channels for the benchmark tool. Figure 5-8 shows channels for the core insert. In this figure, the heat transfer oil is first pumped through a 0.25" diameter insert, then divided into 5 parallel branches, mixed at the other end of the mold by a long channel and flow back through 5 parallel channels. They are eventually combined to a single flow at the outlet. The configuration of the channel system for cavity insert is more complex because the channels have to be placed in 3D space in order to conformal to the cavity shape.

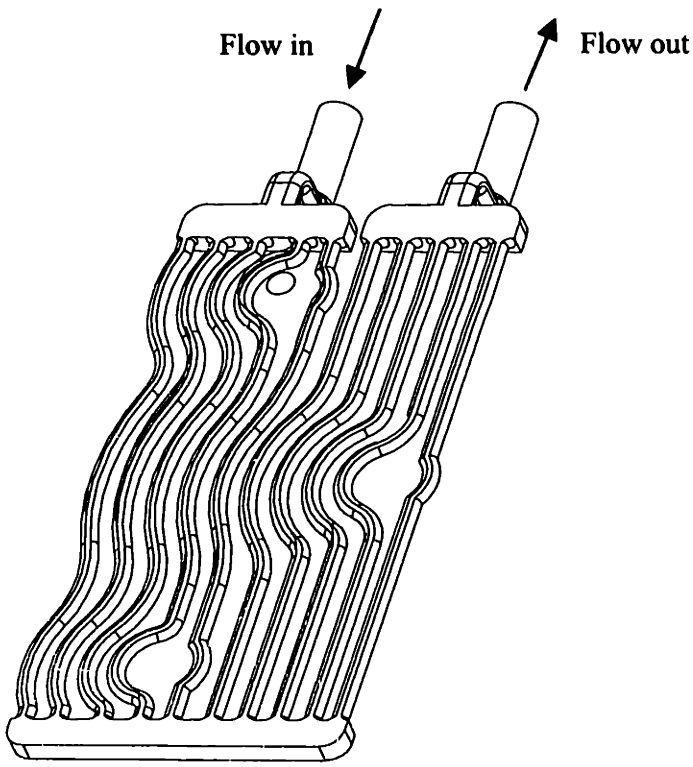

Figure 5-8 The conformal channel set for rapid thermal cycling (core side)

5.2.3 Process parameter design

5.2.3.1 Goals and difficulties

Our objective is to design the process condition for the rapid thermal cycling test that shows major advantages over the conventional molding process. With our customized tool of low thermal inertia we want to achieve the following goals:

1) Demonstrate the ability to mold extremely thin parts with the wall thickness in a range of 0.01" to 0.05".

2) Demonstrate the improvement of the molecular orientation by isothermal filling.
3) Demonstrate the warpage improvement for parts with abrupt thickness change.
4) Demonstrate the improvement in knit line strength.
5) Test the part mechanical property change by rapid thermal cycling.
6) Test the idea of shrinkage compensation by controlled mold surface deflection. Please refer to chapter 4 for detailed description of this concept.
7) All the above goals should be achieved with little sacrifice of the injection cycle time (desired rapid heating time is about 2 sec., desired filling time is about 2 sec. and cooling time is about 10 sec. for the benchmark part shown in Figure 5-2)

In consequence we are facing the following challenges placed by the technical and physical limitations:

1) The strength of the 3D Printed truss structure limits the allowable process pressures. After considering the yield strength of the 3DP material and other issues such as creating a certain mold surface deflection for shrinkage compensation and minimizing the heat loss through truss support, we finally end up with a target injection pressure of 5000psi. This injection pressure corresponds to a clamping force of within 20 ton for the projection area of the part shown below in Figure 5-10.
2) The maximum temperature the oil circulation system can achieve is about 550degF. The target is to increase the mold temperature by 100 degC within 1~2 seconds

5.2.3.2 Design of Experiment

5.2.3.2.1 Design parameters

After reviewing the objectives and challenges of this project, we recognized that the following design parameters have significant influence in the performance of a rapid thermal cycling system: the gate number, the minimum part thickness, the mold temperature and the injection pressure.

The four design parameters discussed above are correlated with each other. For example the effort to minimize the part thickness is hindered by other process factors such as the injection pressure, the gate number and the mold temperature. First of all, since the part solidification time is proportional to the square of the part thickness, the decrease of the part thickness significantly shortens the vitrification time for the polymer melt. In previous section we have demonstrated that the cooling time for a part of 0.01" thick is less than 0.1 sec with the mold temperature of 212degF, while that for 0.02" thick is 0.36

seconds. The short solidification time requires a very strict control of the mold surface temperature so that at any point in the flow path the polymer melt is not frozen. Second, the decrease of the part thickness significantly increases the injection pressure. As shown in equation (5-10) the required injection pressure is inversely proportional to the cube of the part thickness. This means that a reduction of the part thickness from 0.02" to 0.01" will result in the increase of the injection pressure by 800%. The third point is that the decrease of the part thickness will lead to a large viscous shear that may degrade the polymer melt. According to equation (4-50) and (4-51) the shear rate is inversely proportional to the square of the part thickness. This means that a thickness change from 0.02" to 0.01" results in a shear rate increase of 400%.

The above analysis indicates that the effort of reducing the part thickness by a factor of two corresponds to the increase of the technical challenge by at least 4 folds. It also suggests that we distribute technical risks to various design efforts in order to obtain an optimal operational point for rapid thermal cycling. These efforts include: 1) using multiple gates to shorten the flow path and the filling time. 2) increasing the part thickness to make the flow easier. 3) increasing the mold temperature. 4) increasing the injection pressure. Since these efforts are in the mean time constrained by other physical limitations, it is very necessary to develop a systematic way to evaluate and design the combined effect of the above four design factors. We use matrix experiment design method [Phadke, 1989] for this purpose.

Table 5-2 lists four design parameters at different levels. The gate number has two selections: single gate injection or two gate injection. The part thickness is chosen from 0.01" (very challenging), 0.02" (moderate challenging) and 0.03" (not very challenging). The mold temperature setup has three levels: 212 °F (suggested mold temperature for conventional molding of PC), 450 °F (a mold temperature that is easy to achieve by the existing rapid thermal cycling system) and 570 °F(a mold temperature which is very close to the melt processing temperature but beyond the capability of the existing rapid thermal cycling system). The injection pressure has three levels: 3500psi (below the process pressure target), 5000 psi (at the process pressure target), 7500 psi (beyond the process pressure target). A dummy level 2' is introduced in order to construct the orthogonal array for experiment. 2' is a simple duplication of level 2 but it allows the formation of a standard orthogonal array with 9 experiments. Table 5-2 shows the matrix experiment developed based on the orthogonal array.

Factor	Levels		
	1	2	3
A. Gate Number	1	2	2'
B. Part Thickness	0.01"	0.02"	0.03"
C. Mold Temperature	212 °F	450 °F	570 °F
D. Injection Pressure	3500 psi	5000 psi	7500 psi

Table 5-2 Experiment parameter setup at different levels

No.	Experiment Name	A. Gate Number level	B. Part Thickness level	C. Mold Temp. level	D. Injection Pressure level
1	A1B1C1D1	1	1	1	1
2	A1B2C2D2	1	2	2	2
3	A1B3C3D3	1	3	3	3
4	A2B1C2D3	2	1	2	3
5	A2B2C3D1	2	2	3	1
6	A2B3C1D2	2	3	1	2
7	A3B1C3D2	2'	1	3	2
8	A3B2C1D3	2'	2	1	3
9	A3B3C2D1	2'	3	2	1

Table 5-3 List of orthogonal experiment arrays

5.2.3.2.2 Objective function

As we have discussed before there are multiple goals we want to achieve in designing tools for rapid thermal cycling. These goals are listed below in a sequence of priority level:

1) The highest priority is to ensure that the designed process can make a complete part. The moldability criterion is the percentage of the shot volume at the end of filling. This value is denoted as $y1$. The

moldability for the complete filling without short shot is 1, while the moldability for 50% short shot is 0.5.

2) The second highest priority is that the isothermal filling is accomplished in an endurable time. This time includes not only the filling time but also the time to preheat the mold. In order to obtain the time criterion *y2* we divide the summation of the target heating time and filling time by the summation of the actual heating time and filling time. That is:

$$y2 = \frac{t_{h\_target} + t_{f\_target}}{t_{h\_actual} + t_{f\_actual}} \tag{5-17}$$

The target heating time t_{h_target} is set 2 seconds. The target filling time t_{f_target} is 2 seconds. The actual filling time $t_{f\_actural}$ is obtained by MoldFlow analysis. The actual heating time t_{h_actual} is calculated by the following equations:

$$t_{heat} = \tau \ln \frac{T_{final} - T_{oil}}{T_{init} - T_{oil}} \tag{5-18}$$

where τ is the time constant of the mold (typically 2 seconds), T_{final} is the target mold temperature, T_{oil} is the hot oil temperature, T_{init} is the initial mold temperature. For the oil temperature of 600°F and the initial mold temperature of 212°F, the time to heat up the mold up to 450°F is 1.9 seconds, up to 570°F is 5.12 seconds.

3) The next priority level is the mold strength factor denoted by *y3*. As we know, the matrix experiment selects three levels of injection pressures, 3500 psi, 5000 psi and 7500 psi. The criterion *y3* is normalized by dividing these pressure values with the minimum injection pressure 3500 psi.

4) The next objective function considers the capacity of the existing oil delivery system. This criterion is denoted as *y4*. Its value depends on how high we want the mold temperature to achieve during the preheating stage. The *y4* values for both 212°F (MoldFlow suggested temperature for PC) and 450°F (the temperature a typical oil circulation system can delivery) are set to 1 because they are both ready for use. However a higher mold temperature of 570°F still need some effort considering the sealing and safety issues. Therefore the *y4* value for this temperature level is close to 0.

5) The technical leadership demonstrated by the thin wall is denoted as *y5*. We model this value to be inversely proportional to the square of the part thickness. With this model we defines the technical leadership as 1, 0.67 and 0 for the part thickness of 0.01", 0.02" and 0.03" respectively.

The combined objective function y is the summation of the criteria defined above multiplied by weight factors which is defined based on their priority level:

$$y = \frac{w1 \cdot y1 + w2 \cdot y2 + w3 \cdot y3 + w4 \cdot y4 + w5 \cdot y5}{w1 + w2 + w3 + w4 + w5} \qquad (5\text{-}19)$$

In the above equation the weight factors *w1* to *w5* are assigned with 5,4,3,2,1 respectively.

The final objective function η is defined as:

$$\eta = 100\log(y) \qquad (5\text{-}20)$$

5.2.3.2.3 DOE design results

Table 5-4 shows the analysis results for the matrix experiments listed in table 5-3. According to this table one can easily obtain the overall mean over the entire experimental region and the average signal/noise ratios for different factors. Figure 5-9 plots the factor effects.

Experiment	y1	Y2	y3	y4	y5	y	100log(y)
A1B1C1D1	0.54	0.07	1.00	1.00	1.00	0.60	-22.15
A1B2C2D2	1.00	0.24	0.70	1.00	0.67	0.71	-14.60
A1B3C3D3	1.00	0.46	0.47	0.33	0.00	0.59	-22.70
A2B1C2D3	1.00	0.46	0.47	1.00	1.00	0.75	-12.55
A2B2C3D1	1.00	0.23	1.00	0.33	0.67	0.68	-16.46
A2B3C1D2	0.92	0.61	0.70	1.00	0.00	0.74	-13.07
A3B1C3D2	1.00	0.26	0.70	0.33	1.00	0.65	-18.56
A3B2C1D3	0.92	0.71	0.47	1.00	0.67	0.77	-11.49
A3B3C2D1	1.00	0.20	1.00	1.00	0.00	0.72	-14.33

Table 5-4 Analysis result for the orthogonal experiment array

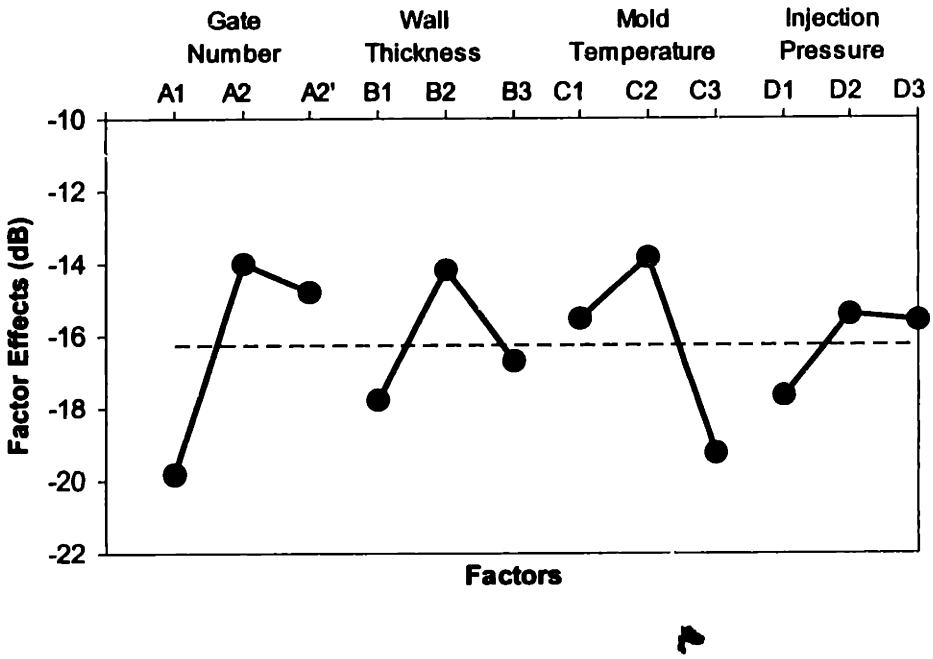

Figure 5-9 Factor effects versus factors plot for the orthogonal experiments

According to the above analysis the best setting for the experiment is A2B2C2D2, which means that we use 2 gate injection to mold the part with the minimum thickness of 0.02". The mold temperature is set 450degF. The injection pressure is set 5000psi.

5.2.3.2.4 MoldFlow analysis for the optimal experiment setup

MoldFlow analysis is performed for the optimal experiment setup discussed above. The material used for flow simulation is generic Polycarbonate. The properties are listed in table 5-1. The melt temperature is set 572 degF, a MoldFlow suggested melt temperature for PC. The solid model is created as shown in Figure 5-10. The model includes a tapered sprue, two branches of runners, two gates and a two dimensional part defined with different thickness values. MoldFlow version 9.0 can not analyze .runners of arbitrary cross section shape. Therefore we use the round runners with the equivalent hydraulic diameter instead.

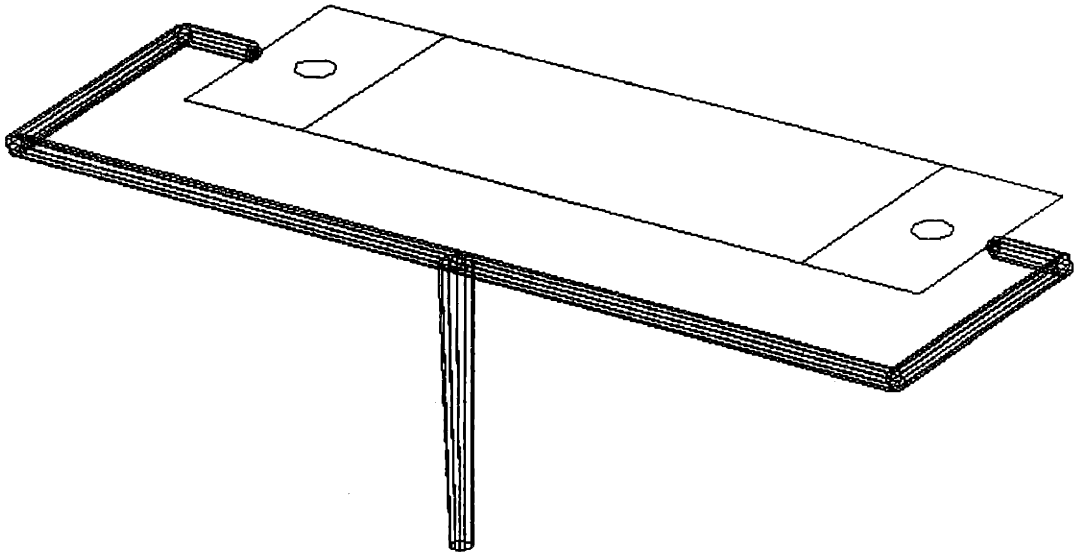

Figure 5-10 Solid model of the part created by MoldFlow modeling module

The MoldFlow fast filling analysis was performed based on Polycarbonate with the target filling time of 2 seconds, maximum injection pressure of 5000psi and mold temperature of 450 degF. The part thickness is set 0.02". The resulting temperature, filling time, shear rate and pressure distributions at the end of the filling stage are listed in Figure 5-11, 5-12, 5-13 and 5-14 respectively.

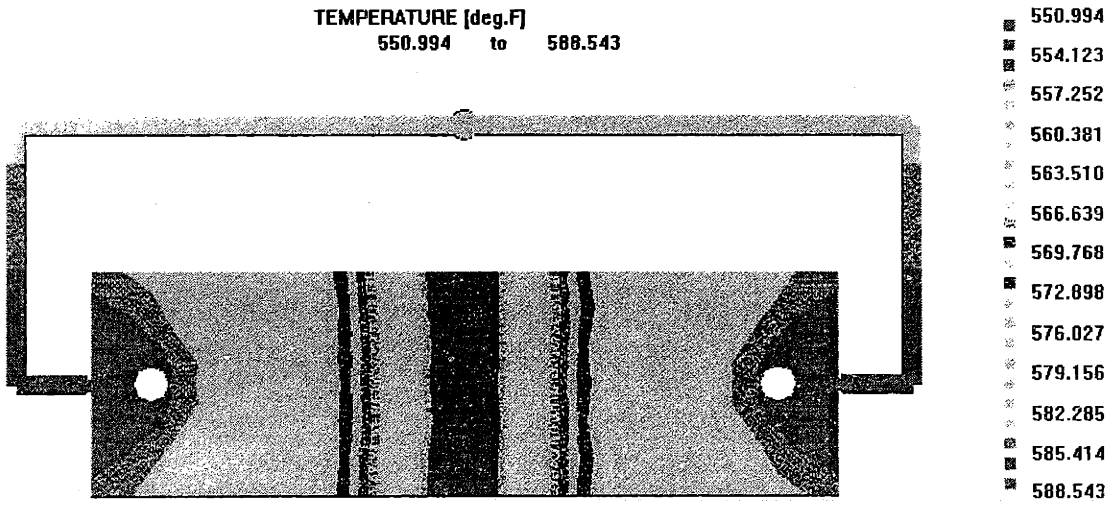

Figure 5-11 Temperature distribution after filling

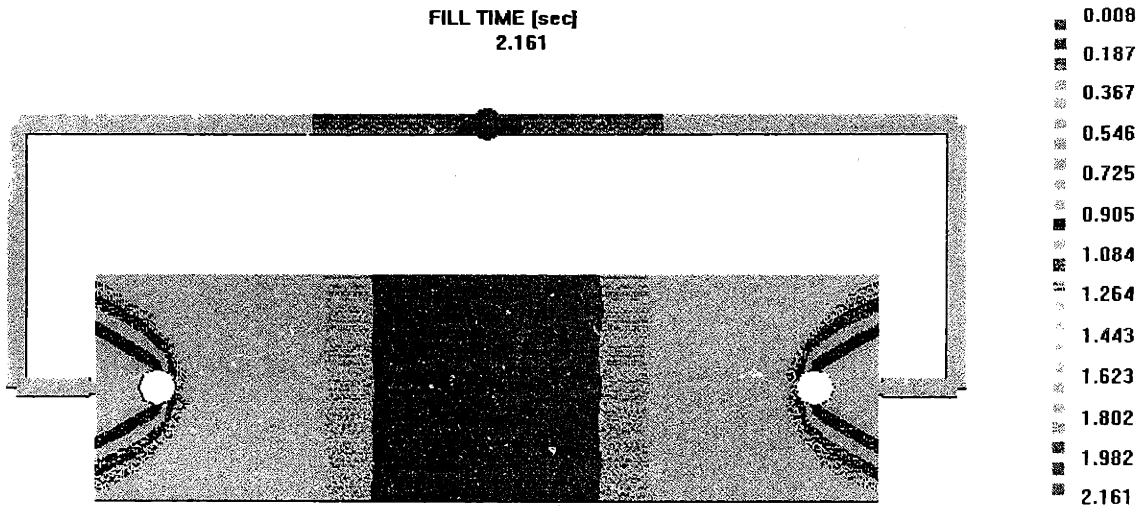

Figure 5-12 Filling time at different positions of the part

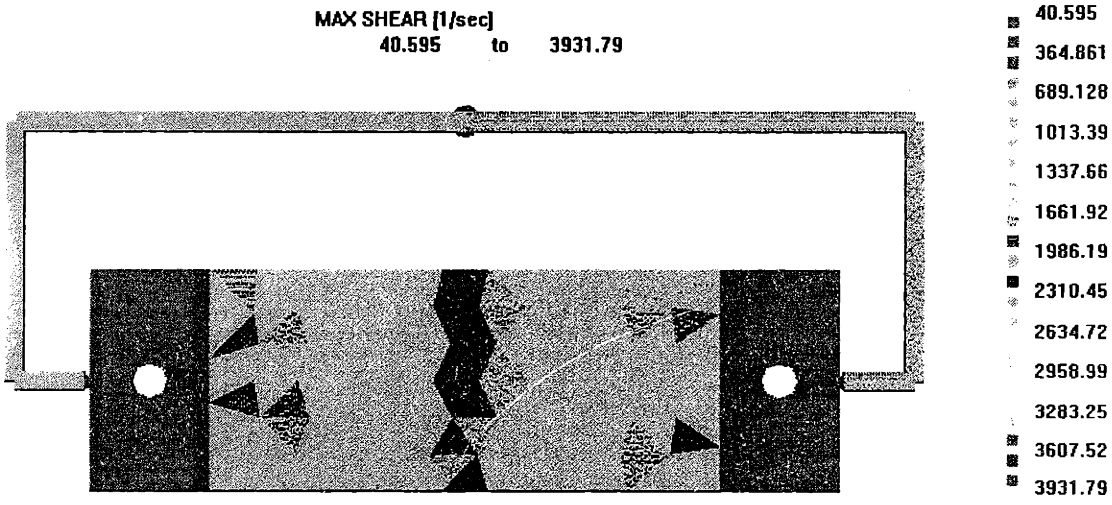

Figure 5-13 Maximum shear rate at different points of the part during filling

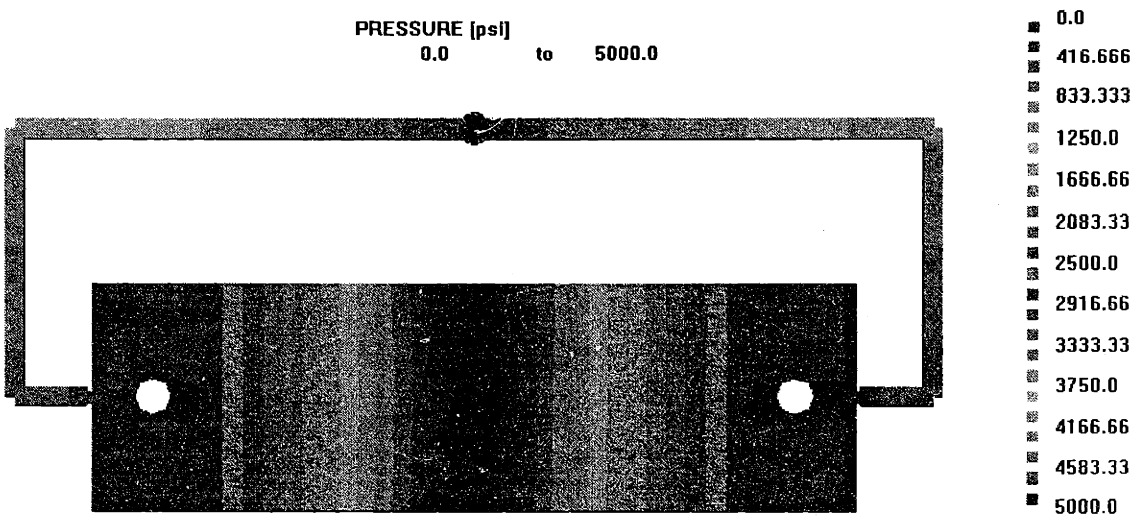

Figure 5-14 Pressure distribution in the part during filling stage

The temperature map in Figure 5-11 is taken at the end of isothermal filling. As one can see from the figure, the minimum melt temperature is 551degF. From the figure we also notice that the maximum melt temperature after filling is 588 degF, 16 degF above the initial melt temperature (572 degF). The temperature increase can be explained by the combined effect of the conductive heat transfer and the viscous heating.

Figure 5-12 shows the filling time at different point of the part. According to the figure the polymer melt takes about 1 second to flow through runners and gates and to fill the thicker areas (0.1") of the part. It then takes another 1 second to fill the thinner area (0.02") of the part. Equation (4-50) shows that the flow rate is proportional to the cube of the part thickness for a given injection pressure. Therefore the effort to further reduce the part thickness will lead to extremely long filling time or very high injection pressure. The flow simulation for the part with the thickness of 0.01" has shown an intolerably long filling time of over several hundred seconds.

Figure 5-13 is the distribution of the maximum shear rate. As one can see the maximum shear rate over the part is lower than 4000 s-1. The close view of the shear rate plot shows that the maximum shear rate of about 3930 s-1 occurs at the gate entrances. The high shear rate at the gate area suggests us to finish gates and make round corners in order to minimize the pressure drop.

The pressure distribution over the part is plotted in Figure 5-14. This plot shows that 1/3 of the total 5000 psi injection pressure is consumed in runners and gates. The net pressure applied to the cavity surface is about 3500psi. The low injection pressure helps to protect the low thermal inertia tool from mechanical failure. Although during the design of the benchmark tool we set the target process pressure of 5000 psi with a combined safety factor above 2, the pressure that an actual tool can stand may be lower than this figure because of the truss defect introduced by the fabrication processes. The actual strength of the benchmark tool is determined by strength test described in chapter 6. A low cavity pressure will no doubt help to elongate the tooling life. In the practical molding test we will slightly adjust the injection pressure setup according to the actual tool strength and the process conditions.

5.2.3.2.5 Order of magnitude confirmations

In this section we will use the order of magnitude analysis developed in chapter 4 to explain the MoldFlow result discussed above. The part is defined in Figure 5-2 and the process parameters are determined by Design of Experiment analysis in section 5.2.3.2. The parameters include: 1) injection pressure 5000psi; 2) melt temperature 572 degF; 3)mold temperature 450degF; 4) target filling time around 2 seconds

The total pressure drop during the filling stage is expressed as:

$$\Delta p = \frac{32\mu L Q}{\pi D^4} + \frac{12\mu L_g Q}{H_g{}^3 W_g} + \frac{12\mu L_1 Q}{H_1{}^3 W_1} + \frac{12\mu L_2 Q}{H_2{}^3 W_2} \qquad (5\text{-}21)$$

In the above equation, the first term is the pressure loss through the runner of diameter D and length L, the second term is the pressure drop through the gate with length L_g, depth H_g and width W_g, the third term is the pressure drop through the thick section of the part with length L_1, thickness H_1 and width W_1, the forth term is the pressure drop through the thin section of the part with with length L_2, thickness H_2 and width W_2. Since the part is gated from both sides, only half of the characteristic lengths should be included in the calculation. For a given pressure drop of 5000psi, the available melt flow rate is 0.062 in^3/sec. The resulting filling time is 2.7 seconds, which is close to the numerical simulation result of 2.16 seconds. Equation (5-21) yields up to 12.3% pressure loss through gates and runners, while the numerical simulation shows over 30% of pressure loss.

The maximum shear rate occurs at two gates and is calculated by equation (4-51). For the benchmark part discussed here, if we stick to the filling time of 2 seconds, the maximum shear rate value at the gate is about 1500s-1. This value is lower than the MoldFlow result (3931.8s-1) because of the simple flow model and constitutive law we have chosen.

The high viscous shear causes the melt temperature rise in Figure 5-11. This temperature rise can be roughly estimated by equation (4-57). The application of equation (4-57) in the design shown in Figure 5-10 yields a maximum temperautre rise of At two gates the temperature rise due to vissous shear is calcualted as

The temperature drop due to conductive heat transfer is obtained by equation (4-59). The application of this equation to the benchmark part discussed here yields a maximinum temperature drop of

5.2.3.2.6 Further discussion on MoldFlow results

Several issues deserve further discussion the numerical simulation by MoldFlow has been performed. The first issue we need to pay special attention is that even belonging to the same material category, the thermal and rheological properties of the polymer are highly different from one supplier to the other. The difference will also effect the simulation result. For example in the simulation discussed above we use a generic PC with material properties listed on table 5-1. But if we choose DOWUSA PC grade DU302, the resulting filling time will be 4.11 seconds instead of 2.16 seconds. From the material property point of view, DU302 has a higher no flow temperature (374 degF) than PC001 (347.4 degF).

The second issue is that to what extend we can elongate the filling time without introducing any side effects such as the short shot. The answer is that there is no upper limit for the filling time. Theoretically speaking the short shot will never occur for a mold temperature of 450degF because the no flow temperature for the polycarbonate material used in this analysis is about 347degF, far below the mold wall temperature. This result is supported by MoldFlow simulation. It provides us some flexibility in process condition design because we can adjust the filling time in order to leave enough time to heat the mold up to a certain target temperature. However it is important to keep in mind that if the polymer melt stay too long at a high temperature it may degrade.

Another important issue is that to what extent we can lower the mold and the melt temperature. As we know the molding above the no flow temperature will result in no short shot. However this does

not mean that we can keep the mold and the melt temperatures very low. One reason is that the low mold and melt temperatures will lead to large injection pressure and intolerably long filling time. The other reason is that the polymer melt can not mix very well at a very low process temperature.

Mold Temperature (deg F)	Melt Temperature (deg F)	Filling Time (second)	Volume% at Maximum Injection Pressure (second)
450	450	12.28	12.77%
350	450	106.52	11.29%
350	536	68.49	23.06%
400	536	16.09	24.5%
450	536	5.96	25.93%
450	572	2.16	87.65%
450	572	4.30	32.68%
450	572	5.19	81.31%

Table 5-5 MoldFlow analysis results for different temperature setups

Table 5-5 lists the filling time and the volume percentage of filling when the injection pressure first reaches the maximum (5000 psi) for mold and melt different temperature combinations. There are two interesting points worth some discussion:

First, if you check the last three rows of the table above you will see exactly same temperature conditions for three cases. But the resulting filling time varies from 2.16 seconds to 5.19 seconds. The variation is caused by different injection pressure profiles. As one can see from the table the profile that reaches the full pressure at 87.65% of full volume yields a filling time of 2.16 seconds, while a profile that reaches full pressure at 32.68% volume results in 4.3 second filling time. A very strange observation is that the filling time shows no monotonic increase or decrease with the volume percentage. As one can see the highest volume percentage (87.65%) results in the shortest filling time, while the intermediate volume percentage (81.31%) shows the longest filling time. This situation seems very conflictive but can be well explained by the shear and pressure dependent viscosity for polymer materials. As the injection speed and the injection pressure increases the resulting increase of the polymer viscosity may on the contrary slow down the filling time. Another possible reason is the viscoelastic behavior of the polymer materials. But this behavior is not considered in the MoldFlow software. The conclusion of this

observation is that we can find an optimum injection pressure profile for the shortest filling time, or a filling you of your preference.

The second issue raised from table 5-5 is that the high mold temperature allows us to reduce the melt temperature, which is very beneficial for part shrinkage control. This point has been discussed in chapter 4 and will not be redundantly discussed here. Table 5-5 gives us an impression that the combination of the mold temperature of 450degF and the melt temperature of 536degF is potentially helpful for the first step experiment because it yields a reasonable filling time of about 6 seconds with a cut down of the melt temperature by 36 degF. The filling time for this temperature combination can be further shortened if the injection pressure profile is optimized.

5.2.4 Structural design

A conceptual design shown in Figure 5-1 has been proposed for low thermal mass, thermal expansion relief, mechanical strength, buckling resistant, small energy loss, and sufficient heat transfer. This design consists of a thin shell of mold wall embedded with conformal oil channels and supported by thousands of miniature columns. The mold wall is floated on truss supports everywhere except the location of the sprue. This structure allows free expansion/shrinkage of the mold wall with minimum thermal stresses built inside. The truss structure with vertical truss columns is considered after comparing with other different structures such as the tetrahedron one and the honeycomb one.

5.2.4.1 Truss column shape design

In order to decide the shape for the individual truss columns we has considered various structural and thermal issues such as the strength, the buckling, the heat loss and the flexibility to relax thermal stress due to expansion/shrinkage. Figure 5-15 lists possible shapes for the truss and compare their performance in terms of the flexibility to relax thermal expansion/shrinkage induced stresses, stress concentration, buckling resistant, manufacturing difficulty, stiffness in vertical (load) direction, as well as the isotropic behavior. According to that table, a structure with both ends tapered (shown in the last column of the table) turns to be the best in terms of the performance. However as we will discuss later in the manufacturing section the practical implementation of this structure significantly increases the file processing time. The surface quality of this type of truss columns is also not that promising. Therefore in the final design we use simple columns with square cross sections, as shown in the first column of Figure 5-15.

Truss type / Performance	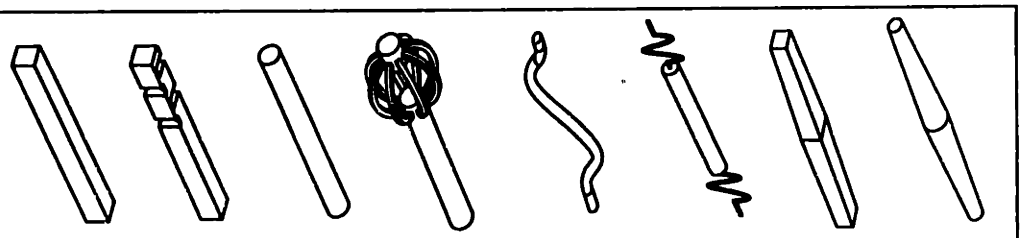							
Flexibility for thermal expansion	poor	excellent	medium	excellent	excellent	excellent	good	excellent
Stress concentration	excellent	poor	excellent	poor	poor	poor	excellent	excellent
Buckling resistant	medium	good	medium	excellent	poor	excellent	excellent	excellent
Ease of manufacturing	excellent	poor	good	poor	medium	poor	medium	excellent
Flexibility in vertical direction	medium	excellent	medium	excellent	excellent	excellent	medium	medium
Isotropic behavior	poor	good	excellent	excellent	poor	medium	medium	excellent

Figure 5-15 Different truss columns and their pros and cons

5.2.4.2 Truss size design

The truss design targets an injection pressure of under 5000 psi, a clamping force of 200kN and a mold temperature increase of 100 degC within 2 seconds. The mold material is 420 stainless steel infiltrated by Bronze. Its thermal and mechanical properties are listed in table 5-6

Density	8000 Kg/m^3
Specific heat	400J/Kg-K
Thermal conductivity	26.3W/m-K
Yield strength	7e8 Pa
Young's Modulus	2e11Pa
Thermal Expansion Coeff.	5.22e-6 m/m/K

Table 5-6 Mechanical and thermal properties for 420 Stainless Steel/Bronze

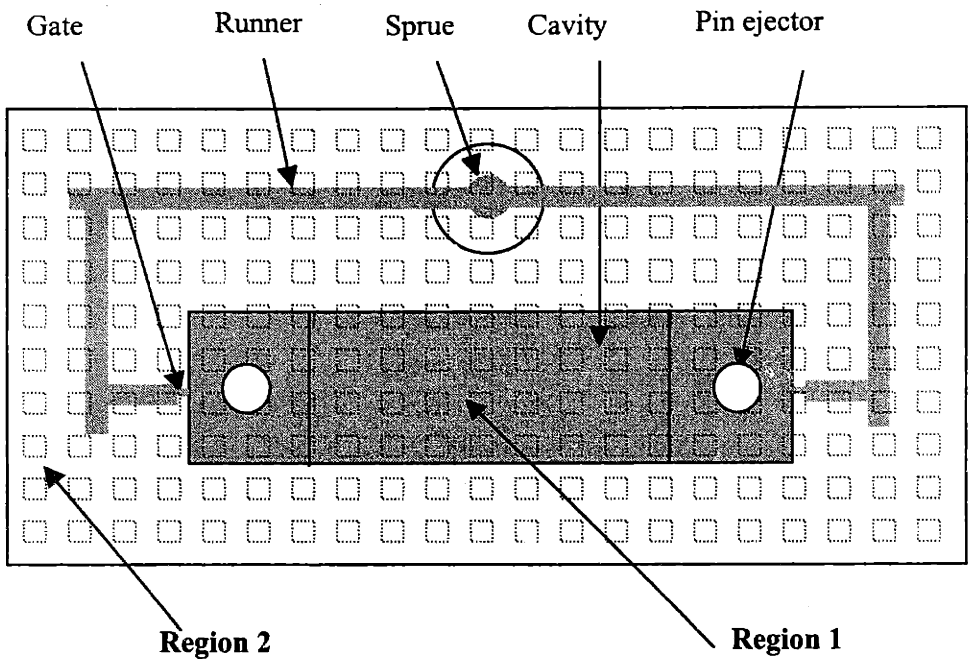

Figure 5-16 Sketch of the benchmark tool viewed from top, showing the cavity, runner, gates and truss columns

. Figure 5-16 sketches the projection view of the cavity insert with truss column supports. The truss-supported area is divided into two regions. Region 1 is underneath the cavity (shown in gray in Figure 5-16) and bears most of the injection and packing pressures during the process. Region 2 is the area surrounding the cavity that takes most of the clamping forces. There are also three scenarios in terms of loads. The first scenario is that only mechanical loads are applied on the truss structure in forms of clamping force, injection pressure and packing pressure. The second scenario is that only the thermal loads are applied on the insert. Under this condition each truss column has a prefixed displacement on the horizontal plane due to the thermal expansion/shrinkage of the top of the insert. The third scenario is that the truss columns undertake both mechanical and thermal loads. The three scenarios discussed above are corresponding with three process conditions in a rapid thermal cycle. The first scenario is the case when two halves of the mold are clamped together before the oil temperature switches. The second scenario corresponds with the case when the mold insert is preheated before the continuos cycle. The thermal scenario reflects the combined loading condition during the actual process cycle. These three scenarios will be analyzed in detail in the following sections.

5.2.4.2.1 Structural analysis with only mechanical loads applied on the insert

When no thermal expansion is considered the truss columns undertake the vertical compressive load. The process pressure p (injection pressure, packing pressure and clamping force) is applied on the top surface of the insert and then evenly distributed onto individual truss columns. Figure 5-17 shows four adjacent columns with length L, size d X d and pitch distance D.. Given the maximum process pressure p = 5000psi and the yield strength of 420 Stainless steel/Bronze system σ=1e5psi, the strength criteria for truss columns in region 1 is then expressed as:

$$pD^2 \le n\sigma d^2 \tag{5-22}$$

where n is the safety factor. For the truss size d = 0.053" and the pitch distance D = 0.1", the safety factor n is calculated as 5.6 under a maximum process pressure of 5000psi. The truss supports occupy 28.1% of the total surface area in region 1.

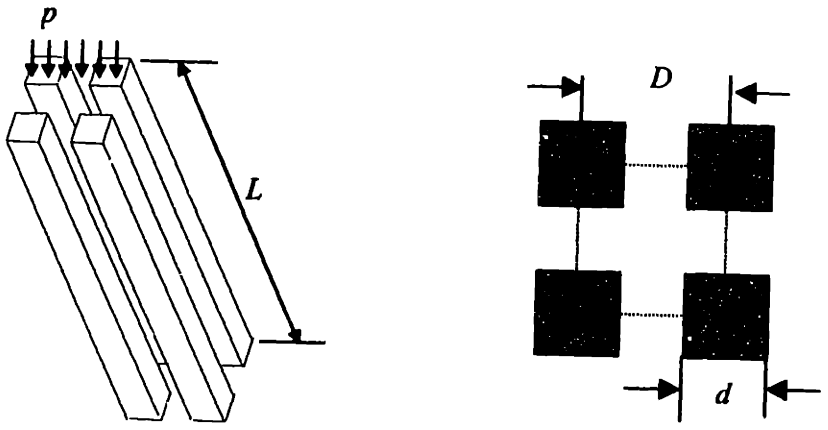

Figure 5-17 Right: truss columns under the process pressure. Left: top view of truss columns showing the dimension

In addition to the strength calculation the critical force is also checked to ensure that the columns are not buckled under the compressive pressure. The critical load that would result in failure of the column is expressed by equation (5-23).

$$P_{cr} = \frac{4\pi^2 EI}{l^2} \tag{5-23}$$

where E is the young's modulus of the truss material, I is the momentum of inertia for the truss column and l is the length of the truss. In our design of the benchmark tool, we choose the truss column size d = 0.053", length l = 1". This design results in a critical buckling force of 762.7lbs. This buckling force results in a distributed compressive stress of 2.72e5psi on each truss column. Considering that the truss columns cover only 28.1% of the insert area, the minimum stress that may lead to the buckling of the

truss structure is therefore 7.63e4psi. However our target process pressure is 5000psi. Therefore the truss columns will not buckle under the target process condition.

5.2.4.2.2 Structural analysis with only thermal loads applied on the insert

In the rapid thermal cycling process when the heat transfer oil switches between hot and cold the top plate of the insert where the oil channels are embedded experiences an abrupt temperature change. This temperature change results in the thermal expansion or shrinkage of the top plate on the horizontal plane. Figure 5-18 shows the top view of the mold insert. As we have discussed before the top plate of the insert is floated on thousands of truss columns except one solid contact with the base of the insert by the post at the sprue area. This is the center point where the rest of the top plate expands around as the hot oil flows through. The maximum distance from the sprue post to the edge of the top plate is denoted as r. The abrupt temperature change during rapid heating is ΔT. Then the maximum thermal expansion of the top plate due to the thermal load is therefore:

$$\delta = \beta \Delta T r \qquad (5\text{-}24)$$

where β is the thermal expansion coefficient of the 3DP material.

For the benchmark mold designed for rapid thermal cycling test, the distance $r \cong 4$", the maximum displacement at the corner of the mold due to thermal expansion is $\delta \cong 0.004$".

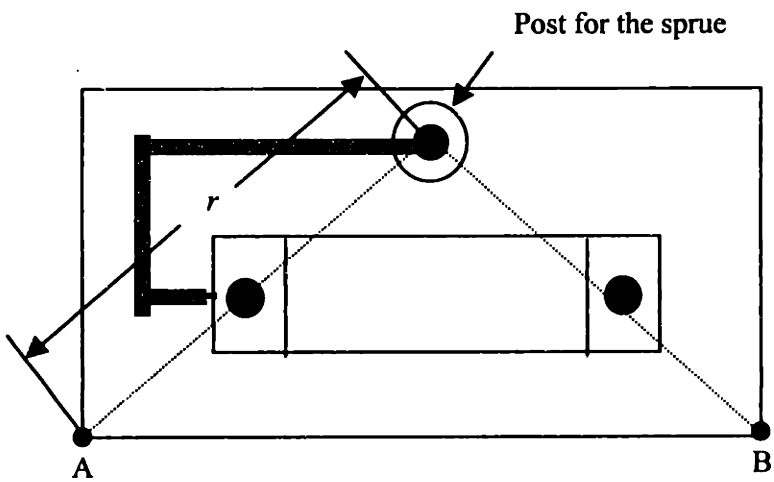

Figure 5-18 Top view of the insert showing the points (A and B) subject to the maximum thermal expansion

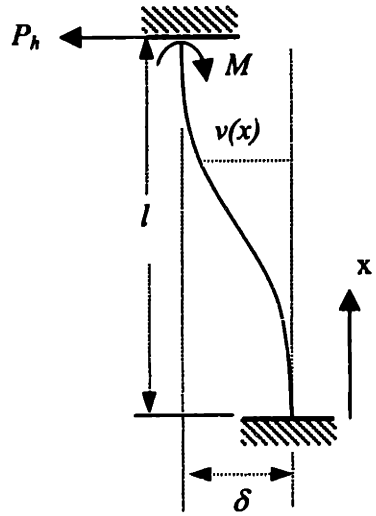

Figure 5-19 Individual truss column with horizontal displacement δ

As the top plate of the insert expands the supporting truss columns are also forced to shift a certain distance δ. This prefixed displacement will introduce the horizontal force P_h and the bending moment M_0 at the top of the column and eventually results in the stress buildup inside the column. Figure 5-19 sketches a single truss column with a horizontal displacement δ, a horizontal force P_h and the bending moment M_0. The equilibrium equation for a point on the column with a distance x to the ground is:

$$M(x) + P_h(l - x) = M_0 \tag{5-25}$$

In the mean time the bending moment $M(x)$ is associated with the deflection $v(x)$ by the following expression:

$$M(x) = -EIv''(x) \tag{5-26}$$

The combination of equations (5-25) and (5-26) yields:

$$-EIv''(x) + P_h(l - x) = M_0 \tag{5-27}$$

The boundary conditions are:

$$\begin{aligned} &v(x = 0) = 0 \\ &v(x = l) = \delta \\ &v'(x = 0) = 0 \\ &v'(x = l) = 0 \end{aligned} \tag{5-28}$$

The solution of equation (5-27) with boundary conditions (5-28) yields:

$$P_h = \frac{12EI\delta}{l^3} \tag{5-29}$$

$$M_0 = \frac{P_h l}{2} \tag{5-30}$$

The maximum stress due to the bending moment is:

$$\sigma = \frac{M_0 d}{2I} = \frac{3d\delta}{l^2}E \tag{5-31}$$

The shear stress due to the horizontal force is approximately:

$$\tau = \frac{P_h}{A} = \frac{d^2\delta}{l^3}E \tag{5-32}$$

The von mises creterion in this case is thus:

$$[\sigma] \geq \sqrt{\sigma^2 + 3\tau^2} \tag{5-33}$$

The application of the above analysis to truss columns for the benchmark tool (d = 0.053", l = 1", δ = 0.004") yields a von mises stress of 1.87e4 psi, leaving a safety factor of 5.34 if we choose the yield strength of the 3DP material as 1e5 psi.

5.2.4.2.3 Structural analysis with both mechanical loads and thermal loads applied

In most of the rapid thermal cycle the truss support undertakes both the mechanical and thermal loads. For each truss column it is simultaneously subject to a vertical compression force P_v (caused by process pressures), a horizontal force P_v (caused by thermal expansion/shrinkage) and a bending moment M, as shown in Figure 5-20. The equilibrium equation at position x on the truss column is:

$$M(x) + P_h(l - x) + P_v(d - v(x)) = M_0 \tag{5-34}$$

where $v(x)$ is the deflection of the beam at position x, $M(x)$ is the bending moment at position x.

Following the similar procedure as shown in the previous section, we can obtain the differential equation in terms of deflection $v(x)$:

$$v''(x)+\frac{P_v}{EI}v=\frac{-P_h x+P_h l+P_v\delta-M_0}{EI} \tag{5-35}$$

If we define:

$$\lambda=\sqrt{\frac{P_v}{EI}} \tag{5-36}$$

Then the solution for the governing equation (5-34) will be:

$$P_h=\frac{P_v\lambda\Delta\sin(\lambda l)}{2-2\cos(\lambda l)-\lambda l\sin(\lambda l)} \tag{5-37}$$

$$M_0=\frac{P_0\Delta[1-\cos(\lambda l)]}{2-2\cos(\lambda l)-\lambda l\sin(\lambda l)} \tag{5-38}$$

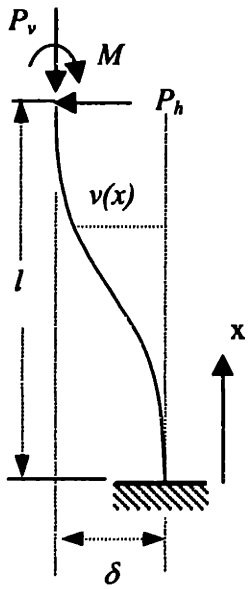

Figure 5-20 Single truss column with loads applied on the top

Buckling occurs as the denominator of equations (5-37) and (5-38) turns to zero. That is:

$$2-2\cos(\lambda l)-\lambda l\sin(\lambda l)=0 \tag{5-39}$$

The above equation leads to two buckling conditions:

$$\sin(\frac{\lambda l}{2})=0 \tag{5-40}$$

$$\tan(\frac{\lambda l}{2})=\frac{\lambda l}{2} \tag{5-41}$$

Equation (5-40) yields the smallest positive critical buckling force as below:

$$P_{cr} = \frac{4\pi^2 EI}{l^2} \tag{5-42}$$

Equation (5-41) yields another smallest positive critical buckling force as:

$$P_{cr} = \frac{8.19\pi^2 EI}{l^2} \tag{5-43}$$

After comparing two equations above, we notice that the smallest buckling force is determined by equation (5-43), which is identical to expression (5-23) in the case of the pure vertical loading without horizontal displacement. We know from the analysis that our design of the truss columns will not lead to buckling under the target process pressure of 5000 psi.

Next we check the stress distribution in truss columns to see if they will fail under the mechanical and thermal loads. Since we have obtained the bending moment, the compressive load and the horizontal force applied on the top of the truss columns, we can calculate von mises stresses in truss columns using equation (5-33). Notice that here the normal stress consists of the part caused by bending moment and the part caused by the compressive load. The truss columns we designed in the benchmark tool yield the maximum von mises stress of 3.57e4 psi, which corresponds with a safety factor of 2.8 for the existing 3DP material.

In the above calculations we did not distinguish between different regions of the insert. We recognize that the clamping force applied on region 2 should large enough to overcome the force applied on the cavity by the injection/packing pressure in order to avoid the flashing of the polymer melt through the parting face. Therefore the clamping pressure p_{clamp} applied in this region observes the following rule:

$$p_{clamp} \geq p_{inj} \frac{A_{cavity}}{A_{clamp}} \tag{5-44}$$

where p_{inj} is the injection pressure, A_{cavity} is the cavity projection area, A_{clamp} is the area of the parting face. In the design of the benchmark part the ratio between A_{cavity} and A_{clamp} is 1:1.8. Therefore the minimum clamping pressure is about 3000psi. This value is then used for the stress analysis.

5.2.4.3 Result of structural design and geometric modeling

By applying design rules and simulations discussed in previous sections, we have successfully designed the benchmark inserts with low thermal inertia, uniform temperature control and strength under pressure pressures and temperature changes. Figure 5-21 shows the CAD model of the cavity insert. As one can see from the figure, the tool consists of thousands of 1 inch long truss columns sandwiched by two parallel plates. The cavity will be EDMed on the flat surface of the top plate. Two big holes on the top surface of the part are for pin ejectors. A big hole in the middle area is for sprue puller. 10 small holes are placed pararrelly on the top of the insert surface for connectivity checking of 10 parallel channels underneath the mold surface (as shown in the cutaway view in right). These 10 holes will be plugged before the debinding process and finally machined after sintering to leave a flat surface for EDM.

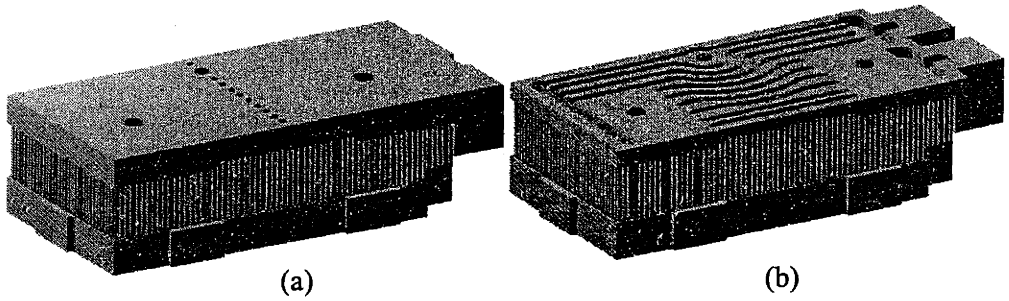

Figure 5-21 (a) solid model of the cavity insert for rapid thermal cycling test. (b) cutaway view of the cavity insert showing the conformal channels inside

5.2.5 Oil delivery system design

The design of the hot/cold oil circulation system for rapid thermal cycling should consider the following issues:

1) Minimum mixture between hot and cold oil. This effort will reduce the unnecessary energy loss, improve the system efficiency and avoid potential hazard.
2) Rapid response to the process control input. That is to say, once the oil delivery system receives the rapid heating signal, it should deliver the hot oil of required temperature in a short time, say within 1 second. Same thing happens for rapid cooling. In order to achieve that the thermal inertia of the system should be kept low.
3) Maintaining the temperature level for hot and cold oil. The system should have the ability to maintain the temperature levels in order to recover the energy change of the hot and the cold oil due to the rapid thermal cycle.

4) Safety issues. The system should run safe and robust. The hazard area should not be exposed to the operator. The high pressure, high flow rate and high temperature area should be minimized and securely protected.

5) Power and pressure capability. The system should have enough power for heating/cooling purpose. The oil pump should have the ability to deliver oil of required flow rate.

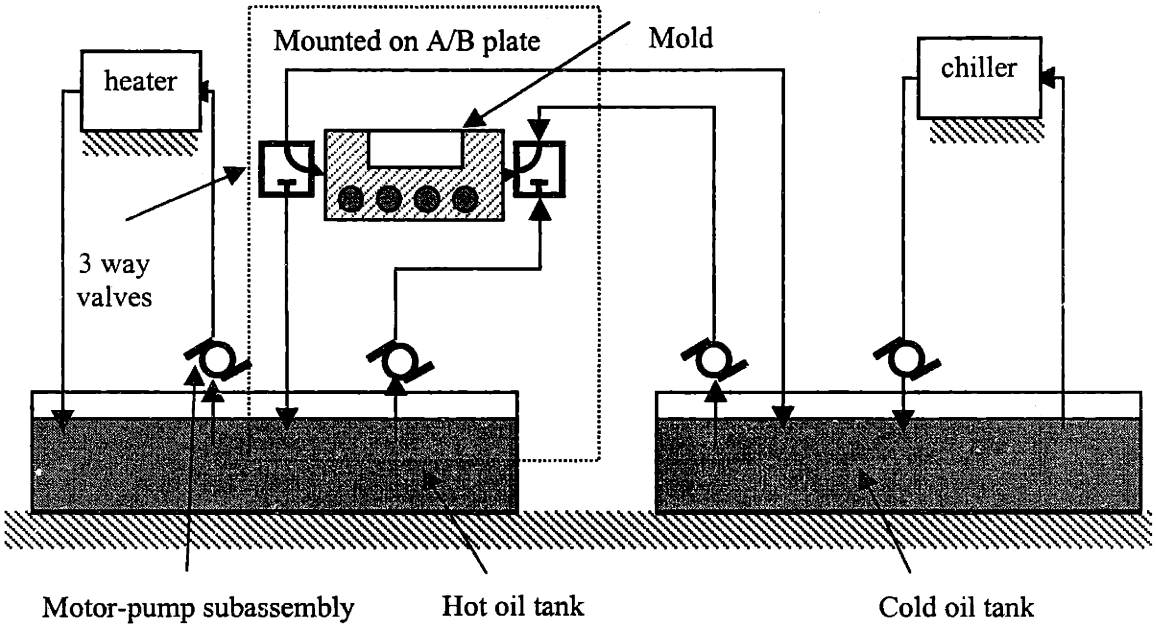

Figure 5-22 A oil circulation system proposed for rapid thermal cycling

A circulation system sketched in Figure 5-22 is proposed. In this figure there are two tanks holding hot and cold oil respectively. For the hot tank, a pump driven by a motor keeps circulating the hot oil through the heater in order to maintain a high temperature level. For the cold tank, a pump keeps circulating the cold oil through the chiller to maintain a low temperature level for the oil. Between the hot oil tank and the cold oil tank is the oil circuit consisting of pumps, 3 way valves and mold inserts. The pumps are regulated to a certain pressure, say 100 psi so that the excessive oil will flow back to the oil tank. The 3 way valves are ball valves operated by pneumatic actuators which is controlled by solenoid cylinders. The details of the valve selection will be discussed in the following subsections. As the rapid thermal cycle starts, both two valves switch to the hot tank side so that the hot oil flows through the mold insert back to the tank. After the rapid heating stage there is residual hot oil left inside channels in the mold insert that may lead to the mixture with the cold oil. In order to minimize this mixture, two 3 way valves are sequenced so that the hot oil rest in the channel is driven back to the hot tank before the cold

oil flow through. This kind of sequencing is achieved by switching the right side 3 way valve first so that the oil from the cold oil tank is pumped into the mold insert to push the rest hot oil back to the hot tank. Once all the hot oil returns the hot tank, the left side 3 way valve switches to the cold oil side too to complete the circuit for the cold oil.

5.2.5.1 Design for heater/chiller capacity.

The heater/chiller size is determined by the following equation.

$$W = c_m M \Delta T / t \tag{5-45}$$

where c_m is the specific heat of the mold material, M is the mass of the insert, ΔT is the desired mold temperature change and t is the time that can be used to recover the energy loss of the oil due to rapid heating, typically it is the cycle time. For a mold insert of 7"X3.25"X0.3", a 5 KW heater is required to heat one side insert by 100 degC assuming the injection cycle time of 10 seconds. A more accurate estimation of the energy consumption in rapid thermal cycling can be performed using the methods discussed in the last chapter.

5.2.5.2 Design for heating/cooling efficiency.

The heater's power estimation in the last section is based on the assumption that the energy delivery from the heater or the chiller to the mold insert is sufficient and prompt. However in most cases the energy transfer is not prompt due to the thermal mass of the insert and the heat transfer condition at the oil channel interface. The larger the oil channel surface area, the more efficiently the insert is heated/cooled. The larger the flow rate, the faster the insert reaches the desired temperature level.

The Reynolds number for the oil flow of a certain flow rate Q in a channel with the size of D is:

$$R_{eD} = \frac{4Q}{\mu \pi D} \tag{5-46}$$

The friction factor is:

$$f = [0.79 \ln(R_{eD}) - 1.64]^{-2} \tag{5-47}$$

The Nusselt number is:

$$N_u = 0.125 f (\mathrm{Re} - 1000) \mathrm{Pr}[1 + 12.7(P_r^{0.4} - 1)(f/8)^{0.5}]^{-1} \tag{5-48}$$

The heat transfer coefficient is therefore:

$$h = \frac{K_c N_u}{D} \tag{5-49}$$

For an insert with the size specified above the total number of the required oil channels are 10, with a total flow rate of 10GPM.

5.2.5.3 Construction of the oil circulation system

The design of the oil circulation system for rapid thermal cycling has to consider the energy efficiency, the response speed, the robustness and the safety. Figure 5-23 sketches the design we have proposed that satisfies the above basic requirements. The figure shows part of the injection molding machine from the backward. On the stationary plate and the mobile plate of the machine stand two solenoid controlled air actuated 3 way ball valves. In a narrow area between the press and the backward safety door is the hot oil tank. The volume of the tank is about 10 liters. It is divided into several regions from the top, but connected all the way on the bottom. Three pump/motor subassemblies are placed on the top of the tank. Subassembly 1 attaches the mobile plate and is responsible for pumping hot oil to the cavity insert on the B side of the mold. It moves with the cavity insert. Subassemblies 2 and 3 are placed stationary on the top of the hot tank. Subassembly 2 is in charge of the hot oil supply to the core insert. Subassembly 3 is in charge of circulating hot oil through the heater which is mounted on the right side of the hot tank. On the same altitude level, outside the molding machine, sits a cold oil tank. There are two pump/motor assemblies installed on the cold oil tank. One is for supplying cold oils for both the cavity and the core inserts. The other is for circulating the cold oil through the chiller which is not shown in the figure.

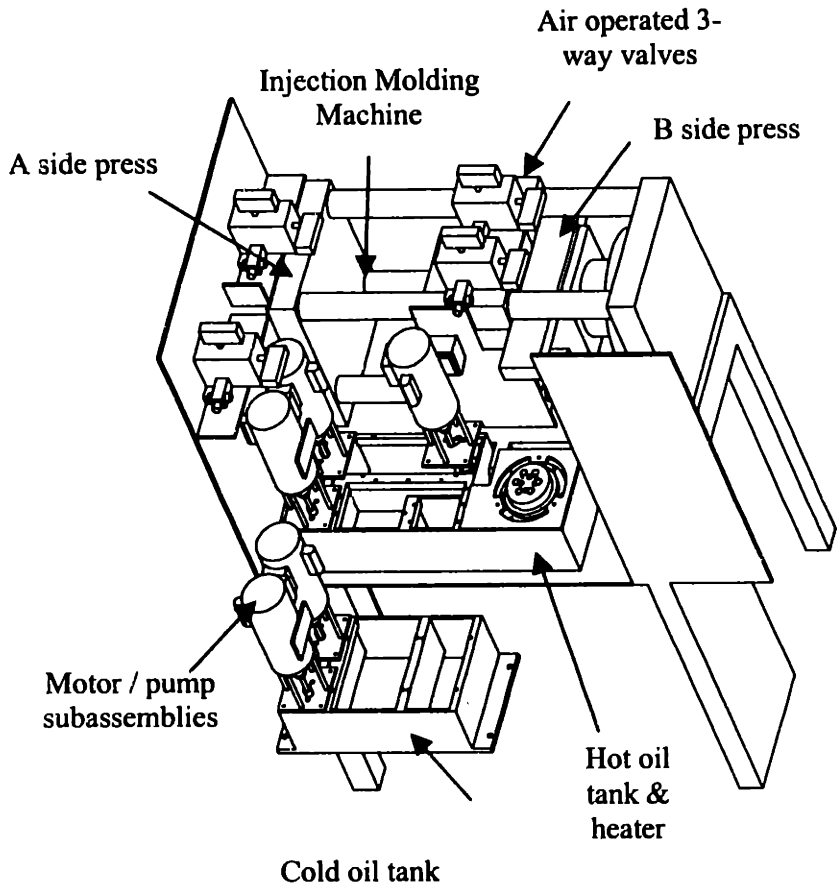

Figure 5-23 Physical construction of the oil circulation system

5.2.5.4 Pump /motor subassembly

The pump/motor subassembly is the key element for the oil circulation system discussed above. It not only circulates the oil through the heater and the chiller but also maintains a certain pumping pressure to the inserts. Figure 5-24 shows the physical model of the pump/motor subassembly. It consists of a AC motor sitting on a plate by four supporting rods and attached by an automobile oil pump. The Dayton 1K063 single phase industrial motor (1/3 HP, 1725 RPM) is chosen for the subassembly. The pump is chosen from one of the automobile oil pumps fabicated by Melling Automotive Products. The part number is M-65B. It is a rotor type assembly integrated with the pressure relief valve. For more inforamtion on this product, please check http://www.melling.com/propump.html. A flexible wafer spring coupling from Berg (part No. CO20-19P) is used to connect between the shaft of the motor and the shaft of the pump. The subassembly provides a flow rate of about 8 GPM at full load using water.

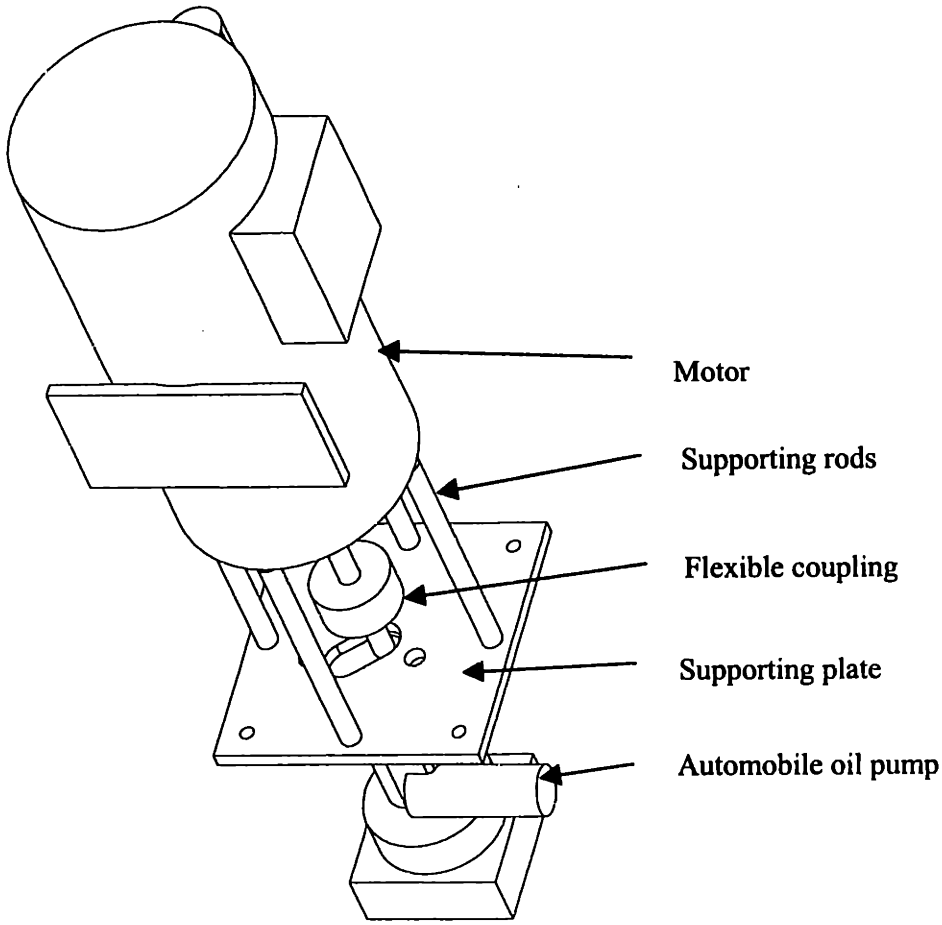

Figure 5-24 Sketch of the pump/motor subassembly

5.2.5.5 Solenoid /actuator /ball valve subassembly

The solenoid /actuator/ball valve subassembly is sketched in Figure 5-25.

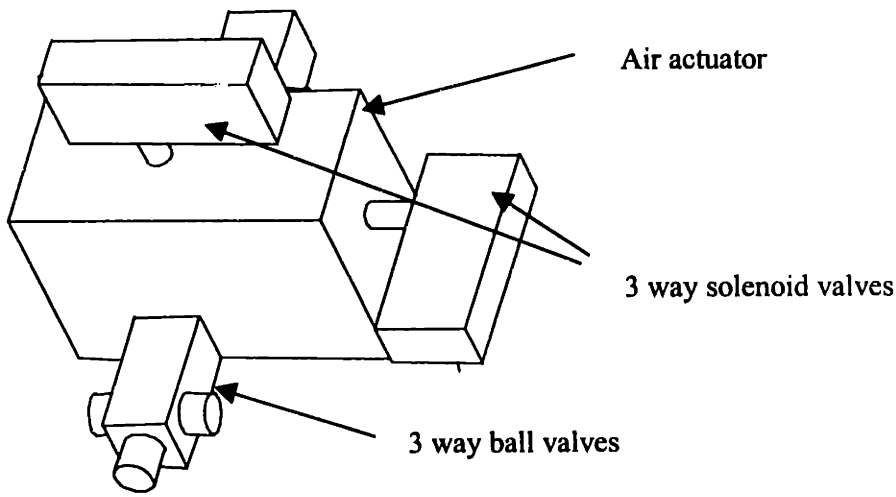

Figure 5-25 Sketch of the solenoid/actuator/ball valve subassembly

In this sketch two 3 way solenoid valves ordered from Air Inc. (part no. 320-120/60NO) were mounted on a air actuator to operate the 3 way ball valve. The air actuator and ball valve assembly was ordered from Cambridge Valve & Fitting Inc., part number SS-62XOPF4-53D. The experiment with this subassembly has demonstrated a fast switching time of less than 0.3 seconds.

5.2.6 Mold base and assembly design

The MUD 08/09 UF quick change "U" style mold frame and the companion T style insert mold are used for the project. Figure 5-26 shows the A-side mold frame assembly designed for the experiment. The assembly is used to mold the part shown on the top of the figure. The core insert with the flat surface is installed in a pocket machined on the 08/09 companion mold with a separation of an insulation plate. Several tapped and clearance holes are made on the on the insert, the insulation plate and the companion mold to locate the insert in z direction with respect to the mold base. On the bottom plate of the insert are platforms on both yz plane and xz plane which are used to align the insert in x and y direction. The whole assembly will be placed vertically with the x direction down. Two screws are used from the side of the mold to push the insert against the wall of the companion mold. In this way we have completely aligned and held the mold insert.

A high temperature insulator sheet made of the glass-reinforced polymer composite [D-M-E] is used for insulation between the insert and the mold base. The function of this insulator sheet is to isolate the insert from the rest of the mold and keep the thermal inertia of the tool low and the energy loss from the oil delivery system low.

For rapid thermal cycling of Polycarbonate, the process temperature is as high as 300 degC, the ejection temperature is 156 degC. The mold base should be kept at an intermediate temperature, say 220 degC, to minimize the energy loss from the insert to the environment. The mold base temperature is maintained by heaters installed on the companion mold, as shown in Figure 5-26.

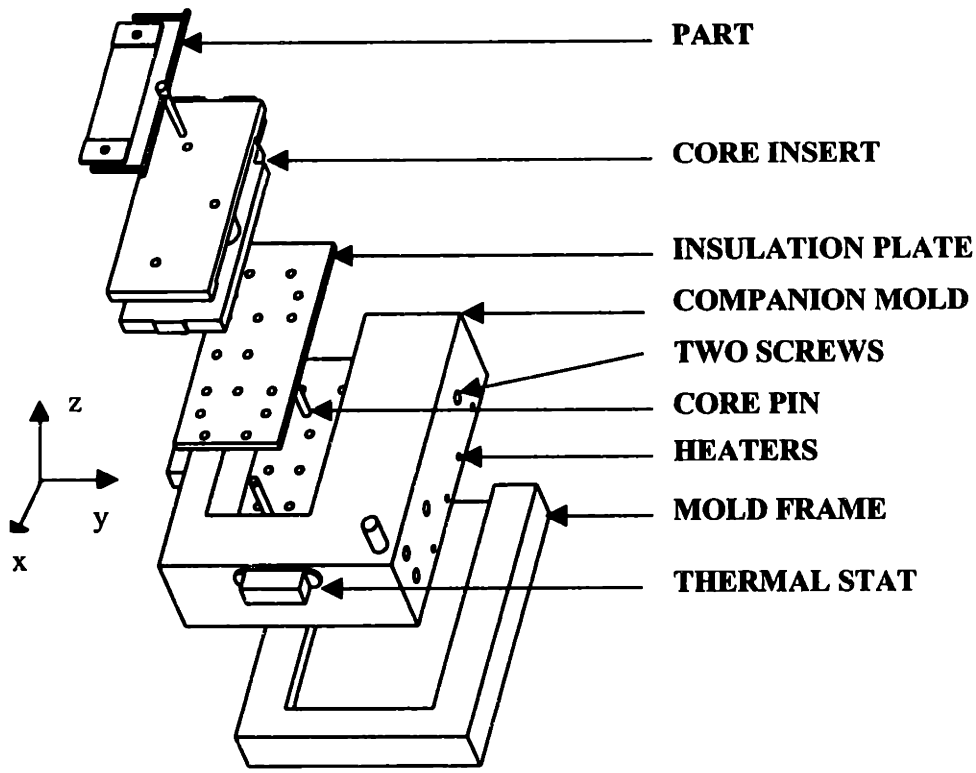

Figure 5-26 B-side mold frame assembly for rapid thermal cycling test

5.3 FABRICATION ISSUES FOR RAPID THERMAL CYCLING

In order to obtain tools for rapid thermal cycling test the first step is to fabricate the green part by selectively printing the Acrysol binder on the stainless steel powder bed on a 3D Printing machine. Then the green part is subject to a standard routine of post processing following a standard routine described in [Guo 1998] in order to obtain the full density. The post-processing procedure is best illustrated by Figure 5-27. In this procedure the first step is called debinding. The green part is placed in a graphite crucible embedded with the Zirconia powder. The water vaporizes above 100degC and the Acrycol binder evaporates at a temperature around 500degC. The debinding is immediately followed by light sintering to give the skeleton a certain degree of sintering strength. The second step is sintering. The purpose for this step is to enhance the strength of the skeleton in preparation for the infiltration. Sinter procedure is performed at a high temperature where a neck is formed among stainless steel particles by solid state diffusion bonding. The third step is called infiltration where the porous skeleton is filled by the liquid bronze by capillary action. After the skeleton is infiltrated a near net-shape tool is ready for further machining.

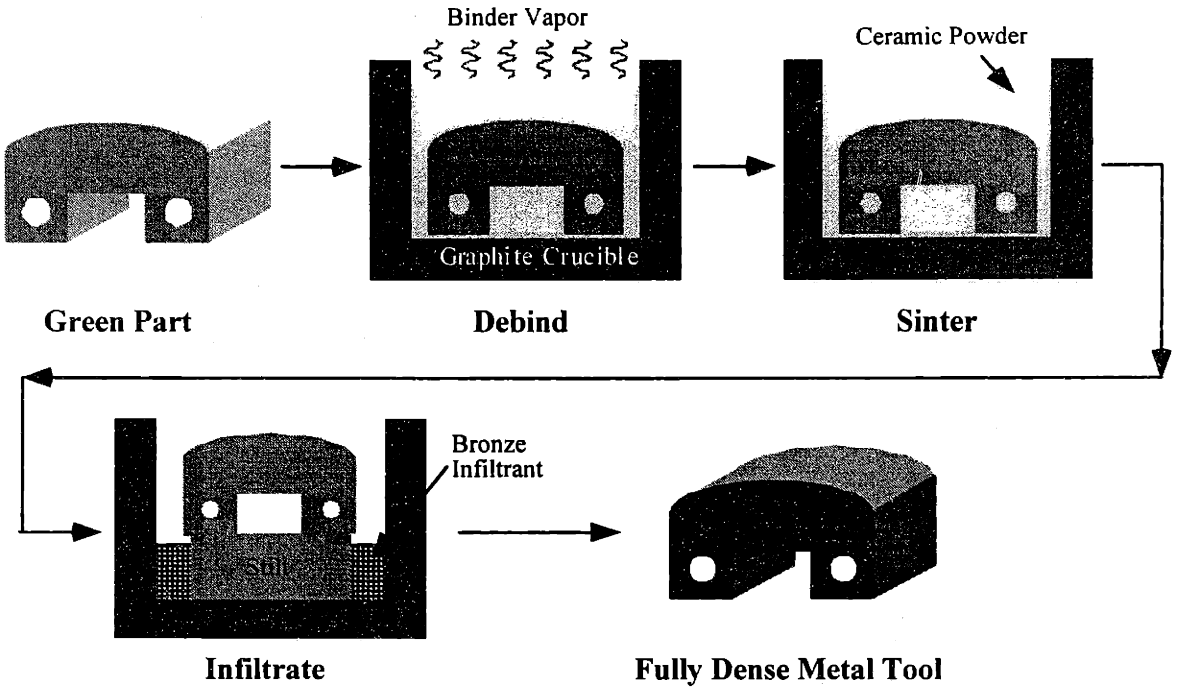

Figure 5-27 Post-processing steps for 3D Printed green parts

5.3.1 Fabrication test by sample structures

There are a lot of quality issues associated with a post process for 3D Printed green part. These issues include the green part strength, the ease of powder removal, the porosity, the deformation and the defect. In order to investigate all these fabrication problems with little cost of processing time, sample truss structures are designed and tested. The sample structure is simply a local copy of the benchmark tool, with top and bottom plates and truss columns of the same size and space as that in the benchmark tool, as shown in Figure 5-28.

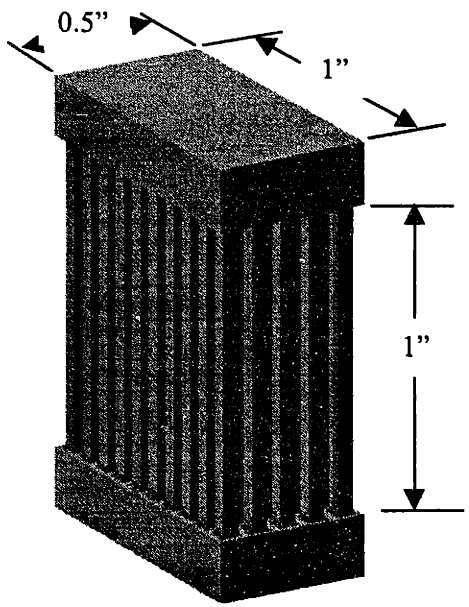

Figure 5-28 The sample truss structure for manufacturing test

The sample in Figure 5-28 has two 1"X0.5"X0.25" plates joined with 50 trusses (5 rows X 10 columns) of 1 inch long. Tests performed on this sample are illustrated by Figure 5-29:

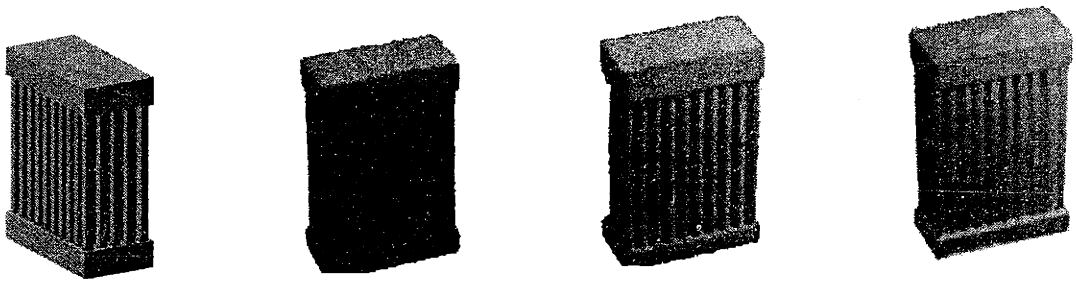

CAD model:	3D Printing:	Debinding/Sintering:	Infiltration:
-model size	-printing defect	-deformation	-part quality
-model quality	-powder removal	-packing powder	-min. stilt height
-data processing	-green part	removal	...
-...	strength	-...	
	-...		

Figure 5-29 Testing procedures for the sample truss structure

At the CAD model stage, the STL models of the truss samples are sliced by Materialise® package and encoded to the 3DP format which is readable by a 3D Printing machine. Truss columns of

different shapes and sizes are modeled and compared in terms of the model size the model quality and the printing data processing time. At the printing stage, the green parts of different truss structures are printed to investigate the printing related issues such as the defect, the ease of the powder removal and the strength the truss columns. After printing the debinding and sintering is performed in a single step in the scalable furnace developed at 3D Printing Lab. The issues such as the resulting buckling of truss columns, the packing powder removal from the sintered part and the strength of the sintered part are investigated. The information is used to improve the process condition for the reduced part deformation. The final stage is infiltration. In this stage the sintered part is put into the same scalable furnace mentioned above for infiltration into full density. The infiltration quality, the minimum stilt height and other issues are investigated during this period. In a word the procedure shown in Figure 5-29 mimics the post-processing procedure for the final benchmark tool, with a certain simplicity and smaller scale. The knowledge obtained from this procedure is directly useful for planning the post-processing of the benchmark tool.

5.3.2 Printing issues

5.3.2.1 Power removal

In the design of truss structures for the low thermal inertia tooling, it is important to determine the size and the density of truss elements so that the loose powder can be easily removed without damaging the fragile trusses after the green part is printed. Different sizes of truss structures have been tested on the sample part. It is proved by experiment that the design with truss equivalent diameter of 0.05" and distribution density of 25% results in the easy removal of loose powder from the green part. The printing defect may lead to small web structures between columns. This web structures as well as some loose powder deposited at corners can be easily removed by jewel's saw after the part is debinded and sintered to a certain strength.

The ease of powder removal is also taken into consideration in the design of the conformal oil channels. One issue is that the cooling channel can not be too small to make the powder removal difficult. The experiment has shown that a channel of 0.1"X0.1" with a total length of 8" is possible to clean the powder. The other issue is how to check the channel connectivity. Basically the channel system shown in Figure 5-8 with single inlet, single outlet and parallel manifolds between them are not favorable because one can hardly identify which channel is blocked. However in many cases the single channel configuration is not practical because of the extremely high pressure drop. In these cases we have to build parallel channels and develop a method for channel connectivity checking. The method is to print small

openings on the insert surface at the middle point of each parallel manifold (as shown in Figure 5-30). By blocking other holes and opening one we can check if the powder is cleaned from the corresponding channel. After each channel has been cleaned, the openings are sealed by 3D Printed plugs before the next step processes of debinding and sintering. The sintering process joins those plugs with the green part. The sintered part is machined later to remove the head of those plugs and obtain a flat surface.

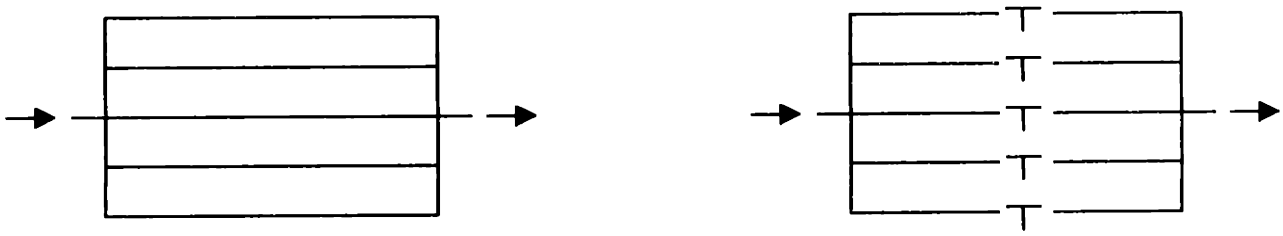

(a) (b)

Figure 5-30 (a) Layout of the cooling channels with single inlet, single outlet and multiple branches. (b) Adding plugs in the middle of individual branches to check the connectivity

5.3.2.2 Printing test for trusses with different column shapes

As we have discussed in the pervious section, the shape of the truss column influences the solid model size, the data preparation time and the green part quality. In Figure 5-31 five different column shapes are designed to test the file preparation and printing related issues.

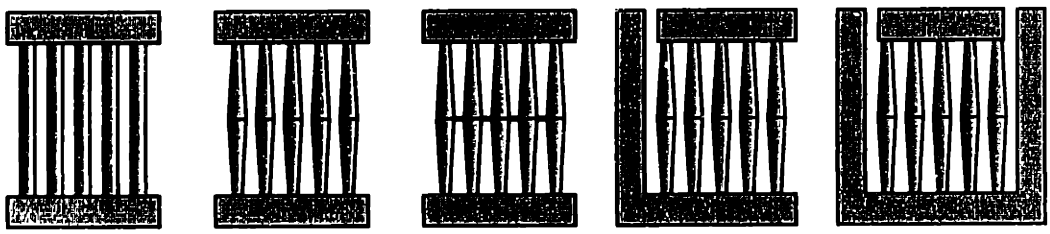

(a) (b) (c) (d) (e)

Figure 5-31 First set of truss samples testing different shapes of truss columns

In the above figure, (a) has straight columns with square or round cross sections, (b) has drum shaped columns consisting of two terraces. The cross sections for columns in (b) are round. (c) is designed to improve the green part strength by linking adjacent columns with thin web. The reason for this design is that we have observed that the truss columns are fragile and easy to be broken in the powder

removal process. Figure (c) and (d) are designed to compensate the powder bed shifting due to one way spreading. In the 3D Printing process, a cylinder moves from one end of the powder bed to the other end in order to prepare a thin layer for printing. However the single direction spreading pushes the powder bed in one direction and may lead to accumulative error in slow axis, even defects in the printed part. In (d) a wall is build next to the truss columns in order to protect the fragile structure from spreading defects. In (e) walls are built on both sides of truss columns. The printing results if these sample parts indicate:

1) Trusses with tapered columns results in a huge STL file size and a significantly long preprocessing time. Although theoretical favorable, these types of truss structures are not practical for the part shown in Figure 5-21 where over 2000 truss columns have to be printed. A simple straight column configuration dramatically reduces the file size and data preprocessing time.
2) Although columns with circular cross sections shows more favorable isotropic behavior under heavy loading, the printing quality is not as high as those with square cross sections. Besides the file size for the former is relatively larger than the latter.
3) Spreading defect is improved by adding two way spreading function to the spreading cylinder. Therefore there is no necessary to add walls in adjacent with truss structures.

The test printing of the samples shown in Figure 5-32 suggests that we use simple straight columns with square cross sections for better printing quality and smaller file size. On observing the printed samples we noticed that the connection between the truss column and the top/bottom plate is so weak that a slight motion will break the truss column. This situation initiates our second round printing of test samples with the fillets and chamfers added to individual truss columns at the connection points.

5.3.2.3 Printing test with fillets and chamfers

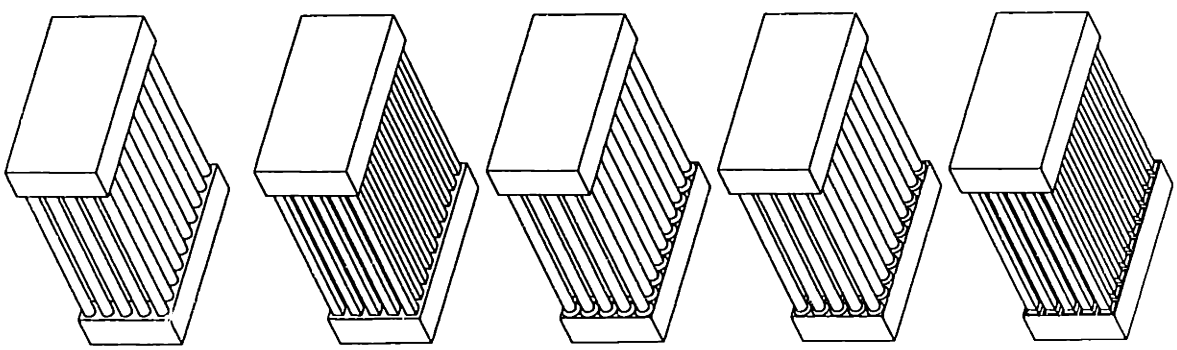

(a) (b) (c) (d) (e)

Figure 5-32 Second set of truss samples testing different fillets and chamfers

It is observed from the printed truss structures that the weakest points are areas where columns connected with upper and bottom plates. In the above figure, 5 samples are made with different joint types and cross section shapes in order to test the improvement on the green part strength. (a) has simple round columns without fillets or chamfers. (b) has simple square columns without fillets or chamfers. (c) has round columns with chamfers at both ends. (d) has round columns with fillets at both ends. (e) has square columns chamfered at both ends. The printing tests on these samples indicate: 1) samples without fillets or chamfers shows lower strength compared with those with fillets or chamfers. 2) Samples with round columns have STL models larger than square columns. 3) Samples with fillets have much larger STL models than those with chamfers.

After combining the printing test results for these two sets of samples, we decided to choose a truss structure of square columns with chamfers as a primitive to build our low thermal inertia mold. The truss column shape is shown in (e) of Figure 5-32.

Other printing related issues we have considered in effort to improve the green part quality include sieving stainless steel powders to size below $62\mu m$, choosing the layer thickness of 150 μm, using 2 way printing instead of 1 way printing, etc.

The green part of the benchmark tool after printing is shown in Figure 5-37.

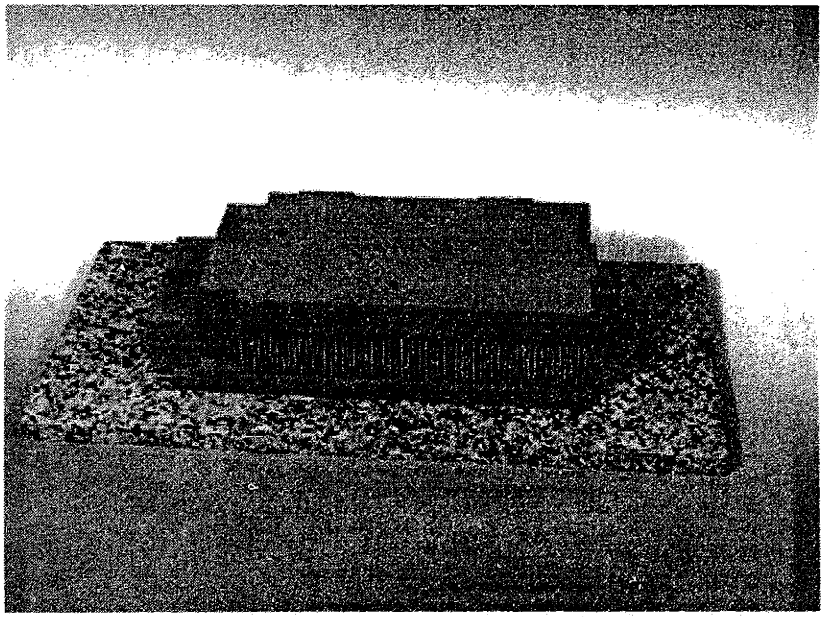

Figure 5-33 The green part of the benchmark tool

5.3.3 Debinding /light sintering and sintering

After the green part is printed, it is heated in an inert gas environment to remove the Acrysol binder. This is called debinding. In the debinding process the binder polymer chains are broken and the binder is evolved as a gaseous product. The debinding process is performed in a low temperature MRF furnace located in building 12. The temperature profile for debinding is sketched in Figure 5-34. As one can see from the figure the green part is first heated up to 200 degC to evaporate the water. Then the furnace temperature ramps up to 500 degC to evaporate the polymer binder. After that the furnace temperature keeps ramping until 1050 degC where the part is lightly sintered in order to keep the shape.

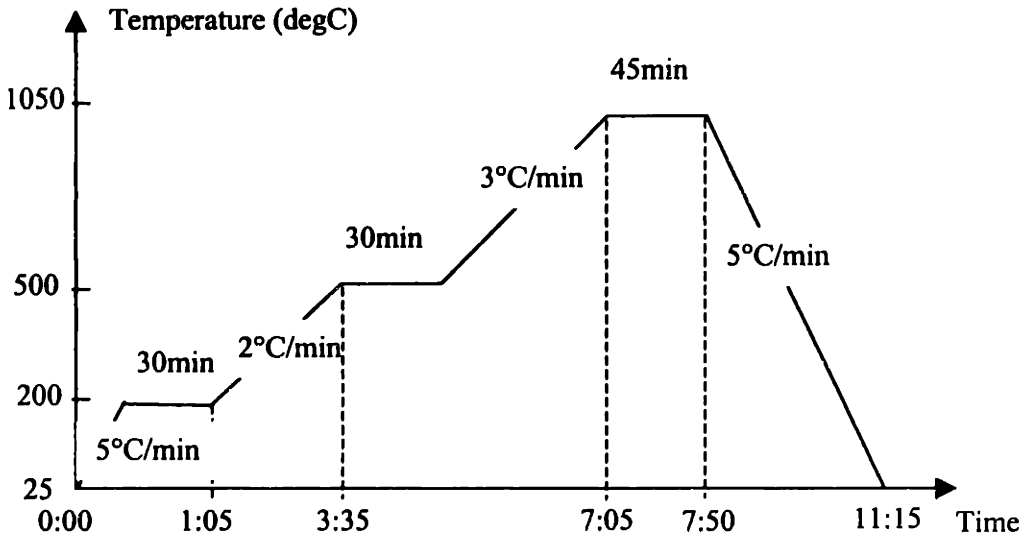

Figure 5-34 The temperature profile for debinding and light sintering

The temperature profile sketched above is a little bit different from the standard one described in [Guo 1998]. The reason is that in our previous sintering test we observed the buckling of the truss columns at the edge of the part. Although there is not an exact explanation of this kind of buckling, we believe that the temperature no-uniformity during debinding and light sintering has big influence in the formation of the truss deformation. Therefore in the modified temperature profile the ramping rates are reduced to 2degC/min and 3degC/min respectively with a hope of reducing the thermal induced truss deformation. Other efforts to reduce the truss deformation includes placing the part vertically in the crucible, put Alumina plate on the bottom of the crucible, etc.

Another issue is that the part should be packed with Zirconia or Alumina powder before the debinding/light sintering operation. The reason is that as the binder burns out the green part gradually loses strength and may result in large deformation even collapse if no supporting material is provided. Figure 5-35 compares the debinded and sintered part with (right figure) and without (left figure) packing powders. Obviously the packing material effectively avoids the collapse and reduces the part deformation.

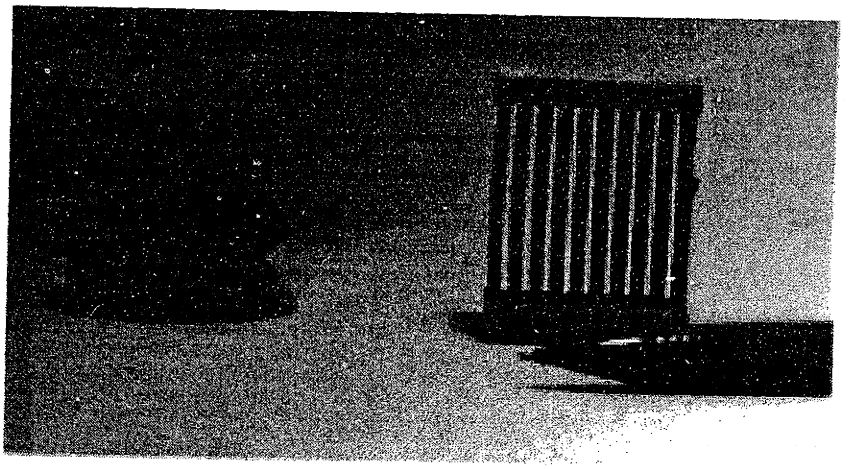

Figure 5-35 Comparison of the sintered parts with (right) and without (left) packing powders

After the part is debinded and light sintered, it is (together with the crucible and packing powder) moved to the high temperature MRF furnace for further sintering. The sintering is in the hydrogen atmosphere and the temperature profile for sintering is sketched in Figure 5-36. The details about sintering have been described in [Guo 1998]. The benchmark tool after debinding and sintering is shown in Figure 5-37.

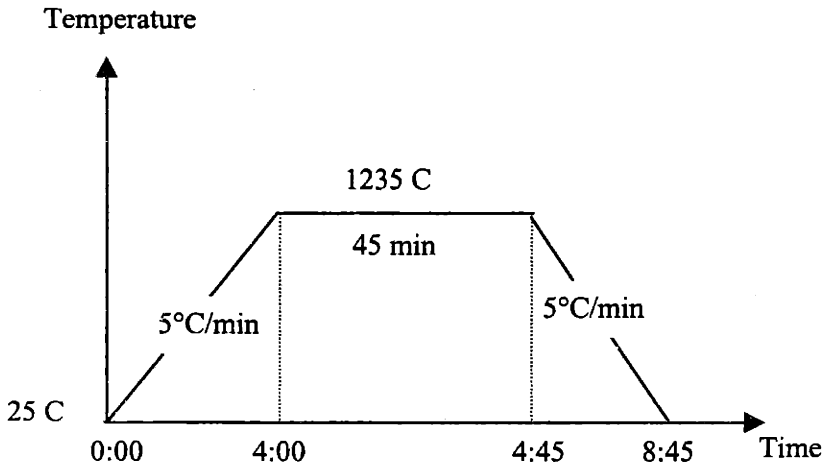

Figure 5-36 Temperature profile for sintering

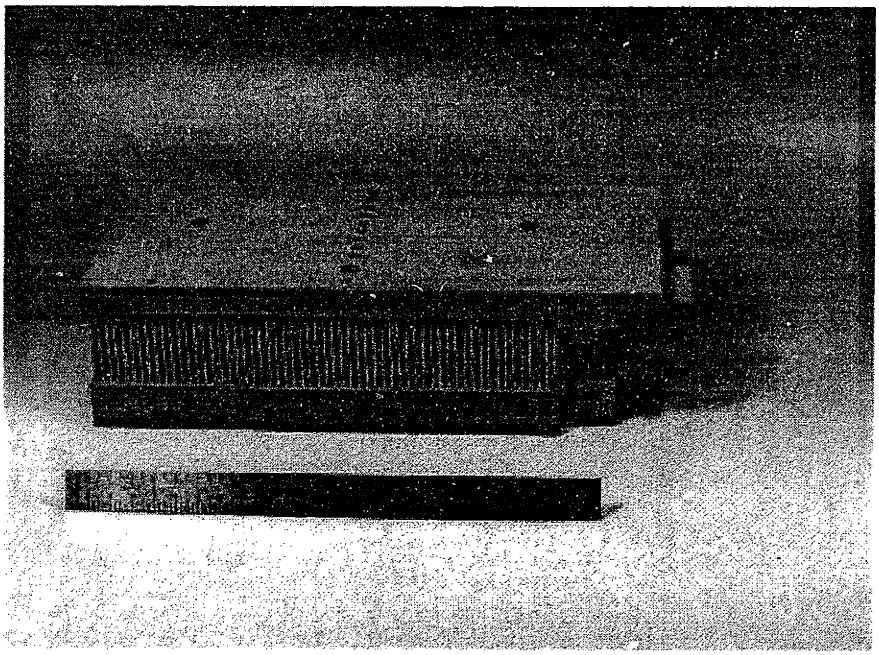

Figure 5-37 Part after debinding and sintering

5.3.4 Infiltration

5.3.4.1 Infiltration temperature profile

After the part has been sintered the next step is the infiltration where the liquid bronze fills the porous stainless steel skeleton by capillary forces. The infiltration is performed at the high temperature MRF furnace at MIT. The temperature profile is shown in Figure 5-38.

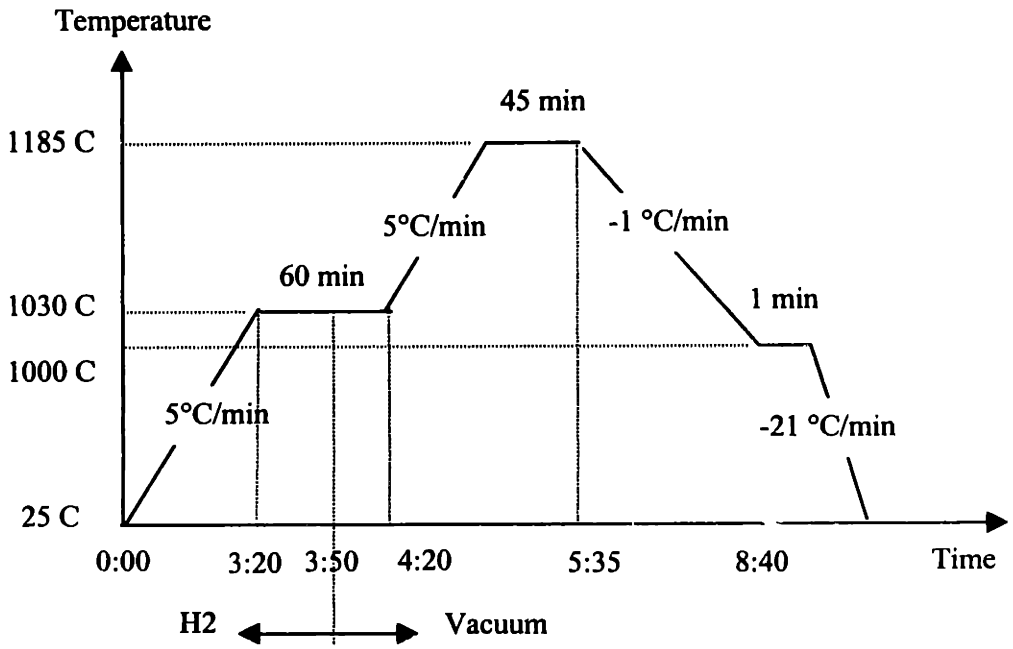

Figure 5-38 Temperature profile for infiltration

For the details on infiltration process please refer to [Guo 1998].

5.3.4.2 Stilt preparation

The infiltration process relies on capillary forces to draw the molten bronze infiltrant up to the stilt and into the sintered part. The stilt supports the part and acts as the porous media for liquid infiltrant to flow through. For the 420 stainless steel/ bronze system the stilt is usually made of 316 stainless steel powder because it is softer and easier to machine after infiltration. Once the infiltration is completed the stilt is cut away from the part and can still be used for the next infiltration as long as it is high enough and the top surface is machined.

The minimum height of the stilt is determined by the capillary force. The capillary force may result in over infiltration (small features such as the truss supports and the conformal channels are clogged

with infiltrant) if the stilt is not high enough. Wylonis derived the equilibrium equation for the infiltrate drawn by capillary force between two flat plates [Wylonis 1995]:

$$2l\gamma\cos\theta = \rho gh(lw); \theta = 0\text{deg}rees \qquad (5\text{-}50)$$

where l is the length of the wall, γcosθ is the surface tension force per unit length of liquid bronze infiltrant, ρ is the density of bronze infiltrant, g is gravity and h is the height of the capillary rise. With this model he successfully predicted the minimum stilt height as a function of the cooling channel width w:

$$h = \frac{2\gamma}{\rho g w} \qquad (5\text{-}51)$$

For a 0.1" wide cooling channel, the above equation yields a minimum stilt height of 0.36".

For the truss structure with square columns, the equilibrium equation is expressed as:

$$4d\gamma\cos\theta = \rho gh(D^2 - d^2); \theta = 0\text{deg}rees \qquad (5\text{-}52)$$

where d is the side width of each square column, D is the pitch distance of adjacent columns, as sketched in Figure 5-17. The above equation yields a minimum stilt height of 0.5" providing that the column width $d = 0.053$" and the column pitch distance $D = 0.1$".

Another issue to consider in the preparation of the silt for infiltration is to make sure that the clearance between the stilt and the crucible has enough room to contain all the required bronze powders for infiltration. The top view and the front view of the crucible, the stilt (part) and the bronze powders are sketched in Figure 5-39. Notice that the stilt is prepared with the same projection area as the part and the height of the bronze powder h should be lower than the top of the stilt.

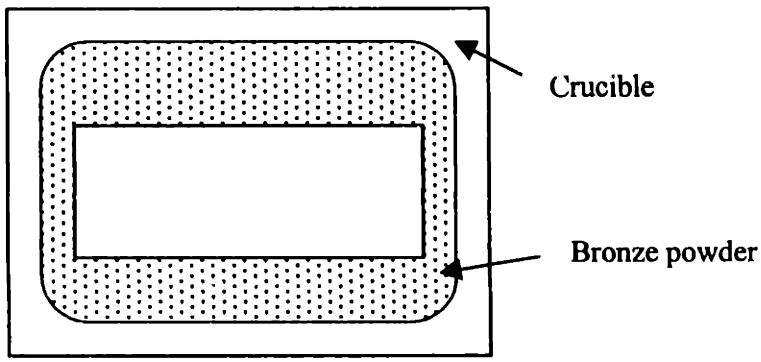

(a) Top view

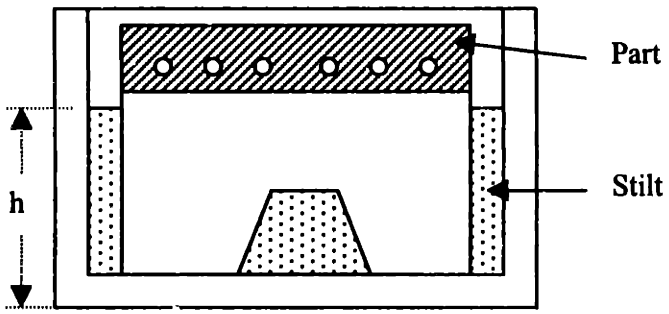

(b) Front view

Figure 5-39 The top view and the front view of the crucible with the part, the bronze powders, and the stilt

The total bronze powder required to fully infiltrate the part and the stilt is roughly the weight summation of the part and the stilt plus 1 kilogram [Guo 1998]: However practically the clearance between the stilt and the crucible is small and can not hold that much bronze powder. There two solutions to this problem. First we can cut some material from the bottom of the stilt (as shown in front view of Figure 5-39) in order to leave extra room for bronze powders. Second we can pre-infiltrate the stilt bock so as to reduce the amount of bronze required for the part infiltration.

The finally infiltrated part and the stilt is shown in Figure 5-40.

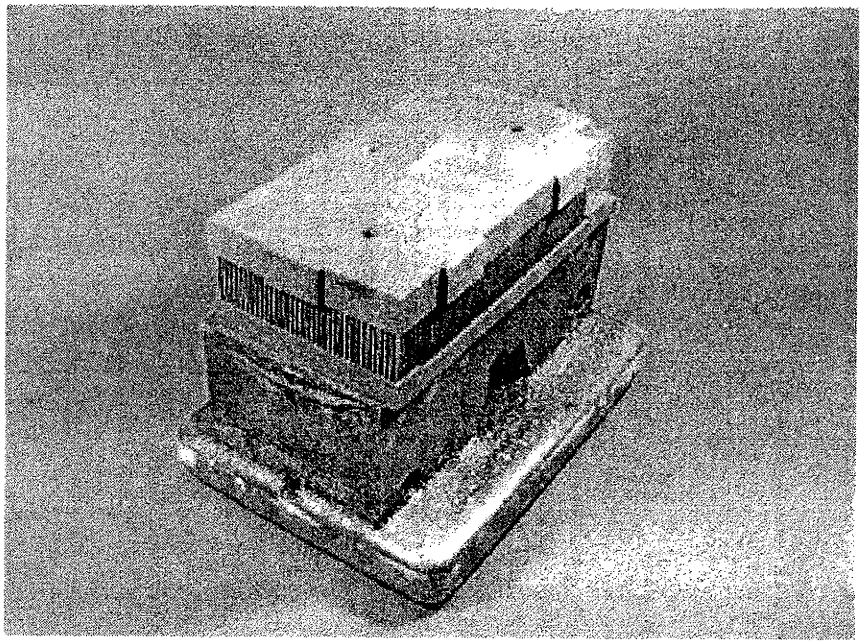

Figure 5-40 The tool and the stilt after infiltration

5.3.5 Post-Machining and Assembling

After infiltration the part is cut from the stilt and ready for further machining works. These machining works include:

1) Milling the top and bottom surface of the insert
2) Drilling and tapping ¼" NPT holes for oil channel connection.
3) Surface grinding the top and bottom of the insert using magnetic chuck
4) Machining the alignment platforms at the bottom plate of the insert
5) Make holes for the sprue bush, pine ejectors and core pins
6) Drill and tap bind holes on the bottom of the insert for installation
7) EDM the cavity pocket on the cavity insert

The part after milling and tappinng is shown in Figure 5-41. Further machining work will be done on this part to get the final dimension and geometry.

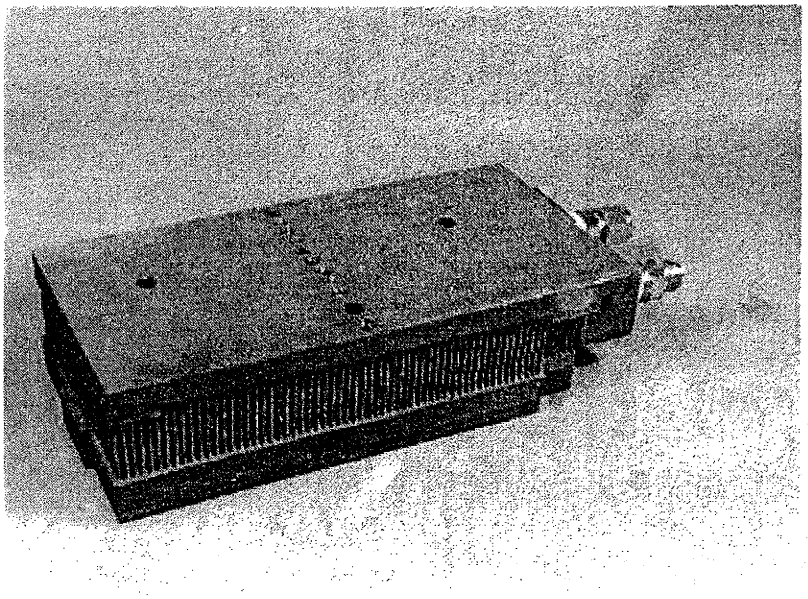

Figure 5-41 The tool after surface milling and tapping for the oil connection

5.4 CONCLUSION

Solid Freeform Fabrication processes have the ability to build injection molding tools with complex internal channels for better control of the mold surface temperature. The rapid cycling of the mold temperature is achieved by running hot and cold oil alternatively through these internal channels. In order to practically implement rapid thermal cycling, the tool has to be dedicatedly designed for low thermal inertia and proper strength and deformation. In this chapter we first discussed the design issues involved in the rapid thermal cycling, then we discussed the fabrication issues. In terms of the design for rapid thermal cycling, we explored a systematic methodology for low thermal inertia tooling design. This methodlogy was supported by a practical design case. The oil circulation system design was as discussed in detail. As to the fabrication issues, we investigated each steps in the tool fabrication. The future work include the rapid thermal cycling test with the low thermal inertia tool discussed in this chapter which has been designed and fabricated.

5.5 REFERENCE

1. Belofsky H., "Plastics: Product Design and Process Engineering", Hanser, 1995
2. Gerhart P. and R. Gross, "Fundamentals of Fluid Mechanics", Addison-Wesley, 1985

3. Guo H., "Alloy Design for Three-Dimensional Printing of Hartenable Tool Materials", Ph.D. Thesis, MIT, 1998
4. Kennedy P., "Flow Analysis of Injection Molds", Hanser, 1995
5. Phadke M., "Quality Engineering using Robust Design", Prentice-Hall
6. Pye R., "Injection mould design", Longman, 1989
7. Rubin I., "Injection Molding Theory and Practice", John Wiley & Sons, Inc, 1972
8. Spencer R. and G. Gilmore, "Residual Strains in Injection Molded Polystyrene", Modern Plastics, December 1950

CHAPTER 6

TESTING AND FUTURE WORKS

CONTENT

FIGURES

6.1 TESTS ON THE BENCH MARK TOOL

6.1.1 Objectives

After the benchmark inserts are fabricated, they are subject to further testing under simulated loading condition to ensure the successful performance and the allowable tooling life during the future molding process. The tests discussed in this chapter evaluate the following critical aspects for the proper performance of a low thermal inertia tool:

1) Thermal response. The rate of the mold temperature change in response to the heat transfer oil temperature change indicates the inertia of the mold that is defined by the mold time constant. In order to shorten the production cycle, it is important to minimize the time for heating and cooling the mold. The thermal response test is designed to evaluate the temperature response of the tool to the abrupt heat transfer fluid temperature change.
2) Temperature uniformity. In order to minimize the residual stress and the warpage caused by the unbalanced heating/cooling, it is important to check the mold surface temperature distribution in order to maintain the mold surface temperature as uniform as possible. Practically speaking, the cooling uniformity is more important that the heating uniformity in the sense that the thermal induced residual stress and birefringence patterns are frozen in the part during the cooling stage while they have chances to get relaxed in the filling stage. The conformal cooling channels designed in the inserts are expected to provide fairly uniform heating/cooling effects to the mold wall. The temperature uniformity can be measured during the heating/cooling processes.
3) Load-displacement curve. The mold insert with top and bottom plates sandwiched with truss columns shows the different stiffness behavior than the normal solid inserts. If the stress-displacement curve of the mold insert is known in advance, the mold deflection under a certain clamping force can be predicted. The prediction can be used to set up the clearance between the parting face of the insert and the top surface of the companion mold so that the companion mold will take part of the compression pressure so as to protect the insert from the damage by the abnormally high process pressures.
4) Failure test under compression load. The failure mode of the truss structure under the compressive loading could be very complex. First truss columns at different places undertake different loading in forms of shear force, compressive force and bending moment. The different loading condition leads to different failure modes such as buckling and yielding for individual truss columns. Second there is no indication of the failure point according to the load-displacement measurement because partial truss columns may fail before the entire insert collapses. This feature indicates that there is no abrupt

change of the load-displacement curve as observed for compression test of a simple column. It is a challenge to identify the point where some of the truss supports starts to fail and evaluate the percentage of the failed truss columns.

5) Loading test under thermal expansion. The working condition for inserts in a rapid thermal cycle is very bad because the inserts have to stand both the thermal expansion / shrinkage due to a temperature change of 100 degC and the large process pressures such as the clamping force and the packing pressure. It is very necessary to do the strength test with both the mechanical loads and the thermal loads applied.

6.1.2 Thermal test

6.1.2.1 Experimental setup

The thermal test was performed on the benchmark tool shown in figure 5-41. The experimental setup is sketched in Figure 6-1, where the benchmark tool is placed on the top of an insulation plate and covered by an Aluminum box. The thermocouples installed on the top of the tool are used to collect the temperature data at different positions on the mold surface. There are a coolant line and a compressed air line connected with the tool and controlled by valve K1 and K2. A hot air gun is used to blow the hot air in order to heat up the tool. At the beginning of the test, valve K2 is turned off and valve K1 is switched to the air side so that the compressed air blows into the channel to clean the residual coolant from the tool. Then the air dryer blows the hot air and heats the tool up to a target temperature (say 75 degC). The thermocouples on the tool are used to monitor the surface temperature. After that the hair dryer turns off and valves K2 turns on so that the coolant (here we use tap water) flows through the internal conformal channels to rapidly cool down the tool. The mold surface temperature during rapid cooling is recorded by the computer.

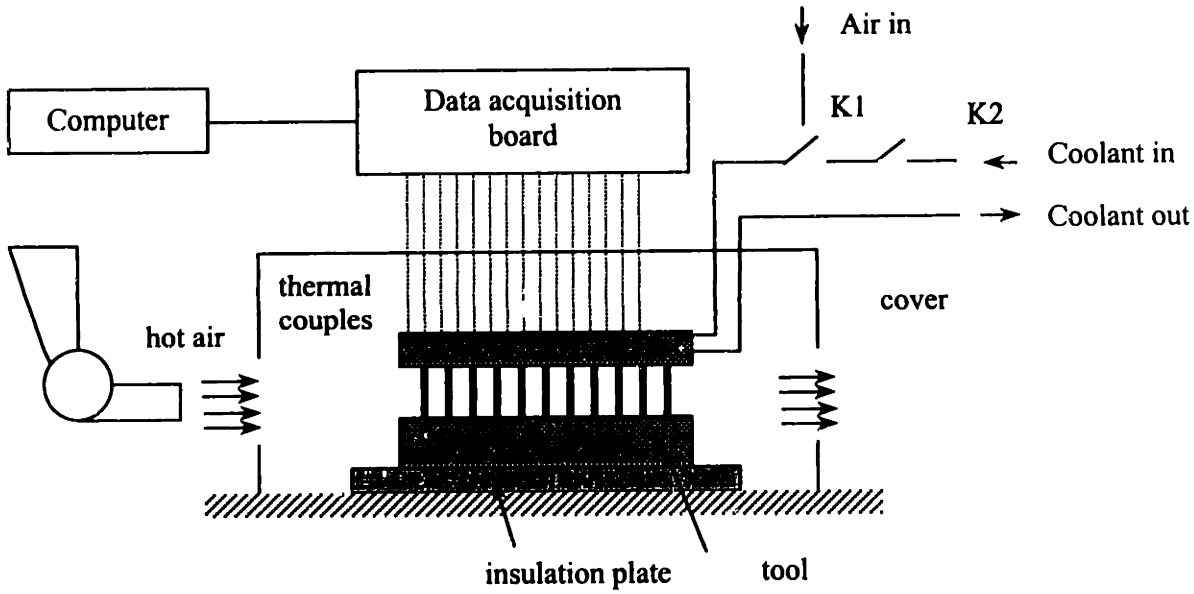

Figure 6-1 Experimental setup for the mold surface temperature measurement

6.1.2.2 Thermocouple selection and installation

J type thermocouples are used for mold surface temperature measurement. The diameter of the wire is 0.020". The bead size varies from 0.035' to 0.038". Since the thermocouples we used were not from OMEGA, it is not clear which insulation material is used for those thermocouples. The thermocouples are installed vertically on the mold surface as sketched in Figure 6-2. In this figure the bead of the thermocouple is placed into a hole of 0.04" in diameter and 0.04" in depth. A high thermal conductive epoxy adhesive (OB-200 by OMEGA Engineering) bonds the thermocouple in the hole. OB-200 has a continuos operation temperature of 500 degF and a very high thermal conductivity of 9.6 W/m-K. The reason to choose the high thermal conductivity epoxy is to minimize the contact resistance and maintain a short response time for the thermocouple. The cure of this material needs a heating time longer than 4 hours in a 170degC oven. After the epoxy adhesive is cured, an instant reactive binder (Delta Bond 155 manufactured by Wakefield Engineering, Inc.) is used to secure the bead to the mold wall and to protect the thermocouple from environment disturbance. The characteristics of Delta Bond 155 are not available. However the thermal conductivity of this material is relatively high., which is not good for the precise measurement of the mold temperature at the specified spots. An improvement is to use the binder with low thermal conductivity. The conversion from the thermocouple reading (voltage signal) to temperature is based on the thermocouple reference table on OMEGA catalogue. The resolution for the measurement is around 0.053 volts/degC. The expected tolerance for the thermocouple s0.75% according to the OMEGA catalogue. This tolerance yields a measurement error of 0.4 degC for the experiment discussed in section 6.1.2.1, where the mold is cooled down from 75 degC to 25 degC by running cold water through conformal channels.

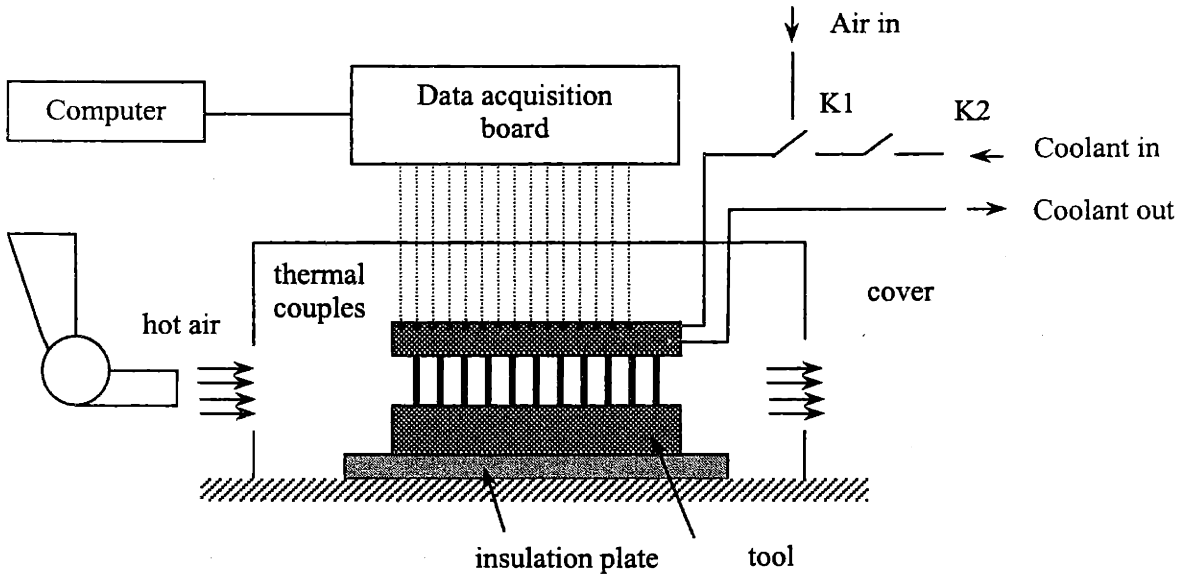

Figure 6-1 Experimental setup for the mold surface temperature measurement

6.1.2.2 Thermocouple selection and installation

J type thermocouples are used for mold surface temperature measurement. The diameter of the wire is 0.020". The bead size varies from 0.035' to 0.038". Since the thermocouples we used were not from OMEGA, it is not clear which insulation material is used for those thermocouples. The thermocouples are installed vertically on the mold surface as sketched in Figure 6-2. In this figure the bead of the thermocouple is placed into a hole of 0.04" in diameter and 0.04" in depth. A high thermal conductive epoxy adhesive (OB-200 by OMEGA Engineering) bonds the thermocouple in the hole. OB-200 has a continuos operation temperature of 500 degF and a very high thermal conductivity of 9.6 W/m-K. The reason to choose the high thermal conductivity epoxy is to minimize the contact resistance and maintain a short response time for the thermocouple. The cure of this material needs a heating time longer than 4 hours in a 170degC oven. After the epoxy adhesive is cured, an instant reactive binder (Delta Bond 155 manufactured by Wakefield Engineering, Inc.) is used to secure the bead to the mold wall and to protect the thermocouple from environment disturbance. The characteristics of Delta Bond 155 are not available. However the thermal conductivity of this material is relatively high., which is not good for the precise measurement of the mold temperature at the specified spots. An improvement is to use the binder with low thermal conductivity. The conversion from the thermocouple reading (voltage signal) to temperature is based on the thermocouple reference table on OMEGA catalogue. The resolution for the measurement is around 0.053 volts/degC. The expected tolerance for the thermocouple s0.75% according to the OMEGA catalogue. This tolerance yields a measurement error of 0.4 degC for the experiment discussed in section 6.1.2.1, where the mold is cooled down from 75 degC to 25 degC by running cold water through conformal channels.

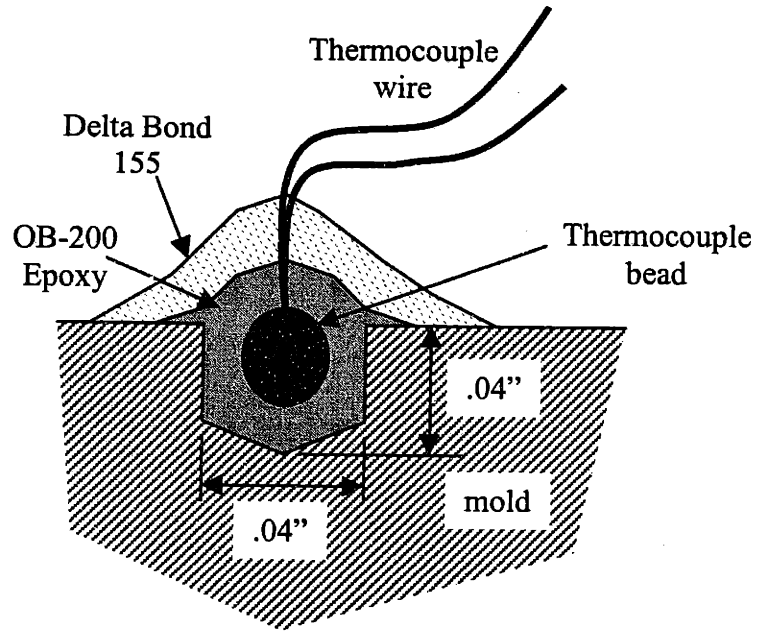

Figure 6-2 Sketch showing installation of the thermocouple

6.1.2.3 Data collection and analysis

Figure 6-3 is the top view of the tool indicating the location of those thermocouples. 13 thermocouples are used to measure the mold surface temperatures at different locations. Points 2, 3, 8, 9, 10, 11, 12, 13 are points that locate within or close to the cavity surface. The dotted lines in the figure correspond to cooling channels.

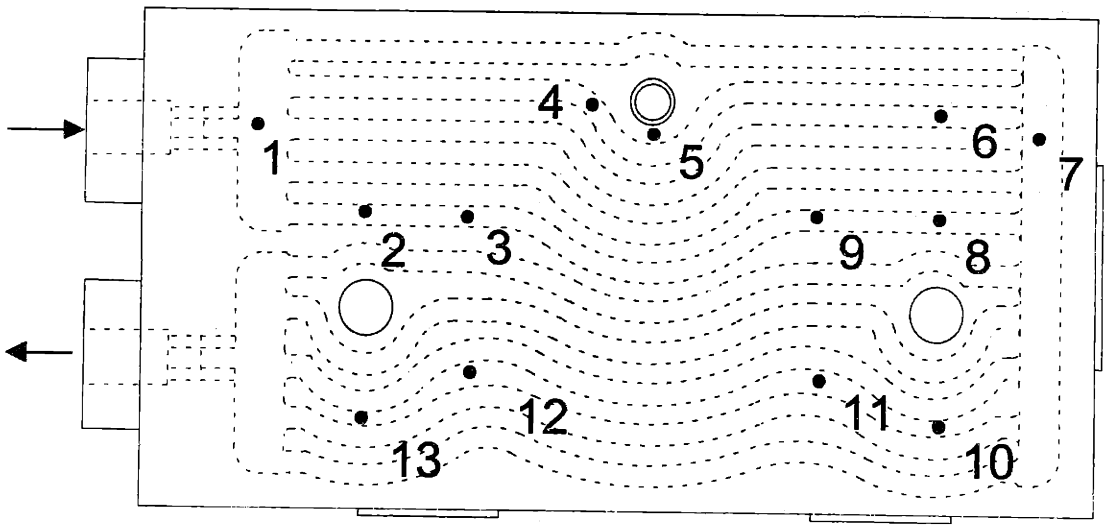

Figure 6-3 Top view of the tool for thermal test

In order to test the stability and the variation of thermocouples, the thermocouples were calibrated in boiling water. The calibration yields a stability within ±.0.75degC for each thermocouple and a

thermocouple to thermocouple variation of ±.1.5degC when they all merged into the boiling water. The temperature variation from channel to channel is not that important from the analysis point of view because we are interested in the time constant of the points on the mold surface instead of the absolute temperature value at those points.

Figure 6-4 is the mold surface temperature data recorded at points 2, 3, 8, 9, 10, 11, 12 and 13. These eight points are located close to the location of the future cavity. Therefore the temperature uniformity for these eight points are very crucial to the molding performance. That is why we select only these eight points for temperature response study. In addition to the cooling period, the figure also plots a short period before rapid cooling. During this period, point 2 maintains a lower starting temperature. The reason is the point 2 is behind pipe connections and the hot air is not quite easy to reach that point. With the hot air gun it is not very easy to maintain the uniformity of the mold temperature. Figure 6-5 is the averaged mold temperature profile for those 8 points. The profile is compared with that predicted by the 1D analytical model (equation (4-1) and (4-5) in chapter 4). Obviously the analytical model and the experiment yield similar results. The analytical model yields a mold time constant of 5.05 seconds for a vertical distance from the top of the cooling channel to the mold wall of 0.18". For the final benchmark tool, the vertical distance from the top of the oil channel to the mold wall is 0.1". This distance corresponds to a mold time constant of 2.34 seconds. Obviously the reduction of the oil chance distance by a factor less than 2 leads to the drop down of the mold time constant by a factor larger than 2. According to equation (4-2), the time constant of the mold should be proportional to the square of the vertical distance from the oil channel to the mold wall. However since we have also considered the convective term in equation (4-1), the actual reduction of the mold time constant associated with the reduction of the vertical distance is no that much.

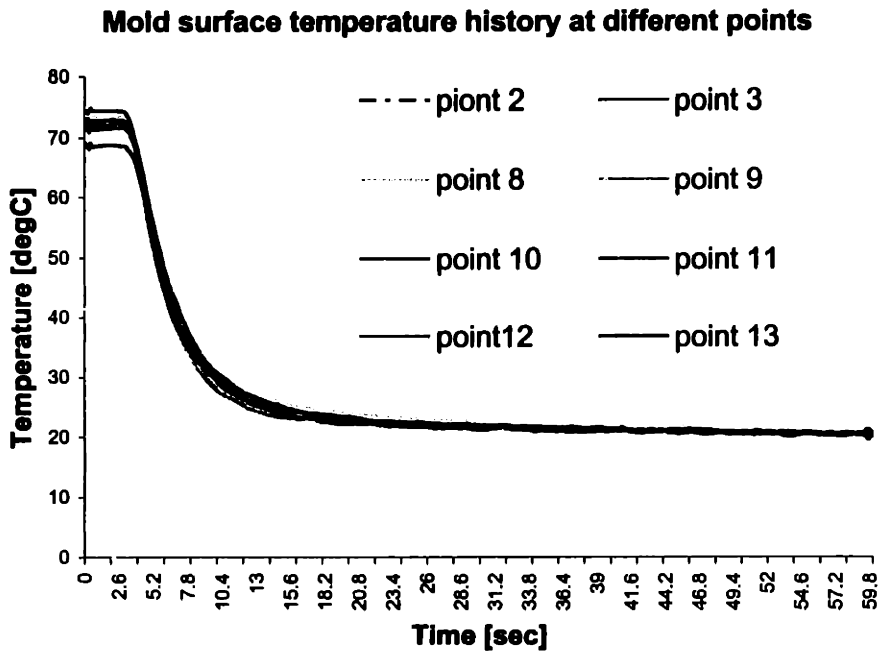

Figure 6-4 Mold surface temperature profiles recorded at points 2,3,8,9,10,11,12,13

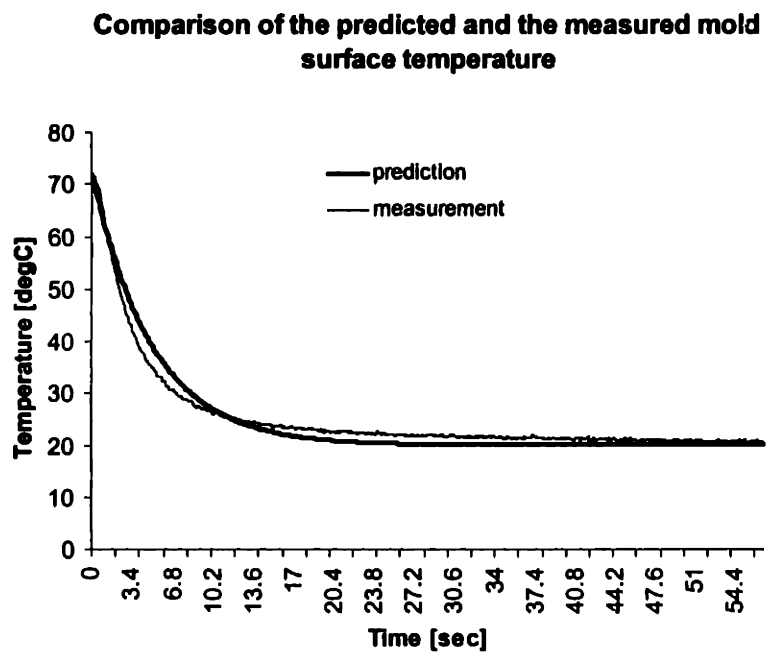

Figure 6-5 Comparison of averaged mold surface temperature profiles by measurement and analytical model

Figure 6-6 shows the temperature variation recorded by thermal couples over the mold surface during rapid cooling. The temperature variation data were obtained by comparing the instant temperature values recorded at points 2, 3, 8, 9, 10, 11, 12 and 13 with the temperature value averaged over these points. Figure 6-6 shows a relatively large temperature variation before the rapid cooling stage. This variation is caused by non-uniform temperature distribution during heating stage. Once the rapid cooling starts the temperature variation from point to point drops down to ±1degC. The temperature variation values measured by thermocouples at steady state reflect the performance variation for different thermocouples. If we shift the temperature variation profiles to the position where the maximum variation and the minimum variation merge after a long cooling time, we can obtain the "net" temperature difference curves shown in Figure 6-7, eliminating the effect of the thermocouple variation. One can conclude from Figure 6-7 that the maximum mold surface temperature difference during the entire cooling period is within 3 degC.

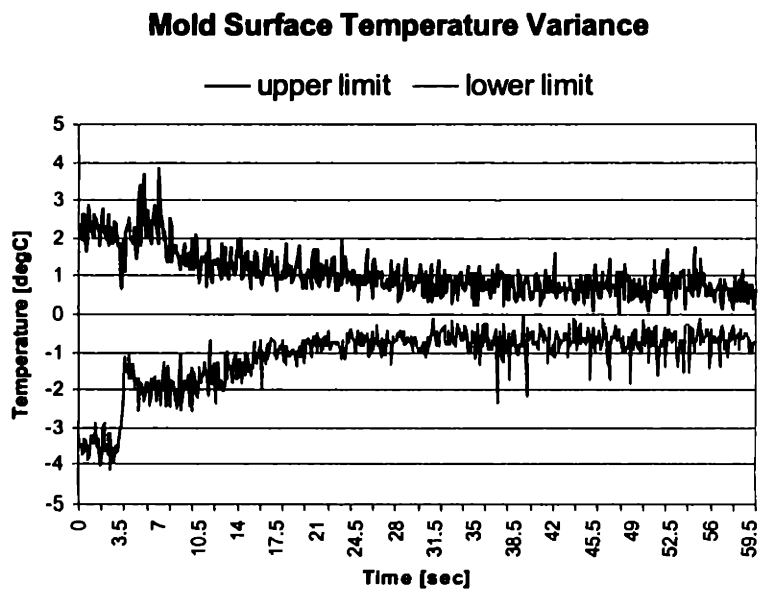

Figure 6-6 Temperature variation on mold surface during rapid cooling

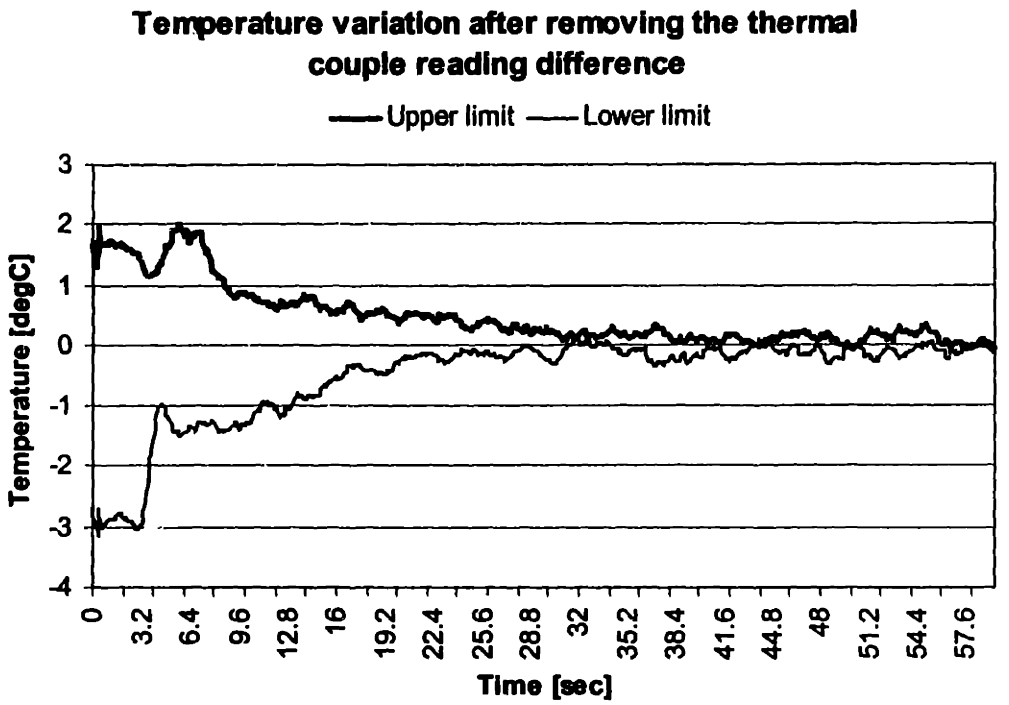

Figure 6-7 Temperature variation on mold surface during rapid cooling after the effect of the thermocouple reading differences are removed

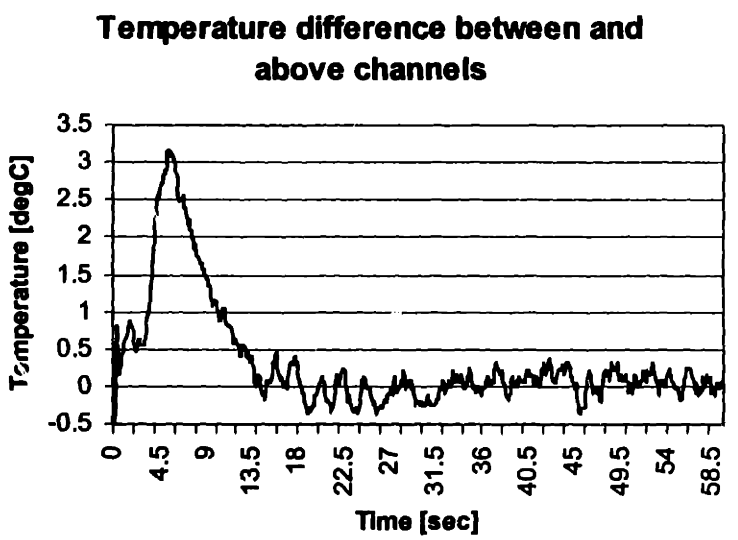

Figure 6-8 Temperature difference on and between channels in rapid cooling

If we compare the mold surface temperature profiles at a point between the channel and that above the channel (for example, points 6 and 8 in Figure 6-3), we obtain the temperature difference between these two points during rapid cooling. This temperature difference profile is smoothed and shifted as we have done in Figure 6-7 and then plotted in Figure 6-8. The plot shows a peak temperature variation of about 3 degC after a continuos cooling of 6 seconds. As the comparison, the numerical simulation with the same cooling condition is plotted in Figure 6-9. The numerical simulation leads to a peak temperature variation of 2 degC after a continuos cooling of about 0.75 seconds. The reason why the experiment shows a much longer time to reach the peak value is not quite clear but might be explained below. 1).As one can see from Figure 6-4, The time to start cooling is delayed by 2 to 3 seconds and the mold temperature is not quite uniformly distributed before cooling. 2) Points chosen for the temperature difference measurement (i.e. point 6 and point 8) are not adjacent with each other but separated by several cooling channels. The unbalanced flow between channels may lead to the different heat transfer conditions for points 6 and 8. 3) The method we used to install thermocouples may also lead to the measurement error. In the experiment small holes with 0.04" in diameter and 0.04" in depth are drilled and thermocouples with bead size less than 0.038" are installed with a type of high thermal conductivity epoxy. The clearance between the bead and the mold surface as well as the variance of the bead size leads to the error in time constant measurement. 4) The binding material used around individual thermocouple as a support is thermally conductive and may also effect the measurement result. 5) The cross-section shapes for parallel channels are designed with rectangular shape and rounded corners. However since these channels are very small it is hard to ensure that all the powder are cleaned. The post process may also effect the cooling channel formation. All these factors reduce the cross-section area of the cooling channel and increases the temperature non-uniformity. As one can see from equation 2-11, the reduction of the cooling channel size will also increases the mold time constant. Alternative approaches will be proposed in section 6.2 for a more accurate mold surface temperature measurement

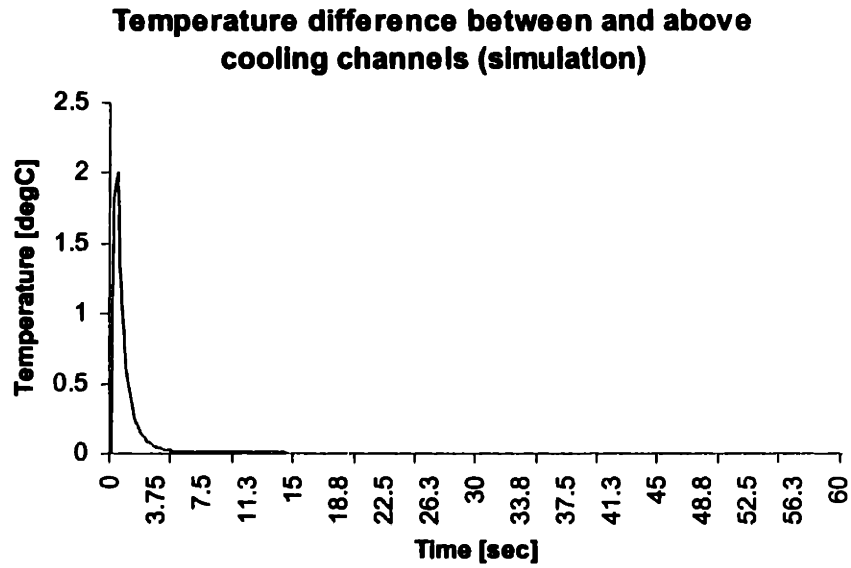

Figure 6-9 Mold surface temperature variation on and between cooling channels predicted by numerical simulation

6.1.3 Mechanical test based on the sample truss structure

In chapter 5 we have discussed the design and fabrication of small truss samples to explore problems that may occur in fabricating the much bigger benchmark tool. We believe that the truss columns are the weakest link of the entire design in terms of CAD design, green part printing and post processing. We notice that truss columns are also the weakest link of the entire mold that may first fail under the process pressures. Three observations support this inference: 1) The truss columns occupy only about 25% of the whole parting face. 2) The truss columns carry all the mechanical load and stress induced by thermal expansion. 3) After printing and post processing the truss columns are slightly buckled which may reduce its mechanical strength. In a word it is very necessary to study the mechanical behavior of the 3D Printed truss structures under the compressive process load. A truss sample shown in figure 6-10 was used for the compression test.

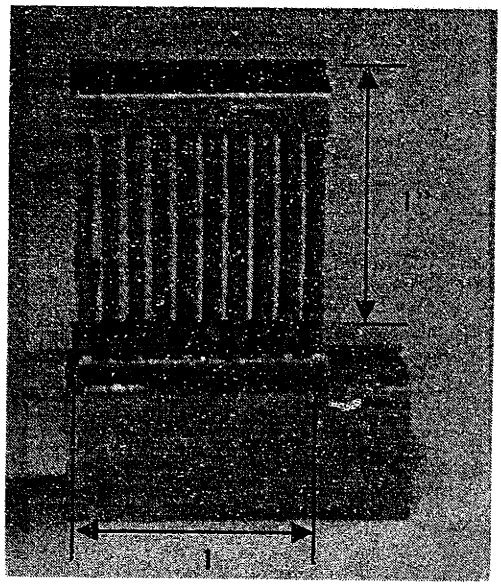

Figure 6-10 Truss sample prepared for the compression test

The compression test was performed on an Instron machine. The sample is placed between two loading heads and is applied with the compression force. In order to ensure the validity of the test result, a dummy sample made from Aluminum was first used, as shown in Figure 6-11. The compression test on the Aluminum sample indicates that there is a necessity for direct measurement of the sample's displacement under a certain load in order to eliminate the effect of the compliance of the rest of the machine on the Young's modulus measurement of the sample. An expansion gage is used for this purpose.

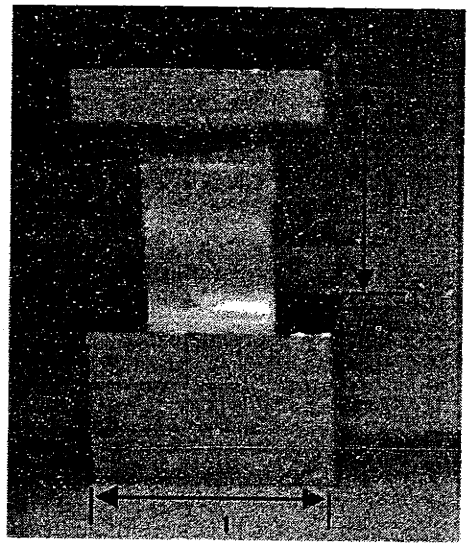

Figure 6-11 Aluminum dummy sample used for Instron test

Figure 6-12 shows the load-displacement curve recorded by Instron for the truss sample shown in Figure 6-10. Figure 6-13 is the corresponding stress-strain curve after considering the cross section area of the truss columns. The yield point corresponding with 2% of the maximum strain is about 28,000psi, according to Figure 6-13. This value is about 25% of the yield strength for typical 3D printed Stainless steel/Bronze parts. Figure 6-14 shows the truss sample after the compression test. It is obvious from the figure that the dominant failure mode for the truss sample is buckling of those truss columns instead of yielding.

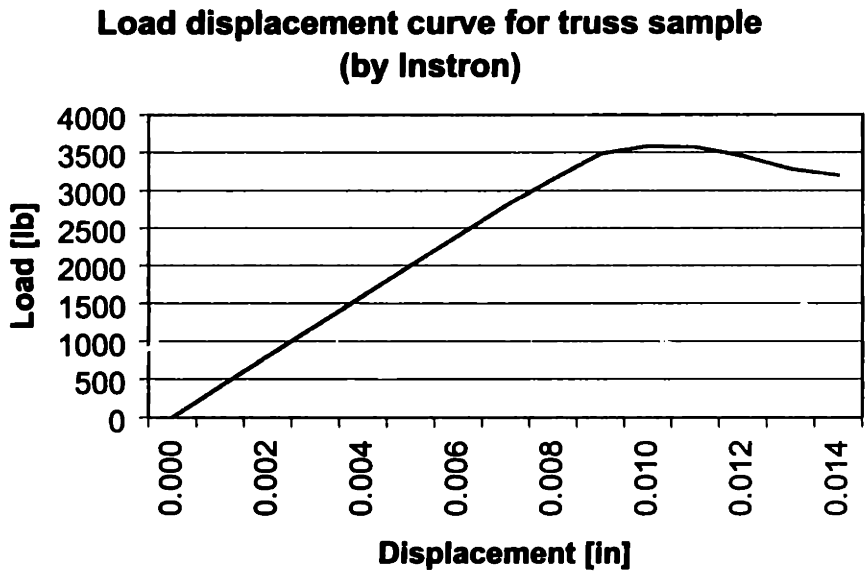

Figure 6-12 Load-displacement curve for the truss sample recorded by Instron

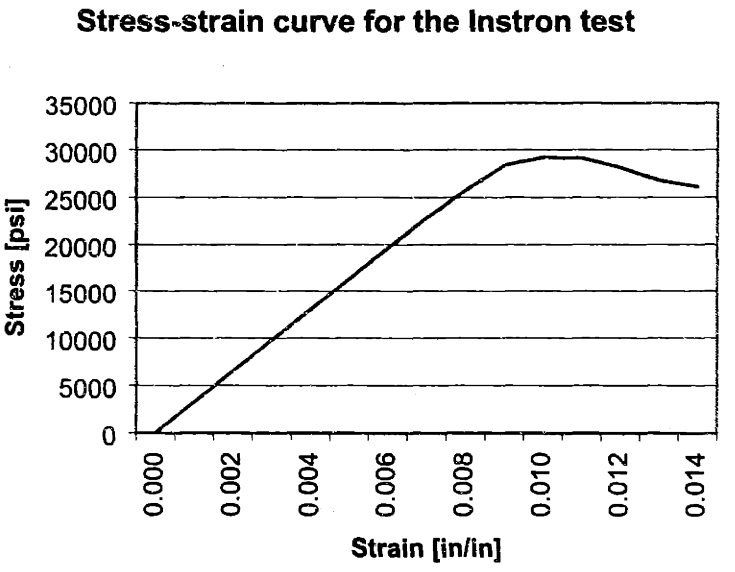

Figure 6-13 Stress-strain curve obtained from the compression test result in figure 6-11

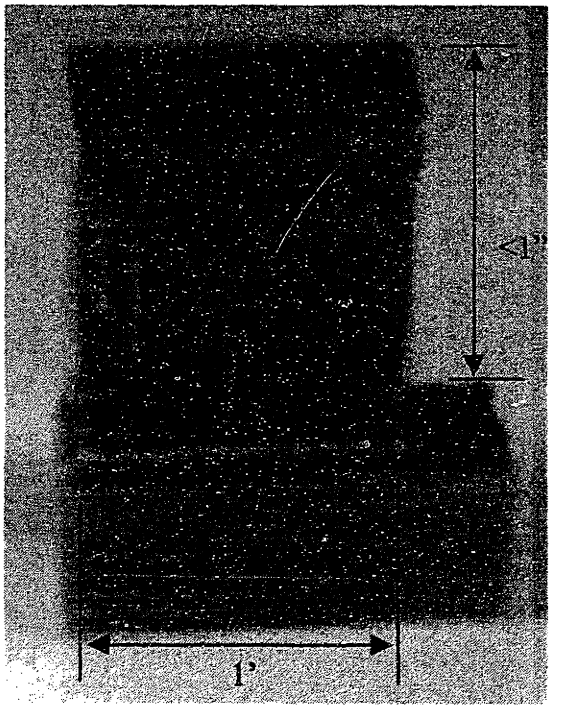

Figure 6-14 Truss sample after compression test

We have recognized that the Young's modulus value obtained from Instron test is not reliable because the compliance of the rest part of the machine is also involved into the result. An expansion gage is used to manually measure the sample displacement at different loading steps. Figure 6-15 shows the resulting displacement-load curve. The calculation based on this curve gives a Young's modulus value of 12.5Mpsi.

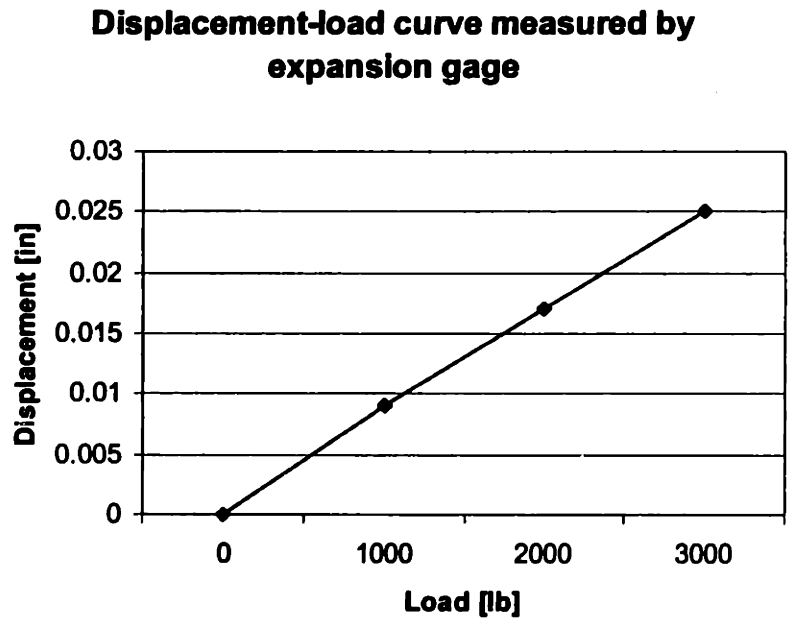

Figure 6-15 Load-displacement curve by expansion gage

6.2 FUTURE WORK

6.2.1 Mold surface temperature recording

As we have discussed in section 6.1.2. The current method for mold surface temperature measurement introduced the relatively large measurement error and it is difficult to install thermocouples properly. Besides, the thermocouples only record the temperature profiles at special points instead of the temperature distribution over the entire mold surface. In this section we will discuss several alternative ways for the temperature measurement. We hope to minimize the system error introduced by the measurement method and obtain a complete map of the temperature distribution. These methods include the infrared thermograph, the infrared thermal couple, the birefringence coating and the liquid crystal thermometer.

6.2.1.1 The infrared thermograph

Infrared is the electromagnetic spectrum beyond red [Kaplan 1999]. All objects radiate energy in the infrared spectrum. The hotter the target, the more energy radiated, the shorter the peak wavelength of the infrared emission. Very hot targets radiate in the visible as well. For example the sun, at 6000K, appears white hot with the emitted energy centered over the visible spectrum with a peak at 500nm, a tungsten filament at 3000K appears yellow, a surface heater at 800K appears red hot. The radiant energy emitted from the target surface and he wavelength of the maximum radiation are calculated by the Spephan-Boltzmann law and the Wien's displacement law respectively:

$$W = \delta \varepsilon T^4 \qquad (6\text{-}1)$$

$$\lambda_m = b / T \qquad (6\text{-}2)$$

where W is the radiant flux emitted per unit area (watts/cm^2), e is emissivity (unity for a blackbody target), d is the Stephan-Boltzmann constant (5.673e-12 watts cm-2K-4), T is the absolute temperature of target (K), λm is the wavelength of the maximum radiation (μm), and b is the Wien's displacement constant (2897 μm-K). The above two equations guide us to choose proper films or other infrared detectors and set up a proper exposure time for a certain range of temperature measurement. The peak wavelength of the infrared emission for the thermal test discussed above is in a range of 7,700nm (100degC) to 22,280nm (20degC).

Now let us explore the methods that can be used to detect the infrared emission at the above wavelength and intensity range. The first question is if the regular camera with infrared sensitive films is appropriate to record the temperature distribution. Before anwsering this question let us see which kinds of infrared films are comericially available. There are four black and white IR films from Agfa, Ilford, Kodak and Konica. There is on color IR slide film from Kodak. Kodak high speed infrared balck and white film (HIE 135-36) is sensitive to IR down to approximately 1000nm. Konica Infrared 750 black and white film has a sensitivity range from 640 to 820 nm in addtion to the intrinsic sensitivity range of AgBr 400-500nm. The peak sensitivity is 750nm. Ilford SFX 200 Black and White has a sensitivity about 800nm. Agfa APX 200S Black and White has a peak sensitivity at 740nm and extends to 775nm.Kodak Ektachrome Color Infrared Slide film is sensitive up to 900nm radiation. More detailed information on IR photography can be obtain from the web site:http://www.freeyellow.com/members6/glsmyth/.

After reviewing all the available IR films we noticed that the IR emission for the temperature range of our interest is in the far-infrared region which is not detectable by conventional IR films. It is necessary to use infrared detectors instead of IR films to record the far-infrared emission associated with

the temperature distribution in the thermal response and the temperature uniformity test. Major manufacturers for infrared imagers include 3M, Inframetrics Inc., GE, Edmund Scientific Corp., Mikron Instrument Co., FLIR Systems, Inc., etc.

6.2.1.2 Infrared thermocouple

The thermal test in section 6.1.2 uses J type thermocouples which need to drill small holes on the mold surface and use the thermal conductive epoxy to install. The thermocouple installation procedure is difficult and time consuming. It also introduces the instability and inaccuracy of the measurement. An alternative way is the non contact temperature measurement by infrared thermocouple. A 2-wire infrred temperature transmitter supplied by OMEGA (model number OS1551-A) is one of the options. This type of the thermocouple has a temperature measurement range of 0 to 200 degC and spectral response of 8 to 14 microns. Its 10 msec time constant make it ideal for use to capture quick temperature changes in rapid cooling stage. The only problem is the price. A basic infrared thermocouple unit costs more than $700. For a test that needs at least 10 such thermocouples, the expense is remarkably large.

6.2.1.3 Photoelasticity

In 1814 David Brewser discovered that the optical properties of some transparent materials were modified when the material was subjected to stresses. This led to the development of photoelasticity. When a object coated with a certain plastic material is illuminated by white light, a colorful fringe pattern will form to reveal the stress/strain distribution due to external or internal load.

The photoelasticity technique can be used to analysis the temperature response and distribution because the mold surface temperature change directly results in the thermal strain which can be indicated by the fringe pattern of the thin plastic coating. This method is an easy and low cost way to check the mold surface temperature uniformity. However the quantitative interpretation of the fringe pattern is not straightforward. Also the stress and the temperature will couple with each other in influencing the fringe pattern.

6.2.1.4 Liquid Crystal

As a special material, liquid crystal has a unique phase between solid and liquid called liquid crystal phase. The distinguishing characteristic of the liquid crystalline state is the tendency of the molecules called mesogens to point along a common axis called the director. There are many types of

liquid crystal states. One is called nematic which is characterized by molecules that have no positional order but tend to point in the same direction (along the director). The nematic phaseshows a phase transition from the marbled texture to the black, isotropic liquid when the material temperature is raised. A special class of nematic liquid crystals called chiral nematic is used for thermometer because of its unique ability to selectively reflect light of different colors depending on different temepratures. A thermometer for practically any temperature range can be built by mixing different compounds of chiral nematic liquid crystals. A more detailed information on liquid crystal thermometer can be found at: http:// abalone.cwru.edu/ tutorial/ enhanced/files/lc/apps/apps.htm. The major application for liquid crystal thermometer is to detect the human body temperature or the food temperature. It might not be a efficient way for precise temperature measurement.

6.2.2 Structural test on the benchmark insert

In section 6.1.3 we have discussed the mechanical test using the small truss samples. It is also beneficial if we can evaluate the strength and the tool life for 3D Printed mold inserts in a simulated rapid thermal cycling process. As we will discuss later this type of test will help the design and fabrication of the mold assembly for the desired performance.

6.2.2.1 Loading condition

The types of loads experienced in a rapid thermal cycle are mainly compressive loads and thermal loads. The compressive loads are those in forms of the clamping force, the injection pressure, the packing pressure, the ejection force, etc. The thermal loads include the cyclic heating by the hot plastic melt and the rapid heating and cooling cycle by the heat transfer oil.

The actual loading condition can be simulated on one of Instron 5500 series universal test systems. This series features a combination of a Windows® based material test software package (Merlin®); high-speed electronics for precise measurement and processing of data; and load frames with drive system for accurate speed, position, strain and load control. The load capacity for this series ranges from 500N to 600KN, which covers the load of interest (about 200KN) in the case of rapid thermal cycling.

Different loading conditions that a mold insert will experience in a rapid thermal cycle are discussed below:

1) Clamping force

In the clamping stage, two halves of the mold are compressed face to face by a clamping force applied by the injection molding machine. This clamping force is less than 200KN for our benchmark tool and is applied on the parting face of each insert in the area surrounding the cavity.

2) Mold surface thermal expansion/shrinkage

In a rapid thermal cycle, the mold surface experiences a rapid temperature change of about 100 degC, which in consequence results in a maximum thermal expansion/shrinkage of 0.004" for our benchmark part. The thermal expansion/ shrinkage is combined with the compression loading and results in a complex pattern for stress build-up in the insert.

3) Injection and packing pressures

A rapid thermal cycle starts with the condition while the two halves of the mold are clamped together to form a void for hot plastic to fill in. While the hot plastic melt is injected into the cavity, a time and position dependent pressure is distributed on the cavity surface until a maximum packing pressure is achieved. At this point the clamping force applied on the shoulder of the mold insert is minimum. The packing pressure gradually drops down while the part starts to shrink in cooling. It is important to notice that the injection and packing pressures are only applied on the cavity surface and the runner systems where the part is formed.

4)Ejection force

Compared with the clamping, injection and packing pressures, the force applied by the ejection pin is a minor issue. However it is necessary to do the assembly test at a high mold temperature in order to check the mobility and the friction between the ejection pins and inserts caused by the thermal expansion at elevated temperature. The mismatch of the pins and the corresponding pin holes on inserts and mold bases may create huge bending moment that eventually damages the ejection pins.

6.2.2.1.1 Cavity surface deflection

In Chapter 4 we have explored the idea of using the mold surface deflection to compensate the part shrinkage during cooling. From the p-V-T curve the part shrinkage is in a range of 5%, which requires a maximum cavity surface deflection of 0.002" for a target part thickness of 0.02". In order to detect the mold surface deflection under the injection pressure, we propose several methods below.

1) Recording maximum deflection by displacement sensor

A displacement sensor or an expansion gage can be used to detect the mold surface deflection at a certain point, say the center of the cavity. The expansion gage can be installed at the center of the cavity. The detected maximum mold surface deflection can be used to estimate the total volumetric change due to deformation. Other displacement sensors that can be used include laser interferometers, ultrasonic distance sensors, piezoelectric micrometers, etc.

2) Recording mold surface profile by thin foil

It is proposed that we place a thin Aluminum or other metal foil between the packing block and the mold cavity. As the mold surface deforms under the packing pressure, the metal foil records the mold surface profile by the permanent deformation. This method is not that promising in measurement accuracy because the spring back of the metal foil after the force is released and the error introduced when the foil and the rubber are taken out of the chamber.

3) Recording mold surface profile by chemical reaction

An alternative way to record the mold surface profile is to replace the rubber with the reactive binder such as Epoxy or silicon RTV. The cavity is filled with this reactive binder and pressed by a sealed loading head. After applying for the compression load for enough time with the target packing pressure, say 5000psi, a permanent shape which is conformal to the deformed mold surface will be formed.

4) Recording cavity strain by strain gage

Several pieces of stain gages can be installed on the mold surface to measure the strain experienced by the mold cavity after the packing pressure is applied. The mold surface profile can be calculated by integrating the strain value along the cavity surface. The strain gage has to be calibrated in advance to eliminate the effect of the high normal pressure applied on it.

6.2.3 Rapid thermal cycling test

As we have discussed before the main focus of this project is to demonstrate the potential advantages of the rapid thermal cycling process over the traditional injection molding process. The experiment discussed below is designed for verifying these advantages. The molding material in these tests is chosen from Polysterene and Polycarbonate because of their transparent shape that allows the

visualization of defects and birefringence patterns. Although the design of the tool and the oil circulation system targets Polycarbonate, a popularly used molding material, it is recommended that the first rapid thermal cycling test is done with Polysterene. Polysterene is widely used for the injection molding research because of its relatively low stress optical coefficient in the glass state [K. Jansen and A. Flaman, 1994] and its relatively low process temperature.

6.2.3.1 Moldability test for thin wall molding

Thin wall molding is defined as injection molding of parts having a normal wall thickness of 1mm (0.04") or less and a surface area of 50cm^2 (8 square inches) or more. The traditional methods for thin wall molding include to use polymer material with low viscosity, to fill the mold cavity with great injection pressure and high injection speed, and to elevating barrel temperatures beyond recommended ranges [Fassett, 1995]. These methods result in the high stress and sink in the part, high levels of molecular degradation and subsequent part failures.

By introducing rapid thermal cycling for thin wall molding the shortcomings associated with the traditional molding process can be eliminated and the length of filling can be further improved. Researchers have investigated the variation of the length of filling with injection pressure and injection speed for the conventional cavity and the low thermal inertia mold. [Wadhwa & Kim, 1988]. The MoldFlow simulation also demonstrated that the rapid thermal cycle of the mold significantly improved the filling time and the short shot defect for thin wall parts.

The test proposed on the benchmark is to study how thin the part can be made by rapid thermal cycling. For this purpose the parting face of the cavity insert can be machined in order to get different web thickness starting from 0.05" to 0.01" to test the moldability. This test results will be compared with those by conventional molding to see how much the rapid thermal cycling process improves the part quality. We also want to know how thin the process can go before factors other than short shot block the molding process.

6.2.3.2 Shrinkage compensation by mold deflection

The plastic part shrinks during cooling. The conventional way to compensate the shrinkage is by packing. After the polymer melt is injected into the mold cavity a high packing pressure is applied. The packing pressure has two functions. First of all, according to the Spencer-Gilmore equation the high

packing pressure reduces the volumetric shrinkage of the part after cooling. Second while the part start to shrink after cooling, the extra melt will be fed through the gate under high packing pressure until the gate is totally sealed. Although the traditional packing stage effectively compensates for the cooling induced part shrinkage, it leads to density non-uniformity and the residual stress in the part. An alternative way is to utilize the deformation of the mold cavity to hold extra melt for shrinkage compensation. This idea can be tested in the rapid thermal cycling process by setting up proper packing pressure and proper time for gate sealing. A runner (or gate) switch can be designed to rapidly cut off the runner/gate in order to hold the desired packing pressure in the cavity after the material is completely filled and packed. The resulting part thickness (especially the thickness at the middle web area) is compared with that made by rapid thermal cycling with low packing pressure to see the difference.

6.2.3.3 Birefringence observation for rapid thermal cycled part

Birefringence observations are a quick and easy way to qualitatively establish the degree of residual strain and/or molecular orientation in transparent injection-molded part. When viewed between crossed polaroids, a clear plastic part exhibits a series of colored band, each color representing a fixed amount of strain or molecular orientation, depending on the plane of observation. The birefringence photographs took by different researchers have demonstrated a significant improvement of the rapid thermal cycling in residual stress and molecular orientation.

A quantitative definition of birefringence was reviewed by Isayev [Isayev, 1990]. During molding the orientation at every point of the molded part can be characterized by the following symmetric tensor of refractive index:

$$n_{ij} = \begin{pmatrix} n_{11} & n_{12} & n_{13} \\ n_{12} & n_{22} & n_{23} \\ n_{13} & n_{23} & n_{33} \end{pmatrix} \tag{6-3}$$

For one-dimensional flow this tensor can be simplified to:

$$n_{ij} = \begin{pmatrix} n_{11} & n_{12} & 0 \\ n_{12} & n_{22} & 0 \\ 0 & 0 & n_{33} \end{pmatrix} \tag{6-4}$$

Three mutually independent components of birefringence are defined as:

$$\Delta n = \sqrt{(n_{11} - n_{22})^2 + 4n_{12}^2}$$
$$n_{11} - n_{33} \qquad (6\text{-}5)$$
$$n_{22} - n_{33}$$

The above birefringence components (Δn, n_{11}- n_{33}, n_{22}- n_{33}) are measured on thin slices, where the thickness is along the 3, 2, 1 directions of the cavity respectively, as shown in Figure 6-5. Among them Δn is the main birefringence which is always measured by many researchers. Jansen and Flaman [Jansen & Flaman, 1994] also used this measurement to study the influence of surface heating on the birefringence distribution. The various components of birefringence discussed above are always measured by a polarizing microscope with a calibrated compensator.

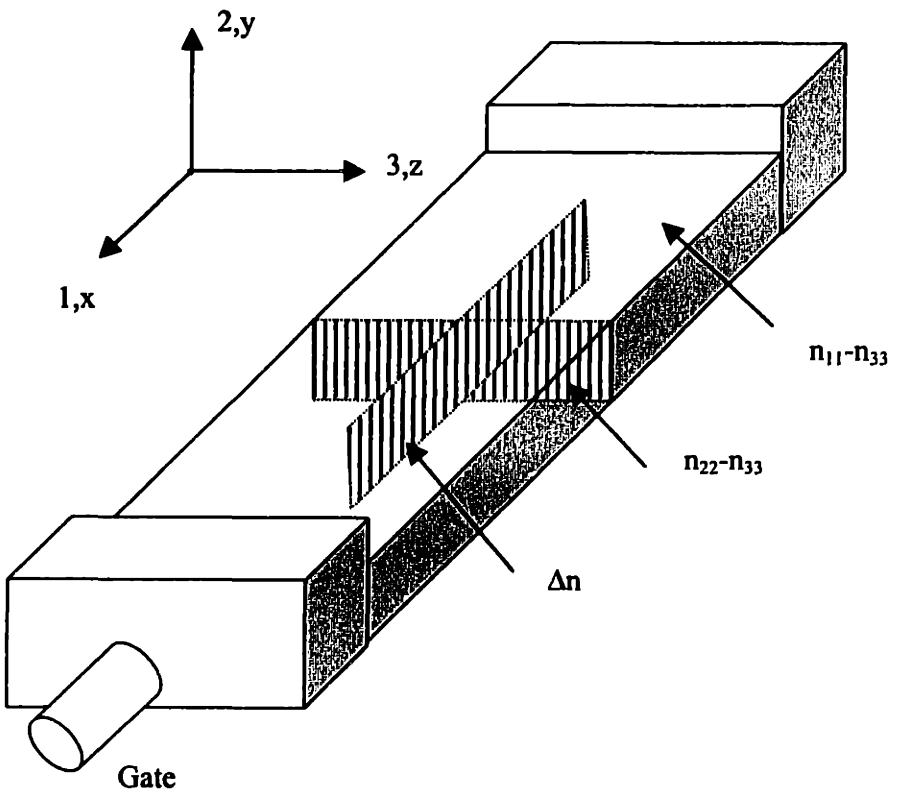

Figure 6-16 Birefringence test for the part

Furthermore, the stress-optical rules can be applied to estimate the part stress distribution and molecular orientation from the birefringence values obtained above. The stress-optical rules consist of two rules. The first rule states that the birefringence Δn is linearly proportional to the principle stress difference $\Delta\sigma$. The second rule is that the orientations of the optical axes and the principal stresses

coincide. The more detailed description on these two rules and their applications are discussed in [Isayev, 1987].

6.2.3.4 Mechanical property test for rapid thermal cycled part

Previous research has demonstrated that the low thermal inertia molded part shows more isotropic mechanical properties. Some researchers also observed the lost of the tensile strength as well as the toughness by isothermal filling [Stipkovic 1994]. However such an observation was based on the limited test samples and the molding process involves only isothermal filling under low pressure. This condition indicates that a certain packing pressure is valuable for maintaining the mechanical strength of the molded part in rapid thermal cycling. Furthermore the well controlled vitrification will further improve the part mechanical properties. The mechanical properties for the rapid thermal cycling molded part can be examined by the following tests performed on an Instron machine:

a. Tensile test to check the knit line strength in the middle area of the part. For the part shown in Figure 4-2, the two-gate filling leads to a knit line in the middle area of the part. This knit line is subject to the tensile testing in order to evaluate the improvement of the knit line strength by isothermal filling. The test result is then compared with the machined sample of the same dimension.
b. Expansion test to check the knit line strength surrounding two tapered holes. In the part shown in Figure 4-2, there are two tapered holes at both ends. The formation of these two holes lead to knit lines in the thicker area of the part. The expansion force will be applied on these holes to evaluate the strength of the formed welding line. Similarly, the test result will be compared with the machined sample of the same dimension.
c. Residual stress measurement by layer removal method. Thin layers of uniform thickness are removed from one surface of the specimen, thus upsetting the residual stress equilibrium in the piece. The reestablish equilibrium, the specimen warps to the shape of a circular arc. We can calculate the gap wise residual stresses in the part by measuring the resultant curvature as a function of depth of material removed. The technique was first developed by Treuting and Read and discussed in detail in [Isayev 1987].

6.2.4 Residual stress and warpage improvement by active process control

Research work in Cornell has demonstrated theoretically that the minimum residual stress can be achieved by optimizing the mold temperature history in the cooling stage. The optimum mold temperature

profile can be achieved on a 3D Printed tool by running hot and cold oil through conformal channels. The thermal circuit model discussed in chapter 4 has the potential to build up the entire algorithm for optimum process control based on the system dynamic analysis. It is promising that we can actively control the mold surface temperature by selectively running hot and cold oil so that the part molded with such a process will have the minimum wrapage. The optimization also considers the cost of the production rate.

6.3 REFERENCES

1. DME Product Catalogue
2. Fassett J., Thin Wall Molding: Differences in Processing Over Standard Injection Molding, ANTEC' 95, p430-433
3. Kaplan H., Practical Applications of Infrared Thermal Sensing and Imaging Equipment, SPIE Optical Engineering Press, 1999
4. Reese R., W. Kawahara, Handbook on Structure Testing, The Fairmont Press, 1993
5. Stipkovic C., Comparison of Mechanical Properties Between Isothermal Molding and Injection Molding, ANTEC'94, p3675-3677